

Exploitation and Optimization of Reservoir Performance in Hunton Formation, Oklahoma

**FINAL REPORT
BUDGET PERIOD I**

Submitted by

Mohan Kelkar
Department of Petroleum Engineering
The University of Tulsa
Tulsa, Oklahoma 74104

Contract Date: March 7, 2000

Completion Date: March 6, 2005

Budget Period I: March 7, 2000 – March 6, 2002

Work Performed Under Contract No. DE-FC26-00NT15125

Prepared for

U.S. Department of Energy
Assistant Secretary for Fossil Energy

Contracting Officer
Mr. Richard Rogus
U.S. Department of Energy
National Energy Technology Laboratory
Post Office Box 10940 MS 921-143
Pittsburgh, PA 15236-0940

DISCLAIMER

“This report was prepared as an account of work sponsored by an agency of the United States Government. Neither the United States Government nor any agency thereof, nor any of their employees, makes any warranty, express or implied, or assumes any legal liability or responsibility for the accuracy, completeness, or usefulness of any information, apparatus, product, or process disclosed, or represents that its use would not infringe privately owned rights. Reference herein to any specific commercial product, process, or service by trade name, trademark, manufacturer, or otherwise does not necessarily constitute or imply its endorsement, recommendation, or favoring by the United States Government or any agency thereof. The views and opinions of authors expressed herein do not necessarily state or reflect those of the United States Government or any agency thereof.”

ACKNOWLEDGEMENTS

The research effort described in this report was supported by the U.S. Department of Energy under Contract No. DE-FC26-00NT15125. Additional support is provided by Marjo Operating Company, Inc., the University of Houston, Joe Podpechan and James R. Derby and Associates, Inc. The computer facilities were provided by The University of Tulsa.

We would like to thank Brian Keefer from Marjo Operating Company, Inc. for his valuable contribution and insight to our work. Our special thanks also go to Rhonda Lindsey and Dan Ferguson from the Department of Energy for their enthusiasm and valuable suggestions.

March 2002
Mohan Kelkar

TABLE OF CONTENTS

DISCLAIMER	ii
ACKNOWLEDGEMENTS	iii
TABLE OF CONTENTS	iv
LIST OF FIGURES	vii
LIST OF TABLES	xi
ABSTRACT	xiii
1. EXECUTIVE SUMMARY	1
2. INTRODUCTION	4
3. OBJECTIVES	7
4. TECHNICAL PROGRESS	8
4.1. Data Collection	8
4.2. Geological Analysis	11
4.2.1. Overview	11
4.2.2. Introduction	14
4.2.3. Stratigraphy	20
4.2.4. Structural Setting	23
4.2.5. Depositional History	27
4.2.6. Migration History	31
4.2.7. Production	32
4.2.8. Core Description, Methodology, and Interpretation	35
4.2.8.1. Facies	38
4.2.8.2. Paleontology, Stratigraphic Correlation, and Facies Interpretation	40
4.2.8.3. Porosity Types.....	50
4.2.8.3.1. Distribution of Pore types.....	53
4.2.8.4. Log Interpretation of Porosity	53
4.2.8.5. Karst	54
4.2.9. Conclusions	56
4.3. Engineering Analysis	57
4.3.1. Core – Log Correlation.....	57
4.3.1.1. Development of Correlation between Core and Log Data	58
4.3.1.1.1. Discriminant Analysis and Determination of Geological Pore types	58
4.3.1.1.2. Cross Validation	60
4.3.1.2. Electrofacies Analysis	60
4.3.1.2.1. What is Electrofacies?	60
4.3.1.2.2. Principal Component Analysis	61
4.3.1.2.3. Cluster Analysis	62
4.3.1.2.4. Discriminant Analysis	65
4.3.1.2.5. Comparison of Electrofacies and Geological Facies	65
4.3.1.3. Porosity – Permeability Correlation	67
4.3.1.4. Static to Dynamic Relationship.....	69
4.3.1.4.1. Pickett Plots using geological pore types	71

4.3.1.4.2.	Buckles plot.....	81
4.3.1.4.3.	Hydrocarbon Mapping	90
4.3.1.4.4.	Electrofacies mapping	92
4.3.1.4.5.	Production mapping	94
4.3.1.4.6.	Comparison of the Static data with the Dynamic data.....	98
4.3.1.4.7.	Prediction of In-fill well Locations	100
4.3.2.	Production Data Evaluation.....	102
4.3.2.1.	Introduction	102
4.3.2.2.	Background	102
4.3.2.2.1.	Gas Solutions.....	106
4.3.2.3.	Analytical Framework of Hunton Model	107
4.3.2.3.1.	Procedure.....	108
4.3.2.3.2.	Liquid Production (Oil or Water) Calculation Procedure	109
4.3.2.3.3.	Gas Production Calculation Procedure.....	110
4.3.2.4.	Synthetic Data Example.....	111
4.3.2.4.1.	Liquid Case.....	112
4.3.2.4.2.	Gas Case.....	114
4.3.2.5.	Field Case Example.....	116
4.3.2.6.	Analysis of Results.....	125
4.3.2.7.	Conclusions.....	126
4.3.3.	Laboratory Testing of Cores.....	126
4.3.3.1.	Methodology	126
4.3.3.2.	Results.....	128
4.3.3.2.1.	CT Scan.....	129
4.3.3.2.2.	Wettability.....	131
4.3.3.2.3.	Relative Permeability	132
4.3.3.2.4.	Thin-section.....	136
4.3.3.2.5.	Mercury Porosimetry.....	140
4.3.3.3.	Conclusions.....	141
4.3.4.	Flow Simulation Study	142
4.3.4.1.	Model Characteristics.....	142
4.3.4.1.1.	Free Gas Cap	143
4.3.4.1.2.	Presence of Fractures.....	148
4.3.4.1.3.	Relationship between oil and gas production	151
4.3.4.1.4.	Limited Aquifer	152
4.3.4.1.5.	Bulk of the hydrocarbon production is through water zone	154
4.3.4.2.	Analytical Model.....	155
4.3.4.2.1.	Model Assumptions.....	156
4.3.4.2.2.	Results	161
4.3.4.2.3.	Limitations.....	163
4.3.4.3.	Flow Simulation Study.....	163
4.3.4.3.1.	Single Well Model.....	164
4.3.4.3.2.	Field-Wide Model	169
4.3.5.	Excess Water Disposal	175
5.	TECHNOLOGY TRANSFER.....	178
5.1.	Overview.....	178
5.2.	Project Web Page.....	183
5.2.1.	Members	183
5.2.2.	Announcements	184
5.2.3.	Publications	185

5.2.4.	Well Data.....	186
5.2.4.1.	Basic Well Data.....	187
5.2.4.2.	Production Data.....	189
5.2.4.3.	Well Bore Data.....	192
5.2.5.	Archive.....	193
5.2.6.	Search.....	194
5.2.7.	Discussions.....	195
6.	REFERENCES.....	196
7.	APPENDICES.....	200
7.1.	Geologic Appendix.....	200
7.1.1.	Structural Map of West Carney Hunton Field, showing location of cross-sections.....	200
7.1.2.	Hunton Isopach Map of West Carney Hunton Field, showing location of cross-sections.....	201
7.1.3.	Location of Well Cores in and near West Carney Hunton Field, on Hunton Isopach Map.....	202
7.1.4.	E – W Hunton Well-log Cross-section of West Carney Hunton Field.....	203
7.1.5.	N – S Hunton Well-log Cross-section of West Carney Hunton Field.....	204
7.1.6.	Table of Wells Cored.....	205
7.1.7.	Introduction to Core Description and Explanation of Terminology.....	206
7.1.8.	Core Descriptions of Individual Wells.....	210
7.1.9.	Explanation of Coding of Porosity and Facies Type.....	228
7.1.9.1.	Table of Porosity Types and Codes.....	228
7.1.10.	Tables of Core Porosity, Grain Density, Porosity and Facies Codes of Individual Wells.....	232
7.1.11.	Graphic Core Data and Well Log Plots of Individual Wells, with graphic plots of Porosity Types and Lithofacies Types on described cores.....	244
7.1.12.	Preliminary Report on Conodont Faunas of the Hunton Group (PaleoAppendix1).....	262
7.1.13.	Tables of Conodonts Recovered from 8 Wells (PaleoAppendix2).....	267
7.1.14.	Thin Section Samples of Individual Wells.....	271
7.1.15.	Introduction to Core Photographs.....	279
7.1.16.	Core Photographs of Individual Wells.....	279
7.2.	Geologic Appendix.....	280
7.3.	Production Appendix.....	282
7.4.	Laboratory Testing Appendix.....	285

LIST OF FIGURES

Figure 2-1: Location of the West Carney Field.....	5
Figure 2-2: Marjo Operating Company acreage.....	6
Figure 4-1: The West Hunton Field is located in T. 15-16 N., R. 1-3 E. in Logan and Lincoln Counties.....	15
Figure 4-2: Structural framework of Oklahoma (after Fritz, 1978 ¹).....	16
Figure 4-3: Map showing outline of Oklahoma Basin and other major features that existed in early Paleozoic time (after Johnson, 1988 ²).....	16
Figure 4-4: Surface and Subsurface distribution of Pre-Woodford rocks in Oklahoma (after Jordan, 1965 ³). The patterned rock represents Formations of the Hunton Group. Note the NW-trending narrow “outlet” of zero Hunton in central Ok., which is a complex structural uplift and pre-Woodford erosional feature, the Seminole Uplift.....	17
Figure 4-5: Production data from the first 120 days of the Marjo Operating Co. No. 1 Schwake demonstrates the unique characteristics of early well performance.....	18
Figure 4-6: Isopach map of Mississippian strata in northwestern Lincoln County, Oklahoma. Contour interval is 10 ft. Hachures represent isopach “thins”. The abrupt thickening of Mississippi strata in the south central portion of the map correlates well with the northeast-southwest trending fault. (Reproduced from Rottmann, 2000 ⁹).....	25
Figure 4-7: a) Structure map of the base of the Hunton Group in the West Carney Hunton Field. Contour interval is 50 ft.....	26
Figure 4-8: A brief interpretation of the depositional history of the West Carney Hunton Field. The figures represent a profile from west to east across the field.....	28
Figure 4-9: Map view of generalized facies combinations in the West Carney Hunton Field.....	29
Figure 4-10: Map of Vitrinite reflectance (reproduced from Comer, 1992, Figure 13 ¹²).....	32
Figure 4-11: Map showing cored wells employed in this study.....	37
Figure 4-12: Four well cross-section showing unconformities, Formations, and lithology across the West Carney Hunton Field. The cross-section is constructed from west to east, its locality referenced in Figure 4-11.....	42
Figure 4-13: Local zonation of Conodont stratigraphy divided into 7 zones.....	43
Figure 4-14: West Carney Hunton Field Formations and Facies.....	46
Figure 4-15: West Carney Hunton Field Lithology and Pore Types.....	47
Figure 4-16: Facies model for Early Silurian Shores and Shelves of North America and Siberia. B.A. 0 – 6 indicate Benthic Assemblage zones (from M. Johnson et al., 1997 ¹⁴).....	48
Figure 4-17: Core porosity vs. average log porosity.....	53
Figure 4-18: Scree plot showing the different principal components and their variance percentage.....	62
Figure 4-19: Cluster plot using seven groups.....	63
Figure 4-20: Cluster plot using five groups.....	64
Figure 4-21: Comparison of Electrofacies with Geological Pore Types.....	66
Figure 4-22: Log porosity vs. Ln K.....	67
Figure 4-23: Correlation between Log porosity and Core porosity.....	68
Figure 4-24: A typical Pickett plot.....	71
Figure 4-25: Pickett plot for the well Danny #2; Legends: ef = electrofacies.....	75
Figure 4-26: Production from well Danny #2.....	75
Figure 4-27: Pickett plot for Schwake ; Legend ef = electrofacies.....	76
Figure 4-28: Production from well Schwake.....	76
Figure 4-29: Pickett plot for well Townsend ; Legend ef= electrofacies.....	77
Figure 4-30: Production from well Townsend.....	77
Figure 4-31: Pickett plot for well Carter ; Legend ef= electrofacies.....	78
Figure 4-32: Production from well Carter.....	78
Figure 4-33: Pickett plot for well Lewis ; Legend ef = electrofacies.....	79
Figure 4-34: Production from well Lewis.....	79
Figure 4-35: A typical Buckles plot.....	81
Figure 4-36: Buckles plot showing different zones.....	82

Figure 4-37: Buckles plot showing different zones present in the West Carney Hunton Field.....	83
Figure 4-38: Buckles plot for Limestone with coarse matrix and vuggy pore types; Legend cr = coarse matrix.....	85
Figure 4-39: Buckles plot for Limestone with Fine matrix and Fracture pore types; Legend f= fine matrix and fr= fracture.....	85
Figure 4-40: Buckles plot for Dolomite and partly dolomitized limestone with coarse matrix and vuggy pore types; Legend cr= coarse matrix.....	86
Figure 4-41: Buckles plot with electrofacies # 1.....	87
Figure 4-42: Buckles plot with electrofacies # 2.....	88
Figure 4-43: Buckles plot with electrofacies # 3.....	88
Figure 4-44: Buckles plot with electrofacies # 4.....	89
Figure 4-45: Buckles plot with electrofacies # 5.....	89
Figure 4-46: Distribution of Hydrocarbons in place (Barrels per acre foot) in the area of study.....	91
Figure 4-47: Distribution of electrofacies 1+2+3 in the area of study.....	92
Figure 4-48: Distribution of electrofacies # 4+5 in the area of study.....	93
Figure 4-49: Distribution of oil production in the area of study, calculated for a six year period.....	94
Figure 4-50: Distribution of the cumulative oil production from the area of study, calculated as log of the original production (STB).....	95
Figure 4-51: Distribution of gas production in the area of study, calculated for a six year period.....	96
Figure 4-52: Distribution of hydrocarbons in place (BAF) for the electrofacies # 1+2+3 in the area of study.....	97
Figure 4-53: Distribution of hydrocarbons in place (BAF) for the electrofacies # 4+5.....	97
Figure 4-54: Plot of the rank of wells based on water production vs. K*H. The K*H has been calculated using 1 st percentile K values (228 md). The ranks are plotted in decreasing order, rank 1 corresponds to the best and rank 27 corresponds to the worst.....	99
Figure 4-55: Three-layer no cross-flow model.....	108
Figure 4-56: Rate vs. t_{eL} plot used to determine where the pss period begins.....	113
Figure 4-57: q_{DdL} vs. Q_{DdL} plot for synthetic liquid case using only pss data.....	113
Figure 4-58: Oil rate vs. time plot for the oil synthetic production data as well as the oil production data calculated using the matched reservoir parameters.....	114
Figure 4-59: Rate vs. t_{eG} plot used to determine where the pss period begins for the gas synthetic data.....	115
Figure 4-60: q_{DdG} vs. Q_{DdG} plot for synthetic gas case using only pss data.....	116
Figure 4-61: Gas rate vs. time plot for the synthetic gas production data as well as the gas production data calculated using the matched reservoir parameters.....	116
Figure 4-62: Carter Ranch #2-15 q_{DdL} vs. Q_{DdL} plot for pss oil production used to determine r_e	121
Figure 4-63: Carter Ranch #2-15 oil rate vs. time plot of the real production data as well as the production data calculated using the calculated values of r_e , k , and s_f	122
Figure 4-64: Carter Ranch #2-15 q_{DdL} vs. Q_{DdL} plot for pss water production used to determine r_e	122
Figure 4-65: Ranch #2-15 water rate vs. time plot of the real production data as well as the production data calculated using the calculated values of r_e , k , and s_f	123
Figure 4-66: Carter Ranch #2-15 q_{DdG} vs. Q_{DdG} plot for pss gas production used to determine r_e	124
Figure 4-67: Carter Ranch #2-15 gas rate vs. time plot of the real production data as well as the production data calculated using the calculated values of r_e , k , and s_f	124
Figure 4-68: Cross-sectional CT scan at 2, 4, and 6 cm from on side of Core 3.....	130
Figure 4-69: Longitudinal CT scale of Core 3.....	130
Figure 4-70: Cross-sectional CT scan at 2, 4, and 6 cm from one side of Core 4.....	130
Figure 4-71: Longitudinal CT scan of Core 4.....	131
Figure 4-72: Cross-sectional CT scan at 2, 4, and 6 cm from one side of Core 8.....	131
Figure 4-73: Imbibition relative permeability of Mary Marie 4968.6-7 (Cores 3-4).....	133
Figure 4-74: Imbibition relative permeability of Wilkerson 4974.9 (Core 5).....	133
Figure 4-75: Imbibition relative permeability of Carter 4995.2 (Core 6).....	134
Figure 4-76: Correlation between end point water imbibition relative permeability and wettability.....	134
Figure 4-77: Drainage relative permeability of Mary Marie 4968.6-7 (Cores 3-4).....	135
Figure 4-78: Drainage relative permeability of Wilkerson 4974.9 (Core 5).....	135

Figure 4-79: Drainage relative permeability of Carter 4995.2 (Core 6).....	136
Figure 4-80: Horizontal thin-section of Mary Marie 4968.6-7 (Cores 3-4).....	137
Figure 4-81: Horizontal thin-section of Mary Marie 4968.6-7 (Cores 3-4).....	137
Figure 4-82: Horizontal thin-section of Wilkerson 4974.9 (Core 5).....	138
Figure 4-83: Vertical thin-section of Wilkerson 4974.9 (Core 5).....	138
Figure 4-84: Horizontal thin-section of Carter 4995.2 (Core 6).....	139
Figure 4-85: Vertical thin-section of Carter 4995.2 (Core 6).....	139
Figure 4-86: Mercury capillary pressure curves for Cores 4-6.....	140
Figure 4-87: Correlation between absolute permeability, porosity and wettability.....	141
Figure 4-88: Condensed liquid volume in CCE experiment.....	144
Figure 4-89: Gas-oil ratio for Danny #1 well.....	145
Figure 4-90: GOR plot of Schwake well.....	146
Figure 4-91: Water rate plot for Danny #1 well.....	148
Figure 4-92: Water-oil ratio for the Schwake well.....	149
Figure 4-93: Effect of Wilkerson #2 on the production of Wilkerson #1.....	150
Figure 4-94: Oil and Gas rate plot for Danny #2 well.....	151
Figure 4-95: Relation between oil and gas rate for the wells.....	152
Figure 4-96: Bottomhole pressure of wells.....	153
Figure 4-97: Water production for wells, McBride North and McBride South.....	154
Figure 4-98: Two layer model.....	156
Figure 4-99: Water Production Rate.....	162
Figure 4-100: Water Production for Case 2.....	163
Figure 4-101: Three-layer model.....	164
Figure 4-102: Oil rate match for Schwake well.....	167
Figure 4-103: Gas rate for Schwake well.....	167
Figure 4-104: GOR for Schwake Well.....	168
Figure 4-105: Grid structure and the Well locations.....	171
Figure 4-106: Cumulative oil production of the field.....	172
Figure 4-107: Cumulative Gas Production of the Field.....	172
Figure 4-108: Oil Rate for the Boone well.....	173
Figure 4-109: Gas Rate for the Boone well.....	174
Figure 4-110: GOR plot of Well Danny #1.....	174
Figure 5-1: TUCRS home page.....	180
Figure 5-2: Hunton Project home page (non-restricted access).....	181
Figure 5-3: Hunton Project member home page.....	182
Figure 5-4: Hunton Project Members page.....	183
Figure 5-5: Hunton Project Announcements page.....	184
Figure 5-6: Hunton Project Publications page.....	185
Figure 5-7: Hunton Project Well Data page.....	186
Figure 5-8: Hunton Project Basic Well Data page.....	187
Figure 5-9: Well Data Sheet.....	188
Figure 5-10: Hunton Project Well Production Data page.....	189
Figure 5-11: Hunton Project Well Production Data, Oil Rate page.....	190
Figure 5-12: Hunton Project Well Production Data, Oil Rate page with query information displayed.....	191
Figure 5-13: Hunton Project Well Bore Data page.....	192
Figure 5-14: Hunton Project Archive page.....	193
Figure 5-15: Hunton Project Search page.....	194
Figure 5-16: Hunton Project Discussions page.....	195
Figure 7-1: Structural Map of West Carney Hunton Field, showing location of cross-sections.....	200
Figure 7-2: Hunton Isopach Map of West Carney Hunton Field, showing location of cross-sections.....	201
Figure 7-3: Location of Well Cores in and near West Carney Hunton Field, on Hunton Isopach Map.....	202
Figure 7-4: E – W Hunton Well-log Cross-section of West Carney Hunton Field.....	203

<i>Figure 7-5: N – S Hunton Well-log Cross-section of West Carney Hunton Field</i>	204
<i>Figure 7-6: Geological and petrophysical classification of vuggy pore space based on vug interconnection. The volume of separate vug pore space is important for characterizing the petrophysical properties. From Lucia, 1995¹³</i>	209
<i>Figure 7-7: Marjo Anna well log plot</i>	244
<i>Figure 7-8: Bailey 2-6 well log plot</i>	245
<i>Figure 7-9: Marjo Boone 1-4 well log plot</i>	246
<i>Figure 7-10: Marjo Carney Extension SWDW well log plot #1</i>	247
<i>Figure 7-11: Marjo Carney Extension SWDW well log plot #2</i>	248
<i>Figure 7-12: Marjo Carney Townsite 2-5 well log plot</i>	249
<i>Figure 7-13: Marjo Carter well log plot</i>	250
<i>Figure 7-14: Marjo Carter Ranch well log plot</i>	251
<i>Figure 7-15: Marjo Danny 2-34 well log plot</i>	252
<i>Figure 7-16: Marjo Griffin well log plot #1</i>	253
<i>Figure 7-17: Marjo Griffin well log plot #2</i>	254
<i>Figure 7-18: Marjo Henry 1-3 well log plot</i>	255
<i>Figure 7-19: Marjo Joe Givens 1-14 well log plot</i>	256
<i>Figure 7-20: Marjo Mary Marie 1-11 well log plot</i>	257
<i>Figure 7-21: Marjo McBride South 1-10 well log plot</i>	258
<i>Figure 7-22: Marjo Toles 1-10 well log plot</i>	259
<i>Figure 7-23: Marjo Wilkerson 1-3 well log plot</i>	260
<i>Figure 7-24: Marjo Williams 1-3 well log plot</i>	261
<i>Figure 7-25: Local zonation of Conodont stratigraphy divided into 7 zones</i>	266
<i>Figure 7-26: Explanation for Lithology and Pore Type Symbols</i>	280
<i>Figure 7-27: Explanation for Facies Type Symbols</i>	281

LIST OF TABLES

<i>Table 4-1: List of Marjo wells in West Carney Hunton Field</i>	9
<i>Table 4-2: Age, lithology, and thickness of units above and below the Hunton Group in the West Carney Area</i>	20
<i>Table 4-3: Biostratigraphic correlations of the Hunton Group (reproduced from Stanley, 2001³)</i>	22
<i>Table 4-4: List of cored wells and cored intervals currently employed in this study. Also described are the wireline derived log depths for the top and base of the Hunton Group</i>	38
<i>Table 4-5: Numeric codes for 14 identified Lithofacies</i>	39
<i>Table 4-6: Distribution of Conodont Faunas</i>	44
<i>Table 4-7: Table of Facies Code symbols used with Figure 4-14 and Table of Pore Codes used with Figure 4-15</i>	45
<i>Table 4-8: Depth ranges of Silurian Benthic assemblages (from M. Johnson, 1987¹⁵)</i>	49
<i>Table 4-9: Comparison between log and core data</i>	54
<i>Table 4-10: Petrophysical, electrofacies and production characteristics of some of the wells</i>	80
<i>Table 4-11: Time taken by some of the wells to go on vacuum after acid treatment</i>	100
<i>Table 4-12: Synthetic data as well as calculated results for the synthetic liquid (oil) case</i>	112
<i>Table 4-13: Synthetic data as well as calculated results for the synthetic gas case</i>	115
<i>Table 4-14: Carter Ranch #2-15 known reservoir and fluid properties input used for the oil production analysis</i>	118
<i>Table 4-15: Carter Ranch #2-15 initial estimates and min and max values for permeability and skin factor used for the oil production analysis</i>	118
<i>Table 4-16: Carter Ranch #2-15 calculated reservoir parameters based on oil production rate and core data values</i>	118
<i>Table 4-17: Carter Ranch #2-15 known reservoir and fluid properties input used for the water production analysis</i>	119
<i>Table 4-18: Carter Ranch #2-15 initial estimates and min and max values for permeability and skin factor used for the water production analysis</i>	119
<i>Table 4-19: Carter Ranch #2-15 calculated reservoir parameters based on water production rate and core data values</i>	119
<i>Table 4-20: Carter Ranch #2-15 known reservoir and fluid properties input used for the gas production analysis</i>	120
<i>Table 4-21: Carter Ranch #2-15 initial estimates and min and max values for permeability and skin factor used for the gas production analysis</i>	120
<i>Table 4-22: Carter Ranch #2-15 calculated reservoir parameters based on gas production rate and core data values</i>	120
<i>Table 4-23: List of cores</i>	129
<i>Table 4-24: Core properties and Amott Wettability</i>	132
<i>Table 4-25: Comparison between WEHLU and West Carney Field</i>	147
<i>Table 4-26: Input Data used for Single Well Simulation</i>	166
<i>Table 7-1: Table of Wells Cored</i>	205
<i>Table 7-2: Pore-type classification of carbonate rocks (Lucia, 1995)¹³</i>	208
<i>Table 7-3: Core Description, Marjo Anna 1-15</i>	210
<i>Table 7-4: Core Description, Marjo Bailey 2-6</i>	211
<i>Table 7-5: Core Description, Marjo Boone 1-4</i>	212
<i>Table 7-6: Core Description, Marjo Carney Townsite 2-5</i>	213
<i>Table 7-7: Core Description #1, Marjo Carter 1-14</i>	214
<i>Table 7-8: Core Description #2, Marjo Carter 1-14</i>	215
<i>Table 7-9: Core Description #1, Marjo Carter Ranch 2-15</i>	216
<i>Table 7-10: Core Description #2, Marjo Carter Ranch 2-15</i>	217
<i>Table 7-11: Core Description, Marjo Danny 2-34</i>	218
<i>Table 7-12: Core Description, Marjo Henry 1-3</i>	219

Table 7-13: Core Description, Marjo Joe Givens 1-15	226
Table 7-14: Core Description #1, Marjo Mary Marie 1-11.....	227
Table 7-15: Core Description #2, Marjo Mary Marie 1-11.....	228
Table 7-16: Core Description, Marjo McBride South 1-10.....	228
Table 7-17: Core Description #1, Marjo Toles 1-10.....	229
Table 7-18: Core Description #2, Marjo Toles 1-10.....	230
Table 7-19: Core Description #1, Marjo Wilkerson 1-3	231
Table 7-20: Core Description #2, Marjo Wilkerson 1-3	232
Table 7-21: Core Description, Marjo Williams 1-3.....	233
Table 7-22: Table of Facies Codes.....	237
Table 7-23: Marjo Anna Porosity and Facies Codes	238
Table 7-24: Bailey 2-6 Porosity and Facies Codes	239
Table 7-25: Boone 1-4 Porosity and Facies Codes	240
Table 7-26: Carney Townsite 2-5 Porosity and Facies Codes	241
Table 7-27: Carter 1-4 Porosity and Facies Codes.....	242
Table 7-28: Carter Ranch 2-5 Porosity and Facies Codes	243
Table 7-29: Danny 2-34 Porosity and Facies Codes.....	244
Table 7-30: Henry 1-3 Porosity and Facies Codes.....	245
Table 7-31: Joe Givens #1-15 Porosity and Facies Codes.....	245
Table 7-32: Mary Marie Porosity and Facies Codes	246
Table 7-33: McBride South 1-10 Porosity and Facies Codes	247
Table 7-34: Marjo Toles 1-10 Porosity and Facies Codes.....	248
Table 7-35: Marjo Wilkerson 1-3 Porosity and Facies Codes.....	249
Table 7-36: Williams 1-3 Porosity and Facies Codes	250
Table 7-37: Local Biostratigraphic relationship of selected wells in the West Carney Hunton Field.....	277
Table 7-38: Conodont Samples, Marjo Bailey 2-6.....	279
Table 7-39: Conodont Samples, Marjo Boone 1-4.....	279
Table 7-40: Conodont Samples, Carney Townsite 2-5.....	280
Table 7-41: Conodont Samples, Marjo Carter 1-14.....	280
Table 7-42: Conodont Samples, Marjo Griffin 1-14	281
Table 7-43: Conodont Samples, Mary Marie 1-11	281
Table 7-44: Conodont Samples, Marjo W. Carney Extension SWDW No. 1	282
Table 7-45: Thin Sections, Marjo Anna 1-15.....	283
Table 7-46: Thin Sections, Marjo Bailey 2-6	284
Table 7-47: Thin Sections, Marjo Boone 1-14.....	285
Table 7-48: Thin sections, Marjo Carney Townsite 1-14.....	285
Table 7-49: Thin section, Marjo Carter 1-14.....	286
Table 7-50 Thin section, Mary Marie 1-11.....	287
Table 7-51: Thin section, McBride South 1-10.....	288
Table 7-52: Thin section, Marjo Toles #1.....	288
Table 7-53: Thin Section, Marjo W. Carney Extension SWDW 1-14.....	289
Table 7-54: Thin section, Marjo Wilkerson 1-3	290
Table 7-55: Hydrodynamic Properties of the fluids used in the experiment	297
Table 7-56: Imbibition Relative Permeability of core#3 by JBN method.....	297
Table 7-57: Drainage Relative Permeability of core#3 by JBN method.....	298
Table 7-58: Imbibition Relative Permeability of core#5 by JBN method.....	299
Table 7-59: Drainage Relative Permeability of core#5 by JBN method.....	300
Table 7-60: Imbibition Relative Permeability of core#6 by JBN method.....	301
Table 7-61: Drainage Relative Permeability of core#6 by JBN method.....	302

ABSTRACT

The West Carney Field in Lincoln County, Oklahoma is one of few newly discovered oil fields in Oklahoma. Although profitable, the field exhibits several unusual characteristics. These include decreasing water-oil ratios, decreasing gas-oil ratios, decreasing bottomhole pressures during shut-ins in some wells, and transient behavior for water production in many wells.

This report explains the unusual characteristics of West Carney Field based on detailed geological and engineering analyses. We propose a geological history that explains the presence of mobile water and oil in the reservoir. The combination of matrix and fractures in the reservoir explains the reservoir's flow behavior. We confirm our hypothesis by matching observed performance with a simulated model and develop procedures for correlating core data to log data so that the analysis can be extended to other, similar fields where the core coverage may be limited.

1. EXECUTIVE SUMMARY

(Note: When viewing this document electronically in MicroSoft Word, please be advised that bold text that specifically references a Table, Figure, Equation, or document Section is cross-referenced via hyperlinks to the noted object. To view, point at the text and Ctrl+Click. To return to your place in the text, make sure that your Web toolbar is enabled (View, Toolbars, and select Web) and click the green back arrow. These links will not work in Adobe Acrobat.)

The West Carney Field in Lincoln County, Oklahoma, produces from the Hunton Formation. Although prolific and profitable, the production exhibits unusual characteristics. The purpose of this project was to explain the unusual characteristics of the reservoir, and develop methods for extending the analysis to other infill well locations as well as other potential fields. We have been successful in achieving these objectives. Specifically, we can derive the following conclusions from the study. These conclusions are based on detailed geological and engineering evaluations included in the report.

1. The mechanism by which oil and gas in the West Carney Field is stored is through two displacements. Oil is migrated in a water wet reservoir rock filling up large pores and some of the small pores. Due to the polarity of oil, the wettability of the rock changed. Some of the invaded rock became oil wet and some remained water wet. Over geological time, water migrated into the reservoir again. Due to the changed nature of wettability, water migrated into large pores, leaving oil in the small pores.

2. Hydrocarbons in the reservoir can be described as either volatile oil or condensate gas. Small reductions in the pressure can result in two phases – oil and gas – separated in the reservoir. Both phases co-exist in the pores where hydrocarbons are located. Therefore, if the well produces oil, there is good correlation between oil and gas production.

3. The reservoir is partially fractured, mostly vertical. These fractures are located mostly in fine pore matrix. The fractures have relatively high permeability compared to other parts of the reservoir. Water selectively moves through these highly permeable fractures.

4. The source for water is the coarse matrix and vugs in the reservoir. It is a finite source, and as the water is produced, the reservoir pressure is slowly depleted.

5. As the pressure in the fractures is reduced, oil and gas located in the fine matrix migrates into the fractures, and starts producing along the fractures. Eventually, the water rate decreases and the hydrocarbon rate increases. Since oil and gas have to migrate into fractures before they are produced, the effective permeability of the water zone is significantly higher than the effective permeability of the oil and gas zones.

6. The majority of hydrocarbons, which are accessible, are the only ones located in fine matrix. Therefore, a good spatial correlation exists between hydrocarbons produced and the presence of fine matrix.

7. The percentage of fine matrix at different spatial locations can be identified by using available log data at existing wells. By identifying log signatures and dividing them into various clusters, different pore types can be spatially mapped. The fine pore matrix represents the highest possibility of producing the most oil, since it includes the two ingredients for a successful well – presence of fractures and fine pore matrix filled with hydrocarbons.

8. Flow simulation of simplified reservoir description confirms the mechanistic model proposed to explain the reservoir behavior. Most of the unique characteristics exhibited by the West Carney Field can be reproduced using this model.

9. The geological and reservoir properties description indicates the highly heterogeneous nature of the reservoir with little spatial correlation. Therefore, it is difficult to correlate isochronal intervals in the field using the available core and log data. However, we can still map the spatial concentration of various facies, resulting in potential in fill well locations.

Future work in the Budget Period II would include:

- Develop better PVT characteristics for the field.
- Develop quantitative characteristics to predict success of newly drilled wells
- Build a geologically consistent reservoir model to match the existing production data, and use the model to predict future performance under various scenarios
- Evaluate alternate mechanisms to improve the performance of the reservoir.
- Conduct several technical workshops to disseminate the technical knowledge gained in this project.
- Upgrade the existing web site so that member parties are able to download different combinations of well data.

We believe that we will accomplish these tasks in Budget Period II.

2. INTRODUCTION

The West Carney Field is located in Lincoln County, Oklahoma. The location of the field is shown in **Figure 2-1**. The field, which was discovered in 1980, produces from the Hunton Formation in a shallow-shelf carbonate reservoir. The early development in the field was sporadic. Many of the initial wells were abandoned due to high water production and constraints in surface facilities for disposing excess produced water. Field development by Altex Resources began in earnest in 1995. Altex recognized that production from this field was only possible if large volumes of water could be disposed. Since Altex already had a disposal well to that could handle large amounts of water, they were able to aggressively drill several producers. With few exceptions, all these wells exhibited similar characteristics. The initial production indicated trace amounts of oil and gas with mostly water as a dominant phase. As the reservoir was depleted, the oil cut eventually improved, making the overall production feasible. The decreasing oil cut (ROC) behavior is not completely understood. However, the field has been subjected to intense drilling activity due to the success of Altex Resources.

Currently, three operators dominate this area: Altex Resources, Dominion, and Marjo Operation Company. Of the three, we are working closely with Marjo Operating Company. The acreage of Marjo Operating Company is shown in **Figure 2-2** below. For this report, therefore, we will concentrate on this area.

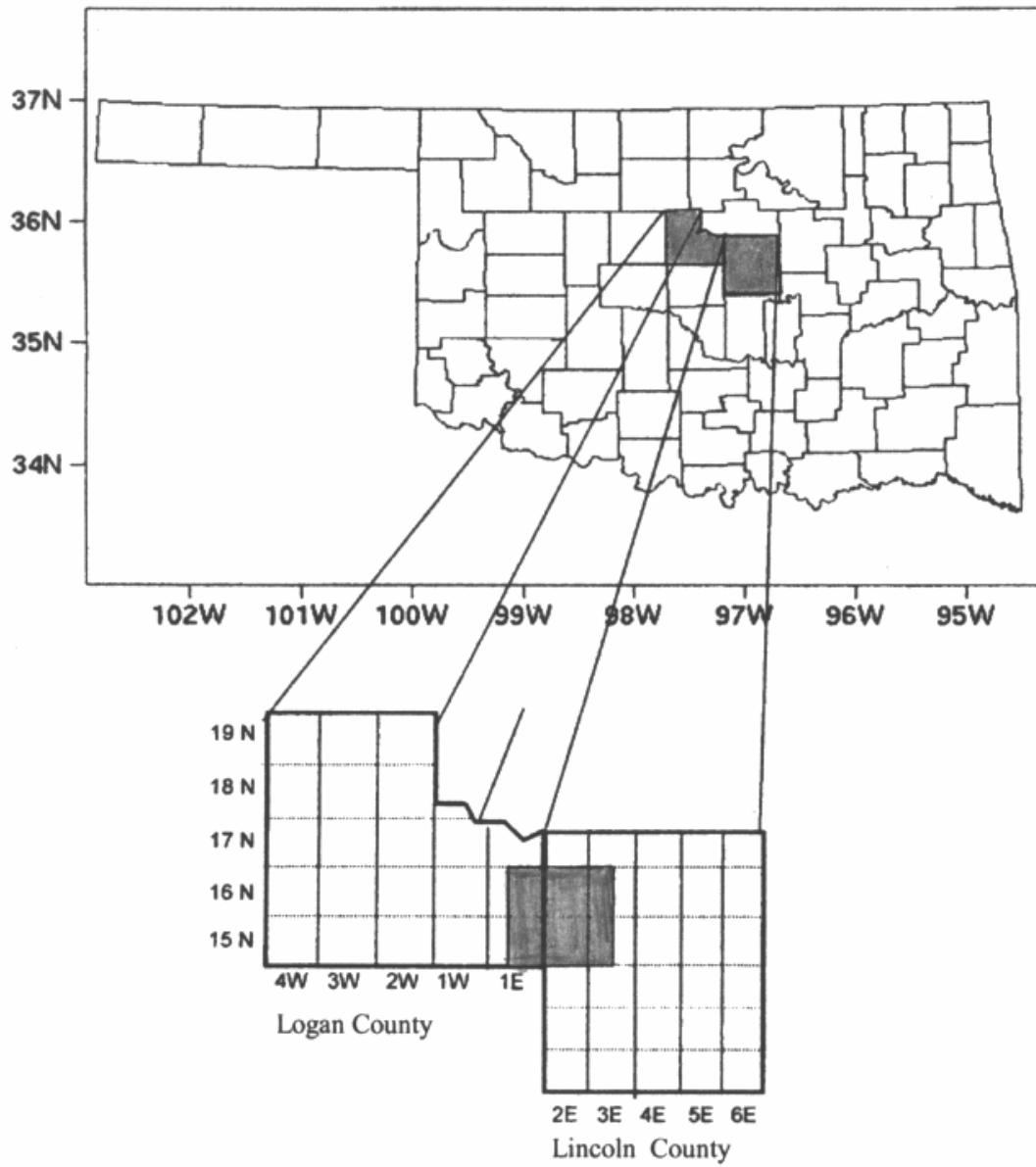


Figure 2-1: Location of the West Carney Field

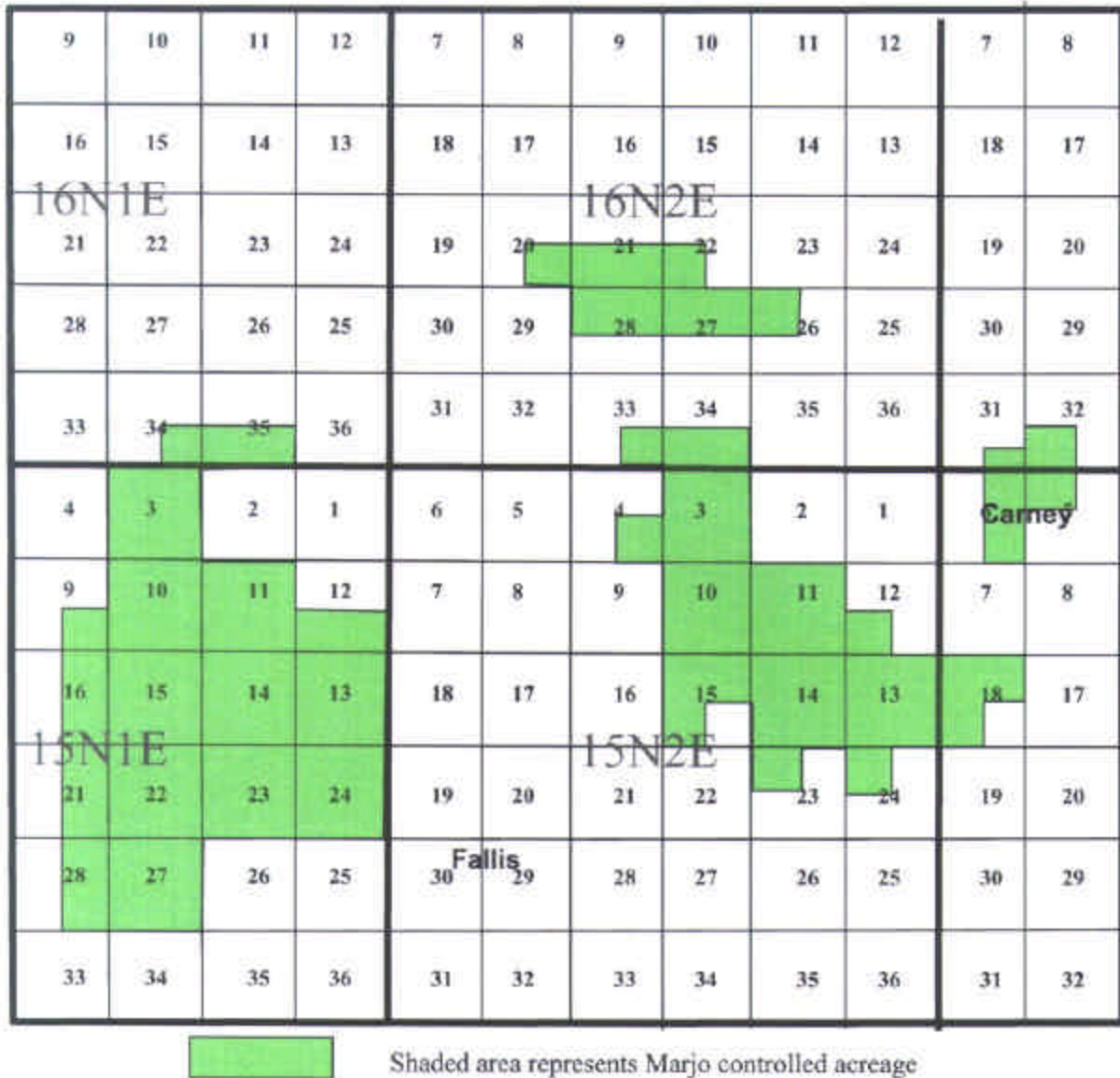


Figure 2-2: Marjo Operating Company acreage

3. OBJECTIVES

The main objectives of the proposed study in Budget Period I can be summarized as follows:

1. To understand and evaluate an unusual primary oil production mechanism that results in decreasing (retrograde) oil cut (ROC) behavior as the reservoir pressure declines.
2. To build a depositional model to explain the geological characteristics of the reservoir.
3. To develop areal distribution of geological facies and rock types to understand the geological heterogeneity of the reservoir.
4. To improve calculations of initial oil in place so as to determine the economic feasibility of completing and producing a well.
5. To optimize the location of new wells based on understanding of the geological and petrophysical properties heterogeneities.
6. To develop correlation between rock types and log curves so that the evaluation can be extended to other areas where limited core data are available.
7. To develop decline type curves methods for evaluating performance of existing and new wells, and to estimate reservoir properties based on production characteristics.
8. To correlate static reservoir description with dynamic data.
9. To improve techniques for water disposal to reduce the cost of excess water handling.
10. To effectively transfer the technology so that other operators can use the knowledge gained in this work.

4. TECHNICAL PROGRESS

The technical progress made in Budget Period I is presented in the following sections. Most of the objectives stated in the previous section have been accomplished, except the water disposal problem. The reasons for this exception are explained below.

4.1. Data Collection

Mohan Kelkar (The University of Tulsa)

One of the primary goals of the project was to collect sufficient information for proper evaluation of the field. Careful evaluation of all the logs revealed that log data from 186 wells can be used for further analysis. The logs collected from these wells included gamma ray, neutron, density and deep resistivity. Based on the evaluations of cored wells, we have noted that the most useful logs providing information about the characteristic of the reservoir are neutron, density and deep resistivity. We found 186 wells for which all three logs were available. We have digitized the data from these wells.

In addition to collecting log data from wells, we also have collected core data from various wells. In the original proposal, we had intended to collect core data from six wells. However, we decided to core many more wells so that we will have extensive core coverage in the field. **Table 4-1** shows the number of wells that have been drilled in the field, and the wells which have been cored. The core data includes standard measurements such as permeability, porosity and saturation as well as core photographs and fluorescence analysis. In addition, several core samples were further investigated for relative permeability measurements as well as fracture distributions. We also made 140 thin sections and sent 85 samples for conodont studies.

Table 4-1: List of Marjo wells in West Carney Hunton Field

Well Name	Comp Date Completed	Location Section	Twp/Blk	Rng/Survey	County	State
Ables 1-34	4/10/2000	C SE SW Sec. 34	16N	2E	Lincoln	OK
Adams #1-A	9/11/2001	NE NE NE Sec. 5	14N	3E	Lincoln	OK
Alan Ross 1-11		NE SW NE NE Sec. 11	15N	2E	Lincoln	OK
Anna #1-15 **	9/29/2000	SE NW NE Sec. 15	15N	2E	Lincoln	OK
Bailey #2-6 **		SE NE SW Sec. 6	15N	3E	Lincoln	OK
Bailey 1-6		SW/4 Sec 6	15N	3E	Lincoln	OK
Boone #1-4	8/21/2000	C SW SE Sec. 4	15N	2E	Lincoln	OK
Bracken #1	1/5/2002	SW Sec. 33	15N	3E	Lincoln	OK
Cal #1-11 **	3/27/2001	C NE SE 11	15N	1E	Logan	OK
Carney Townsite #2-5 **	11/27/2000	NW NW NW Sec. 5	15N	3E	Lincoln	OK
Carney Townsite 1-5		SW NE SW NW Sec. 5	15N	3E	Lincoln	OK
Carter #1-14 **		C NE SE Sec. 14	15N	2E	Lincoln	OK
Carter Ranch #2-15 **	2/7/2001	NW NW SE Sec. 15	15N	2E	Lincoln	OK
Castine #1		Sec. 22	16N	2E	Lincoln	OK
Chandler SWDW #1 **	11/20/2001	SW NE NE NE Sec. 5	14N	3E	Lincoln	OK
Christy 1-15	2/26/2000	W/2 SE NE NW Sec 15	15N	2E	Lincoln	OK
Danny 1-34	3/28/2000	SE/4 Sec 34	16N	2E	Lincoln	OK
Danny 2-34 **		C SE SE Sec. 34	16N	2E	Lincoln	OK
Denney #1-31	8/24/2000	NE SW SE SE Sec. 31	16N	3E	Lincoln	OK
Denney #2-31	10/23/2001	SW NE SW SE Sec. 31	16N	3E	Lincoln	OK
Franny 1-11		NE SW NE SE Sec. 11	15N	2E	Lincoln	OK
Garrett 1-11		N/2 S/2 NW SW Sec. 11	15N	2E	Lincoln	OK
Geneva #1-32		32	16N	3E	Lincoln	OK
Geneva #2-32 **	2/1/2001	C NE SW Sec. 32	16N	3E	Lincoln	OK
Gerry 2-6	10/28/1998	SW NW NW Sec 6	15N	3E	Lincoln	OK
Gilmore Price Horizontal #1-33	8/16/2001	NW SE Sec. 33	16N	2E	Lincoln	OK
Green #1-26		SW NW Sec 26	16N	2E	Lincoln	OK
Griffin #1-14 **	8/30/2001	NW NW SW Sec. 14	15N	1E	Logan	OK
Henry #1-3 **		NW/4 Sec 3	15N	2E	Lincoln	OK
Houser #1-11 A **	9/27/2001	SE NE 11	15N	1E	Logan	OK
JB #1-13 **		S2 NW NW 13	15N	1E	Lincoln	OK
Joe Bryan #2		SE SE) Sec. 32	15N	3E	Lincoln	OK
Joe Givens #1-15 **		W2 NE NE SW Sec. 15	15N	2E	Lincoln	OK
Katheryn #1-14		NE SW NE NW Sec. 14	15N	2E	Lincoln	OK
Kathryn #2-14 **	1/15/2001	NW NW NW Sec. 14	15N	2E	Lincoln	OK
Mary Marie #1-11 **		SW NE SE NW Sec. 11	15N	2E	Lincoln	OK
Mary Marie #2-11	5/2/2000	SW NE NE NW Sec. 11	15N	3E	Lincoln	OK
McBride North #1-10		W/2 E/2 NE NE Sec. 10	15N	2E	Lincoln	OK
McBride South #1-10 **	8/3/2000	SE/4 Sec. 10	15N	2E	Lincoln	OK
Mercer #1-28 **	7/16/2001	E2 NW NE Sec. 28	17N	2E	Lincoln	OK
Morrow #1-27 **	10/15/2001	NW NE NW Sec. 27	16N	2E	Lincoln	OK
Parkview #1-3	2/14/2000	C SE SE Sec. 3	15N	2E	Lincoln	OK
Pearl #1-12		NE SW NE SW Sec. 12	15N	2E	Lincoln	OK
Pearl SWDW #1		SE NW NW NE Sec 15	15N	2E	Lincoln	OK
Points #1-13 **	5/31/2001	C NE SE Sec. 13	15N	1E	Logan	OK
Ranch SWDW #1		SW SW NE Sec 3	15N	2E	Lincoln	OK
Saunders #1-13 **	5/16/2001	NW NE NE 13	15N	1E	Logan	OK
Schwake #1-10		N/2 SW NE SW Sec 10	15N	2E	Lincoln	OK
Shons #1-23	2/1/1994	SE NE NW	23	15N	Logan	OK
Short #1-22	7/30/2001	S2 SE SE Sec. 22	17N	2E	Lincoln	OK
Stevenson #1-14 **	12/26/2001	N2 S2 NW NW Sec.14	15N	2E	Logan	OK
Toles #1-10 **		SW NE SW NW Sec 10	15N	2E	Lincoln	OK
Townsend #1-13		NW SE NW NW Sec 13	15N	2E	Lincoln	OK
West Carney Extension SWDW #1 **		NE SE SW NE Sec. 14	15N	1E	Logan	OK
White #1-27		C W/2 SE NE Sec 27	16N	2E	Lincoln	OK
Wilkerson #1-3 **		N/2 S/2 NE NE Sec 3	15N	2E	Lincoln	OK
Wilkerson #2-3	10/31/2000	NW SE SE NE Sec. 3	15N	2E	Lincoln	OK
Williams #1-3 **		SW Sec. 3	15N	2E	Lincoln	OK
Wilson # 1-6		SW NE NE Sec 6	15N	3E	Lincoln	OK

** Cored wells

For Marjo wells, we collected water, oil and gas production data on daily basis. Some wells were equipped with bottomhole pressure gauges which allowed us to measure both the rates and pressure variations. After each well was swabbed, we checked to see if the well would go on vacuum and how fast. The production data for wells operated by other operators was collected through the public domain.

To understand the PVT characteristics of the fluid produced, we collected one sample and analyzed it. This was useful in understanding the fluid behavior of the field.

Originally, we proposed to conduct a single well tracer test to determine the oil saturation. This was based on our initial belief that the resistivity logs may not reflect true saturation in the reservoir. Therefore, we felt the need to use a single well tracer test to measure the oil saturation. Subsequent to the contract, we collected more than thirty cores and measured the saturations in those samples. We observed that the saturations measured in the cores were consistent with the values obtained from the log data. This gave us confidence in our measurement of saturation using log data only.

The single well tracer test to measure the oil saturation required that we inject a partitioning tracer into a well, which partitions between oil and water and, depending on how long it takes to flow back in the producing well, one could determine the oil saturation. The problem was that the method would only determine the residual oil saturation which is not mobile. That is, the tracer will contact the residual oil and partition between the residual oil and mobile water. That is because when the tracer is injected along with water, all the fluid is pushed back except immobile oil and water. This type of approach is good to determine residual oil saturation for water flooding, but may not reflect the oil saturation in West Carney Field. Our current understanding of the reservoir assumes that most of the oil is produced through the water zone, and it is mobile when it enters the water zone. Most of the injected tracer will selectively go into the water zone and will not be able to measure oil saturation in the small pores. In order to determine the oil reserves, we need to measure oil

saturation in the small pores. Since this is not possible using a single well tracer test, we decided not to conduct the single well tracer test.

4.2. Geological Analysis

James R. Derby (Derby & Associates, Inc.), Joe Podpechan and Jason Andrews (Independent Geologists), and Sandeep Ramakrishna (The University of Tulsa)

4.2.1. Overview

The goal of the Geological Analysis effort in Budget Period I has been to describe and interpret the geology and petrophysical reservoir characteristics of the Hunton reservoir. The project proposal included study of 3 cores; to date, 27 wells have been cored, of which 14 have been described in detail, and 23 have been studied to various degrees. It was anticipated that well-logging suites would include sonic logs and borehole imaging; both have been eliminated in favor of additional coring. It was anticipated that the reservoir would be a traditional Mid-Continent layered reservoir, divisible into widely correlative horizons of similar characteristics. The abundance of core data reveals that the reservoir is heterogeneous laterally and vertically, and is not readily divisible into horizontal zones of similar characteristics. Consequently the geological investigation has expanded greatly in the magnitude of wells studied, and therefore has departed significantly from some of the goals outlined in the project proposal. These goals are listed below in italics, followed by a statement of the work completed or planned and the principal workers. Copies of core descriptions and other data are to be found in the **Geologic Appendix**. The general conclusions and interpretations derived from the Geological Analysis are included in the Report on the Petroleum geology of West Carney Hunton Field, which follows.

Geological analysis will consist of the following elements:

- Detailed sedimentological and lithologic description of core, including thin section description. Fourteen (14) cores have been described, including lithology, sedimentology, facies and pore type characterization, with separate descriptions of fracture, karst, and stylolite features. 140 thin sections were prepared and partly described. Thirteen (13) cores remain to be described, including several that contain markedly different facies from those already described. All of the thin sections need re-study and complete descriptions. (Derby and Ramakrishna)
- Identify secondary porosity types to calibrate borehole imaging to a well-studied core. Porosity types, most of which are secondary, are identified both in the general description, and in a foot-by-foot description linked to the core-lab analysis. Borehole imaging has not been performed to date. Much of the needed thin-section work is to quantify the various porosity types. (Derby)
- Core-lab analysis of core and determination of “cementation factor” for log analysis. Core-lab analysis by Stim-Lab of every foot of every core cut by Marjo. Derby and Keefer selected 10 samples that were analyzed by Stim-Lab to determine cementation factor “m”.
- Selection of samples for micropaleontology, primarily conodont studies. 85 samples from 8 wells have been studied for conodonts by Dr. James Barrick of Texas Tech. An additional 20 samples await processing. All wells will be analyzed to verify stratigraphic correlations. (Derby and Podpechan)
- Plot biostratigraphic age determinations (conodont zones) to the stratigraphic section derived from the core and log correlations, compare to known worldwide Silurian Sea-level curve to identify probable position of sequence boundaries. As each well is analyzed the data is plotted and interpreted. Three sequences have been identified, subdivided into Lower

Cochrane, Upper Cochrane, and Clarita formational sequences. (Derby and Barrick)

- Stratigraphic correlation at the finest possible scale, interconnected across the area. Well-log cross-sections have been constructed, showing the relations of the identified formations. (Podpechan)
- Preliminary division into stratigraphic units, at individual sequence level, if possible. Ongoing, see above. (Podpechan and Derby)
- Identify sequence boundaries and major unconformities within the Hunton to project intervals of karsting. At least three periods of subaerial exposure and Karsting have been identified: post Lower Cochrane, post Upper Cochrane, and post Clarita. (Derby and Podpechan)
- Project sedimentary facies derived from core description and log correlations across the area, select wells for additional sample analysis to verify projections. This is an on-going part of the project; see the discussion of sedimentary environments in the narrative below. A sedimentary facies code is assigned to each foot of each core, so that sedimentary facies can be quantitatively analyzed (See **Section 7.1.9 - Explanation of Coding of Porosity and Facies Type**). (Derby, Podpechan, and Ramakrishna)
- Capillary pressure analysis of selected core intervals, with coordinated thin-section and Scanning Electron Microscope imaging to define porosity systems. Capillary pressure analysis has been performed on three samples at the University of Houston. Five samples have been studied by SEM. Further microscopic analysis is deferred to Budget Period II. We will attempt to characterize all significant reservoir systems.
- Pore space classification for reservoir characterization and quantify porosity systems from micropores to macropores, e.g., from submicron to millimeter sized. Dominant pore types have been macroscopically identified for each foot of core. Thin sections were examined to determine

pore types at control points. (See **Section 7.1.14 - Thin Section Samples of Individual Wells.**) All 140 thin sections and additional new ones will be re-studied in detail to gain understanding of porosity types. Scanning Electron Microscopy (SEM) will be coordinated with additional thin section work to better characterize micropore systems.

- Computerized analysis and lithologic interpretation of logs. Conventional lithologic interpretation of gamma ray, neutron-density, and resistivity logs has been performed. All team members.
- Innovative log analysis techniques to predict porosity and permeability types from well logs alone, or combined with borehole data. Lack of sonic logs prevents the innovative log techniques originally proposed. Sonic logs are generally not available on wells in this area. The engineering team is performing studies to improve interpretations of existing logs.

4.2.2. Introduction

The West Carney Hunton Field (WCHF) is located in Logan and Lincoln Counties in North Central Oklahoma in T. 14-16 N., R. 1-3 E (**Figure 4-1**). The field is in an area generally described as the Central Oklahoma Platform or Eastern Oklahoma Shelf; a structural element bounded by the Nemaha Range immediately to the west, the Ozark Uplift on the east and northeast, the Hunton-Pauls Valley Uplift on the south, and the Arbuckle Uplift and Arkoma Basin on the south and east (**Figure 4-2**). This location was on the northeast flank of the Oklahoma Basin (**Figure 4-3**) during deposition of the Hunton, but was separated from the deeper part of the Basin by the Uplift of the Nemaha Range during Pennsylvanian time.

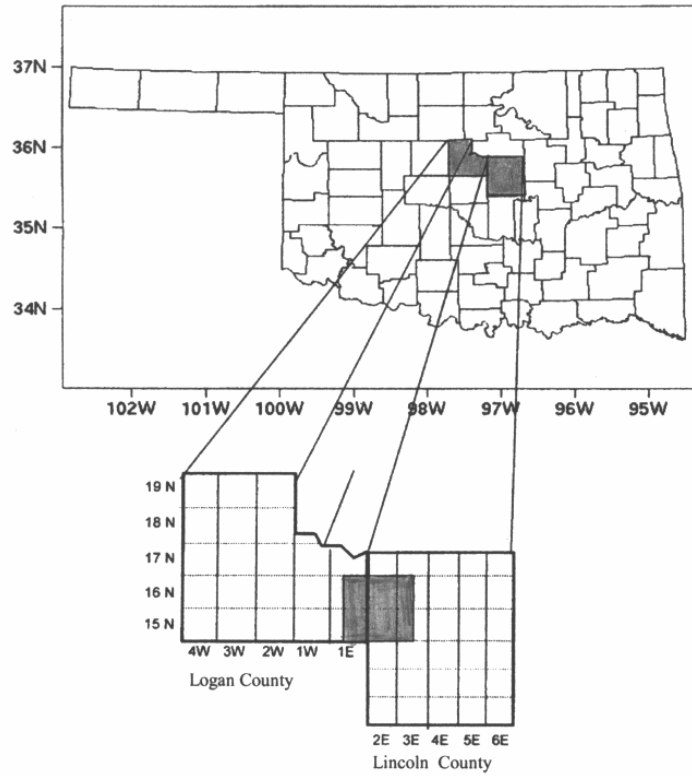


Figure 4-1: The West Hunton Field is located in T. 15-16 N., R. 1-3 E. in Logan and Lincoln Counties

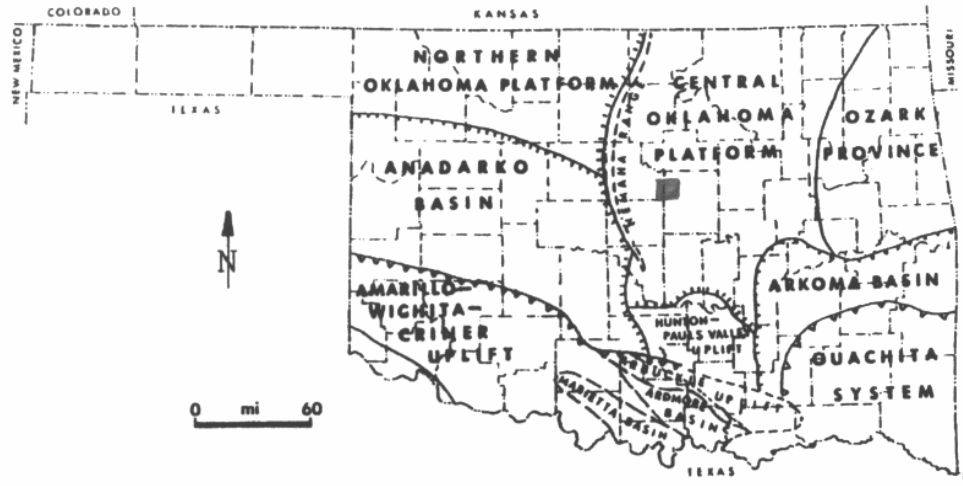


Figure 4-2: Structural framework of Oklahoma (after Fritz, 1978¹)

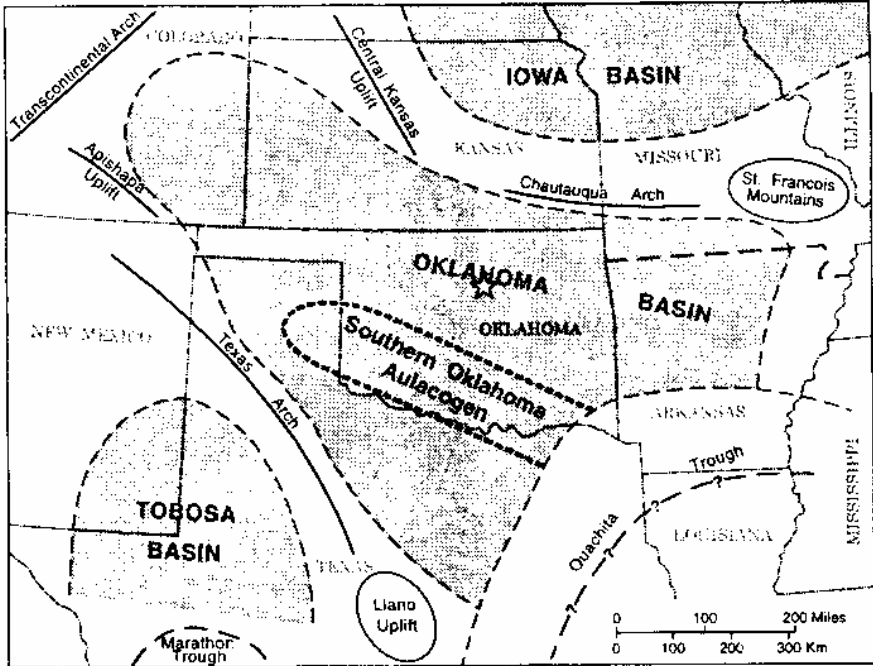


Figure 4-3: Map showing outline of Oklahoma Basin and other major features that existed in early Paleozoic time (after Johnson, 1988²)

West Carney field produces oil and gas from the Hunton Group, which is a major target for petroleum exploration in the southern Midcontinent. The Hunton Group is located stratigraphically between the subjacent Sylvan Shale and the superjacent Woodford Shale. The West Carney Hunton Field is located about 6 miles southwest of the updip or northeast pinchout of the Hunton beneath the Woodford Formation as shown on the Pre-Woodford map of Oklahoma (**Figure 4-4**). Although this map (after Jordan, 1965³), shows a large area of Hunton Group subcrop, it only crops out in eastern Oklahoma, on the flanks of the Ozark Uplift and in southern Oklahoma, in the Arbuckle Mountain Complex. Because of its limited exposure and its distance from the study area, understanding of the Hunton Group in north-central Oklahoma must be obtained through core data and wireline logs. This study has exceptional control in terms of wireline log data and core data.

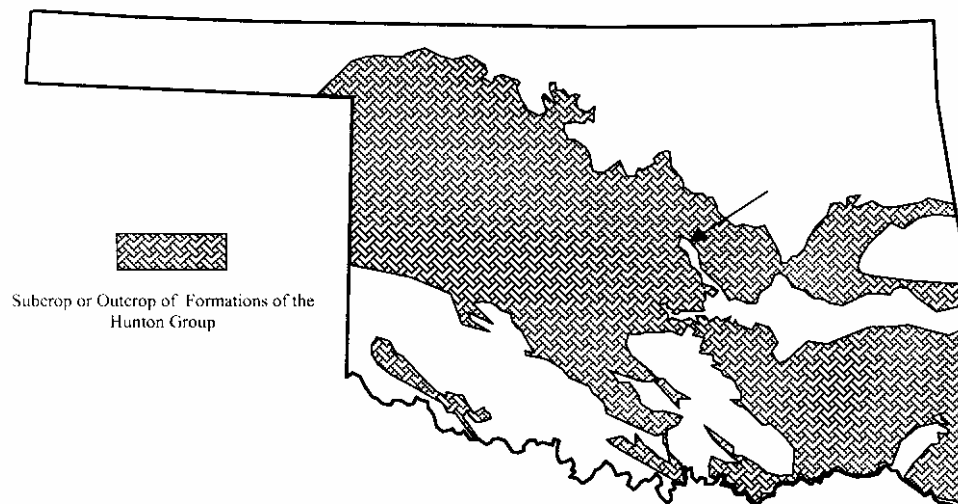


Figure 4-4: Surface and Subsurface distribution of Pre-Woodford rocks in Oklahoma (after Jordan, 1965³). The patterned rock represents Formations of the Hunton Group. Note the NW-trending narrow “outlet” of zero Hunton in central Ok., which is a complex structural uplift and pre-Woodford erosional feature, the Seminole Uplift

The West Carney Hunton Field has been aggressively developed since it began in 1996, when Altex Resources placed the Decker # 1 (NE, 1-15N-2E) on a large beam pump and soon realized that large quantities of oil and gas could be produced by moving large amounts of water. Four companies operate a majority of the wells in the field: Altex Resources, New Dominion, Craig Elder, and Marjo Operating Company. The field, which covers nearly 30,000 acres, currently has more than 230 producing wells and 16 saltwater disposal wells. The field produces an average of 6000 barrels of oil, 55,000 MCF gas, and 86,000 barrels of water daily.

This study and the high level of interest concerning it, was prompted at least in part, by the unique characteristics in association to how the field produces commercial quantities of oil and gas. When initially completed, wells in the field produce large amounts of water with a relatively low oil and gas cut. As the water within the reservoir is pumped, the gas volume slowly begins to increase, followed by an increase in oil cut (**Figure 4-5**). Somewhere within a few days to a few months, depending on several factors, the well becomes profitable.

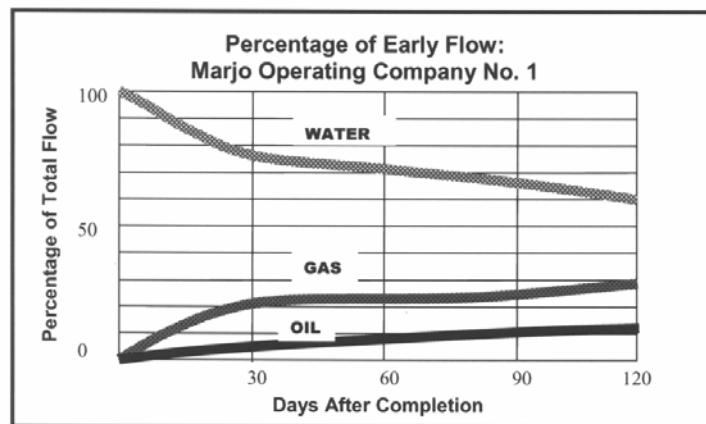


Figure 4-5: Production data from the first 120 days of the Marjo Operating Co. No. 1 Schwake demonstrates the unique characteristics of early well performance

This portion of the project deals with building a geological understanding of the Hunton group in the West Carney Hunton Field, especially in relation to optimizing reservoir performance and exploitation of the Hunton reservoir. When faced with large initial water rates associated with producing from this type reservoir, most oil and gas companies would cease operation before significant oil and gas production is realized, resulting in a field of this nature being easily bypassed. Alternatively, it is important to identify and define the unique characteristics of this type of reservoir in order to avoid the economic disaster caused by operators completing and pumping every new well in the mistaken hope that commercial production will result, when in fact, the reservoir is “wet” in the conventional sense and producible oil is not present. Understanding the geology behind the reservoir within the West Carney Hunton Field, may help in the early assessment of other similar type reservoirs elsewhere.

4.2.3. Stratigraphy

The complete stratigraphic section in the West Carney area is shown in **Table 4-2**. Units both above and below the Hunton Group are expressed in terms of general lithology, age, and thickness. Permian strata of the Garber and Wellington Formations and the underlying Chase Group crop out at the surface within the area. Depth to the Hunton Group in the field averages about 5000 feet.

Numerous formations in the Pennsylvanian produce oil in the area. The Ordovician Bromide sand (“Second Wilcox” of drillers nomenclature) also is a major petroleum producer in the area and the target of most wells that fully penetrate the Hunton strata. Although the Arbuckle Dolomite does not produce oil and gas in the area, it is an excellent zone for the disposal of salt water.

The interval of specific interest in the West Carney Hunton Field is as follows:

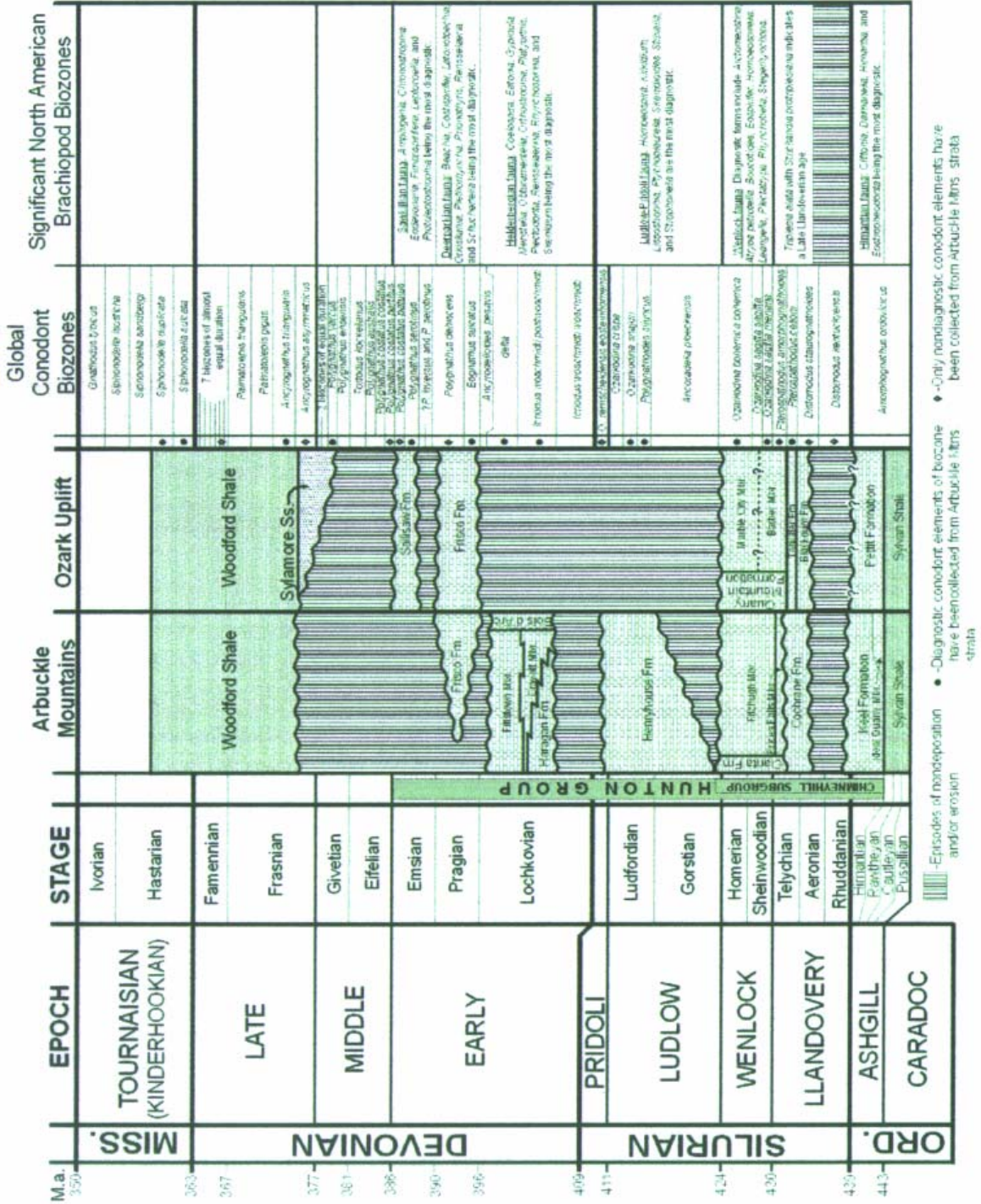
- Woodford Formation- a black shale and rich hydrocarbon source-rock. The Woodford is reported to be the source of 70% of the oil produced in Oklahoma (Comer and Hinch, 1987⁴).
- Hunton Group- a shallow shelf carbonate of Latest Ordovician through Middle Devonian age. Detailed subdivisions of the Hunton Group are shown in **Table 4-3**. Only the Early Silurian portion has been found in the West Carney Hunton Field.
- Sylvan formation- a gray-green marine shale, commonly containing graptolites, suggesting that it was deposited in relatively deep water.

Table 4-2: Age, lithology, and thickness of units above and below the Hunton Group in the West Carney Area

AGE	FM. Or GROUP	LITHOLOGY	THICKNESS
Permian	Sumner-Admire Groups	Mixed: dom. Shale	Combined = 4800 Feet
Pennsylvanian	Complete sequence	Sh, Ss, Ls	
M. & Lt. Miss.	<i>(Largely missing-Major Unconformity)</i>		
E. & Mid. Miss.	Osage & Meramec Fms.	Limestone	0-100 Feet
Lt. Dev.-E. Miss.	Woodford Fm	Shale, black, source rock	30-100 Feet
E. & M. Devonian	<i>(Missing- Major Unconformity)</i>		
Lt. Ord, Silurian	Hunton Group	Ls, Dolomite	0-140 Feet, avg. 60
Lt. Ordovician	Sylvan Shale	Marine shale	100 Feet
	Viola Group	Dol. & Ss	150-250 Feet
Mid. Ordovician	Simpson Group	Bromide	Ss ("2 nd Wilcox")
		McLish	Ss, Sh, Ls
	<i>(Major Unconformity)</i>		
Lt. Camb-E. Ord.	Arbuckle Group	Dolomite	1500 Feet
	<i>(Major Unconformity)</i>		
Pre-Cambrian	Basement Rocks		

The latest and best litho- and time-stratigraphic diagram of the Hunton Group in Oklahoma is shown in **Table 4-3**. This diagram, prepared by Stanley (2001)⁵ and first published in Oklahoma Geological Survey Guidebook 33 shows the biostratigraphic correlation of global Conodont Biozones and North American Brachiopod biozones with the fauna found in the rock units of the Hunton Group in Oklahoma. The Hunton Group ranges in age from Late Ordovician (Hirnation Stage, Ashgill Epoch) about 440 mya through Middle Devonian 377 mya; a time span of more than 63 million years. The Hunton Group in Oklahoma is generally in conformable contact with the subjacent Sylvan shale, and in unconformable contact with the Woodford Shale above.

Table 4-3: Biostratigraphic correlations of the Hunton Group (reproduced from Stanley, 2001⁵)



As determined from Conodont work, the entire West Carney field is composed of the Cochrane and Clarita Formations of the Chimney Hill subgroup; a suite of rock which only represents a ten million year time span. As of now, there is no evidence of the basal unit, the Keel Formation, nor is there evidence for the presence of the Henryhouse, Bois d'Arc, or Frisco Formations above. Therefore, within the West Carney field, the Hunton Group has an unconformable relationship with both the underlying Sylvan Shale, and the overlying Woodford Shale. The missing rock above the Clarita and/or Cochrane Formations in the field, accounts for approximately 47 million years of rock that was either never deposited or deposited, then eroded away. Therefore, only about 16 percent of "Hunton time" is represented in the rocks in the Carney area

4.2.4. Structural Setting

The West Carney Hunton Field lies along the northern flanks of the Paleozoic Oklahoma Basin (**Figure 4-3**). The strata deposited in most parts of the Oklahoma Basin are widespread and laterally persistent, indicating the relative tectonic and orogenic stability of the region during the early Paleozoic. The Hunton Group was deposited in a broad, shallow epicontinental sea. From Late Cambrian through Devonian the area of the present day West Carney Hunton Field had a gentle depositional slope southwestward into the more rapidly subsiding part of the basin, the Southern Oklahoma Aulocogen. This southwest dip was enhanced by Late Devonian (pre-Woodford) time with the uplift of the broad Chautauqua Arch (**Figure 4-3**). Following deposition of the Mississippian carbonates, the development of the Nemaha Uplift tilted the West Carney Hunton Field area eastward, causing the truncation of the Mississippian, Woodford, and Hunton. The regional outcrop pattern of the Hunton through Mississippian strata on the Pre-Pennsylvanian Subcrop Map (Jordan, 1962⁶) clearly suggests an

eastward dip; an east-west transect in Township 14 N. from R. 1 E. to R. 4 E., shows a pattern of successively younger strata southeastward. The eastward tilting apparently continued throughout the remainder of Paleozoic, as evidenced by the east-southeast thickening of the Pennsylvanian sequence (cf. Levorsen, 1967, p. 543⁷), locally about 10 feet per mile. The area was subsequently tilted southwestward during the Mesozoic (probably Jurassic) with a resultant modern structural dip of about 45 feet per mile southwestward.

This simple structural scenario is complicated by paleotectonic movements and selective erosion both prior to and following Hunton deposition in the Carney area. A regional thin in the Viola under the West Carney Hunton Field suggests that Hunton deposition may have been affected by a slight paleotopographic high. Possibly the absence of Keel in the field is due to non-deposition, or deposition and subsequent erosion over this “high.” Post-depositional structural movements in the area are evidenced by the fault cutting the field, which did not affect Hunton thicknesses, but did control the thickness of the Mississippian (compare **Figure 4-6** and **Figure 4-7**). This shows the fault to be post Hunton, probably pre-Mississippian. However, post-Hunton – pre-Woodford movements in the area are evidenced by erosion of the Hunton along the Seminole Uplift (**Figure 4-4**) and local areas of “zero Hunton” both southeast and northeast of West Carney Hunton Field as shown by Amsden (1975, pl. 9⁸) on his pre-Woodford map. At this point in the study, we have no clear-cut evidence of tectonic activity affecting deposition or early erosional history.

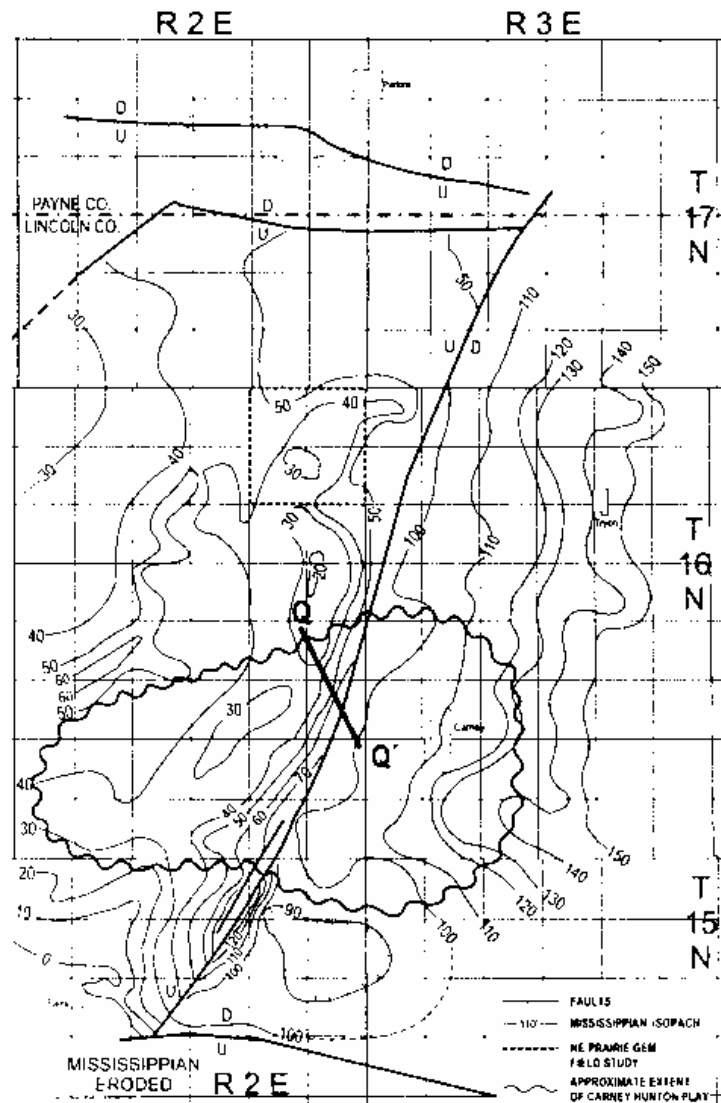


Figure 4-6: Isopach map of Mississippian strata in northwestern Lincoln County, Oklahoma. Contour interval is 10 ft. Hachures represent isopach “thins”. The abrupt thickening of Mississippian strata in the south central portion of the map correlates well with the northeast-southwest trending fault. (Reproduced from Rottmann, 2000²)

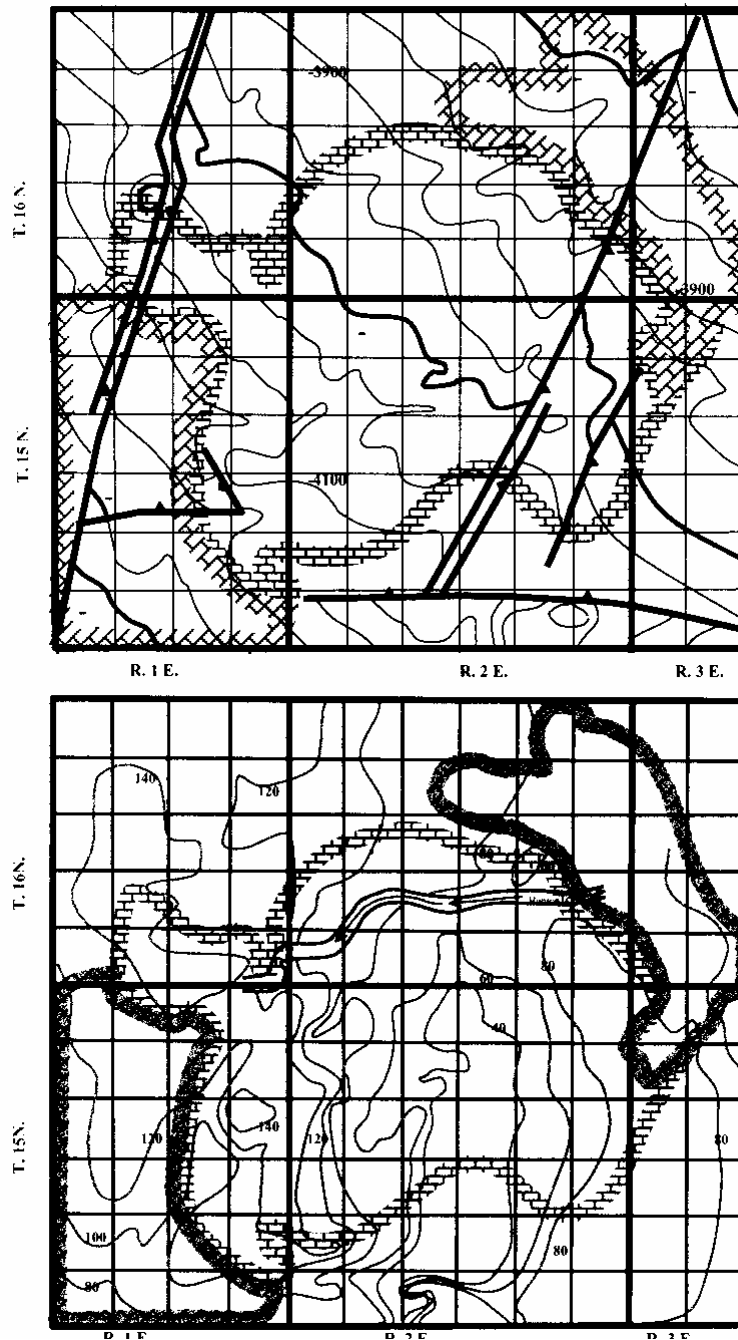


Figure 4-7: a) Structure map of the base of the Hunton Group in the West Carney Hunton Field. Contour interval is 50 ft.

b) Thickness isopach map of the Hunton Group in West Carney Hunton Field. Contour interval is 20 ft.

4.2.5. Depositional History

The rock units of the Hunton Group in the West Carney Hunton Field, and in all of Oklahoma, suggest a depositional history of episodic cycles of deposition and erosion (**Figure 4-3**, **Figure 4-8**), that is clearly related to world-wide sea-level, oceanic, and climatic events (Barrick, 2001¹⁰; Jeppsson, 1998¹¹). The lower portion of the Hunton Group in Oklahoma is composed of the Chimney Hill Subgroup, which includes in ascending order, the Keel Formation, Cochrane Formation, and Clarita Formation (**Table 4-3**). The Keel Formation, or lowermost unit, is late Ordovician (Ashgill Epoch) to early Silurian (Llandovery Epoch) in age, but appears to be absent in the West Carney Hunton Field. The Keel generally consists of oolitic Limestone indicating a shallow, high-energy carbonate depositional environment.

At present, neither have oolitic limestone facies been found, nor have paleontology studies found representative “Keel-aged” fauna from the available core data. Apparently the Keel Formation was deposited in the West Carney Hunton Field and later eroded away, or it simply was never deposited. Therefore, the relationship between the top of the Sylvan Shale, and the base of the Cochrane Formation in the Carney area is unconformable and the “normal” basal sequence of the Hunton Group is missing in the West Carney Hunton Field.

The basal portion of the Hunton Group in the West Carney Hunton Field is the Cochrane Formation, consisting of a variety of fossiliferous open marine limestone facies. Conodont data, in combination with the relative stratigraphic position of the rock units indicate that a widespread Lower Cochrane unit is unconformably overlain locally by an Upper Cochrane unit. The Cochrane

Formation within the West Carney Hunton field is composed of a central fossiliferous limestone macrofacies, flanked by a nonporous mudstone facies (Figure 4-8 and Figure 4-9); however, the age of the flanking mudstone facies has not yet been confirmed by paleontology or detailed core studies.

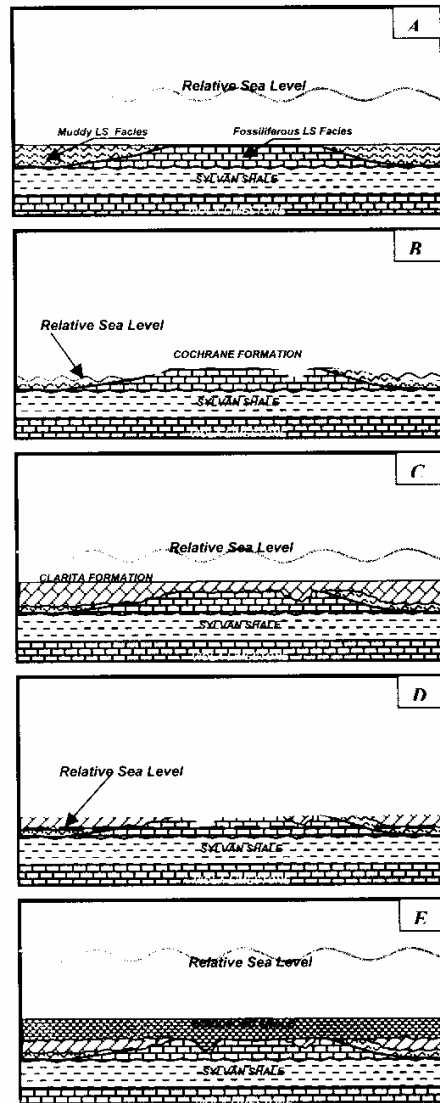


Figure 4-8: A brief interpretation of the depositional history of the West Carney Hunton Field. The figures represent a profile from west to east across the field.

A) The Cochrane Formation is deposited directly on top of the Sylvan Shale. A fossiliferous limestone macrofacies is deposited within the central portions of

the field, and a nonporous carbonate mudstone facies is deposited on its flanks. An unconformity exists within the Cochrane formation, but is not shown here.

B) Fall in relative sea level results in subsequent erosion of Cochrane rocks. The central portion of the field was more resistive to erosion than were the flanks of the field.

C) Relative sea level rises, resulting in the deposition of the Clarita Formation, primarily a dolomite facies.

D) A fall in relative sea level leaves an erosional unconformity at the top of the Clarita Formation on the flanks of the field, and on the Cochrane Formation in the central portion of the field. The unconformity represents approximately 43 million years of rock that was either not deposited or deposited, then eroded away.

E) Relative sea level rises, depositing the Woodford Shale.

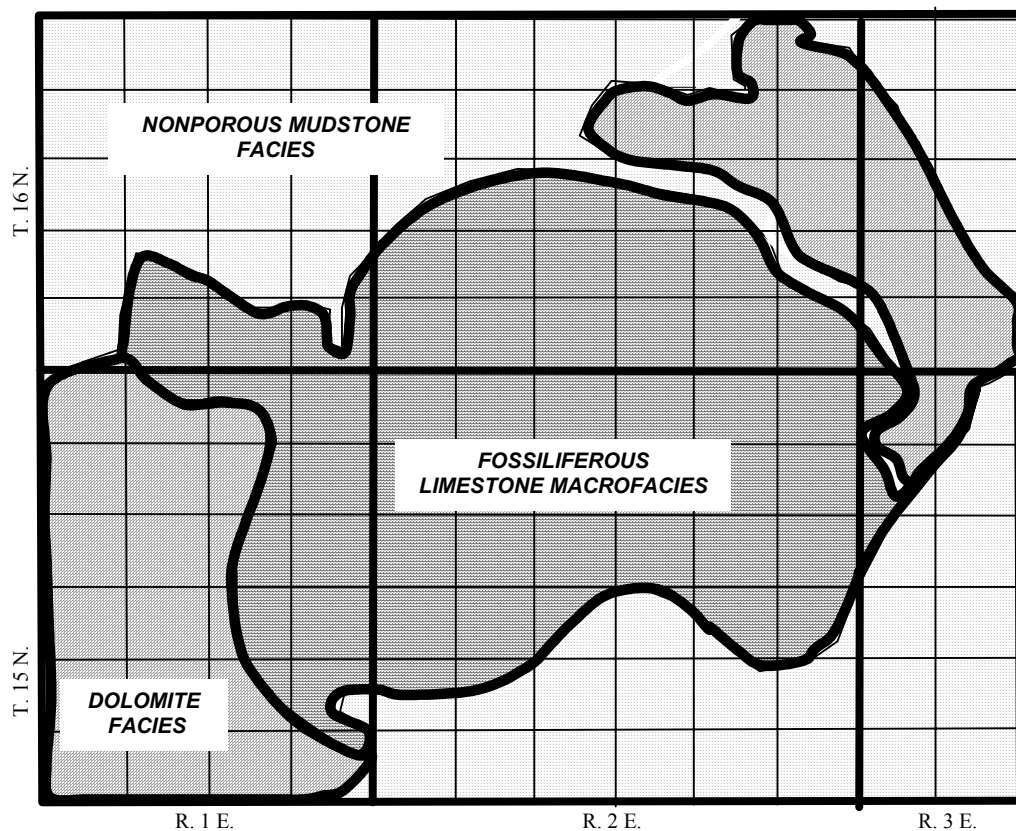


Figure 4-9: Map view of generalized facies combinations in the West Carney Hunton Field

The deposition of the upper Cochrane Formation was followed by a fall in relative sea level. As sea level dropped the Cochrane was eroded differentially; the fossiliferous limestone macrofacies within the center portion of the field (**Figure 4-9**), was more resistive to erosion than the nonporous mudstone facies on the flanks of the field. This differential erosion resulted in a topographic high composed of the fossiliferous Cochrane limestone (**Figure 4-8B**).

When relative sea level began to rise again, the Clarita Formation was deposited across the area (**Figure 4-8C**). Relatively thick sequences of Clarita, generally a shoal- water dolomite or dolomitized limestone are found on the east and west sides of the field, where the Clarita was deposited in the post-Cochrane paleotopographically lower areas.

The deposition of the Clarita Formation is the last unit of the Hunton Group recorded in the strata of the West Carney Hunton Field. The absence of the overlying Hunton Formations represents approximately 47 million years of time that is gone from the rock record (**Figure 4-8D**, **Table 4-3**). The depositional history of the Carney area between the Clarita Formation and the deposition of the Woodford Shale is purely speculative. Hunton regional geology suggests that at least the Henryhouse Formation, if not the Haragan-Bois d'Arc, and the widespread but rarely preserved Frisco Formation, were deposited across the field (see Amsden, 1980, Text-fig. 23⁸). As explained by numerous authors, each of these formations is unconformity-bounded, and some contain many sequences that are also unconformity bounded. Consequently multiple episodes of deposition and erosion followed the deposition of the Clarita Formation, the final episode being a sea level low stand and a long period of erosion and subaerial exposure during the 10 million years between the deposition of the Frisco and

onset of Misenor/Woodford deposition. Extensive karst development, including multiple generations of cross-cutting karst dissolution and sedimentation, is evident in nearly every core of the field. Karst effects are visible to the bottom of the Hunton in numerous cores, attesting to complete emergence during sea level lowstands.

After the final episode of erosion and subaerial exposure, relative sea level increased again, resulting in the deposition of the Woodford Shale across the region. In the West Carney Hunton Field, the Woodford was deposited evenly through most of the field, but is exceptionally thick where the underlying Cochrane Formation (where Clarita is absent) has been incised by erosion (**Figure 4-8E**).

4.2.6. Migration History

The Woodford Shale is considered to be the primary source rock for oil and gas accumulations within the Hunton reservoir, with perhaps minor amounts of hydrocarbons derived from the Sylvan Shale. Numerous studies have shown that approximately 5000 feet of burial is required to bring sedimentary organic matter to the state of thermal maturity to begin oil generation. The Woodford Shale most certainly achieved this depth of burial in the West Carney Hunton Field by the end of Permian time. In fact, the depth was likely greater, as an unknown amount of Permian and Mesozoic strata have been eroded from the region. The Woodford in the area has reached the Early Oil Generation stage as indicated by vitrinite reflectance (Comer, 1992, fig 13¹²; reproduced as **Figure 4-10**). Higher thermal maturity values are present eastward, reflecting the eastward thickening of post-Woodford strata.

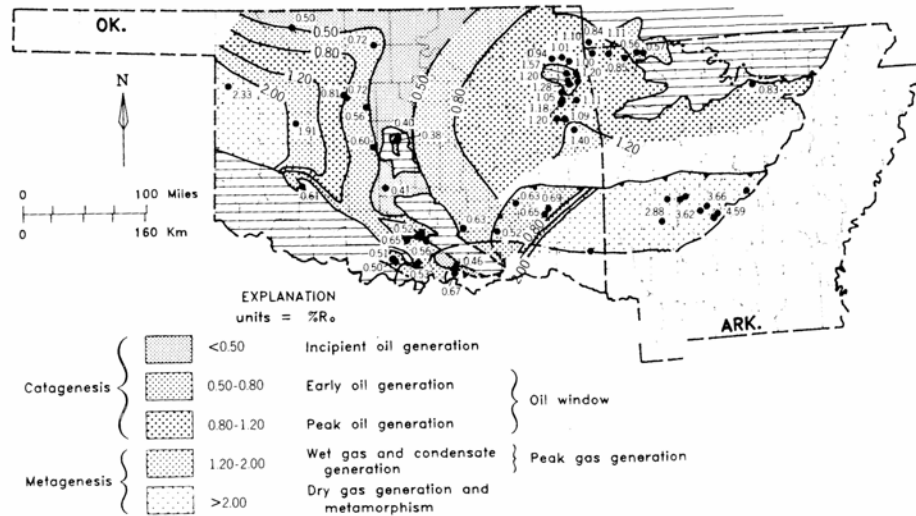


Figure 4-10: Map of Vitrinite reflectance (reproduced from Comer, 1992, Figure 13¹²)

Oil generated to the east would have migrated updip to the west, possibly filling reservoirs in the West Carney Hunton Field area by mid-Mesozoic time. The subsequent southwest tilting would have altered the reservoir configuration, possibly partially breaching the seal of the reservoir, allowing water to invade a previously oil-filled reservoir, leading to the complex conditions observed today.

4.2.7. Production

The Hunton Group in the West Carney Hunton Field produces oil and gas from the Chimney Hill Subgroup. The reservoir ranges from 24 to 146 feet thick throughout the area. A gentle homoclinal dip of approximately 40 feet per mile to the southwest and little to no structural closings (**Figure 4-7a**), suggest a

stratigraphic mechanism of entrapment. The producing portion of the field is currently believed to be approximately 30 thousand acres.

The field now hosts around 230 producing wells and 16 saltwater disposal wells. All saltwater disposal wells are open-hole completed in the nearly 2000 feet of Arbuckle dolomite. Approximately 50 (22%) wells are located in the portions of the field composed primarily of dolomite facies, while approximately 180 (78%) wells produce from the limestone macrofacies (**Figure 4-9**). As of now, 8 horizontal wells have been drilled and completed in the West Carney Hunton Field. Relative success of horizontal wells compared with “straight-hole” (vertical) wells has yet to be determined; however, early indications are encouraging.

The field currently produces 6000 barrels of oil per day, 55,000 MCF gas per day, and 86,000 barrels of water per day. An average well will produce 26 barrels of oil per day, 239 MCF gas per day, and 374 barrels of water per day. An exceptional well produces in excess of 100 barrels of oil per day, .5 to 1 million cubic feet of gas per day, and in excess of 1500 barrels of water per day. The average reserves per well is expected to be near 50,000 barrels oil, and 350,000 MCF gas. Volumetric calculations from wireline logs indicate that roughly 5% of the oil in place is being recovered. One of the goals of this study is to optimize reservoir performance, and increase the percentage of recoverable hydrocarbons.

As mentioned in the introduction, the West Carney Hunton Field is being studied at least in part, because of its unique production characteristics. The heterogeneous nature of the field prohibits the use of the term “typical” in reference to any single well; however, wells generally perform in this manner: 1. Wells produce large initial water rate with low oil and gas cut. 2. The rate of gas

production increases within a few days. 3. Finally, the rate of oil production increases (**Figure 4-5**).

The heterogeneity of the field may contribute to this behavior. The Hunton Group reservoir rock within the West Carney Hunton Field is believed to have a dual permeability system: a higher permeability component consisting of vugs and solution enhanced fractures, and a lower permeability component consisting of microporosity and intercrystalline porosity. At this time it is believed that fluids move readily through the higher permeability component but that more hydrocarbons are stored in the lower permeability component. As a result, wells when initially completed produce large quantities of water with a relatively low oil and gas cut indicating that the higher permeability component of the dual porosity system is being “flushed.” Eventually enough of the fluid contained in the higher permeability component is removed, thus creating a pressure differential between the low and high components of the dual permeability system. As a pressure differential develops, fluid contained within the microporosity of the low permeability system mobilizes, and moves from an area of high pressure to an area of low pressure, thus it “bleeds” into the high permeability component of the system. When the fluid reaches the higher permeability component, it becomes recoverable. Gas, having a lower viscosity is more readily moved than oil; therefore, the production of gas increases prior to the production of oil.

As the gas and oil cut slowly increases, the well becomes commercial, and hopefully profitable. Moving and disposing of such large amounts of water is a costly endeavor. The drilling of saltwater disposal wells is a must in the area, at a cost between \$450,000 and \$600,000; an upfront cost needed before substantial production can begin. A producing well costs between \$400,000 and \$500,000 and costs an additional \$2,000 to \$6,000 each month to operate. On average the

return on investment is between 2:1 and 3:1, depending significantly on oil and gas prices.

4.2.8. Core Description, Methodology, and Interpretation

Early in the project, the operating company, Marjo, determined that coring every well gave the best data for their purposes. To date, 27 wells have been cored. **Figure 4-11** is a map of cored wells. Marjo's policy is to run two 60-foot core barrels and take whatever core can be recovered in those two runs. Cores are listed in **Table 4-4** (all wells cored to date), which shows that core recovery of Hunton rocks ranges from 9 feet to 117.5 feet. Every core is taken directly to Stim-Lab of Duncan, Ok., where the following is performed:

- Whole core plain light photography
- Whole core ultraviolet light photography, showing fluorescent oil-saturated intervals
- Whole core porosity/permeability/ grain density analysis at one foot intervals
- Cut and separately box a thin slab
- Plain light photography of the slabbed core.

These data and the well log data, typically gamma-ray, neutron-density, and resistivity logs, are made available to the geologist. Prior to description of the core we prepare a core/log comparison sheet (see core/log displays of each well in **Section 7.1.8**), in which we adjust the core data to the log so that the core-derived porosity, permeability, and grain density values can be compared after accurate depth adjustment. This depth adjustment is critical to the log analysis and engineering studies that follow.

During a preliminary study of each core, samples are taken for petrographic thin sections, and for paleontologic (conodont) analysis. Prior to detailed description of a core it is desirable to have at least a preliminary description of each thin section to accurately identify grain types and diagenetic fabrics in each well. These microscopic data are entered on the data sheets, as a guide to accurate macroscopic recognition of pore types, grain types, and facies (See **Section 7.1.9**, Porosity and Facies codes,). During core description, each analyzed interval is assigned a Porosity type code and a Facies code. The core is also described in conventional lithogenetic or sedimentological units, and principal porosity types are identified. Because secondary porosity is so significant in the Hunton reservoir, the pore classification of Lucia (1995)¹³ is utilized and the percentage of Touching Vugs is estimated for each described interval (**Section 7.1.6** Explanation of core descriptive terminology). Finally, the karst features, stylolites, and fractures of each core are described separately.

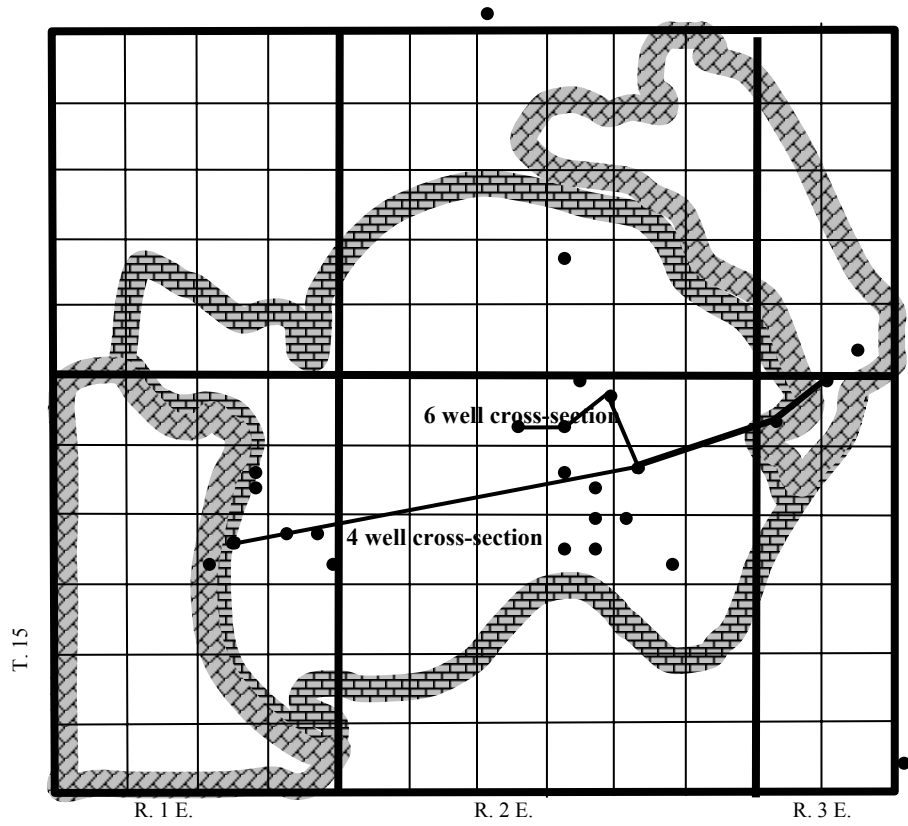


Figure 4-11: Map showing cored wells employed in this study

Table 4-4: List of cored wells and cored intervals currently employed in this study. Also described are the wireline derived log depths for the top and base of the Hunton Group

DOE/TU West Carney Hunton Project															
TABLE OF WELLS CORED: Thickness, Core/Log adjustment, Data															
X = top or base of Hunton not cored;; (footage) = top or base of core; <i>italicized depth</i> is "core depth" of fm top or base picked on logs															
		Hunton Top		Core/log	Hunton Base		Thickness	Status & Data. * = Completed							
		Core	Log	adj.	Core	Log		Wk	TS	PC	SEM	Cono	UH	Wett	Lithology
1	5705 - Mary Marie 1-11	4961	4944	17	5003.5		42.5	C	33	C	4	14*	10	4	Ls/ 2'dol
2	5712 - Wilkerson 1-3	4953.4	4937.5	15.8	4999.8	4984	46.4	C	17*	C	1		8	1	Ls/ 2'dol
3	5733 - Toles 1	4964	X	na	5003.7	X	39.7	C	8*	C					Ls/ 2'dol
4	5818 - Henry 1-3	X (4966)	4958	7.5	X (4996.6)		30.6+	C		C					Ls/5' dol/lis
5	5838 - Danny 2-34	X (4930)	4918	10.8	4984.3		54.3+	C		C			4	1	Ls
6	5874 - Joe Givens 1-15	5017.8	5010	9	5044		26.2	C		C					Ls/ 0.1' dol
7	5887 - Williams 1-3	4943.5	4934	9.5	4983.7	4974	40.2	C		C			8		Ls/ 5' dol
8	5899 - McBride South 1-10	X (4962)	4947	13.3	4996.2	4983	34.3	C	1*	C		1*	4		Ls/dol/lis
9	5913 - Boone 1-4	X (5037)	5028	6.5	5066.5	5060	29.5+	C	6*	C		6*	4	1	Ls/ dol Ls/ 4' dol
10	5934 - Carter 1-14	X (4940)	4927	13.3	4995.8	4983	56.1	C	16	C		18*	4	2	1'dol/ Ls/ 2'dol
11	5943 - Anna 1	4967.1	4947	20.1	5004.7	4985	37.6	C	10	C					Dol
12	5992 Carney Townsite 2-5	X (4906)	4907	1.3	X (4966); 4979.3L	4978	60 cored; 73.3 log	C	8*	C		10	4		Dol/Ls
13	6011 - Bailey 2-6	X(4876)	4875	-2.8	X(4934)	4964	58 cored; 89 log	C	20	C		12			14' Dol/Ls
14	6029 - Kathryn	X(4994)	4990	2.5	5030.5	5028	36.5 core 38 log								Ls/Dol/Ls/Dol
15	Geneva						9 ft cored		1						Ls(Cri pkstn)
16	6051-Carter Ranch	5006	5000	6	5035.1	5030	29.1 cored	C	5	C					
17	6061-Carney Ext SWDW	5042.7	5039.2	3.5	X(5131); =5156 L	5151	88.7 core 112 log	IP	15			10			Ls
18	6088-Cal 1-11	X(5034)	5025	4.2	5135.8	5134	101.8 core 108.5L								
19	6100-Mark Houser 1-11	X(4961)	4940		X(5077.6)	5066	116.6 core 126L								
20	6112-JB 1-13	4971.9	4964.5		X(5058.8)	5120	86.9 core 155.5L								
21	6131-Saunders 1-13	4917.3	4911		X(4940.5)	5053	23.2 core 142L								
22	6143-Points 1-13	4989.5	4978	11.5	X(5107)	5096	117.5 core 118								Ls
23	Mercer 1-28	X(4527)	4526		X(4583)	4606	56 cored 80L	IP							
24	6209-Griffen 1-14	X (5082)	5077	5	X(5142); 5191.5	5186.5	60 cored 109.5L	IP				14			Ls/dol/limy dol
25	Morrow	X(4905)	4886		4956.4	4956	51.9 cored 69L								
26	Chandler SWDW	X(4810)	4797.5		X(4869.8)	4865	59.8 core 68L								
27	Stevenson	X(5143)	5101		X(5167.6)	5186	24.6 core 42.5L								

Wk = Work status (Core description), PC = Porosity Codes. Core description, Pore codes: C = Completed; IP = In Process.
 TS = Thin Sections, # made, * described ; SEM = Scanning Electron Microscopy, Cono = Conodont micropaleontology, # of samples, * completed
 UH = Core Plug samples at Univ. Houston; Wett = Wettability Analysis,
 Numbers in front of Well Name is StimLab well Identification Number

4.2.8.1. Facies

Individual lithofacies are objectively described, as they are encountered, in attempt to characterize the stratigraphy and depositional environments of the Hunton in West Carney Hunton Field. In the fourteen wells described to date,

we have identified 11 distinct lithofacies in the Hunton, (and 3 non-Hunton lithofacies). Preliminary studies of the additional cores suggest that more lithofacies will be identified. In most cases, the original depositional lithofacies can be identified regardless of the degree of dolomitization. All facies can be recognized in limestone, partially dolomitized limestone, and dolomite, so long as the allochems are recognizable. Facies #2 is the descriptor for completely recrystallized or totally crystalline of primary origin rock in which no pre-cursor sediment is recognizable. The specific rock type is described in the pore code, which distinguishes between limestone, partially dolomitized limestone, and dolomite.

Table 4-5: Numeric codes for 14 identified Lithofacies

1. Argillaceous Dolomite (Greenish-gray, resembles Sylvan Fm)
2. Crystalline Dolomite (No fossils or allochems identifiable)
3. Small Brachiopod Grainstone/Packstone/Wackestone
4. Fine Crinoid Grainstone/Packstone/Wackestone
5. Coarse Crinoid Grainstone/Packstone
6. Mixed Crinoid-Brachiopod Grainstone/Packstone/Wackestone
7. Big Pentamerid Brachiopod Coquina
8. Coral and Diverse Fauna
9. Coral and Crinoid Grainstone-Wackestone
10. Sparse Fossil Wackestone
11. Mudstone, carbonate
12. Fine- Medium Grainstone
13. Shale (Woodford, Sylvan)
14. Fine Sandstone (Misener SS)

4.2.8.2. Paleontology, Stratigraphic Correlation, and Facies Interpretation

Initial attempts at stratigraphic correlation of lithofacies yielded unsatisfactory results because of what appeared to be too abrupt lateral changes in facies. The addition of paleontological data allowed us to recognize that the West Carney Hunton Field stratigraphy consists of three separate sequences, with major topographic relief at the unconformities. Cross-section (**Figure 4-12**) shows four wells distributed from west to east, showing how over 100 feet of Lower Cochrane has been deeply eroded, is overlain by an Upper Cochrane sequence, which is in turn deeply eroded and overlain by a Lower Clarita sequence.

Figure 4-13 shows the conodont zonation for the late Ordovician and Silurian, divided into 7 “zones”. **Table 4-6** shows the distribution of conodont faunas in the 8 wells analyzed to date. Data for these conclusions and the interpretations of the conodont specialist, Dr. James Barrick of Texas Tech, is given in **Section 7.1.12**.

Lithofacies relations between wells, as shown in **Figure 4-14** (6-well section) are amenable to interpretation as Silurian Benthic Assemblages on an open marine shelf, as shown by Markes Johnson, et al (1997¹⁴, reproduced here as **Figure 4-15**) and easily given depth and fossil assemblage equivalence as shown in **Table 4-8** (from Johnson, 1987¹⁵). The big pentamerid brachiopod (facies 7) assemblage is diagnostic for Benthic Assemblage 3, which indicates water depths of 30 to 60 meters in an outer or lower part of the shallow shelf. This facies is locally more than 60 feet thick, and occasionally makes a spectacular reservoir rock with huge vugs between the large brachiopod shells; alternatively these vugs may be filled with karst infill and tightly

cemented, resulting in a poor reservoir. The coral, stromatoporoid, and crinoid dominated facies (4,5,6,8,9) suggests a B.A. 2 or mid shallow shelf position, in water depths of 10 to 30 meters. Therefore, almost all of the Cochrane units described can be interpreted as lower to middle shallow shelf depositional environments. This lithofacies and macrofossil environmental interpretation is supported by the microfossil (conodont) data (see **Section 7.1.12**). In contrast to the “layer-cake” stratigraphy characteristic of peritidal settings, the lateral relationships of facies, shown in Figure 4-14 demonstrate the heterogeneity common in some open shelf environments. Large brachiopod shell mound accumulations grade laterally, in some cases in less than one mile, to crinoidal grainstones or to coral or stromatoporoid-dominated wackestones.

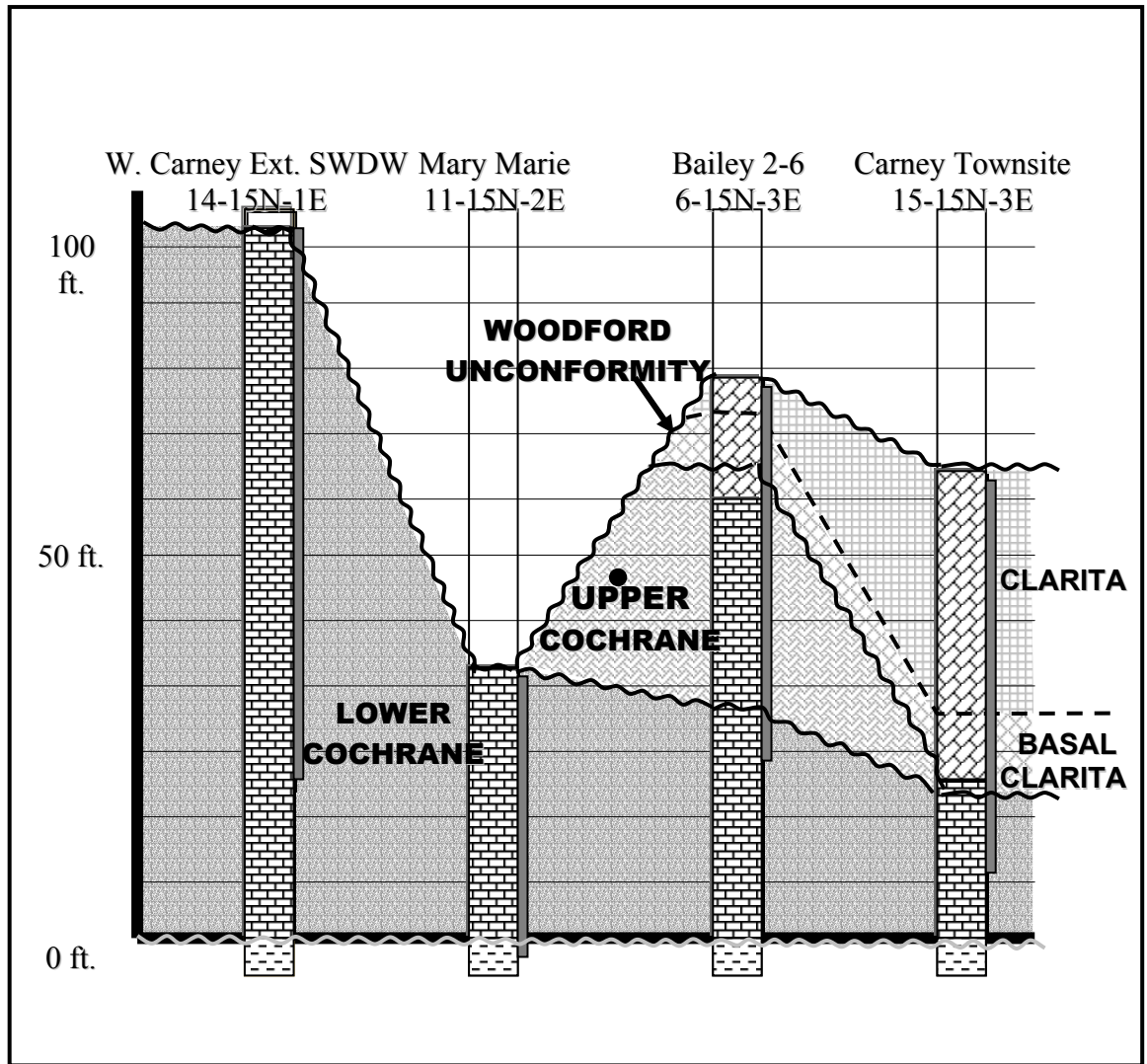


Figure 4-12: Four well cross-section showing unconformities, Formations, and lithology across the West Carney Hunton Field. The cross-section is constructed from west to east, its locality referenced in Figure 4-11.















	SERIES	STAGES	CONODONTS	"Zone"	Formation			
SILURIAN	PRIDOLI		<i>O. eastonhorvathi</i> - <i>O. s. ditoria</i>					
			<i>O. remscheldensis</i> Interval zone					
		LUDLOW		<i>O. crassa</i>				
				<i>O. snajdri</i> Interval zone				
				<i>P. siluricus</i>				
			<i>A. ploeckensis</i>					
			<i>K. "variabilis"</i>					
	WENLOCK	HOMERIAN		<i>O. bohemica</i>	5	Clarita		
				<i>O. sagitta sagitta</i>				
		SHEINWOODIAN		<i>K. ortus ortus</i>				
				<i>K. walliseri</i>				
				<i>O. rhenana</i>				
				<i>K. ranulliformis</i> Superzone				
				<i>P. p. procerus</i> Superzone				
				<i>Ps. bicornis</i> Superzone				
		TELYCHIAN		<i>P. a. amorphognathoides</i>			5a	Basal Clarita
				<i>P. celloni</i>			4	Upper Cochrane
			<i>P. seopennatus</i>					
	LLANDOVERY		AERONIAN		3	Lower Cochrane		
				<i>D. staurognathoides</i>				
RHUDDANIAN		<i>D. kentuckyensis</i>	2	Generally Missing				
		<i>O. ? natheni</i>						
Ordovician			1	Keel				
		<i>A. Ordovicicus</i>	0	Sylvan Shale				

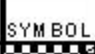











Figure 4-13: Local zonation of Conodont stratigraphy divided into 7 zones

Table 4-6: Distribution of Conodont Faunas

Age	Series	Formation	Zone	Selected Wells with Completed Conodont Study							
SILURIAN	Wentlock	Upper Clarita	6	Marie Marie No.1	Mcbride South No. 1	Boone No. 1	Carter No. 1	Carney Townsite No. 2	Bailey No. 2	W. Carney SWDW No. 1	Griffin No. 1
		Lower Clarita	5	Marie Marie No.1	Mcbride South No. 1	Boone No. 1	Carter No. 1	Carney Townsite No. 2	Bailey No. 2	W. Carney SWDW No. 1	Griffin No. 1
	Llandoverly	Upper Cochrane	4	Marie Marie No.1	Mcbride South No. 1	Boone No. 1	Carter No. 1	Carney Townsite No. 2	Bailey No. 2	W. Carney SWDW No. 1	Griffin No. 1
		Lower Cochrane	3	Marie Marie No.1	Mcbride South No. 1	Boone No. 1	Carter No. 1	Carney Townsite No. 2	Bailey No. 2	W. Carney SWDW No. 1	Griffin No. 1
		Missing	2	Marie Marie No.1	Mcbride South No. 1	Boone No. 1	Carter No. 1	Carney Townsite No. 2	Bailey No. 2	W. Carney SWDW No. 1	Griffin No. 1
	ORDOVICIAN	Ashgill	Keel	1	Marie Marie No.1	Mcbride South No. 1	Boone No. 1	Carter No. 1	Carney Townsite No. 2	Bailey No. 2	W. Carney SWDW No. 1
Sylvan			0	Marie Marie No.1	Mcbride South No. 1	Boone No. 1	Carter No. 1	Carney Townsite No. 2	Bailey No. 2	W. Carney SWDW No. 1	Griffin No. 1
Local Biostratigraphic relationship of Selected Wells in the West carney Hunton Field, Logan County, Oklahoma.				Marie Marie No.1	Mcbride South No. 1	Boone No. 1	Carter No. 1	Carney Townsite No. 2	Bailey No. 2	W. Carney SWDW No. 1	Griffin No. 1

Table 4-7: Table of Facies Code symbols used with Figure 4-14 and Table of Pore Codes used with Figure 4-15

CODE	SYMBOL	DESCRIPTION	CODE	SYMBOL	DESCRIPTION
1		ARGILLACEOUS DOLOMITE	8		CORAL AND DIVERSE FAUNA
2		CRYSTALLINE DOLOMITE	9		CORAL AND CRINOID GRAINSTONE/WACKESTONE
3		SMALL BRACHIOPOD GRAINSTONE/PACKSTONE/WACKESTONE	10		SPARSE FOSSIL WACKESTONE
4		FINE CRINOID GRAINSTONE/PACKSTONE	11		CARBONATE MUDSTONE
5		COARSE CRINOID GRAINSTONE/PACKSTONE	12		FINE TO MEDIUM GRAINSTONE
6		GRAINSTONE/PACKSTONE/WACKESTONE	13		SHALE
7		BIG PENTAMERID BRACHIOPOD	14		FINE SANDSTONE

CODE	SYMBOL	DESCRIPTION	CODE	SYMBOL	DESCRIPTION
1		INTERCONNECTED VUGGY POROSITY LIMESTONE	7		MEDIUM TO FINE CRYSTALLINE POROSITY/ DOLOMITE
2		COARSE MATRIX POROSITY/ LIMESTONE	8		FRACTURE/ DOLOMITE
3		FINE MATRIX POROSITY/ LIMESTONE	9		VUGGY OR MOLDIC POROSITY/ DOLOMITIC LIMESTONE
4		FRACTURE/ LIMESTONE	10		COARSE CRYSTALLINE POROSITY/ DOLOMITIC LIMESTONE
5		VUGGY OR MOLDIC POROSITY/ DOLOMITE	11		MEDIUM TO FINE CRYSTALLINE POROSITY/ DOLOMITIC LIMESTONE
6		COARSE CRYSTALLINE POROSITY/ DOLOMITE	12		FRACTURE/ DOLOMITIC LIMESTONE

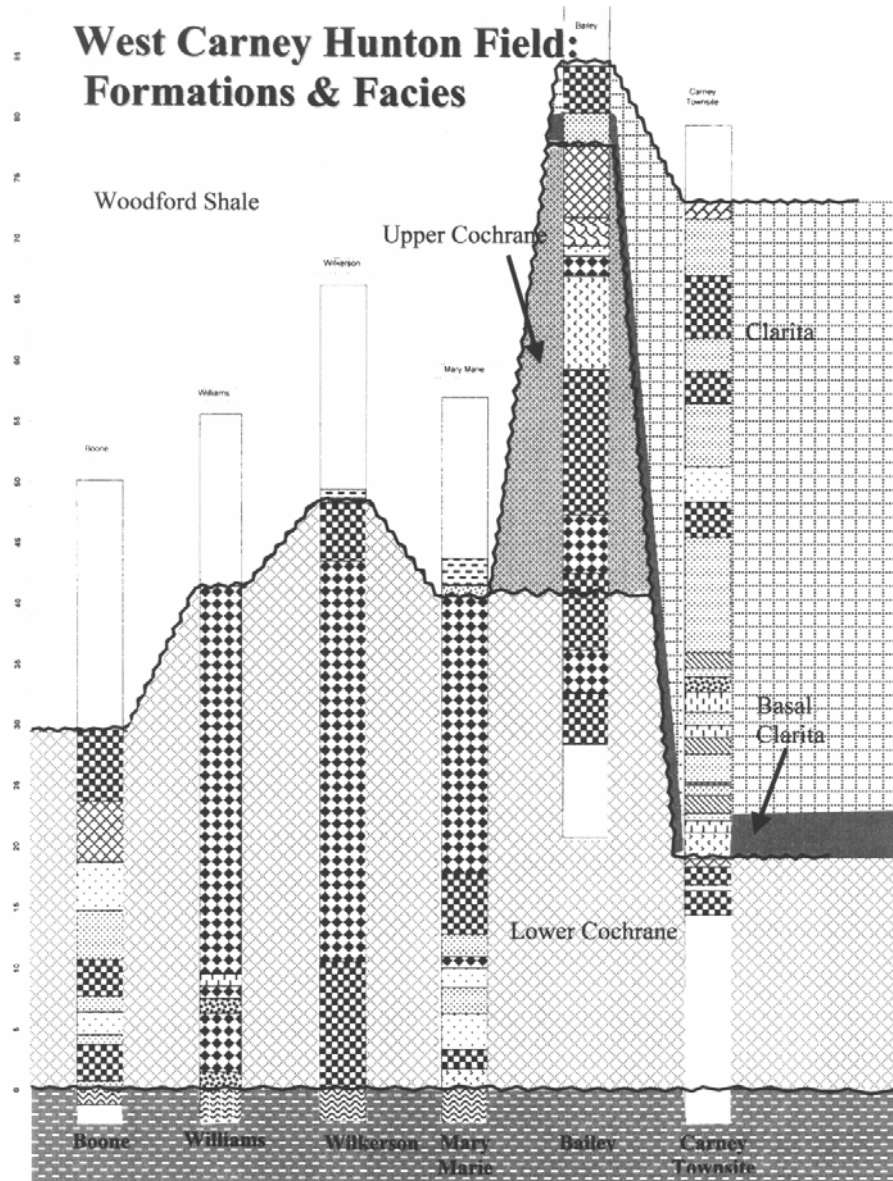


Figure 4-14: West Carney Hunton Field Formations and Facies

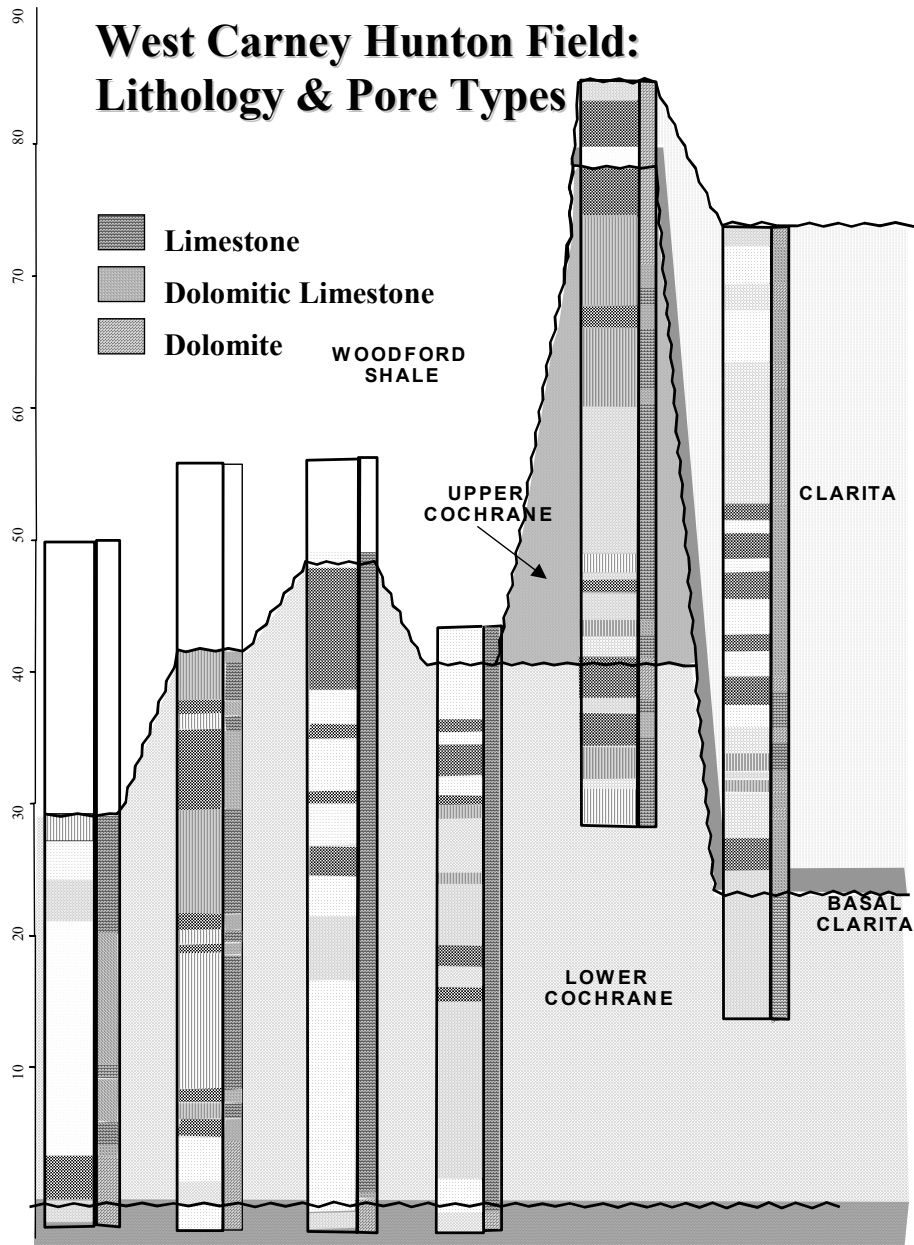


Figure 4-15: West Carney Hunton Field Lithology and Pore Types

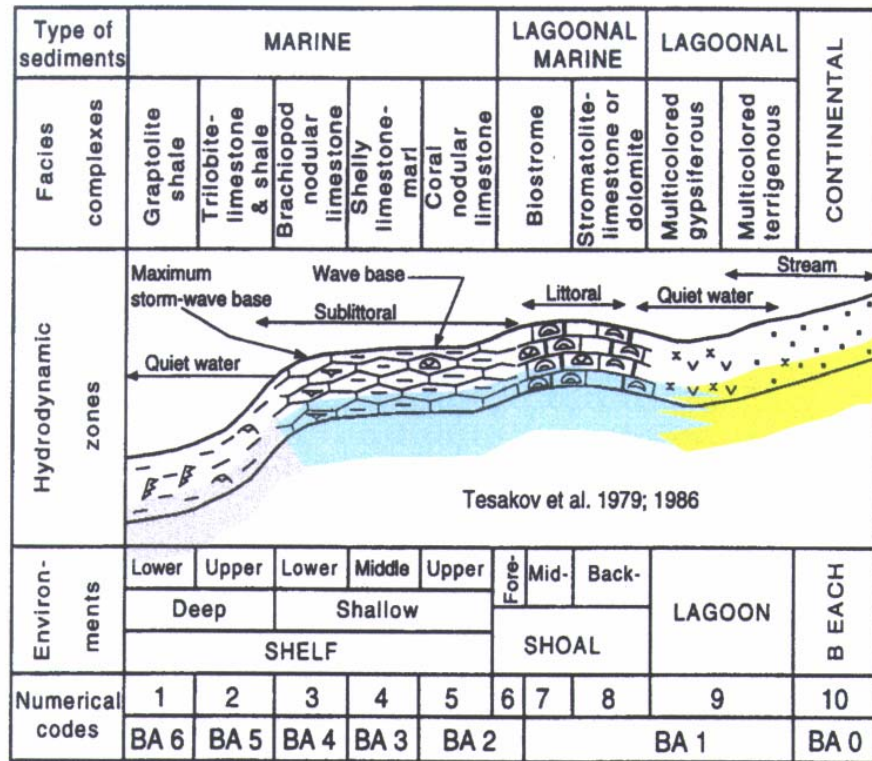


Figure 4-16: Facies model for Early Silurian Shores and Shelves of North America and Siberia. B.A. 0 – 6 indicate Benthic Assemblage zones (from M. Johnson, et al., 1997¹⁴)

Table 4-8: Depth ranges of Silurian Benthic assemblages (from M. Johnson, 1987¹⁵)

BATHYMETRY OF EARLY SILURIAN MARINE COMMUNITIES								
Welsh Basin ZIEGLER (1965)		Williston Basin JOHNSON & LESCINSKY (1986)		Michigan Basin JOHNSON & CAMPBELL (1980)		East Iowa Basin JOHNSON (1980)	depth (m)	
0	Rocky shore	0	Red beds & frosted sands				0 ±	
1	Lingulid	1	Stromatolite	1	Stromatolite		0-10	
2	Eocoeliid	2	Coral-Stromatoporid	2	Coral-Stromatoporid	2	Coral-Stromatoporid	10-30
3	Pentamerid	large size variation in Cyclocrinid algae lower photic zone limits		3	Pentamerid	3	Pentamerid	30-60
4	Stricklandiid				4	Stricklandiid	60-90	
5	Clorindid	BEADLE & JOHNSON (1988)						90-120
6	Graptolite	Sedimentary Environments						120-?
← clastics →		← platform carbonates →						

In contrast, the Clarita, which is dominated by dolomitized fine grainstones and some fine mudstones with sedimentary features suggestive of very shoal to intermittently emergent conditions would fall in B.A. 1. The geographically abrupt transition from BA 3 (in the Cochrane) to BA 1 (in the Clarita) is extremely unlikely, except by the now obvious fact that they are two separate depositional events. Recognition of these two distinctly different sequences allows the regional log correlation interpretation shown in the well-log cross sections in **Appendix Section 7.1.4** and **7.1.5**. We now have confirmation of the correctness of this interpretation in the results from the Griffin well on the west side of the field. Conodont data (**Section 7.1.13**) show that these dolomitized grainstones are indeed Clarita.

Paleoenvironmental interpretation of the Clarita remains problematic. The mix of lithofacies, including fine to medium crinoidal and small brachiopod wackestones, packstones, and grainstones, all suggest a very shoal, moderately high energy environment. A few beds of mudstone with sub-

horizontal mottles suggest sabkha conditions,. The overprint of early karst and early dolomitization also suggests a shoal to emergent environment, namely BA 1. In contrast, the contained conodont fauna (see **Appendix Section 7.1.12**) is a deep-water open marine fauna consistent with the well-know fact that the Wenlock transgression is one of strongest and most extensive Silurian sea level rises. A probable explanation is that the Clarita dolomitized packstone and grainstones in the West Carney Hunton Field area are marine bioclastic sediments, largely derived from deeper water settings, but transported to and deposited in a shoal water shoreline setting surrounding an island in the Silurian sea. The emergent part of the island is composed of the thicker portions of the Lower and Upper Cochrane (**Figure 4-12** and **Figure 4-14**).

4.2.8.3. Porosity Types

Porosity development in the Chimneyhill Subgroup in West Carney Hunton Field is a combination of original sediment type, early, and late diagenesis. Most of the sediment is so severely altered by early to middle diagenesis, that original sediment type no longer is a factor. For example, much of the section is coarse grainstone, but most coarse grainstones are so strongly affected by early dissolution that the grainstone fabric is totally collapsed into a tight matrix of coarse, inter-sutured grains, with virtually no fine matrix or secondary spar. Other grainstones are more conventionally filled with porosity-occluding spar or syntaxial overgrowths. Especially Pelmatozoan (“Crinoid”) grains are subject to development of syntaxial overgrowths which totally occlude any effective porosity. In many Hunton packstones, effective porosity is developed only as result of dissolution of fine carbonate mud matrix.

A classification of porosity types for this study is given below, and in **Section 7.1.9.1**. This is simply an *ad hoc* listing of porosity types encountered so far and does not preclude other types in the future. In **Section 7.1.9.1**, each sample analyzed by Stim-Lab is assigned a porosity code, providing a foot-by-foot description of the reservoir. Many of these porosity code assignments may be modified in the future by more detailed information resulting from thin section or acetate peel analysis of selected intervals. Porosity types are shown below.

Limestones (grain density 2.71 to <2.73)

1. Interconnected Vuggy porosity

Vug or Moldic (MO) with inter-granular (IG), solution fracture (SF) or other connection, touching vugs (TV) general, Vug general. Not vugs with tight matrix.

2. Coarse Matrix porosity

Inter-particle (IP), IG or inter-crystalline (IX) of coarse-grained rock, > .25 mm particle size. Many include dissolution porosity that is inter-particle micro vugs (dissolution of spar or matrix).

3. Fine Matrix porosity

Inter-particle (IP), IG or IX of medium to fine-grained rocks, < .25 mm particle size. Includes fine non touching vugs and non touching fine Moldic (MO) porosity along with intra-particle porosity

4. Fracture

FR or SF without significant matrix or vugs.

For this study, includes solution-enhanced fractures with sand in-fill.

Dolomite (> 50% dolomite; grain density 2.79 or higher)

5. Vuggy (vug) or Moldic (MO) in coarse crystalline (IX) matrix (> .25 mm)
6. Coarse crystalline with Inter-crystalline porosity (IX) (> .25 mm)
7. Medium to fine crystalline (IX) (.25 mm to .02 mm)
8. Fracture FR or SF without significant matrix porosity

Partly Dolomitized Limestone (10 – 50 % dolomite; gr density 2.73-2.78)

9. Interconnected Vuggy porosity

Vug or MO with IG, SF or other connection, TV general, Vug general.
Not vugs with tight matrix.

10. Coarse Matrix porosity

Inter-particle (IP), IG or IX of coarse-grained rock, > .25 mm particle size.
May include dissolution porosity that is inter-particle micro vugs (dissolution of spar or matrix).

11. Fine Matrix porosity

Inter-particle (IP), IG or IX of medium to fine-grained rocks, < .25 mm particle size. Includes fine non touching vugs and non touching fine Moldic (MO) porosity along with intra-particle porosity

12. Fracture

FR or SF without significant matrix or interconnected vuggy porosity.
For this study, includes solution-enhanced fractures with sand in-fill.

4.2.8.3.1. Distribution of Pore types

Figure 4-15 illustrates the vertical and lateral distribution of pore types in a 6-well cross-section. This demonstrates the reservoir is extremely heterogeneous both vertically and laterally, with no individual flow-units creating neat geometric compartments of reservoir types. Modeling of the reservoir must accommodate this known heterogeneity.

4.2.8.4. Log Interpretation of Porosity

Because of the complex porosity structure, we compared the core porosity vs. log porosity to make sure that we are obtaining reasonable representation of porosity values using log data. As an example, **Figure 4-17** shows a plot of running average of core porosity vs. average log porosity (average of density and neutron porosity)

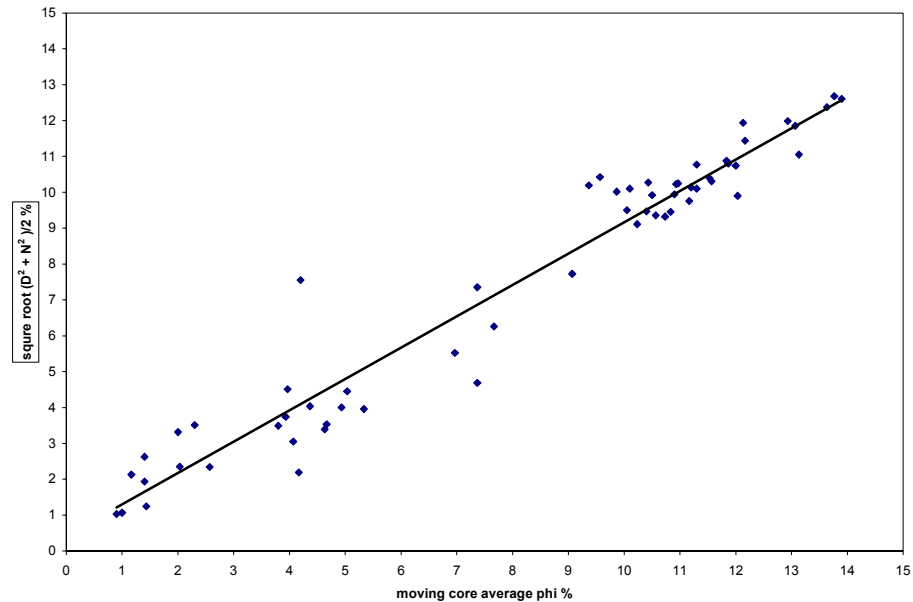


Figure 4-17: Core porosity vs. average log porosity

For the wells described so far, we compared the moving average porosity data with density porosity, neutron porosity and a square root average of neutron and density porosities. The results are shown below in **Table 4-9**. This table shows that for a majority of wells, an average of the two porosities correlates the best with core data. There is only one well where density log provides a superior correlation. However, a closer examination of that well (Givens) reveals that the correlation coefficient for all the three methods is low. It is easy to see that the average method works well even for the wells where one of the other methods is found to be superior in terms of correlation coefficient. In essence, the average method provides a good correlation irrespective of dominant rock type environment.

Table 4-9: Comparison between log and core data

Well Name	Density Log	Neutron Log	$((D^2+N^2)/2)^{0.5}$	The Best Correlation	Dominant Rock Type
Boone 1-4	0.1016	0.7393	0.8066	average	Dolomitic limestone
Carney Townsite 2-5	0.8196	0.9437	0.9452	average	Dolomitic Limestone
Carter 1-14	0.4771	0.6682	0.8862	average	Limestone
Danny 2-34	0.7259	0.5043	0.7791	average	Limestone
Henry 1-3	0.3592	0.6495	0.668	average	Limestone
Joe Givens 1-15	0.3017	0.1343	0.283	Density	Limestone
Mary Marie 1-11	0.7291	0.806	0.7803	Neutron	Limestone
McBride South 1-10	0.0753	0.6543	0.6192	Neutron	Limestone
Wilkerson	0.5775	0.8466	0.8271	Neutron	Limestone

4.2.8.5. Karst

Karst is universally present in all cored wells, but is highly variable between wells. The development of karst and its effects on potential reservoirs is well-illustrated in a recent paper by Loucks (1999)¹⁶. The features illustrated are present abundantly in West Carney Hunton Field cores and are listed in the

karst features part of each well core description (**Section 7.1.8**) The reader is urged to read Loucks's paper in its entirety, especially the portion on the areal extent of karst.

The core descriptions include a separate section describing the effects of karst, separate from the stratigraphic sequences. Effects of karst ranges from open fissures extending through the entire Hunton and thick collapse breccias with steeply dipping beds to minor fracture breccia and vuggy porosity. One well, the Houser 1-11, shows evidence of a cave 11 feet high, completely filled with a combination of collapse breccia, cavern-fill parabreccia, and laminated void-filling silt (See **Appendix Section 7.1.16**, Houser 1-11 at 5061 to 5072). The abundance of collapse breccias suggests that Hunton thickness in West Carney Hunton Field may be significantly affected by karst. We plan to prepare isopach maps of overlying units to see if the karst dissolution and collapse is reflected in younger sediments.

Karst sediment ranges from medium sand to clay, and fills open fissures, caverns, vugs, inter-particle space in collapse breccias, and intra-fossil cavities. Karst sediments may occlude porosity and reduce permeability, at least as recognized by core analysis. For example, the Joe Givens #1-15 is heavily karsted, with sand-filled fissures extending to the base of the Hunton; however it shows very poor porosity on both well logs and core analysis. (Some of the karst passages are obviously not filled, as the Joe Givens has a high fluid flow and is one of the better producers.)

Engineering data and drilling experience clearly show open karst channels interconnect the wells. The Marjo Geneva 2-32 (NE-SW-32-16N-3E) well was being drilled in January 2001 when it lost circulation while coring, and pumped in Lost Circulation Material (LCM). A nearby operator was swab-testing the Altex Covey Heirs 3-32 (SE-NW-32-16N-3E) 1,320 feet away,

almost immediately recovered the LCM in their swab test. Formation pressure data has also verified the free interconnection between some wells. At this time we have not yet attempted to create an appropriate model for karst channels in West Carney Hunton Field, as is clearly needed to simulate fluid flow through karst channels.

4.2.9. Conclusions

We can derive the following conclusions based on geological analysis:

1. 27 wells cored, 14 described, 7 with paleontology studies.
2. In West Carney Hunton Field Hunton is Chimneyhill: Cochrane and Clarita Formations, subdivided into 3 sequences.
3. The field is mostly in Lower Cochrane limestone, open marine, outer to mid shallow shelf facies.
4. An Upper Cochrane unit is present, heretofore unknown in middle US.
5. Clarita Formation is present, deposited in topographic lows lateral to the older Cochrane
6. Clarita is shoal facies, dolomite and dolomitic limestone;
7. Entire Hunton section is Karsted, present as solution-enlarged fractures, mosaic breccias, breccia-filled caverns, sand, clay, and carbonate sediments, and solution collapse.
8. Dual Porosity system dominates; an extremely high permeability system of solution-enlarged fractures, and a matrix system of largely secondary vuggy and leached intergranular pores.
9. Neither sedimentary facies nor porosity “zones” correlate laterally, both create a mosaic of facies and heterogeneous reservoir types.

4.3. Engineering Analysis

Sandeep Ramakrishna, Rahul Joshi, Vineet Marwah, Jeff Frederick, and Mohan Kelkar (The University of Tulsa), Kishore Mohanty (The University of Houston)

The Engineering Analysis is divided into several sections. In the first section, we discuss the relationship between core and log data and our efforts to use log information to infer geological knowledge. The section also provides the relationship between the static data and the dynamic production information. The second section discusses the methods utilized for analyzing production data using available production data. We have developed a procedure for analyzing the production data which is collected under variable rate and variable production conditions. Using the procedure, we can determine the reserves as well as various reservoir parameters. In the next section, we discuss the rock and dynamic characteristics of the core samples based on the lab studies. The lab data indicate slightly oil to mixed wet characteristics of the reservoir, which is consistent with other observations in the field. In the last section, we integrate many of our observations to understand the primary mechanism by which the reservoir is produced. We accomplish this by conducting a flow simulation study and matching the field data with the simulated data.

4.3.1. Core – Log Correlation

This section discusses the use of log data in evaluation of reservoir performance. The first part discusses the development of correlation between the log and the core data so that core analysis can be extended to other wells, in the second part we correlate log data to dynamic information.

4.3.1.1. Development of Correlation between Core and Log Data

The development of the correlation began with the geological description of the cores. The geologist provided detailed core description from fourteen wells in terms of lithology, pore and facies types, fractures, stylolites and karst. The core analysis showed three lithologies namely; Limestone, Dolomite and partly Dolomitized Limestone to be present in the West Carney Hunton Formation (West Carney Hunton Field). The geologist identified four pore types: vugs, coarse matrix, fine matrix and fractures in each of the rock type and fourteen facies types. **Figure 7-26** and **Figure 7-27** give a detailed account of the pore types and facies types identified from the fourteen-cored wells in the West Carney Hunton Field. A detailed account of the geology is presented in the geological analysis of this report. Please refer to the appendix for the core-log plots for more information on the fourteen-cored wells.

4.3.1.1.1. Discriminant Analysis and Determination of Geological Pore types

Our goal was to develop a correlation that would help us determine the pore types for the uncored wells, using only the available log data. Limited digitized log data was available and hence we had to digitize most of the log data from hard copies of logs taken from the log library. Since the Gamma ray and PE logs do not reveal a lot of characteristics of the Hunton formation we decided to digitize only the deep resistivity, density porosity and neutron porosity logs from 139 uncored wells in the West Carney Hunton Field. We began to analyze the data based on similar characteristics. We made groups based on similar rock type and similar pore types. Since the geological facies and rock types did not show us

very good correlations, we decided to analyze the data based on the pore types. Hence the twelve pore types described by the geologist were further divided into four groups by grouping vugs and coarse matrix together and fine matrix and fractures together for limestones and dolomites. We included partly dolomitized limestone along with dolomite to obtain better correlation. This data was then used to perform discriminant analysis.¹⁷

Discriminant Analysis is a method of creating a function or a model that explains the grouping of the given individuals, and can further be used to assign additional observations to the correct group. Relationships among feature variables (principal components of log data) to the grouping variable (cluster type) are expressed by their mean values and their variance-covariance matrices.

The discriminant analysis was performed on data available from 13 cored wells, as well as the logged wells. We used the log-derived data from 13 cored wells and assigned them into 4 groups as mentioned above. Each data point was assigned its corresponding group from the deep resistivity, density porosity and neutron porosity from log signatures. Then discriminant analysis was performed on this data set. The principal components of each logs are calculated and link the groups assigned to each data with its corresponding principal components creates a discriminant function. This is then applied to other raw datasets to classify that data into four groups. Now we have all the data from 152 wells divided into four groups based on pore types.

4.3.1.1.2. Cross Validation

The cross validation is done by using the same dataset (cored wells) that was used to generate the discriminant function. Upon cross validation the match was observed to be 65% i.e. only about 65% of the groups assigned by the discriminant function to a particular data matched the original assignment of the groups. That is, geological assignments match 65% of the times with log signatures.

We could not further improve this match using the geological pore types. Hence we thought of another approach, generation of the electrofacies. The following sections would explain electrofacies and then we would discuss the different approaches considered to develop a relationship between the static and the dynamic data based on the geological pore type and the electrofacies.

4.3.1.2. Electrofacies Analysis

4.3.1.2.1. What is Electrofacies?

The concept of electrofacies¹⁸ is introduced to extend the information about porosity-permeability obtained from cored wells to log data for the uncored wells. The underlying principle of electrofacies is purely statistical in nature, but its results are seen to be geologically consistent. Using this concept, the data obtained from logs is classified into groups, which are homogeneous within themselves and distinct from each other. The electrofacies calculation involves three basic statistical procedures explained below.

4.3.1.2.2. Principal Component Analysis

Principal Component Analysis¹⁸ (PCA) is a statistical method used to reduce data to lower dimensions (reducing the number of variables) with minimal information loss. The principal components are the eigen-vectors of the variance-covariance matrix of the variables. The eigen-vectors constitute the directions of principal component axes in the transformed space, whereas the eigen-vectors determine the length of the axes. By multiplying the original data by the components of eigen-vectors the principal component scores are obtained. The variance-covariance matrix of this transformed data is a diagonal matrix, whereby each diagonal term represents the variance of the data independent of the other. Typically the first diagonal term explains the maximum variance of the data followed by the second and so on. Usually the first three or four principal components explain about 90% of the variance of the data. In this way, the number of variables are reduced, with the loss of at most 10% of the variance.

Three logs (density porosity, neutron porosity and deep resistivity) were selected and principal component analysis was carried out. Since there were only three variables, all the three principal components were taken into consideration for further analysis.

We also used five logs (density porosity, neutron porosity, deep resistivity, density correction and photo electric) for our analysis; however, we did not see any significant improvement by adding two more logs. Hence we continued with the three log analysis.

Figure 4-18 shows a scree plot that describes the variance percentage of the Principal components. As can be seen, the first component explains

66% of the variance of data; and the first two components explain 88% of the variance.

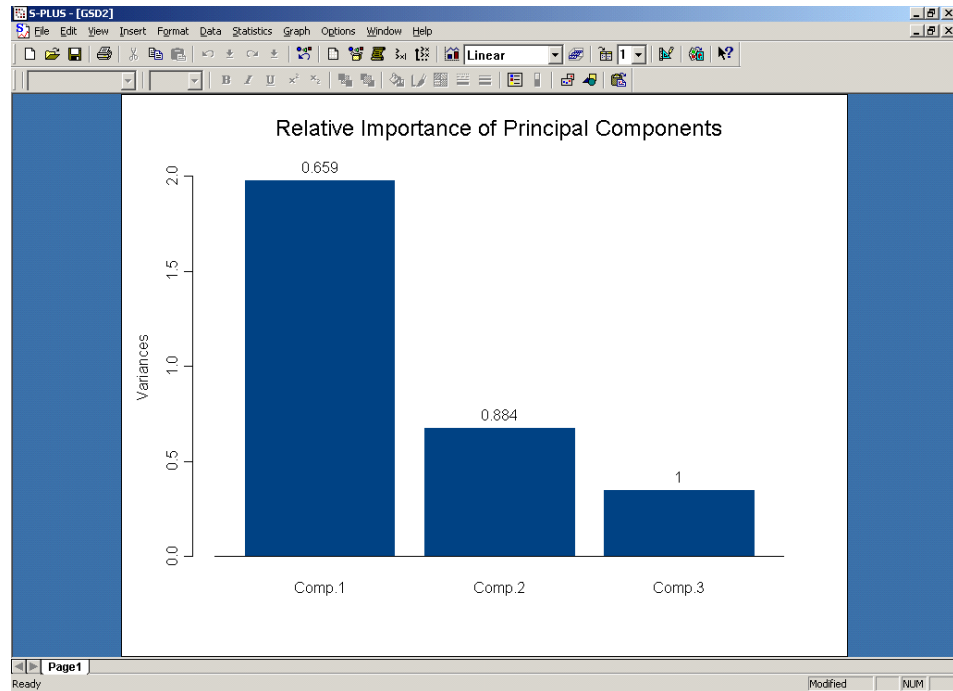


Figure 4-18: Scree plot showing the different principal components and their variance percentage

4.3.1.2.3. Cluster Analysis

Cluster Analysis is the method for classifying the data (principal components) into clusters, which are distinct from each other. These clusters will represent the electrofacies. The process by which these clusters are assigned is mathematical in nature. The algorithm used is a *k-means partitioning around medoids*. In this algorithm k representative objects called medoids are computed and each object is assigned a cluster corresponding to the nearest medoid. These k representative objects should minimize the sum of dissimilarities of all objects to their nearest

medoid. The algorithm basically proceeds in two steps. In the first step called the *build up*, the algorithm sequentially selects k centrally located objects. In the second step called the *swap step* the selected object is swapped with an unselected object if the objective function can be minimized with this operation. This process is continued till the objective function is minimized and each data is assigned a particular cluster. Selecting the number of clusters to be used is a trial and error process, the best indication of which is obtained by observing a cluster plot as shown in **Figure 4-19**. In **Figure 4-19**, too many clusters are concentric.

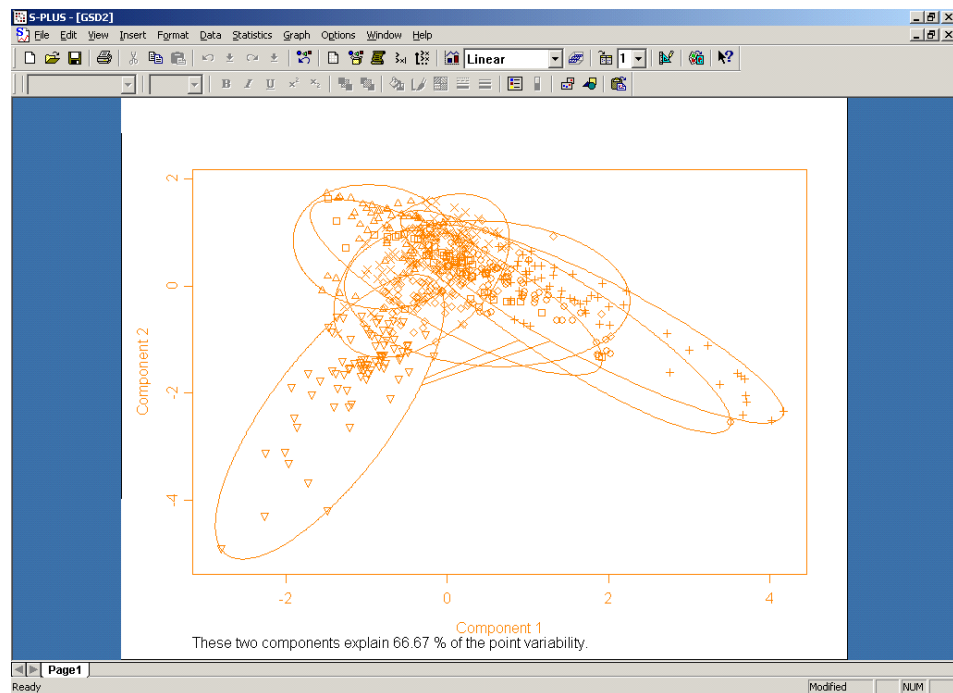


Figure 4-19: Cluster plot using seven groups

From the plot it can be seen that the more the number of clusters specified the more concentric ellipsoids are observed showing that they are

unrealistic and do not actually occur. This gives an indication that the number of clusters needs to be reduced.

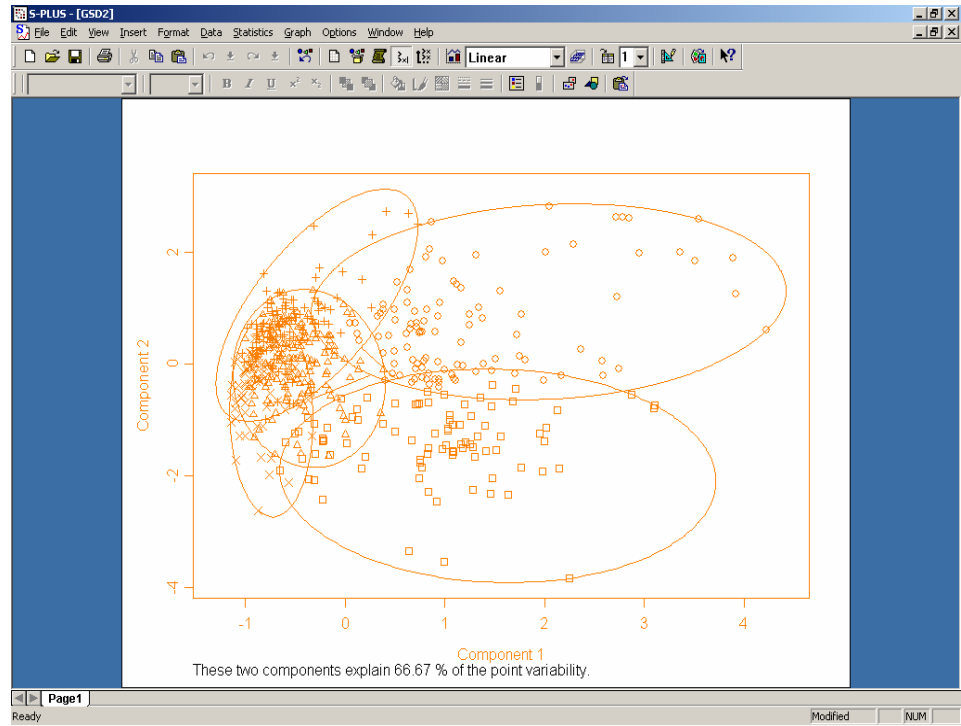


Figure 4-20: Cluster plot using five groups

Figure 4-20 shows a plot with 5 clusters. By trial and error we found that 5 clusters would be the best way to group the data.

In our analysis we considered the 13 cored wells and each log data was assigned a particular cluster. By trial and error and reviewing the cluster plot we found that using 5 clusters gives us a good classification. Hence the number of electrofacies is 5. Once the principal components for each log data and its corresponding electrofacies is known, the information is applied to other uncored logged wells using Discriminant Analysis.

4.3.1.2.4. Discriminant Analysis

The Discriminant Analysis is a method used to extend the information to any number of logged wells. The Discriminant Analysis creates a discriminant function using the cluster number and the principal components of the data of the cored wells. It then applies this function on the principal components of the logged data from uncored wells and generates clusters for each log data value. In this way all the log data from 139 wells were assigned a cluster (electrofacies). Hence we had a complete data set of the 152 wells from the West Carney Hunton Field, those that were considered in our study divided into 5 electrofacies.

4.3.1.2.5. Comparison of Electrofacies and Geological Facies

Once the electrofacies were assigned to each log data for all the cored wells, a comparison was done with the assigned geological facies. During the comparison different geological facies were combined together with one electrofacies depending on the way they were assigned. The **Figure 4-21** shows the results of electrofacies analysis and its comparison to geological facies.

Comparison of Electrofacies and Geological pore types

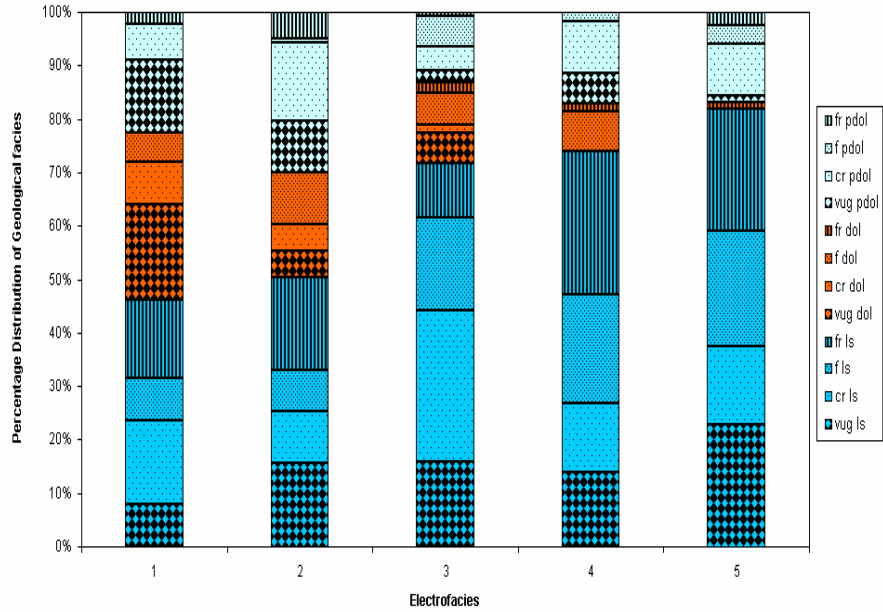


Figure 4-21: Comparison of Electrofacies with Geological Pore Types

Please refer to Appendix Error! Reference source not found. and **Figure 7-27** to understand the legends shown above.

We see from the **Figure 4-21** that Electrofacies 1,2,3 show substantial proportions of coarse matrix and vugs in limestone, dolomite and some partly dolomitized limestone. The amount of dolomite decreases going from electrofacies #1 to electrofacies # 3 and is reduced significantly in #4 and #5. Electrofacies # 4 and # 5 show substantial proportions of limestone with fine matrix and fractures. It can be seen that electrofacies analysis is successfully able to obtain a compositional segregation. Although there is some overlap, we can state that electrofacies # 4 and # 5

mostly are comprised of fine matrix and fractures; whereas, electrofacies # 1, 2 and 3 are comprised of coarse matrix and vugs.

4.3.1.3. Porosity – Permeability Correlation

The electrofacies analysis helped us to generate the electrofacies at 152 wells considered in our study. We had very good core coverage in the area of study, 17 wells, which were cored as well as logged. These were used to develop porosity - permeability correlation.

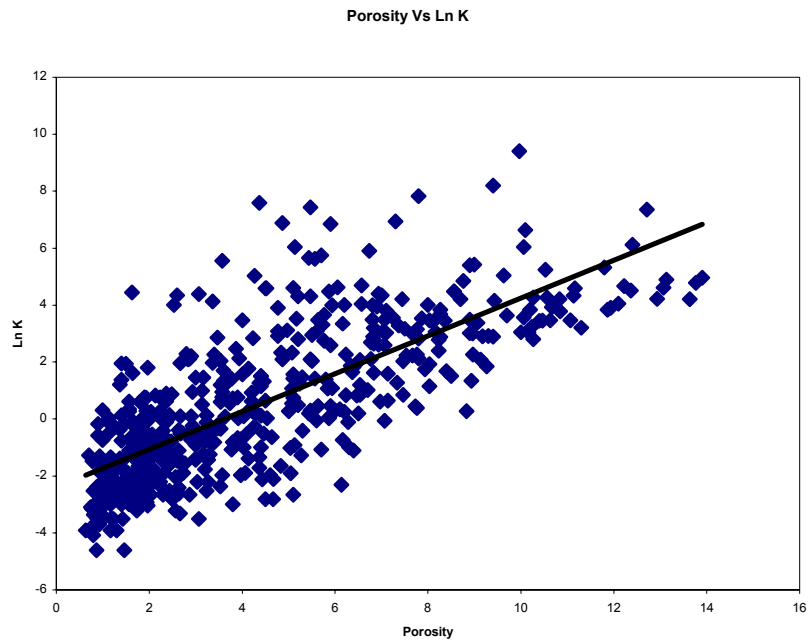


Figure 4-22: Log porosity vs. Ln K

Figure 4-22 shows a plot of log porosity versus Ln K. We used this correlation to obtain permeability values at uncored wells.

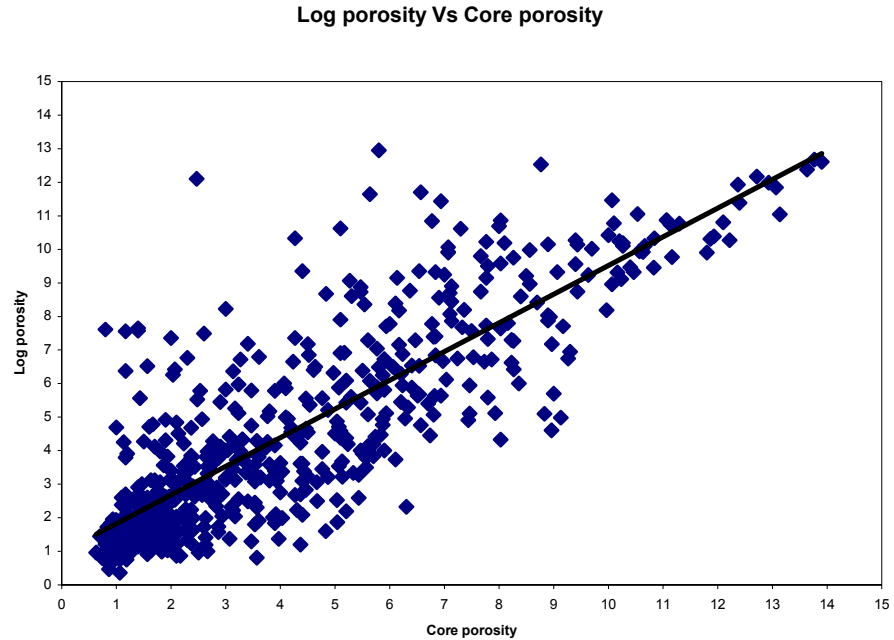


Figure 4-23: Correlation between Log porosity and Core porosity

Figure 4-23 shows good correlation between Log derived porosity and core derived porosity.

We examined correlations developed for each individual electrofacies, but this did not provide significantly different results as compared to the correlation using all the data together. Hence the correlation equation that was developed using all the available porosity permeability data was used to generate permeability values at uncored wells. In the development of the correlation, we were not able to capture some of the extreme values that we suspect are from highly fractured regions and could be a key to the successful production from certain wells.

Once the permeability data was generated at all the well locations, we began to calculate the Productivity ($K \cdot H$). All the permeability data was ranked and the 1st, 5th and 10th percentile values were calculated. The values were found to be 228 md, 40 md and 9 md for 1st, 5th and 10th percentile of the permeability data. Then the productivity was calculated for all the wells having permeability's greater than the cutoffs considered. It was necessary to recognize these high conduit zones as they were considered to be the key to good water production. Some of the results obtained from these correlations are discussed in the following sections.

4.3.1.4. Static to Dynamic Relationship

The aim of this analysis was to determine a relationship between the static data and dynamic data, and to be able to recognize some diagnostic characteristics of the static data responsible for the production success of a well. Two approaches were tried to better understand and study this relationship: the Pickett plot¹⁹ approach and the Buckles plot¹⁹ approach. Both these are discussed in detail in the following sections.

As discussed in the previous section, the geological pore types were assigned at every data point in all the 152 wells. We considered, for calculation purposes, that each pore type represented a small unit thickness of the West Carney Hunton Field reservoir. We also calculated the corresponding porosity, resistivity, water saturation, bulk volume water and hydrocarbons in place associated with that unit thickness. Based on those calculations we were able to calculate the hydrocarbons in place for all the 152 wells from the West Carney Hunton Field considered in our study.

As mentioned earlier the main highlight of this correlation was to understand some of the diagnostic characteristics of the static data like the porosity, permeability, rock type, pore type, facies data and also be able to address the question; what makes a good producer? Hence we had to study the dynamic data such as the oil and gas production, (availability of water production data was limited, but has been studied wherever available), and we determined the decline rates and the cumulative oil and gas produced from the 152 wells. The oil production had to be viewed at similar time periods; hence we have chosen to view the production on a 6 year basis. We have extrapolated the production to match 6 years of producing life for each well using 50% a year as the decline rate. That is, we have either used cumulative production of oil and gas for six years, if available, or have extrapolated cumulative production to six year period by assuming a decline rate of 50% per year. The decline rate is based on average decline rate observed in other producing wells.

The results from the various approaches are discussed below.

4.3.1.4.1. Pickett Plots using geological pore types

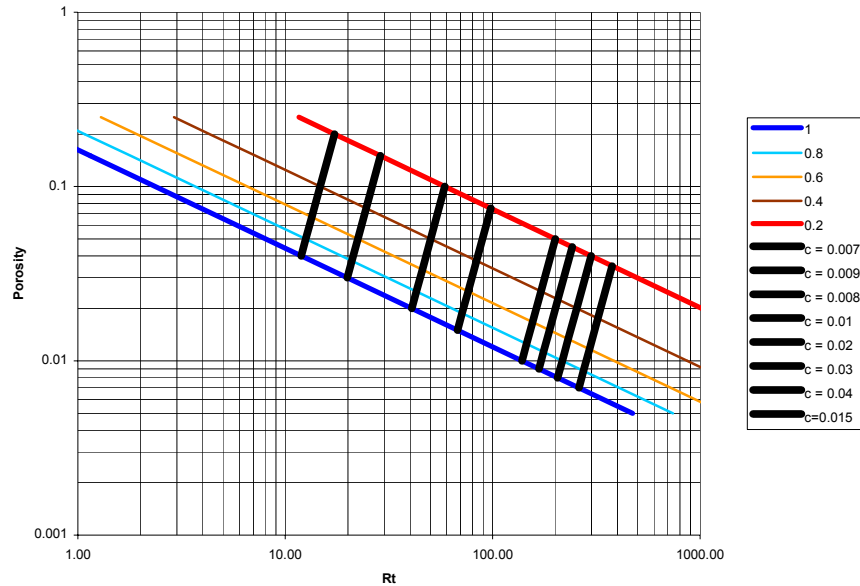


Figure 4-24: A typical Pickett plot

Figure 4-24 is an example of the Pickett plot. Porosity is calculated from the neutron porosity and density porosity logs and is plotted against the resistivity data obtained from the deep resistivity log. Porosity is plotted on the 'Y' axis with a logarithmic scale ranging from 0.1 % to 100 % while the resistivity is plotted on the 'X' axis with a logarithmic scale ranging from 1 to 1000 ohm meter. The colored inclined lines represent water saturation; dark blue line indicates 100%, decreasing as we go towards red, which is 20% water saturation. The dark black lines that are perpendicular to the colored water saturation lines are the bulk volume water lines. The value of these lines is decreasing as the resistivity is increasing.

4.3.1.4.1.1. Porosity calculation:

Porosity was calculated using the data available from the neutron and density porosity logs using the following equation:

$$\sqrt{\frac{D^2 + N^2}{2}}$$

Equation 4-1

Where,

D = Density porosity

N = Neutron porosity

4.3.1.4.1.2. Water Saturation (Sw) calculation

Water saturation was calculated using Archie's formula

$$S_w = \left[\frac{a}{\phi^m} \cdot \frac{R_w}{R_t} \right]^{1/n}$$

Equation 4-2

Where,

ϕ = porosity

R_t = True resistivity of formation

R_w = Water resistivity, (Analysis were done on water samples and the value was found to be 0.035)

m = Cementation factor, (Analysis were done on formation samples and the value was found to be 1.77)

$n = 2$

$a = 1$

4.3.1.4.1.3. BVW calculation

Bulk volume water is the product of the porosity and water saturation. ($\phi * S_w$)

Where,

ϕ = Porosity

S_w = Water saturation

The Pickett plots with geological pore types did not show any correlation to production data, hence we had to abandon that approach and consider plotting the electrofacies on the Pickett plot.

We had access to the daily production records of the wells operated by Marjo Oil Company. We considered 27 wells for which we had log data and classified them into three groups, good average and bad producers. Then, we made the Pickett plots using electrofacies for all these 27 wells, and began examining the data.

The figures below show some of the Pickett plots using the electrofacies along with the production data for some of the good and bad producers amongst the 27 Marjo wells that we considered for this study. Our aim was to determine the diagnostic characteristics, based on these 27 wells and then validate using the data from the remaining wells.

In the following figures, we have cited Schwake and Danny#2 as examples of good producers, Townsend as an example of average producers and Carter and Lewis as examples of bad producers. The production from all the 27 wells considered in this study was viewed at the same time period and the plots were generated. Alan Ross was the first well to produce, amongst the 27 wells considered in this study with the Pickett plots. Wells that came into production at a later stage have been plotted with respect to the producing life of Alan Ross. It can be seen from the plot that the production for Danny #2 starts from the 250th day. This means that the well Danny #2 began producing 250 days after Alan Ross. Comments about mechanical problems associated with the production from the wells are also mentioned on the plots.

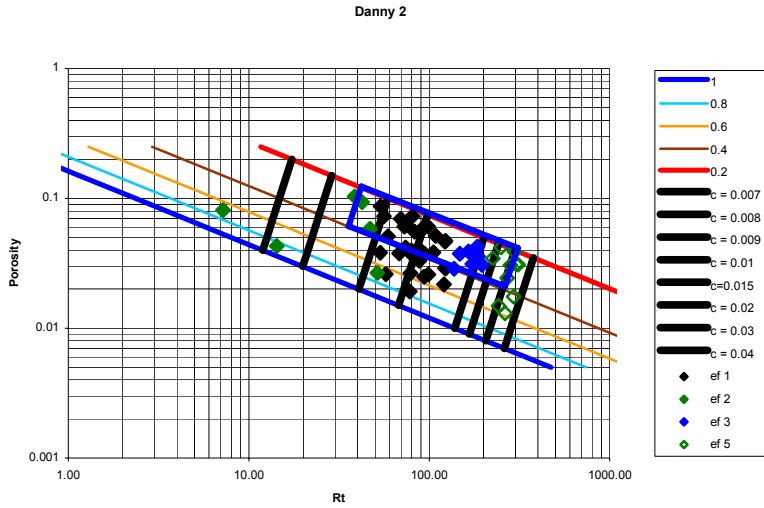


Figure 4-25: Pickett plot for the well Danny #2; Legends: ef = electrofacies

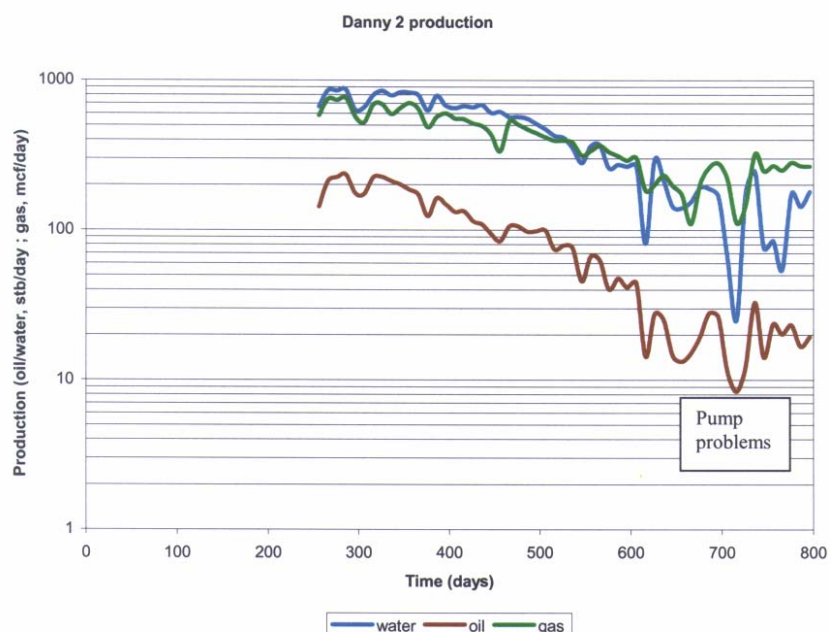


Figure 4-26: Production from well Danny #2

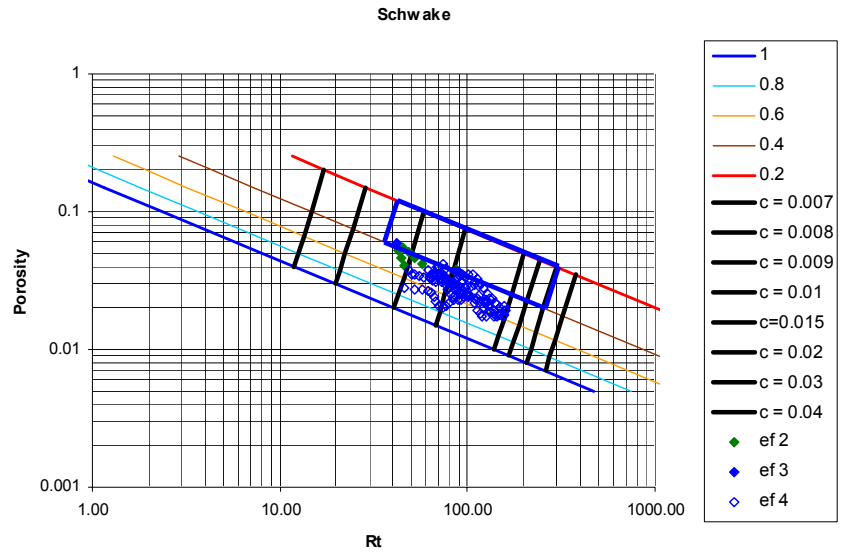


Figure 4-27: Pickett plot for Schwake ; Legend ef = electrofacies

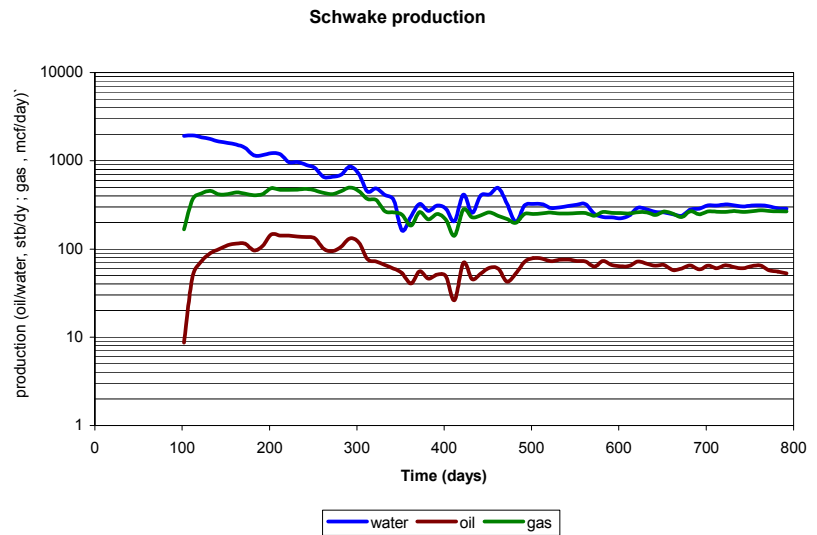


Figure 4-28: Production from well Schwake

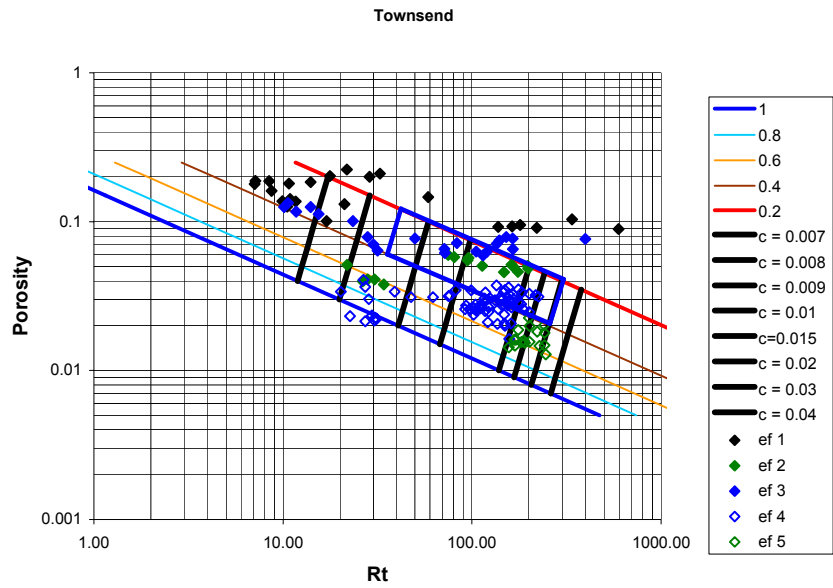


Figure 4-29: Pickett plot for well Townsend ; Legend ef= electrofacies

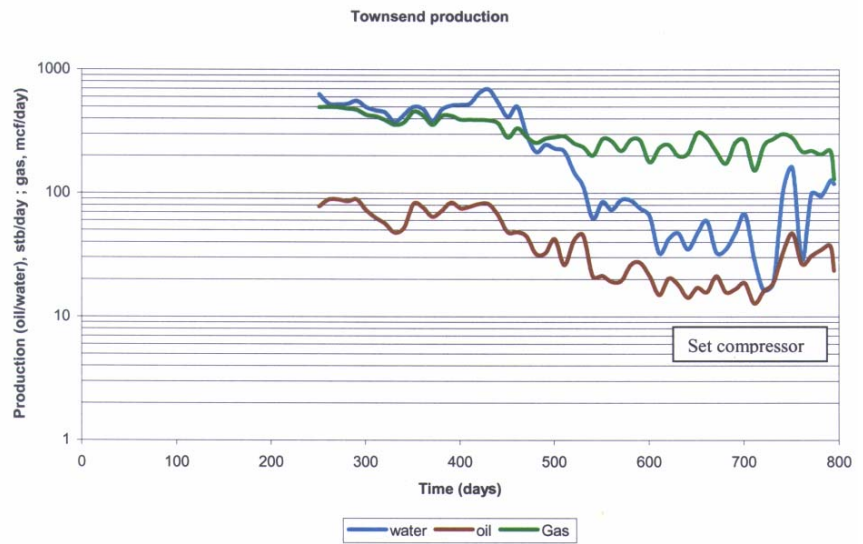


Figure 4-30: Production from well Townsend

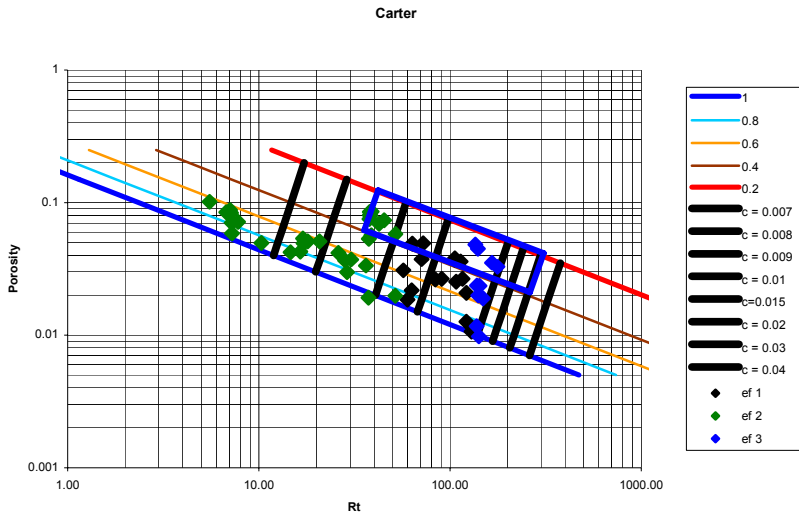


Figure 4-31: Pickett plot for well Carter ; Legend ef= electrofacies

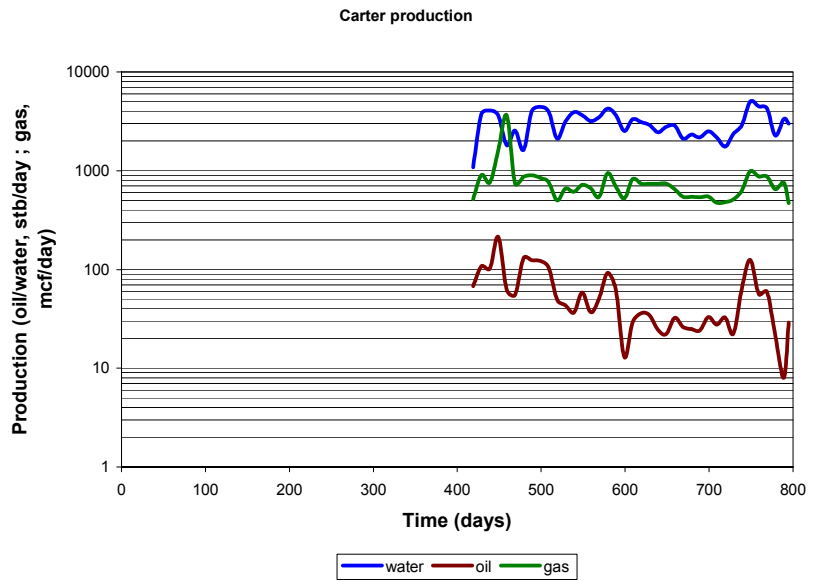


Figure 4-32: Production from well Carter

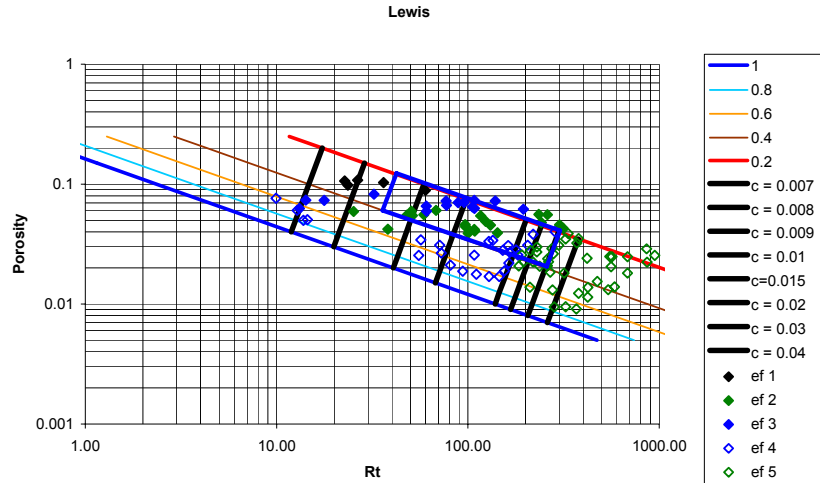


Figure 4-33: Pickett plot for well Lewis ; Legend ef = electrofacies

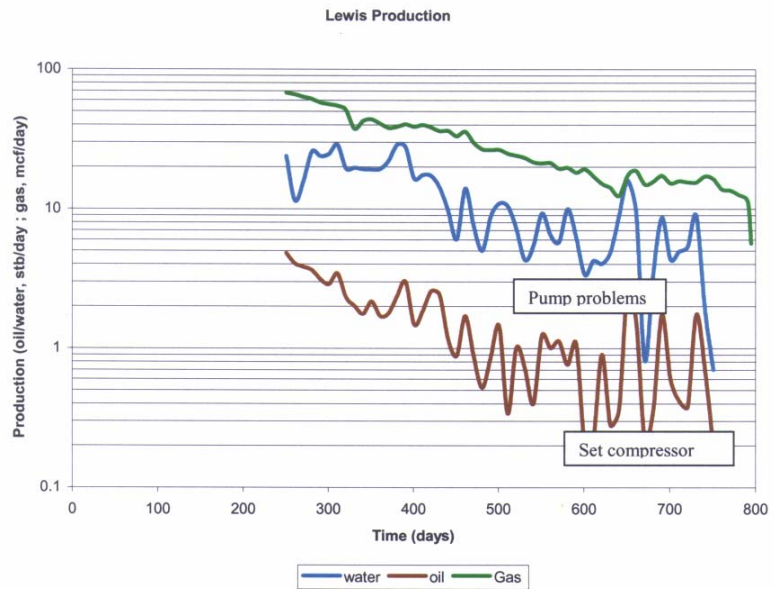


Figure 4-34: Production from well Lewis

Correlation of the static data from the logs with the dynamic data from daily production began with comparison of the Pickett plots with the oil, gas and water production. Similar plots as shown in the figures above were made for every well. The Petrophysical

characteristics, electrofacies and the production data were observed and studied for each well. The results are shown in **Table 4-10**.

Table 4-10: Petrophysical, electrofacies and production characteristics of some of the wells

Well Name	Production Characteristics	Electrofacies	Petrophysical characteristics
Carter 1	High WOR (100 approx), low oil production rate	Mostly 1 & 2, some 3	More than 50 % data has lower than 4 % porosity
Henry	High WOR (50 - 100 approx)	Mostly 1 & 2, some 3	More than 50 % data has greater than 4% porosity
Cal	Low water and oil producer	All present	90 % data has lower than 4 % porosity
Schwake	Low WOR , (4-5 approx) sustained oil & water production, GOR constant	Bulk of the data 4, with some 2 & 3	Bulk of the data between 2 & 4 % porosity, high perm in type 4
Alan Ross	Sustained production, low water, Gas rate decreasing	Large % of 4 with some 2,3,5	Characteristics similar to schwake
Townsend	Sustained oil and water rate, gas rate decreasing	Bulk 4 with significant 1 & 3	Porosity greater than 2 %, 15 % data having porosity greater than 10 %
Franny	Sustained production, WOR (approx 6), gas rate decreasing	Bulk 4, some 1 & 2	Bulk of porosity greater than 2 %
Lewis	WOR (approx 8), poor producer	Equal distribution of all electrofacies	No porosity greater than 10 %
Wilkerson 1	Sustained water rate, WOR (approx 4), sustained gas production, GOR decreasing	Bulk 1,2 & 3	Bulk of porosity greater than 3 % (connected, hence oil coming from somewhere else)
Danny 2	WOR (approx 5), good producer, sustained gas production, GOR decreasing	Bulk 1,2 & 3	Bulk of the porosity greater than 3 % (well connected, hence oil coming from elsewhere)
Williams	Oil and gas rate sustained, water rate decreasing, WOR (approx 10)	1,2,3 & 5, all in equal proportions	Bulk of the porosity is greater than 2 %
Wilson	Sustained oil, water and gas production WOR (approx 2)	High % of 4	Bulk of the porosity is less than 2 %

The study of these plots did not successfully answer our question; what makes a good producer, but then we could infer some of the probable reasons for a good producer from this study. Some wells with substantial proportions of electrofacies 1,2, and 3 having 2%

and greater porosity OR substantial proportions of 4 and 5 having 4% and greater porosity, seemed to be good producers. But we were not able to identify any diagnostic characteristics, which can consistently identify good producers.

4.3.1.4.2. Buckles plot

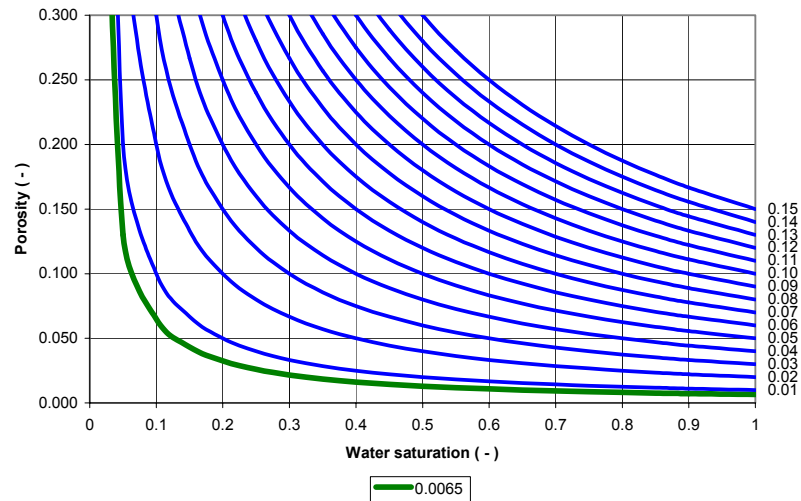


Figure 4-35: A typical Buckles plot

Figure 4-35 is an example of the Buckles plot. Porosity is plotted against the water saturation. Porosity is plotted on the ‘Y’ axis with a scale ranging from 0 to 30% porosity (shown in decimals) while Water saturation is plotted on the ‘X’ axis with a scale ranging from 0 to 100% (shown in decimals) water saturation. The blue lines represent lines of constant bulk volume water. The scale for bulk volume water lines (blue lines) ranges from 0.01 to 0.15 and is shown as a secondary ‘Y’ axis. The green line (value 0.0065) is also a bulk volume water line that is used to demarcate between the reservoir and transition zones.

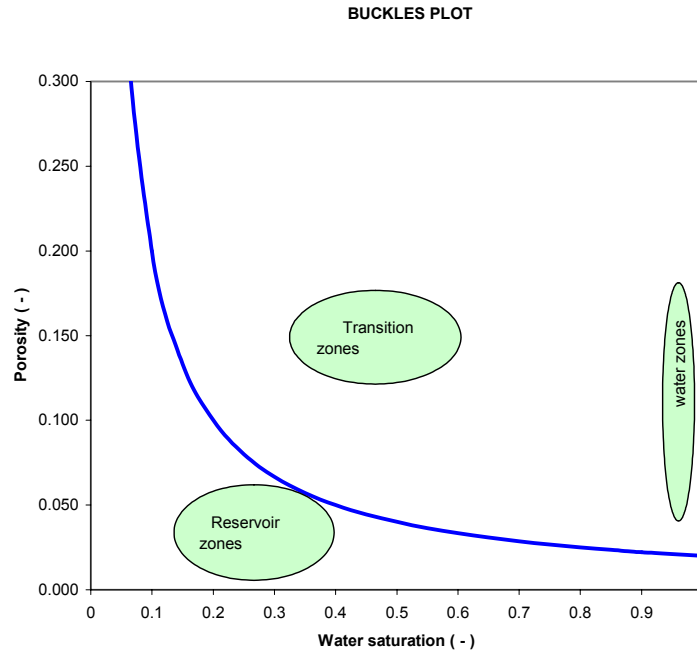


Figure 4-36: Buckles plot showing different zones

The **Figure 4-36** explains a typical Buckles plot. The implicit assumption in the Buckles plot approach is that the product of irreducible water saturation and porosity is constant. The region closest to the blue line (bulk volume water line) is considered to be the reservoir zones, since they contain irreducible water saturation. The regions above and away from the blue line are considered as the transition zones and the regions close to 100% water saturation are considered as the water zones. This type of analysis is useful in traditional oil reservoirs to identify oil zones and water zones. The well will be completed in the oil zone to minimize the water production. In West Carney Hunton Field, however, such traditional approach will not work since water is present and is mobile in all parts of the reservoir.

The **Figure 4-37** shows Buckles plot constructed to explain the unusual behavior of the West Carney Hunton Field. The reservoir is considered to have two zones: the original oil zone and the invaded zone. The invaded zone represents the invasion of water subsequent to oil accumulation.

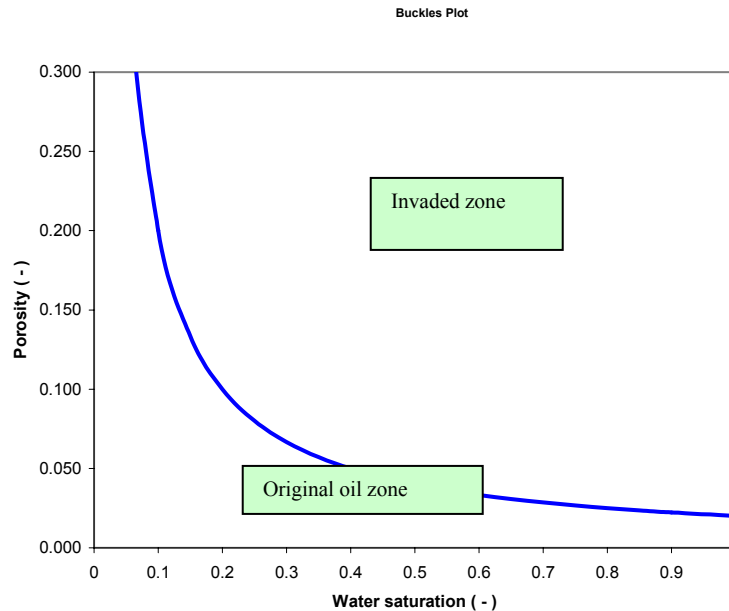


Figure 4-37: Buckles plot showing different zones present in the West Carney Hunton Field

The geological pore types were plotted individually and in combination with one another and the best match was obtained on combining the coarse matrix and the vugs together and the fine matrix and the fractures together. Geological core descriptions also confirm that in most cases the fine matrix rock is fractured. Hence, we decided to combine the fine and fractured pore type together, and the coarse and the vuggy pore types together.

At this point, as we discuss the Buckles plots, we would like to comment on the wettability of the West Carney Hunton Field reservoir rock and also refer to some of the unique characteristics of the reservoir.

The West Carney Hunton Field reservoir rock was originally thought to be water wet. The oil migrated into the reservoir and was trapped in place for a very long time. The oil migrated preferably to the larger pores and vugs. In due course, the wettability of the West Carney Hunton Field began to change to oil wet. Oil began to enter the smaller pores and displaced the water. During the later stages of geological time, water migrated into West Carney Hunton Field and selectively entered larger pores and vugs because of oil wet characteristics. Oil remained trapped in the smaller pores. This is seen in Buckles plots, which show the fine matrix rock to be coincident with irreducible water saturation, whereas, coarse matrix rock to be in the invaded zone.

Figure 4-38 shows the Limestone vug and coarse matrix pore type data plotted on a Buckles plot.

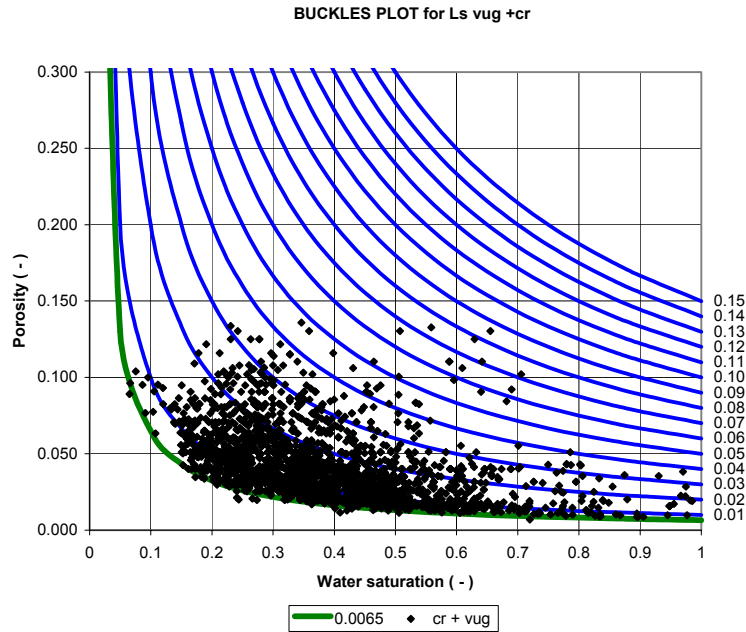


Figure 4-38: Buckles plot for Limestone with coarse matrix and vuggy pore types; Legend cr = coarse matrix

Figure 4-39 shows Limestone fine matrix and fracture pore type data plotted on a Buckles plot.

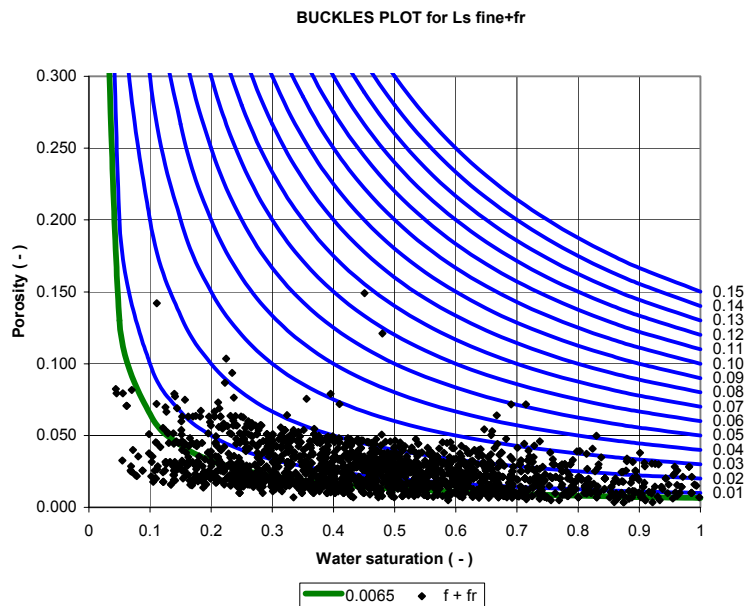


Figure 4-39: Buckles plot for Limestone with Fine matrix and Fracture pore types; Legend f= fine matrix and fr= fracture

By reviewing the two plots shown above, we can see that the rock having fine matrix and fracture pore types are representing the irreducible water saturation, and the rock with coarse matrix and the vuggy pore types are representing the invaded zones along with some reservoir zones.

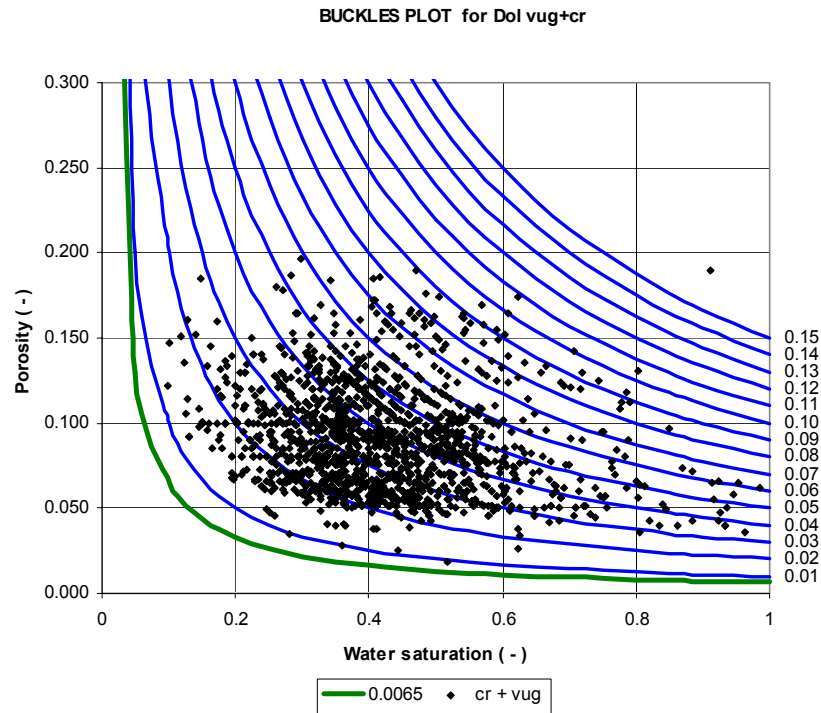


Figure 4-40: Buckles plot for Dolomite and partly dolomitized limestone with coarse matrix and vuggy pore types; Legend cr= coarse matrix

Figure 4-40 shows the coarse matrix and vuggy pore types for dolomite and partly dolomitized limestone. **Figure 4-40** suggests that the coarse matrix and the vugs contain water. The Buckles plot with fine matrix and fracture pore types for dolomite and partly dolomitized limestone did not show us the expected results. That is, the data did not fall on a constant bulk volume water line. Hence, we could not establish a good relationship between the static and the dynamic data using the geological pore types on Buckles plot.

Hence, a different approach was necessary and an attempt was made using electrofacies instead of the pore types for establishing a good relationship between the static and the dynamic data.

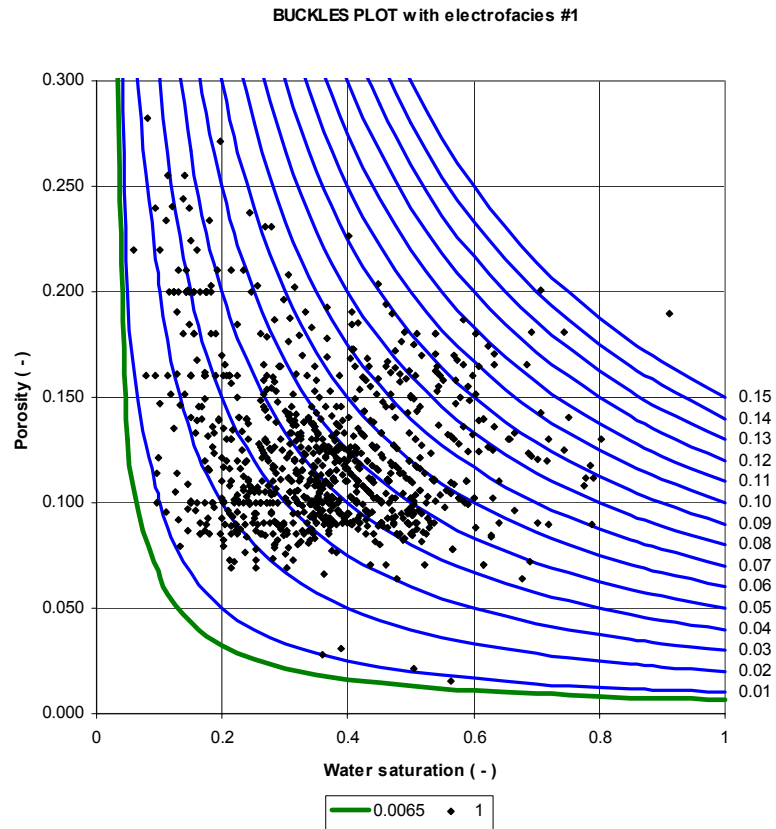


Figure 4-41: Buckles plot with electrofacies # 1

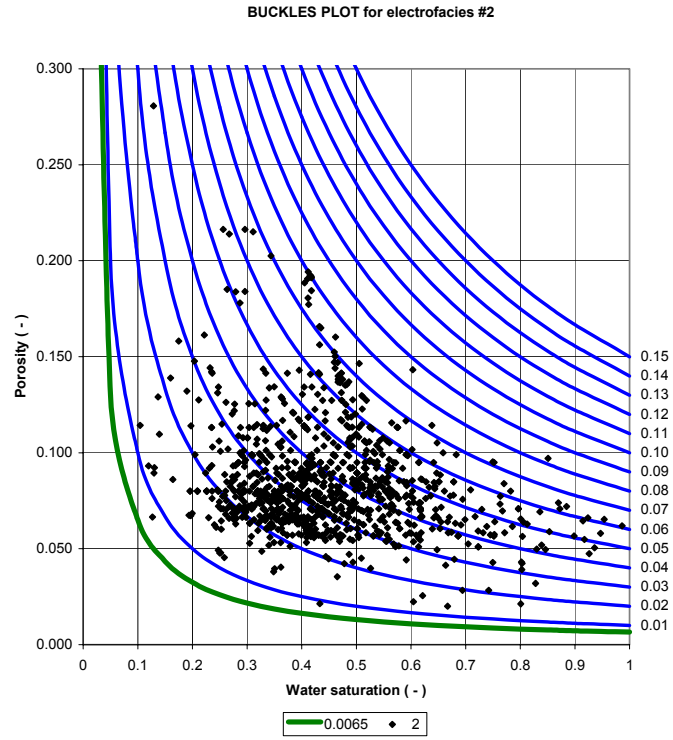


Figure 4-42: Buckles plot with electrofacies # 2

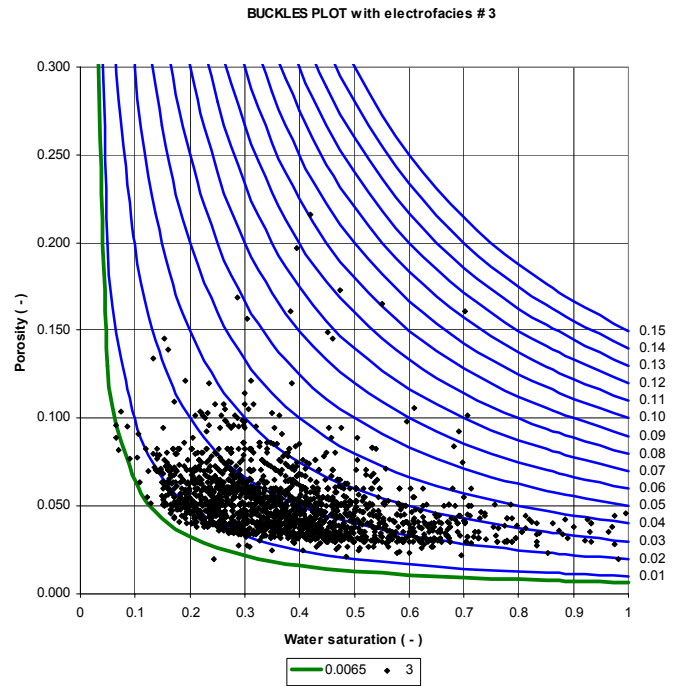


Figure 4-43: Buckles plot with electrofacies # 3

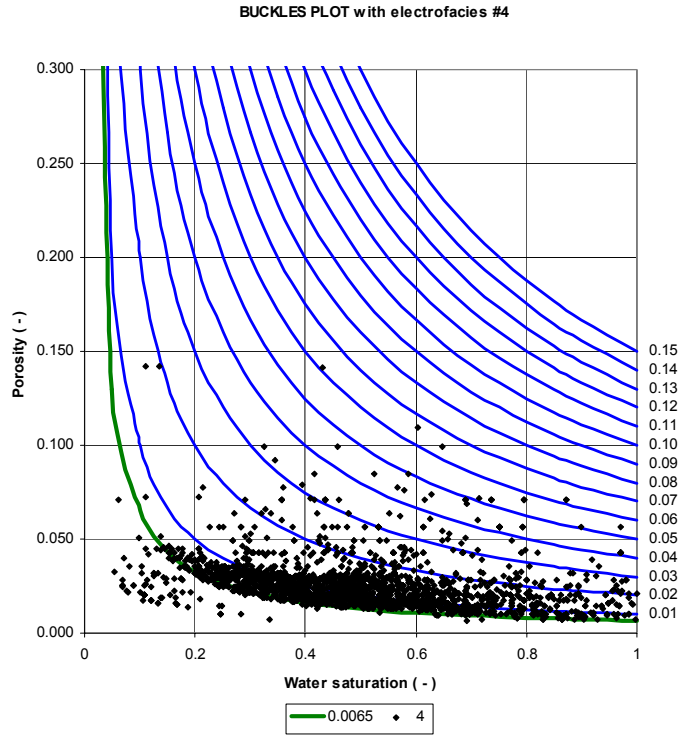


Figure 4-44: Buckles plot with electrofacies # 4

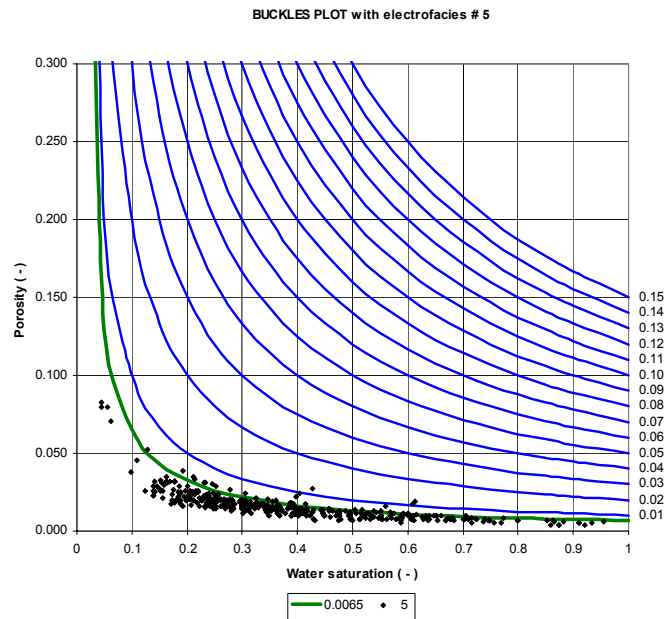


Figure 4-45: Buckles plot with electrofacies # 5

Observing the Buckles plots with electrofacies, **Figure 4-41** through **Figure 4-45**, we see that as we go from electrofacies #1 to #5, we move from the invaded zone to the original oil zone. Electrofacies analysis shows better differentiation between the original oil and invaded zones as compared to the geological pore types. Electrofacies 4 and 5 mainly represent fine matrix and fracture pore types. Water did not invade the fine matrix, the bulk volume saturations is constant in those two facies. The porosity is also low. In contrast, electrofacies 1, 2 and 3 mainly represent vugs and coarse matrix pore types. Water has invaded these pores, bulk volume saturations vary in these three facies. The porosity is also high.

4.3.1.4.3. Hydrocarbon Mapping

Using all the available log data we computed the hydrocarbons in place for each of the 152 wells from the West Carney Hunton Field considered in our study. Then by interpolation we generated the map shown in the **Figure 4-46**.

Figure 4-46 shows the hydrocarbons in place (Barrels per acre foot), plotted in the area of study, i.e. 15N and 16N Townships with 1E, 2E and 3E Ranges; sections 5, 6, 7, 8, 17, 18, 19 and 20 in T15N.R3E, sections 1 to 24 in T15N R2E, sections 1, 2, 3, 10, 11, 12, 13, 14, 15, 22, 23 and 24 in T15N R1E, sections 19, 20, 29 and 30 in T 16N R3E, sections 19 to 36 in T16N R2E and sections 22, 23, 24, 25, 26, 27, 34, 35 and 36 in T16N R1E.

Please note that, hereafter, the area of study in the report refers to the above-mentioned sections from T15N and T 16N, R1E, R2E and R3E.

The hydrocarbons in place for each well were calculated using the equation shown below.

$$\text{BAF} = \{\Sigma[H(\phi - \text{BVW})] * 43560\} / \{\text{Ht} * 5.615$$

Equation 4-3

Where,

BAF = Barrels per acre-foot

ϕ = porosity

BVW = Bulk volume water ($\phi * S_w$)

Ht = Hunton thickness

H = unit thickness represented by a data point (note that for each well Ht = ΣH)

S_w = Water saturation.

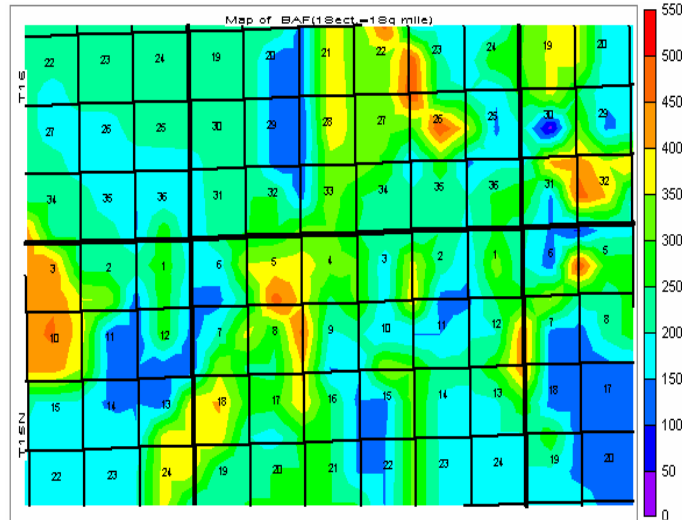


Figure 4-46: Distribution of Hydrocarbons in place (Barrels per acre foot) in the area of study

4.3.1.4.4. Electrofacies mapping

Each of the 152 wells considered in the study comprised of varying proportions of electrofacies, with some wells showing dominance of a certain electrofacies while some of the electrofacies were absent in some wells. The Pickett plots and the Buckles plots with the electrofacies helped us to understand the static data to some extent, but did not help to establish a very good relationship between the static and the dynamic data. Hence we tried the mapping the electrofacies and relating the same with the map of hydrocarbons in place.

Figure 4-47 and **Figure 4-48** show the electrofacies distribution maps generated for the area of study. The proportion of each electrofacies in all of the 152 wells was calculated and mapped. **Figure 4-47** shows the proportion of electrofacies 1,2 and 3 while **Figure 4-48** shows the proportion of electrofacies 4 and 5.

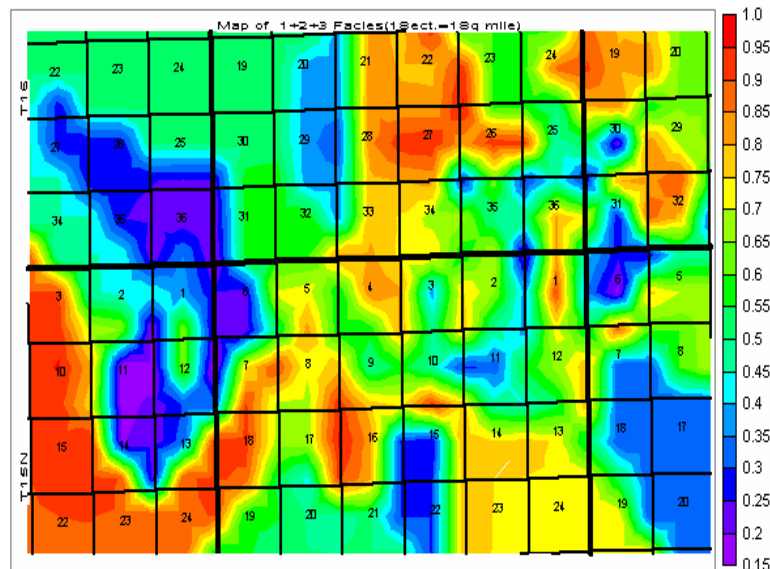


Figure 4-47: Distribution of electrofacies 1+2+3 in the area of study

The color scale ranges from 15% (violet) to 100% (red) shown in decimals. Higher percentages indicate dominance of electrofacies 1+2+3.

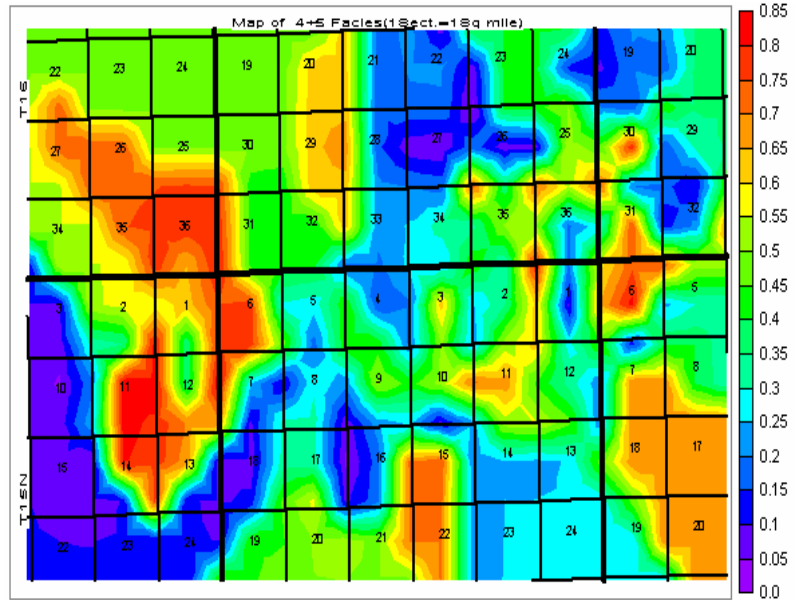


Figure 4-48: Distribution of electrofacies # 4+5 in the area of study

The color scale ranges from 0% (violet) to 85% (red) shown in decimals. Higher percentages indicate dominance of electrofacies 4+5

Comparison of the hydrocarbons in place map with the electrofacies maps show that the map showing the distribution of electrofacies 1+2+3 bears the exact pattern as the hydrocarbons in place map; such that all the areas in showing high values of hydrocarbons in place, show high proportions of electrofacies 1+2+3 and all the regions showing low concentrations of hydrocarbons show high proportions of electrofacies 4+5. There is a clear correlation between the presence of hydrocarbons and electrofacies 1+2+3.

4.3.1.4.5. Production mapping

Oil and gas production data for all wells other than those operated by Marjo Oil Company was taken from NRIS, a service provided by Oklahoma Geological Survey. We have mapped the oil and gas production data; water production data has not been mapped due to limited availability. As mentioned earlier in the report, we chose a six-year period to view the production from every well for a similar time period. When the producing life of a well was less than six years, we extrapolated the production using a 50% per year decline rate.

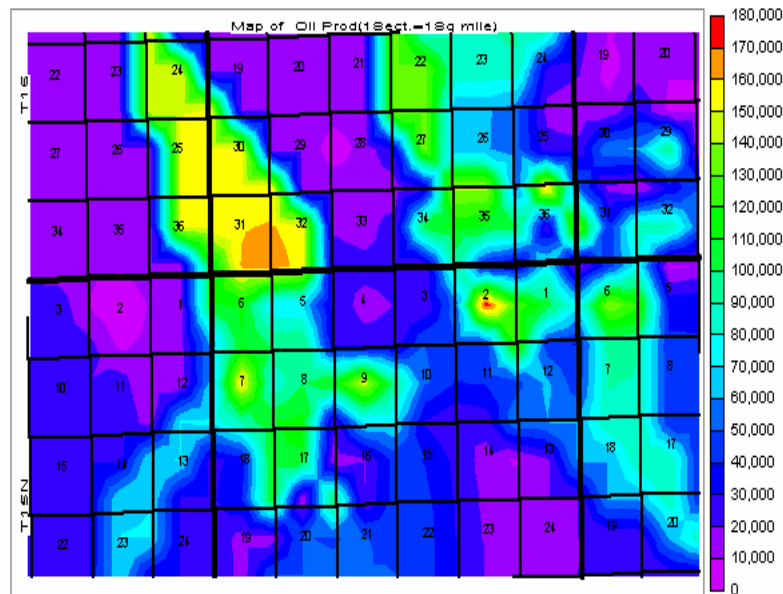


Figure 4-49: Distribution of oil production in the area of study, calculated for a six year period

The color scale ranges from 0 STB (stock tank barrels) to 180,000 STB.

We would like to mention that some of the Leases in the area of study produce from up to three wells and show very high cumulative production.

Hence, the range of scale is too high and does not plot with good resolution. We divided the production by the number of wells in the lease to accommodate for the extremely high values.

We also include a plot showing the log of the cumulative production. By taking the log of the actual values, we honor the production from all the leases in a better way.

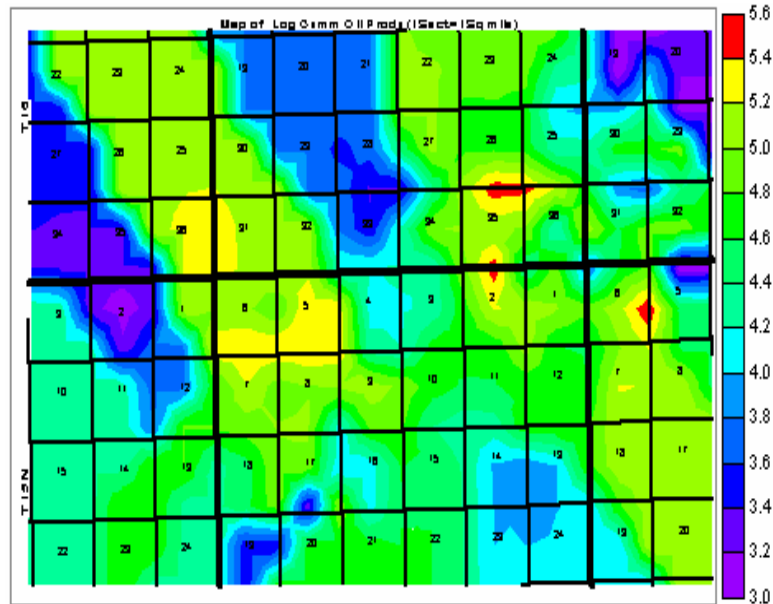


Figure 4-50: Distribution of the cumulative oil production from the area of study, calculated as log of the original production (STB).

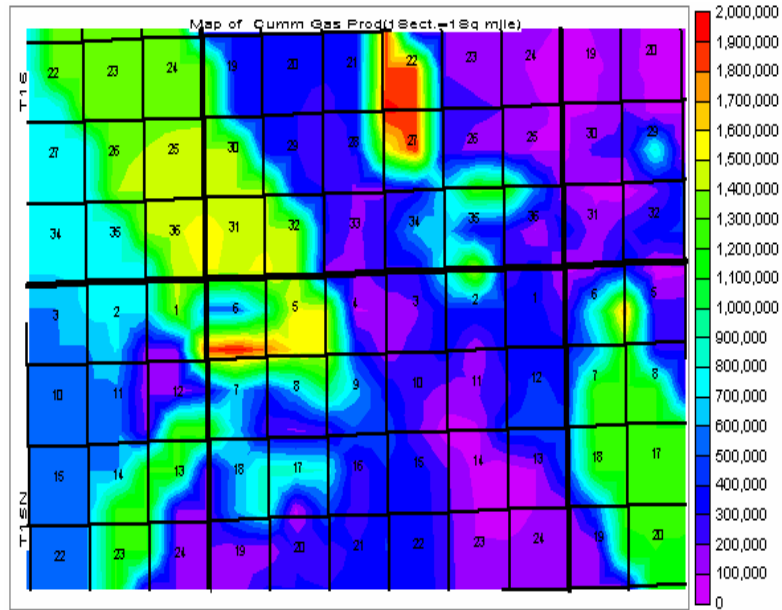


Figure 4-51: Distribution of gas production in the area of study, calculated for a six year period

The color scale ranges from 0 MCF (thousand cubic feet) to 2,000,000 MCF.

Figure 4-52 and **Figure 4-53** show BAF mapped separately for electrofacies # 1+2+3 and for electrofacies # 4+5.

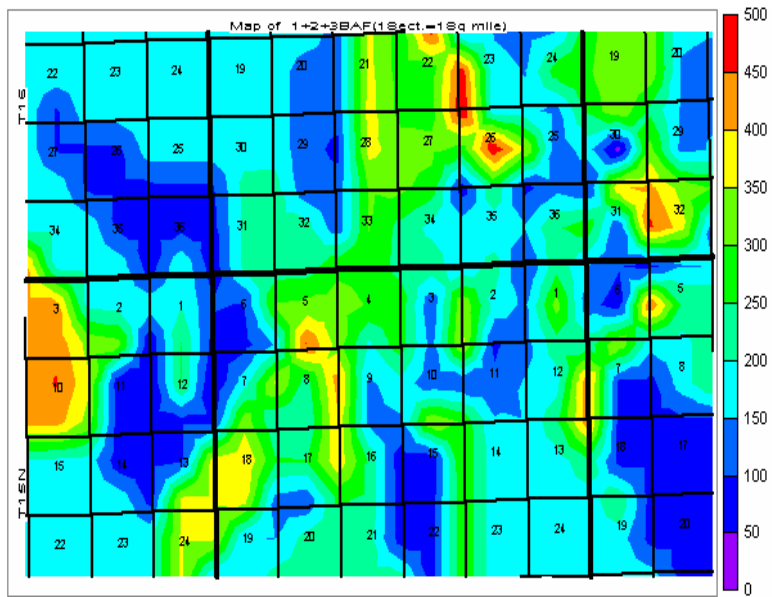


Figure 4-52: Distribution of hydrocarbons in place (BAF) for the electrofacies # 1+2+3 in the area of study

The color scale ranges from 0 (violet) BAF to 550 (red) BAF (Barrels per acre foot).

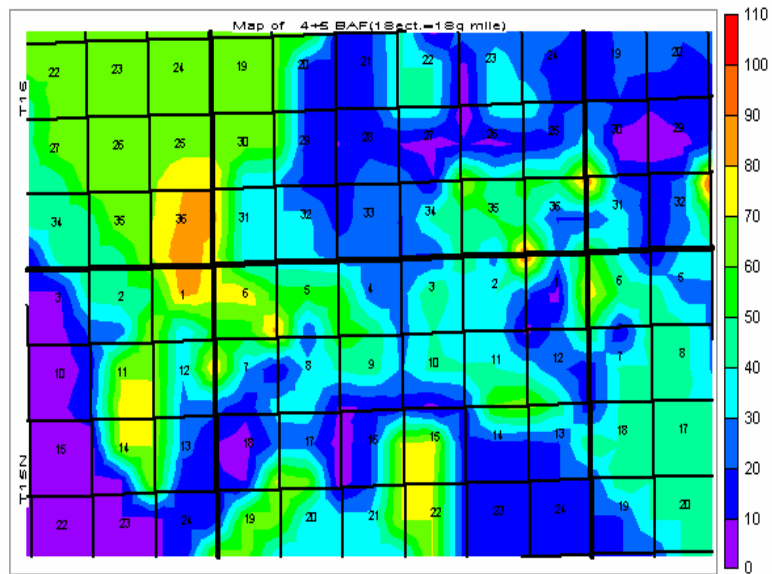


Figure 4-53: Distribution of hydrocarbons in place (BAF) for the electrofacies # 4+5

The color scale ranges from 0 (violet) BAF to 110 (red) BAF (barrels per acre foot).

By comparing **Figure 4-49** and **Figure 4-51**, a clear correlation exists between oil and gas production. This indicates that oil and gas are stored together, and high oil production also indicates high gas production.

The Cumulative oil and gas production maps shown above have a good correlation with the map showing the distribution of electrofacies #4 and 5. This proves that oil recovery has been good in regions where the concentration of electrofacies #4 and 5 is high. This also shows that even though the electrofacies #1, 2 and 3 show high accumulation of hydrocarbons in place (refer to **Figure 4-47**, **Figure 4-49**, and **Figure 4-51**), they do not seem to contribute to the production. The hydrocarbons present in the invaded zone, regions represented by electrofacies 1, 2 and 3, are in isolated globules. It is very difficult to produce them. On the other hand, hydrocarbons present in the original oil zones, regions represented by electrofacies #4 and 5, are well connected by the fracture framework and yield good production. These results are also consistent with our model demonstrating that oil and gas occur together and are present in the fine pores. Fracture systems seem to be the key factor for good production and wells with electrofacies # 4 and 5 show good production.

4.3.1.4.6. Comparison of the Static data with the Dynamic data

As mentioned earlier, 27 wells operated by Marjo Oil Company were considered for this study. Wells were ranked based on their oil production; proportion of electrofacies 1+2+3 and 4+5, productivity calculated using the 1st, 5th and 10th percentile permeability values. These static parameters

were plotted against the production rates, the only good correlation that we observed was the one shown in the figure below.

Figure 4-54 shows the ranks of K^*H calculated using 1st percentile k values plotted against the water rate. The ranks are plotted in decreasing order on both the axis. We can see from the plot that there is a good correlation between the K^*H and water production. The graph is divided into two distinct groups, one of which represent the earlier wells in the field, called the first generation wells and the other group represents the later wells in the field, called the second generation wells. We see that the first generation wells show better ranking in terms of water production than the second generation wells; that is, the first generation wells produced more water than the second generation wells. Hence, we can conclude that the field has a limited aquifer and the newer wells have lesser access to water, as it has have been produced by the earlier wells in the field.

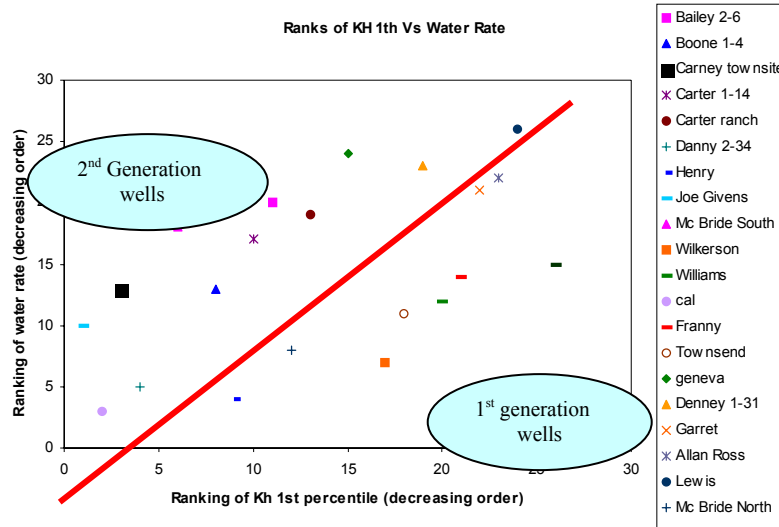


Figure 4-54: Plot of the rank of wells based on water production vs. K^*H . The K^*H has been calculated using 1st percentile K values (228 md). The ranks are plotted in decreasing order, rank 1 corresponds to the best and rank 27 corresponds to the worst.

4.3.1.4.7. Prediction of In-fill well Locations

One of the main aims of this study is to be able to devise a methodology to successfully predict the in-fill well locations from the static data characteristics. Although definitive conclusions may not be possible, some general observations can be made based on the current understanding:

- a. Wells that go on vacuum when treated seem to be good producers. Hence, the time a well takes to go on vacuum after treated is considered to be the best indicator to predict the performance of a well. With few exceptions, if the well goes on vacuum quickly, they are good producers.

Table 4-11 shows some of the wells operated by Marjo Oil Company and the time they took to go on vacuum.

Table 4-11: Time taken by some of the wells to go on vacuum after acid treatment

Immediate	< 5 minutes	< 15 minutes	Never
Alan ross	Franny	Carney townsite 2	Boone
Bailey	Mc Bride North	Danny 2	Cal
Townsend	Schwake	Wilkerson 1	Henry
Joe givens	Wilson	Denney 1	Garrett
Carter	Lewis	Geneva 1	Williams

All the wells that went on vacuum within 15 minutes after they were treated were good producers, except the anomalies which are highlighted. The wells those never went on vacuum are either below average producers or bad producers. Carter and Lewis are anomalies, probably the reason being a limited aquifer and they had to compete with other wells for good production.

- b. Recognition of the fractured zones from the logs could also be one of the key issues to the prediction of a good producer. It has been evident in almost all cases that a well connected well eventually ends up being a good producer. The fracture system has given a very good connectivity network to the field. Hence its very important to recognize the fractures. Unfortunately, we do not have any logs that give us quantitative information about the presence or the extent of fractures. We have to use some qualitative methods to infer the presence of fractures, some of them being the close examination of the separation between the deep and the medium resistivity curves, the caliper curve, the density correction curve. All these would give us some indications of highly porous and permeable zones, which could be thought to be fractures. However, we do not have any quantitative way to compute this information.

- c. Presence of substantial proportions of certain electrofacies. In **Figure 4-48**, **Figure 4-49**, and **Figure 4-51**, we see a good correlation of the cumulative oil and gas production with the presence of electrofacies #4 and 5. We suspect that occurrence of electrofacies #4 and 5 could be the key to good production. One definite conclusion that we draw from this study is that regions, which show high accumulations of hydrocarbons based on calculations from log data, are not always the regions where the wells have been successful producers.

4.3.2. Production Data Evaluation

Jeff Frederick and Mohan Kelkar (The University of Tulsa), Brian Keefer (Marjo Operating Company)

4.3.2.1. Introduction

The West Carney Field initially produced very high water rates and low oil rates, but over time the WOR decreases providing for an increase in the oil rate. The water rate slowly declines and eventually goes to zero in some cases. High water rates result in high lifting costs, so a good estimate of reserves is needed to determine the economic feasibility of the field. With this strange behavior, however, conventional methods for estimating reserves and reservoir parameters (permeability and skin) can no longer be calculated with confidence.

A new production decline method is needed to accurately estimate reserves and reservoir parameters to adequately develop and exploit the West Carney Field. Because the wells are produced at variable bottomhole pressures and variable rates, we have used an equivalent time approach presented by Agarwal *et al.*²⁰. We introduces the use of automatic type curve matching using the Levenberg-Marquardt algorithm. It will be shown, using synthetic data as well as one field example, that using Agarwal *et al.*'s equivalent time and nonlinear regression type curve matching can yield extremely useful results. The production for the three fluids is analyzed separately, allowing for reserve, permeability, and skin estimates for each of the three fluids.

4.3.2.2. Background

Liquid Solutions

Four different solutions are used to analyze radial homogeneous reservoirs in this report: constant pressure production and constant rate production for an infinite reservoir, as well as constant pressure production and constant rate production for a bound reservoir. All of these solutions are derived from the radial diffusivity equation for a radial homogeneous reservoir.

$$\frac{\partial^2 p}{\partial r^2} + \frac{1}{r} \frac{\partial p}{\partial r} = \frac{\phi \mu c}{k} \frac{\partial p}{\partial t}$$

Equation 4-4

First, constant rate production for an infinite reservoir will be discussed. The boundary conditions and initial condition for this case are given in **Equation 4-5**, **Equation 4-6**, and **Equation 4-7** respectively.

$$p(r \rightarrow \infty, t) = p_i$$

Equation 4-5

$$r \frac{\partial p}{\partial r}(r = r_{wa}, t) = \frac{141.2q(t)B_l \mu_l}{kh}$$

Equation 4-6

$$p(r, 0) = p_i$$

Equation 4-7

where,

$$r_{wa} = r_w e^{-S_f}$$

Equation 4-8

The dimensionless variables in field units are defined as,

$$t_D = \frac{0.006328kt}{\phi\mu_i c_t r_{wa}^2}$$

Equation 4-9

$$p_D = \frac{kh(p_i - p)}{141.2q(t)B_l\mu_i}$$

Equation 4-10

$$r_D = \frac{r}{r_{wa}}$$

Equation 4-11

Using the dimensionless variables, the partial differential equation, its boundary conditions, and initial condition are normalized and are given in **Equation 4-12**, **Equation 4-13**, **Equation 4-14**, and **Equation 4-15** respectively.

$$\frac{\partial^2 p_D}{\partial r_D^2} + \frac{1}{r_D} \frac{\partial p_D}{\partial r_D} = \frac{\partial p_D}{\partial t_D}$$

Equation 4-12

$$p_D(\infty, t_D) = 0$$

Equation 4-13

$$\frac{\partial p_D}{\partial r_D}(1, t_D) = -1$$

Equation 4-14

$$p_D(r_D, 0) = 0$$

Equation 4-15

Equation 4-12 and its boundary conditions (**Equation 4-13** and **Equation 4-14**) are transformed into Laplace space and solved using methods described by Myers.²¹ The solution in Laplace space is given in **Appendix Section 7.3** as **Equation A-16**.

Next, the solution for constant rate production for a bounded homogeneous radial reservoir is discussed. The first boundary condition is given in **Equation 4-16** and the second boundary condition and the initial condition are given in **Equation 4-6** and **Equation 4-7** respectively.

$$\frac{\partial p}{\partial r}(r = r_e, t) = 0$$

Equation 4-16

The dimensionless variables are given in **Equation 4-9**, **Equation 4-10**, and **Equation 4-11**. Using these dimensionless variables, the partial differential equation, its boundary conditions, and initial condition are normalized and given in **Equation 4-12**, **Equation 4-17**, **Equation 4-14**, and **Equation 4-15** respectively.

$$\frac{\partial p_D}{\partial r_D}(R_{eD}, t_D) = 0$$

Equation 4-17

Equation 4-12 and its boundary conditions (**Equation 4-17** and **Equation 4-14**) are transformed into Laplace space again solved using methods described by Myers. The solution in Laplace space is given in **Appendix Section 7.3** as **Equation A-17**.

Next, the constant pressure solution for an infinite and bounded homogeneous reservoir is discussed. A relationship in Laplace space exists between constant rate and constant pressure solutions to the radial diffusivity equation. This relationship is,

$$\hat{q}_{D,CP}(r_D; s) = \frac{1}{s^2 \hat{p}_{D,CR}(r_D; s)}$$

Equation 4-18

4.3.2.2.1. Gas Solutions

The radial diffusivity equation used to derive the liquid solutions becomes nonlinear when applied to gas reservoirs. Therefore, it is not possible to generate analytical solutions for gas reservoirs.

Agarwal *et al.* used simulator data to show that the relationship given by **Equation 4-19** holds for both liquid and gas cases, even if the bottomhole pressure is not constant.

$$q_{D,CP}(t_D) = \frac{1}{p_{D,CR}(t_{eD})}$$

Equation 4-19

$q_{D,CP}(t_D)$ is the dimensionless constant pressure solution evaluated at a dimensionless time given by **Equation A-26** or **Equation A-27** in **Appendix Section 7.3** and $p_{D,CR}(t_{eD})$ is the dimensionless constant rate liquid solution evaluated at a dimensionless time given by **Equation A-24** or **Equation A-25** in **Appendix Section 7.3**. Agarwal *et al.* defined the equivalent time for liquid as,

$$t_{eL}(t) = Q(t) / q(t)$$

Equation 4-20

and the equivalent time for gas as,

$$t_{eG}(t) = \frac{\mu_{gi} c_{gi}}{q(t)} \frac{z_i G_i}{2 p_i} [m(p_i) - m(\bar{p})]$$

Equation 4-21

4.3.2.3. Analytical Framework of Hunton Model

Each well drilled into the Hunton is perforated over the entire thickness of the formation. The oil, gas, and water are produced through these perforations and are separated at the surface. It is assumed that oil and gas are in tight matrix blocks and the water is in fractures. Oil and gas percolate into the fracture network and enter the well via the fractures along with the water. For this preliminary work we use a three-layer no cross-flow system to model the reservoir (see **Figure 4-55**). Based on this model the analysis should give three different permeability values, three different external radius values, and three different skin factor values for each case. Although we may have three-phase, dual porosity flow, as a simplification we are going to assume that:

- A. Analysis of water rate as a function of time will predominantly provide us with:
 - a. Aquifer size
 - b. Aquifer permeability (fracture permeability)
 - c. Skin factor associated with water zone
- B. Analysis of oil and gas rates as a function of time will predominantly provide us with:
 - a. Hydrocarbon zone size relative to the water zone (oil or gas)
 - b. Hydrocarbon zone permeability (oil or gas)
 - c. Skin factor associated with hydrocarbon zone (oil or gas)
- C. Dual porosity reservoir can be approximated by a layered no cross-flow model.

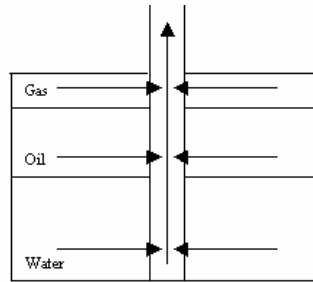


Figure 4-55: Three-layer no cross-flow model

4.3.2.3.1. Procedure

There are a number of calculations involved in determining the external radius, as well as permeability, and skin factor. For this reason a computer program based in Visual Basic was written to provide results quickly and in the case of permeability and skin, automatically. The program uses material balance calculations to determine the external radius and nonlinear regression to calculate permeability and skin. The estimate of external radius allows for the estimation of recoverable oil or recoverable gas. These results, combined with electric log derived saturations at the well provide an estimate of the recovery factor (RF). The values of permeability and skin factor are obtained (if sufficient early time data is present) by using nonlinear regression to minimize the objective function,

$$E(t) = q(t) - q_{\text{model}}(t)$$

Equation 4-22

where for liquid,

$$q_{\text{model}}(t) = [q_{D,CP}(t_D)] \frac{kh(p_i - p_{wf})}{141.2\mu_l B_l}$$

Equation 4-23

and for gas,

$$q_{\text{model}}(t) = [q_{D,CP}(t_D)] \frac{kh[m(p_i) - m(p_{wf})]}{1422(T + 460)}$$

Equation 4-24

where $q_{D,CP}(t_D)$ is obtained using **Equation 4-19** where $p_{D,CR}(t_{eD})$ is evaluated in Laplace space and numerically inverted into real space using the Stehfest inverter.²²

The values of permeability and skin factor have been constrained to prevent convergence on impractical values. The procedures used to constrain the parameters and to minimize the objective function can be found in Carvalho *et al.*'s papers (SPE 24732²³ and SPE 29582²⁴ respectively).

4.3.2.3.2. Liquid Production (Oil or Water) Calculation Procedure

The following is a step-by-step process of the calculations to determine the external radius, permeability, and skin factor for liquid production.

1. Generate t_{eL} using **Equation A-1** and the known $Q(t)$ and $q(t)$ values.
2. Plot $q(t)$ vs. t_{eL} on a log-log plot and determine when the pss (pseudo-steady state) period begins (see **Figure 4-56**).
3. Estimate r_e , k , and s_f .
4. Generate q_{DdL} and Q_{DdL} values using only pss data and the estimate of r_e , k , and s_f from **Equations A-4** and **Equations A-5** respectively.

5. Make a plot of q_{DdL} and Q_{DdL} (see **Figure 4-57**). From the relationship of q_{DdL} and Q_{DdL} given by **Equation A-6** the x-intercept should be 1. If it is not, refine the guess of r_e and proceed back to step 4, otherwise continue to step 6.
6. Calculate recoverable oil (N_{pmax}) using **Equation A-7**.
7. Calculate RF_{oil} or RF_{water} from **Equation A-8** or **Equation A-9** respectively.
8. Calculate t_{eDL} using **Equation A-24**.
9. Evaluate **Equation A-20** or **Equation A-21** at t_{eDL} . The Laplace solution is numerically inverted into real space using the Stehfest inverter.
10. Calculate $q_{D,CP}(t_D)$ using **Equation 4-19**.
11. Calculate the objective function, $E(t)$, using **Equation 4-22** and **Equation 4-23**.
12. Use Levenberg-Marquardt algorithm to minimize the objective function.

4.3.2.3.3. Gas Production Calculation Procedure

The following is a step-by-step process used to calculate the external radius, permeability and skin factor for gas production.

1. Generate a table based on gas properties containing pressure values and the corresponding $m(p)$, μ , c_g , z , and p/z values.
2. Estimate r_e , k , and s_f .
3. Calculate G_i using **Equation A-30** and the estimate of r_e .
4. Generate t_{eG} using **Equation A-2**.
5. Plot $q(t)$ vs. t_{eG} on a log-log plot and determine when the pss period begins (see **Figure 4-59**).

6. Generate q_{DdG} and Q_{DdG} values using only pss data and the estimate of r_e , k , and s_f from **Equation A-10** and **Equation A-11** respectively. To obtain a value for $m(\bar{p})$ needed to calculate Q_{DdG} do the following:
 7. Calculate \bar{p}/\bar{z} using **Equation A-33** and the value of G_i calculated in step 3.
 8. Interpolate from the table generated in step 1 to find $m(\bar{p})$ at \bar{p}/\bar{z} .
 9. Make a plot of q_{DdG} and Q_{DdG} (see **Figure 4-60**). From the relationship of q_{DdG} and Q_{DdG} given by **Equation A-12** the x-intercept should be 1. If it is not, refine the guess of r_e and proceed back to step 3, otherwise continue to step 8.
 10. Calculate recoverable gas (G_{pmax}) by doing the following:
 11. Calculate $m(\bar{p})$ from **Equation A-13**.
 12. Interpolate from the table generated in step 1 to find \bar{p}/\bar{z} at $m(\bar{p})$.
 13. Calculate G_{pmax} using **Equation A-14**.
 14. Calculate RF_{gas} from **Equation A-15**.
 15. Calculate t_{eDG} using **Equation A-25**.
 16. Evaluate **Equation A-20** or **Equation A-21** at t_{eDG} . The Laplace solution is numerically inverted into real space using the Stehfest inverter.
 17. Calculate $q_{D,cp}(t_D)$ using **Equation 4-19**.
 18. Calculate the objective function, $E(t)$, using **Equation 4-22** and **Equation 4-24**.
 19. Use Levenberg-Marquardt algorithm to minimize the objective function.

4.3.2.4. Synthetic Data Example

To test the procedure, as well as the program, two synthetic cases were generated: a liquid case (oil) and a gas case. The liquid case was generated

using constant bottomhole pressure production and the gas case using a reservoir simulator. Both data sets are evaluated using Agarwal *et al.*'s equivalent time and constant rate solutions given by **Equation 4-19** and methods previously outlined.

4.3.2.4.1. Liquid Case

The synthetic oil reservoir and fluid properties are given in **Table 4-12**. The synthetic oil production data is generated using the radial diffusivity equation and constant pressure production (see **Equation 4-19**). The rate vs. t_{eL} plot used to determine where the pss period begins is shown in **Figure 4-56**. The q_{DdL} vs. Q_{DdL} plot used to calculate r_e is shown in **Figure 4-57** and the oil rate vs. time plot is shown in **Figure 4-58**. Nonlinear regression is used to minimize the objective function (see **Equation 4-22**) and compute k and s_f and the results are shown in **Table 4-12**. The results show that the procedure for liquid will converge to the correct values of r_e , k , and s_f .

Table 4-12: Synthetic data as well as calculated results for the synthetic liquid (oil) case

Parameter	Synthetic Data	Calculated Data	Confidence (+/-)	% Difference
r_e (ft)	3000	2,999.999	n/a	0.000%
k (md)	20	20.294	0.007	1.449%
s_f	-3	-2.901	0.001	3.413%
r_w (ft)	1	n/a	n/a	n/a
h (ft)	30	n/a	n/a	n/a
$\bar{\mu}$ (dec)	0.15	n/a	n/a	n/a
P_i (psia)	1300	n/a	n/a	n/a
P_{wf} (psia)	50	n/a	n/a	n/a
$\bar{\mu}$ (cp)	1.1	n/a	n/a	n/a
B_o (RB/STB)	1.16	n/a	n/a	n/a
c_t (psia ⁻¹)	7.00E-06	n/a	n/a	n/a

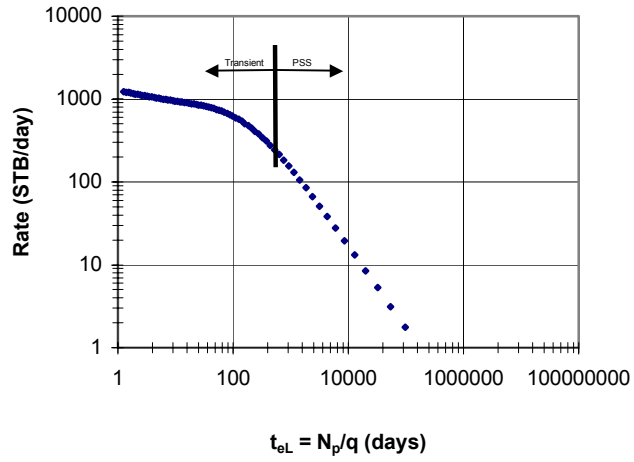


Figure 4-56: Rate vs. t_{eL} plot used to determine where the pss period begins

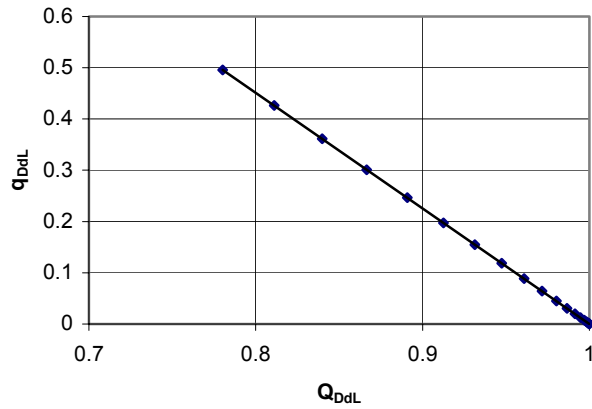


Figure 4-57: q_{DdL} vs. Q_{DdL} plot for synthetic liquid case using only pss data

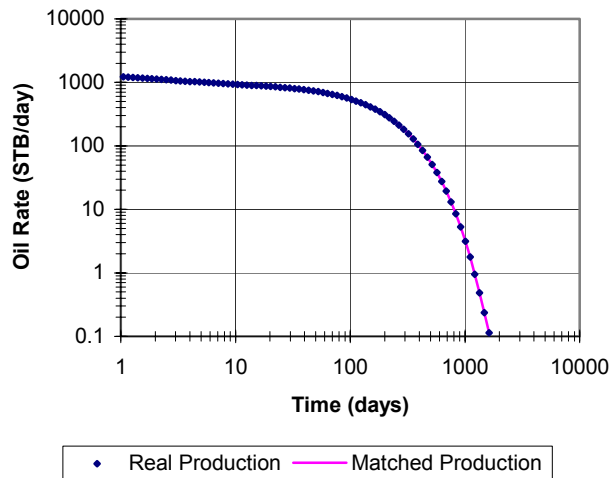


Figure 4-58: Oil rate vs. time plot for the oil synthetic production data as well as the oil production data calculated using the matched reservoir parameters

4.3.2.4.2. Gas Case

Synthetic reservoir and fluid properties for the gas case are given in **Table 4-13**. The synthetic gas production data is given in **Table 4-25**. The q_{DdG} vs. Q_{DdG} plot used to calculate r_e is shown in **Figure 4-60** and the gas rate vs. time plot is shown in **Figure 4-61**. Nonlinear regression is used to minimize the objective function (see **Equation 4-22**) and compute k and s_f . The results are given in **Table 4-13**. The results show that the procedure for the gas case will converge to the correct values of r_e , k , and s_f .

Table 4-13: Synthetic data as well as calculated results for the synthetic gas case

Parameter	Synthetic Data	Calculated Data	Confidence (+/-)	% Difference
r_e (ft)	1490	1,491.363	n/a	0.091%
k (md)	0.5	0.514	0.001	2.724%
sf	0	-0.08	0.019	n/a
r_w (ft)	0.25	n/a	n/a	n/a
h (ft)	100	n/a	n/a	n/a
\bar{q} (dec)	0.1	n/a	n/a	n/a
P_i (psia)	5000	n/a	n/a	n/a
P_{wf} (psia)	893	n/a	n/a	n/a
T (deg F)	200	n/a	n/a	n/a
Gas SG (dec)	0.6	n/a	n/a	n/a
Mol Frac CO2	0	n/a	n/a	n/a
Mol Frac H2S	0	n/a	n/a	n/a

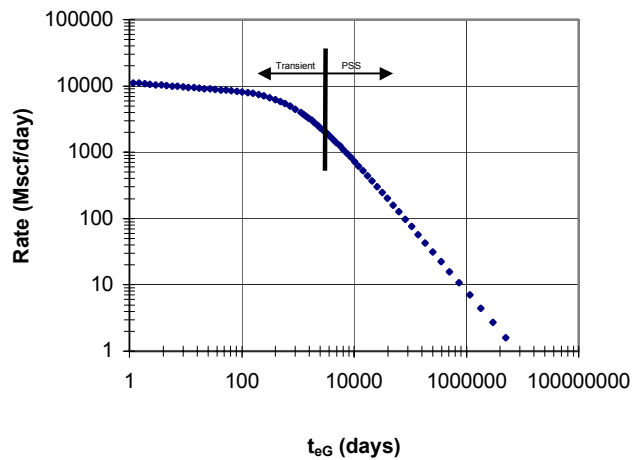


Figure 4-59: Rate vs. t_{eG} plot used to determine where the pss period begins for the gas synthetic data

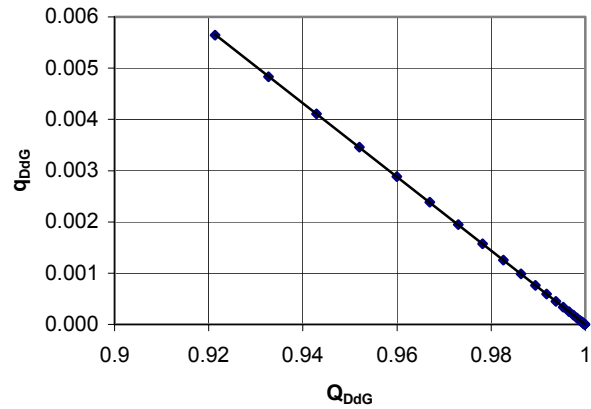


Figure 4-60: q_{DdG} vs. Q_{DdG} plot for synthetic gas case using only pss data

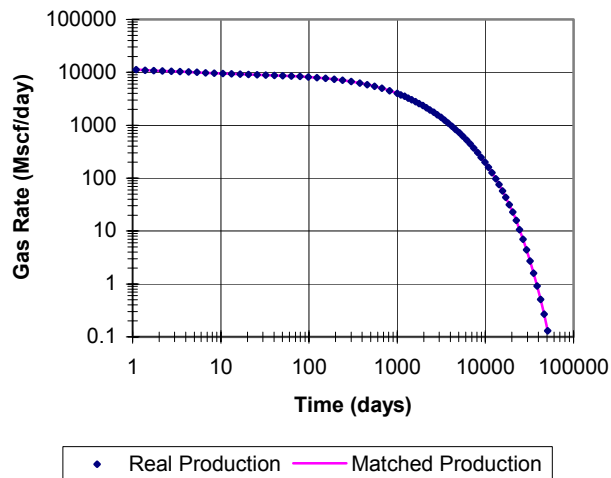


Figure 4-61: Gas rate vs. time plot for the synthetic gas production data as well as the gas production data calculated using the matched reservoir parameters

4.3.2.5. Field Case Example

Now that it has been established that it is possible to calculate r_e and match k and s_f using synthetic data, the program will be tested using a real field case. The well that will be used is the Carter Ranch #2-15. It is currently producing from the Hunton formation in the West Carney Field and the production data

will be analyzed using the approach discussed earlier; each fluid (oil, gas, and water) will be analyzed separately as if it were produced as a single phase from separate layers. For the oil layer the system compressibility is calculated under the assumption that the oil layer has characteristics of a “typical” oil reservoir. It has been calculated using the Vazquez/Beggs correlation for fluid compressibility and the Hall correlation for formation compressibility using the following parameters: API gravity = 43.8, Gas Gravity = 0.8417, Temperature = 110 deg F, reservoir pressure = 1200 psia, GOR = 0.3 Mscf/STB, WOR = 0 STBW/STBO, porosity = 0.0721, water specific gravity = 1.15, and connate water saturation = 0.30. The system compressibility for the water zone is calculated with the same correlations using the following input: reservoir pressure = 1200 psia, porosity = 0.0721, water specific gravity = 1.15, and connate water saturation = 1.0. The estimated values of system compressibility for the oil and water zones can be found in **Table 4-14** and **Table 4-17** respectively.

Estimates for the thickness of the three-layers were determined based on an estimate of water saturation over the entire thickness of the reservoir (28 ft). It was assumed that the water is produced only from the water zone leaving $1 - S_w$ as the hydrocarbon saturation. Furthermore, it was assumed that the oil and gas zones have the same external radius, so the thicknesses of the oil and gas zones were varied until the calculated external radii were about the same. The water and hydrocarbon thicknesses were calculated as $h_{\text{water}} = (h_{\text{total}})(S_w)$ and the hydrocarbon thickness as $h_{\text{oil}} + h_{\text{gas}} = h_{\text{total}}(1 - S_w)$. The estimates of h for the oil, water, and gas layers are given in **Table 4-14** , **Table 4-17**, and **Table 4-20** respectively.

Because it is assumed that the water is produced only from the water layer the initial oil in place (IOIP), given by **Equation A-31** is calculated using $S_w = 0$. Furthermore, the initial water in place (IWIP) given by **Equation A-32** is

calculated using $S_w = 1$. The recovery factors for oil and water (given by **Equation A-8** and **Equation A-9** respectively) are calculated using these estimates for IOIP and IWIP respectively.

Table 4-14: Carter Ranch #2-15 known reservoir and fluid properties input used for the oil production analysis

Parameter	Value	Obtained From
rw (ft)	0.46	Casing Size
h (ft)	10.25	Estimated
μ_{dec}	0.0721	Electric Log
P_1 (psia)	1007	Buildup Test
P_{wf} (psia)	100	Pumping Fluid Level
B_o (RB/STB)	1.231	PVT Data
μ_{cp}	0.81	PVT Data
c_t (1/psia)	1.68E-05	Estimated

Table 4-15: Carter Ranch #2-15 initial estimates and min and max values for permeability and skin factor used for the oil production analysis

Parameter	Initial Estimate	Min	Max
k (md)	1	0.001	50
s_r	-2	-10	5

Table 4-16: Carter Ranch #2-15 calculated reservoir parameters based on oil production rate and core data values

Parameter	Calculated Value	Confidence (+/-)	Core Data		
			Min Value	Median Value	Max Value
r_e (ft)	1,206.225	n/a	n/a	n/a	n/a
N_{pmax} (MSTB)	7.4469	n/a	n/a	n/a	n/a
Recovery Factor	1.524%	n/a	n/a	n/a	n/a
k (md)	1.046	0.117	0.02	1.03	676
s_r	-5.856	0.138	n/a	n/a	n/a

Table 4-17: Carter Ranch #2-15 known reservoir and fluid properties input used for the water production analysis

Parameter	Value	Obtained From
r_w (ft)	0.46	Casing Size
h (ft)	11.6	Estimated
\bar{q} (dec)	0.0721	Electric Log
P_i (psia)	1007	Buildup Test
P_{wf} (psia)	100	Pumping Fluid Level
B_w (RB/STB)	1.012	PVT Data
\bar{q} (cp)	1.12	PVT Data
c_t (1/psia)	7.8E-06	Estimated

Table 4-18: Carter Ranch #2-15 initial estimates and min and max values for permeability and skin factor used for the water production analysis

Parameter	Initial Estimate	Min	Max
k	1	0.001	50
s_r	-2	-10	5

Table 4-19: Carter Ranch #2-15 calculated reservoir parameters based on water production rate and core data values

Parameter	Calculated Value	Confidence (+/-)	Core Data		
			Min Value	Median Value	Max Value
r_e (ft)	4,222.653	n/a	n/a	n/a	n/a
N_{pmax} (MSTB)	58.3291	n/a	n/a	n/a	n/a
Recovery Factor	0.707%	n/a	n/a	n/a	n/a
k (md)	17.687	2.932	0.02	1.03	676
s_r	-4.827	0.558	n/a	n/a	n/a

Table 4-20: Carter Ranch #2-15 known reservoir and fluid properties input used for the gas production analysis

Parameter	Value	Obtained From
r_w (ft)	0.46	Casing Size
h (ft)	6.15	Estimated
β_{dec}	0.0721	Electric Log
P_i (psia)	1007	Buildup Test
P_{wf} (psia)	100	Pumping Fluid Level
γ (air = 1.0)	0.8417	PVT Data
T (deg F)	110	Measured
Mol Frac CO ₂	0	Gas Sales
Mol Frac H ₂ S	0	Gas Sales

Table 4-21: Carter Ranch #2-15 initial estimates and min and max values for permeability and skin factor used for the gas production analysis

Parameter	Initial Estimate	Min	Max
k (md)	1	0.001	50
s_f	-2	-10	5

Table 4-22: Carter Ranch #2-15 calculated reservoir parameters based on gas production rate and core data values

Parameter	Calculated Value	Confidence (+/-)	Core Data		
			Min Value	Median Value	Max Value
r_e (ft)	1,181.232	n/a	n/a	n/a	n/a
G_{pmax} (BCF)	0.14725	n/a	n/a	n/a	n/a
Recovery Factor	92.262%	n/a	n/a	n/a	n/a
k (md)	0.475	0.032	0.02	1.03	676
s_f	-5.637	0.077	n/a	n/a	n/a

The pertinent input data for the oil analysis is available in **Table 4-14** and **Table 4-15**. The monthly production data is used to generate the q_{DdL} vs. Q_{DdL} plot because it eliminates much of the noise associated with daily

production data. The q_{DdL} vs. Q_{DdL} plot for the Carter Ranch is shown in **Figure 4-62**.

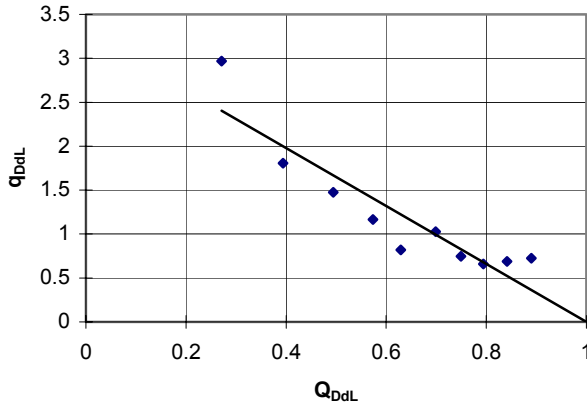


Figure 4-62: *Carter Ranch #2-15 q_{DdL} vs. Q_{DdL} plot for pss oil production used to determine r_e*

Next, the Carter Ranch’s permeability and skin factor based on the oil production are matched and the plot of oil rate vs. time for the real production and the calculated production using the calculated r_e , k and s_f values is shown in **Figure 4-63**. The calculated r_e , N_{pmax} , RF , k , and s_f values are given in **Table 4-16**.

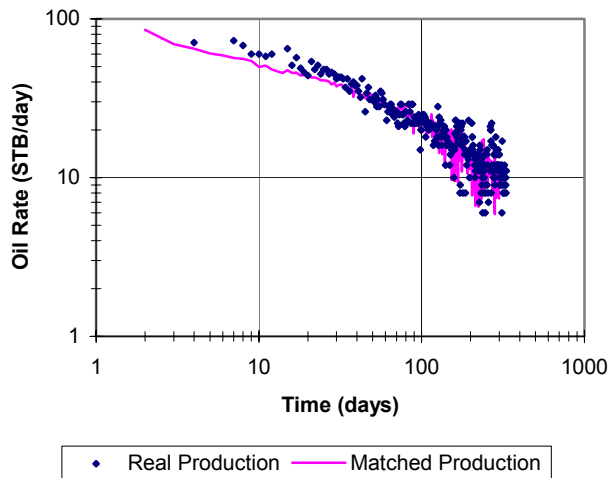


Figure 4-63: *Carter Ranch #2-15 oil rate vs. time plot of the real production data as well as the production data calculated using the calculated values of r_e , k , and s_f*

The input values used for the analysis of the water production are shown in **Table 4-17** and **Table 4-18**. The calculation of the external radius will again be done using the monthly production data because it eliminates much of the noise found when using the daily production. The plot of q_{DdL} vs. Q_{DdL} for the water production is shown in **Figure 4-64**.

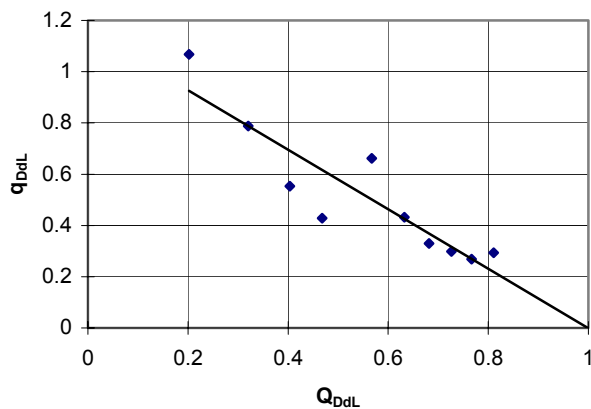


Figure 4-64: *Carter Ranch #2-15 q_{DdL} vs. Q_{DdL} plot for pss water production used to determine r_e*

Next, the Carter Ranch's permeability and skin factor based on the water production are matched and the plot of water rate vs. time for the real production and the calculated production using the calculated r_e , k , and s_f values is shown in **Figure 4-65**. The calculated r_e , N_{pmax} , RF, k , and s_f values are given in **Table 4-19**. When we varied the water layer thickness to a maximum of 28 ft (total zone thickness) we found that r_e was in excess of 3000 ft. The water layer drainage radius is clearly larger than the hydrocarbon layer drainage radius.

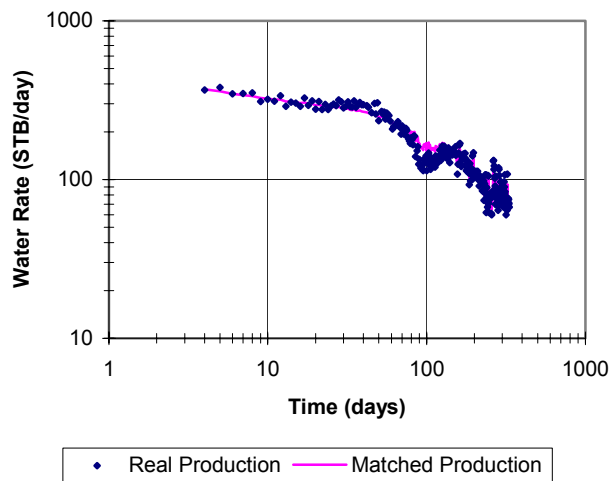


Figure 4-65: *Ranch #2-15 water rate vs. time plot of the real production data as well as the production data calculated using the calculated values of r_e , k , and s_f*

The input values used for the gas analysis are available in **Table 4-20** and **Table 4-21**. Here, the daily gas production will be used to calculate r_e because it is much less noisy than the daily oil and water production. The plot of q_{DdG} vs. Q_{DdG} for the gas production is given in **Figure 4-66**.

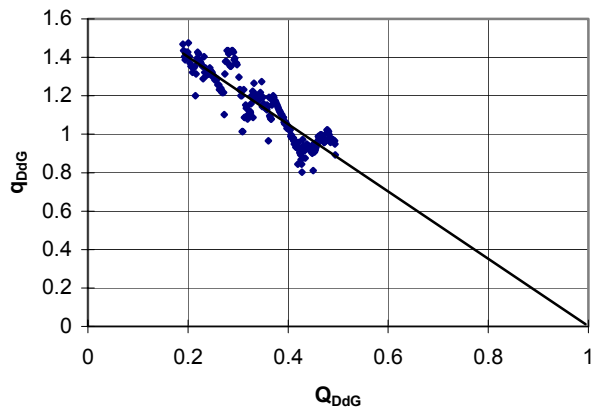


Figure 4-66: Carter Ranch #2-15 q_{DdG} vs. Q_{DdG} plot for pss gas production used to determine r_e

Next, the Carter Ranch's permeability and skin factor based on the gas production are matched and the plot of gas rate vs. time for the real production and the calculated production using the calculated r_e , k and s_f values is shown in **Figure 4-67**. The calculated r_e , N_{pmax} , RF, k , and s_f values are given in **Table 4-22**.

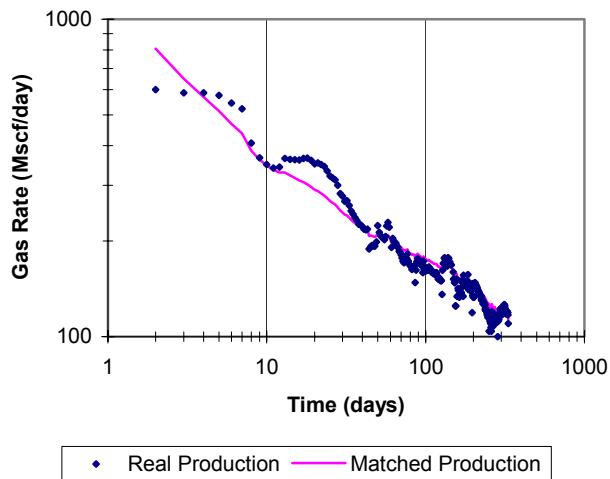


Figure 4-67: Carter Ranch #2-15 gas rate vs. time plot of the real production data as well as the production data calculated using the calculated values of r_e , k , and s_f

4.3.2.6. Analysis of Results

The results of this analysis are consistent with well data and the reservoir model. For example, the skin factors for each case are very similar ($s_{f,oil} = -5.856$, $s_{f,water} = -4.827$, $s_{f,gas} = -5.637$) which is expected since the Carter Ranch #2-15 was acid fractured.

Also, the external radius values computed are consistent with field observations. The Carter Ranch #2-15 is spaced on a 160-acre unit, which should give it an external radius of about 1490 ft, but the calculated oil and gas external radii are less than this ($r_{e,oil} = 1206.225$ ft and $r_{e,gas} = 1181.232$ ft) whereas the water radius is much higher ($r_{e,water} = 4222.653$ ft). Based on field observations it is obvious that the wells are draining a radius greater than that of 1490 ft because pressure depletion is observed when new wells are drilled in adjacent 160 acre units. While the calculated radii of the oil and gas zones are not the true radii (based on previous assumptions), the calculated radii give us an idea of the size of the oil and gas zones relative to the water zone.

It was observed that the calculated external radius is highly dependent on the system compressibility value used for the calculations. Therefore, a good estimate of c_t is required to obtain reasonable results for r_e .

The negative skin factor values provide a good tool for determining the effectiveness of the completions. The calculated skin factor values for the Carter Ranch #2-15 indicate a successful primary acid job. A larger job for this well was probably not necessary. Using skin factor data from previous completions will aid in the design of future acid jobs.

The estimates of r_e and N_{pmax} (or G_{pmax}) can provide a way of calculating a recovery factor. This recovery factor data can then be correlated back to electric log signatures to help direct future field developments and infill drilling.

4.3.2.7. Conclusions

1. It is possible to determine r_e using the material balance calculations discussed. Furthermore, it is possible to use automatic type curve matching using Agarwal *et al.*'s equivalent time method to match values of permeability and skin factor.
2. The results of the field case are consistent with our analytical model of the West Carney Field.
3. The results for skin factor provide a useful tool for analyzing the effectiveness of our completions and will help us effectively design acid jobs in the future.
4. The external radius results can be used along with electric log derived saturations to determine the hydrocarbon reserves and recovery factors for oil and gas. This will allow us to adequately develop and exploit the West Carney Field.
5. The results of this model can be used as a reference for future analysis using other reservoir models.

4.3.3. Laboratory Testing of Cores

4.3.3.1. Methodology

The objective of this part of the work was to determine wettability and relative permeability. The wettability was determined by the standard Amott technique. The relative permeability was determined by the unsteady state

method in the native state. In addition, thin sections and mercury porosimetry were conducted to determine the pore structure.

Core plugs, as received, were scanned by a CT scanner to detect vugs and fractures. Samples without visible fractures were chosen for core analysis. Dead reservoir crude oil was injected into each core with some back pressure (~500psig) to remove all gas. The absolute permeability of the core was determined at this stage. The oil pore volume was determined by a tracer test. The tracer used with the reservoir oil was iododecane. The cores were not cleaned at this stage, so as not to alter original wettability.

For wettability, a core plug was placed in an Amott imbibition cell filled with brine after the determination of initial oil pore volume. The amount of oil expelled from the core was monitored as a function of time. After spontaneous brine imbibition ceased, brine was injected into the core (as a part of the imbibition relative permeability test) and the production of oil was monitored. The brine pore volume was then determined by a tracer method. The tracer used with brine was sodium iodide. The plug was then placed in an imbibition cell filled with reservoir dead oil. Amount of spontaneous oil imbibition was monitored. After the cessation of oil imbibition, the core was flooded with reservoir dead oil and water production was monitored (as a part of drainage relative permeability test). The amounts of spontaneous and forced imbibitions are used in calculation of Amott wettability index.

For imbibition relative permeability, cores were waterflooded at room temperature and pressure after the spontaneous water imbibition step. Pressure drop and effluent oil cut were monitored. JBN analysis was used to extract the imbibition relative permeability. An oil flood was conducted after the spontaneous oil imbibition step to determine the drainage relative

permeability. Pressure drop and effluent oil cut were again monitored. JBN analysis was also used to extract the imbibition relative permeability.

After the wettability and relative permeability tests, the cores were weighed and then extracted in a Dean-Stark extractor. This extraction gave the brine volume. The brine volume obtained from Dean Stark extraction was checked against that expected, from experiments and tracer tests and a reasonable match was obtained in most of the cases. The core was then vacuum dried. The difference between the dry weight and the saturated weight gave the fluid weight. The oil volume was calculated from the difference between the total fluid volume and the brine volume. Porosity and air permeability of the dry core were measured. A part of this core was then used for thin sectioning and another part was used for mercury porosimetry.

4.3.3.2. Results

The cores analyzed are listed in **Table 4-23**. The diameter of the cores was about 2 inches while the length of most of the cores was around 3 inches. They are all limestone except for core 8, which is a dolomite. Cores 1 and 2 were put on a composite and relative permeability of the composite was determined. Core 3 was used for relative permeability where as its adjacent core (Core 4) was used for Amott wettability determination. It was observed that the spontaneous imbibition is low in these cores. In Core 5, spontaneous imbibition is first measured and then relative permeability is measured during the forced imbibition test. Thus both Amott wettability and relative permeability are measured on the same core. Cores 6 and 7 were found to be fractured. Thus relative permeability and wettability tests could not be run on these two samples.

Table 4-23: List of cores

Core	Well	Depth (ft)
1	Mary Marie	4967.7
2	Mary Marie	4967.8
3	Mary Marie	4968.6
4	Mary Marie	4968.7
5	Wilkerson	4974.9
6	Carter	4995.2
7	Danny	4972.0
8	Boone	5065.5

4.3.3.2.1. CT Scan

The CT scan images of Cores 3 and 4 are shown in the figures below. **Figure 4-68** shows the cross-sections at 2, 4 and 6 cm from one edge of Core 3. **Figure 4-69** shows the longitudinal sections through the same core. The darker regions in the image are lower density regions and correspond to vugs. Many vugs are apparent in these scans. There were no visible fractures in these scans. **Figure 4-70** and **Figure 4-71** show the cross-sectional and longitudinal CT sections of Core 4. Again, a few vugs were visible, but no fractures. The major (visible) fractures in such formations are vertical and have a low probability of intersecting cores. **Figure 4-72** shows three cross-sections of Core 8. We observed visible fractures in Cores 7 and 8; these cores were not used in further analysis.

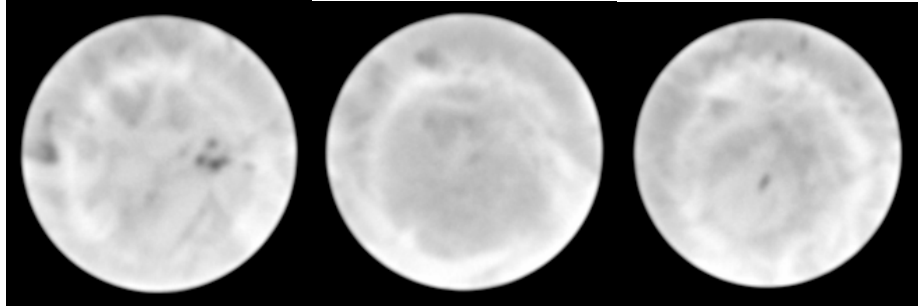


Figure 4-68: Cross-sectional CT scan at 2, 4, and 6 cm from on side of Core 3

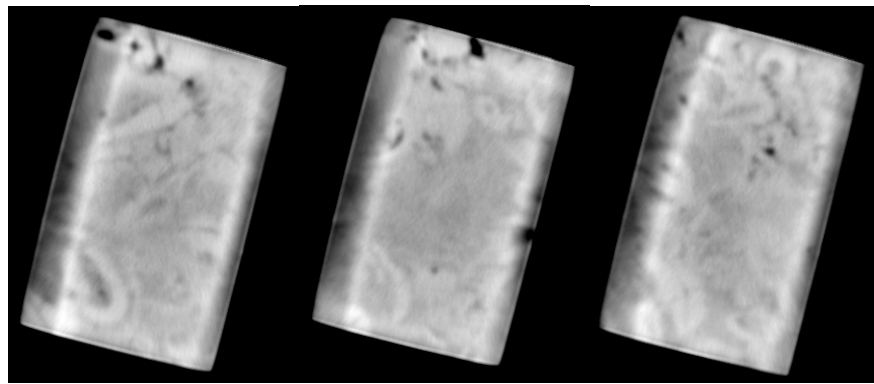


Figure 4-69: Longitudinal CT scan of Core 3

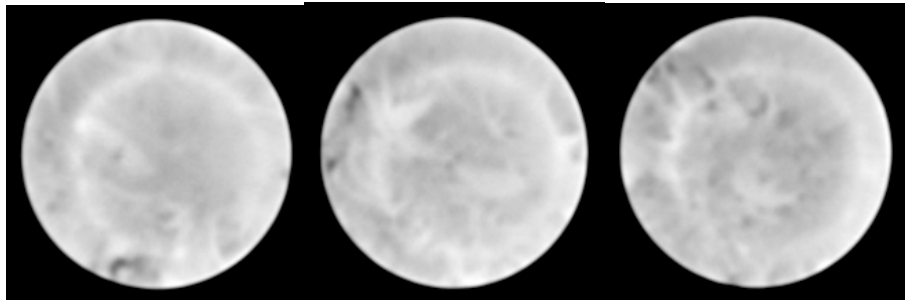


Figure 4-70: Cross-sectional CT scan at 2, 4, and 6 cm from one side of Core 4

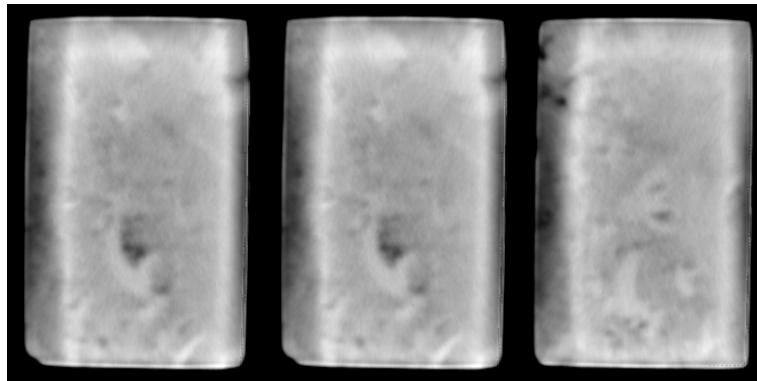


Figure 4-71: Longitudinal CT scan of Core 4

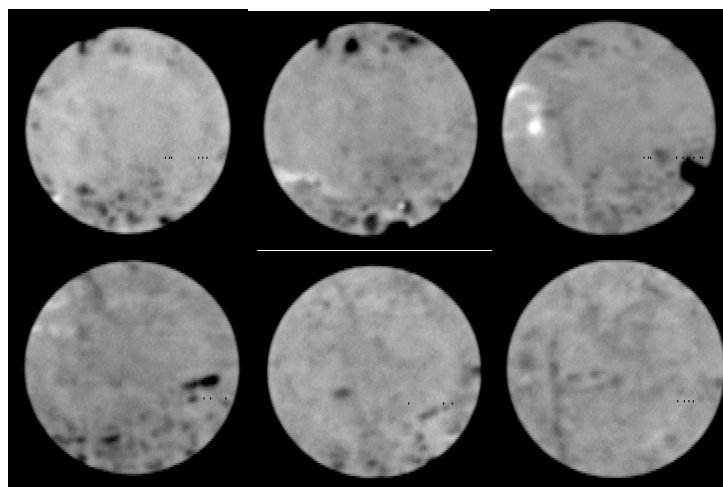


Figure 4-72: Cross-sectional CT scan at 2, 4, and 6 cm from one side of Core 8

4.3.3.2.2. Wettability

Core properties and wettabilities are listed in **Table 4-24**. Cores 3 and 4 from the Mary Marie well had the lowest porosity and permeability. It imbibed spontaneously small amounts of water and oil. The Amott index was 0.04 indicating almost neutral wettability. The Wilkerson core had intermediate permeability. It imbibed no water spontaneously and imbibed only a small amount of oil. The Amott wettability index is slightly negative, indicating slight oil wettability. The Carter core was the most

permeable of these samples. It did not imbibe any water spontaneously, but imbibed a significant amount of oil. Its Amott wettability index is negative, indicating significant oil wettability.

Table 4-24: Core properties and Amott Wettability

	<u>Core 3-4</u>	<u>Core 5</u>	<u>Core 6</u>
	Mary Marie	Wilkerson	Carter 4995.2
	4968.6/4968.7	4974.9	
Porosity (%)	9.7	12.2	11.5
Permeability (md)	1.32	4.4	13.7
Water Index	0.15	0	0
Oil Index	0.11	0.16	0.37
Amott Index	0.04	-0.16	-0.37

4.3.3.2.3. Relative Permeability

Imbibition relative permeabilities of cores 3-4, 5 and 6 are shown in **Figure 4-73**, **Figure 4-74**, and **Figure 4-75**. It can be observed that the brine relative permeability at residual oil saturation is consistently above 0.2, typical of mixed/oil wet reservoirs. This end-point relative permeability is below 0.1 for water-wet reservoirs. The brine-oil cross-over relative permeability is above 0.1, another indication of mixed/oil-wettability. For Core 6, the brine relative permeability is high and almost linear with saturation, an indication of oil wettability. The initial brine saturation is low, from 2% to 25%. The end-point brine relative permeability increases as the oil-wettability of the rocks increase (from samples 3-4 to 6). This is expected because as the oil wettability increases, brine occupies bigger throats and its relative permeability increases. Thus

when the end point imbibition water relative permeability is plotted against Amott wettability index, almost a linear correlation is seen in **Figure 4-76**.

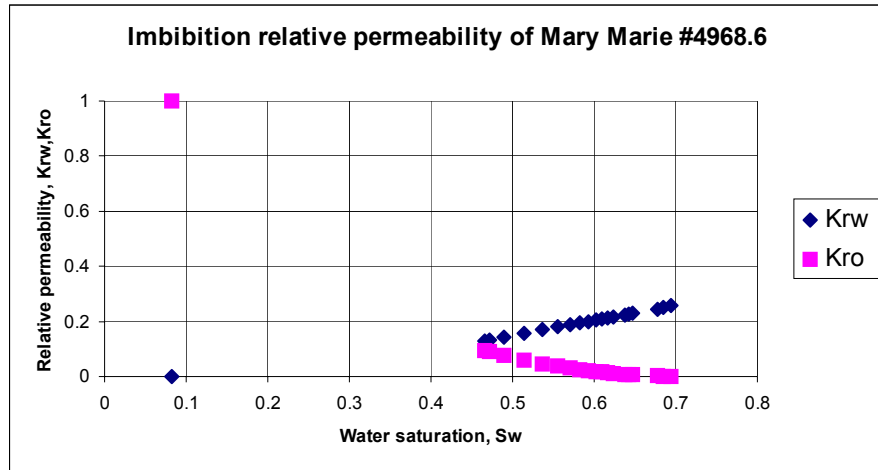


Figure 4-73: Imbibition relative permeability of Mary Marie 4968.6-7 (Cores 3-4)

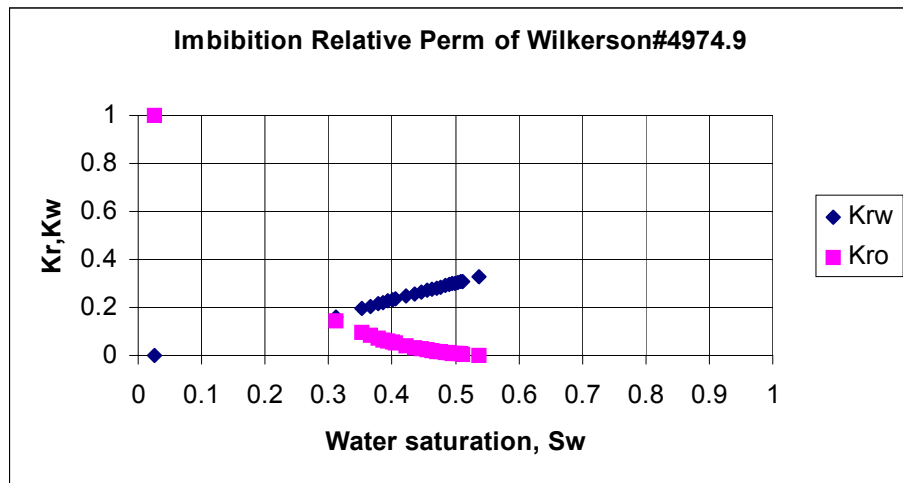


Figure 4-74: Imbibition relative permeability of Wilkerson 4974.9 (Core 5)

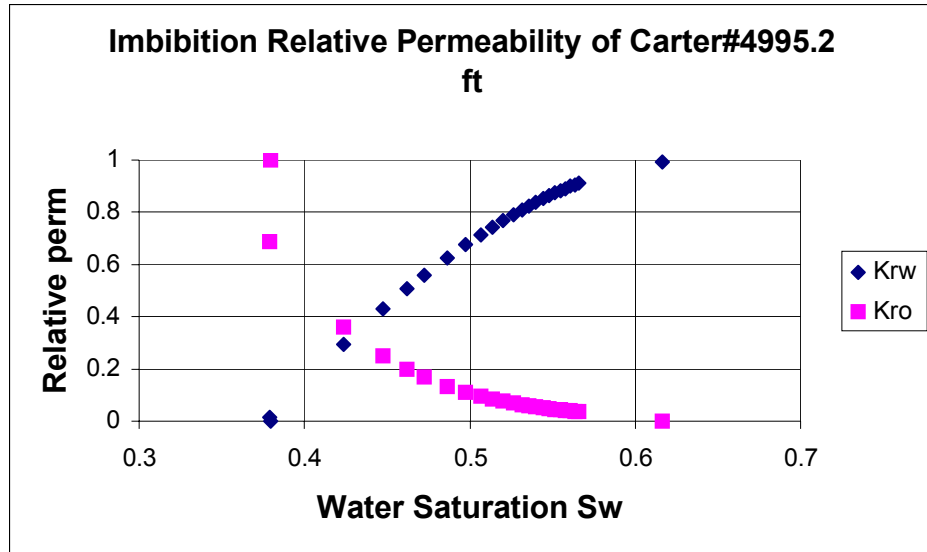


Figure 4-75: Imbibition relative permeability of Carter 4995.2 (Core 6)

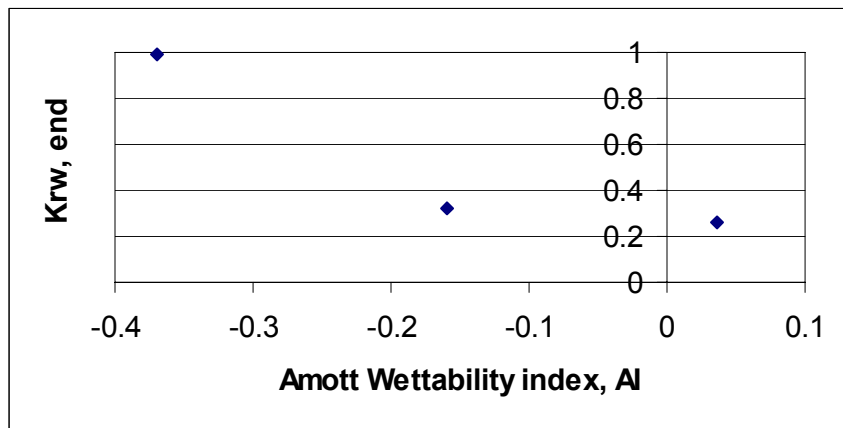


Figure 4-76: Correlation between end point water imbibition relative permeability and wettability

Drainage relative permeabilities of cores 3-4, 5 and 6 are shown in **Figure 4-77**, **Figure 4-78**, and **Figure 4-79**. It can be observed that the brine relative permeability in drainage is lower than that for imbibition.

However, the oil relative permeability is higher. The final brine saturations are quite high, signifying a significant hysteresis.

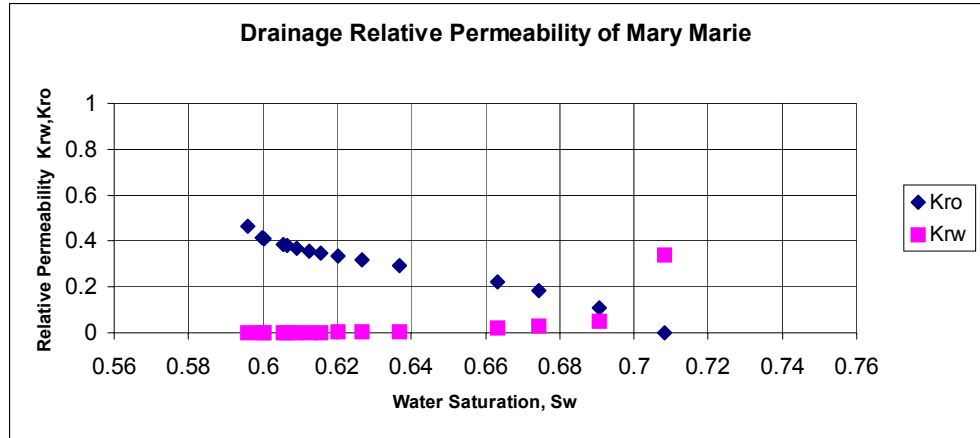


Figure 4-77: Drainage relative permeability of Mary Marie 4968.6-7 (Cores 3-4)

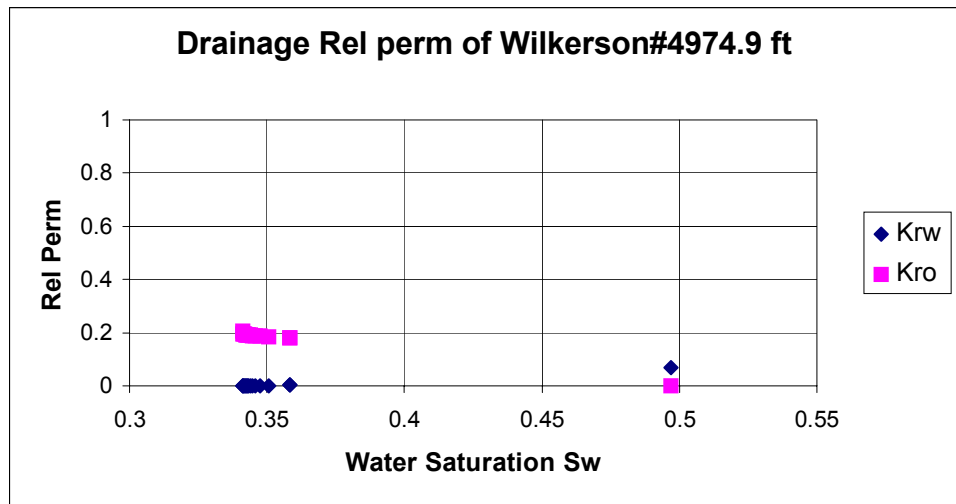


Figure 4-78: Drainage relative permeability of Wilkerson 4974.9 (Core 5)

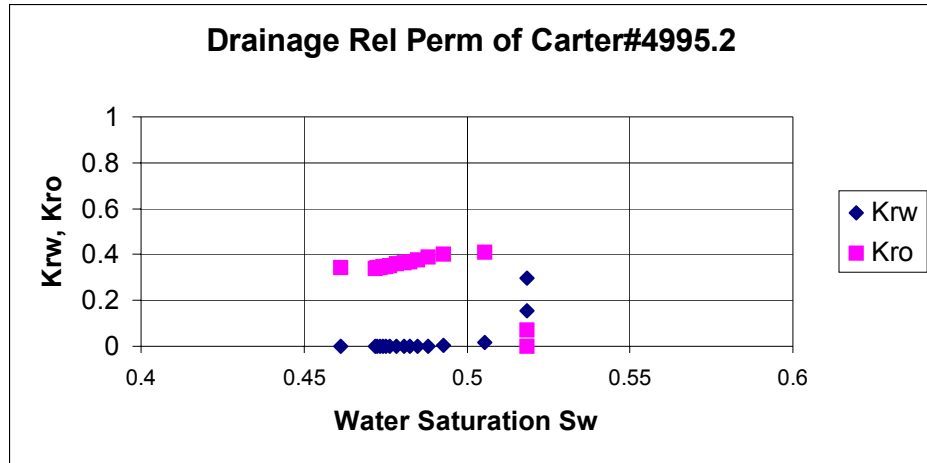


Figure 4-79: Drainage relative permeability of Carter 4995.2 (Core 6)

4.3.3.2.4. Thin-section

The thin-sections of cores 3-4, 5 and 6 are shown in the figures below. All of these samples show extremely tight intergranular pore space with a few vugular pores of the size 50 to 500 μm . The microporosity of the grains cannot be seen in this resolution. The vugs in core sample 6 are larger for than those in the other two samples.

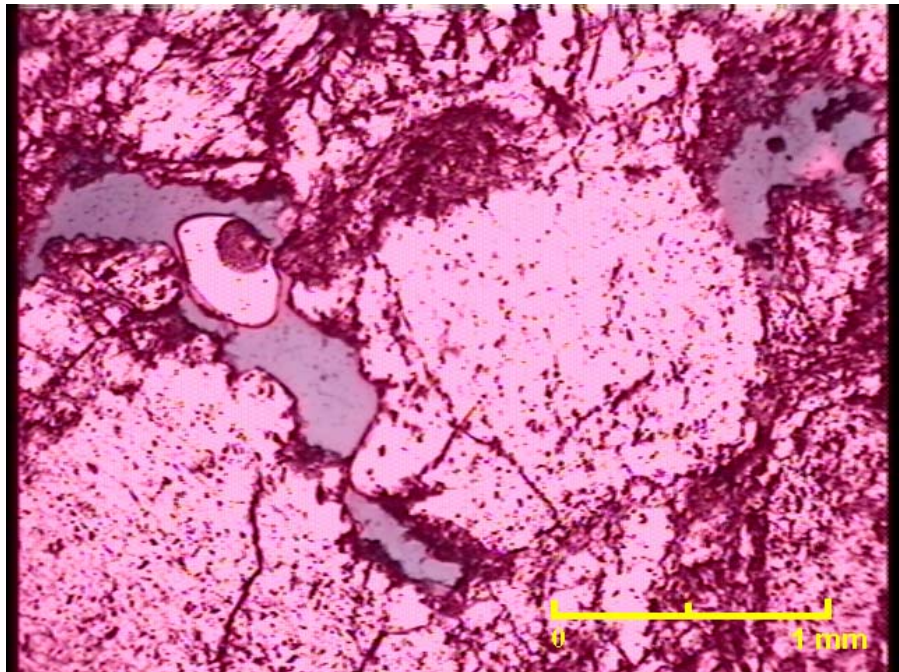


Figure 4-80: Horizontal thin-section of Mary Marie 4968.6-7 (Cores 3-4)

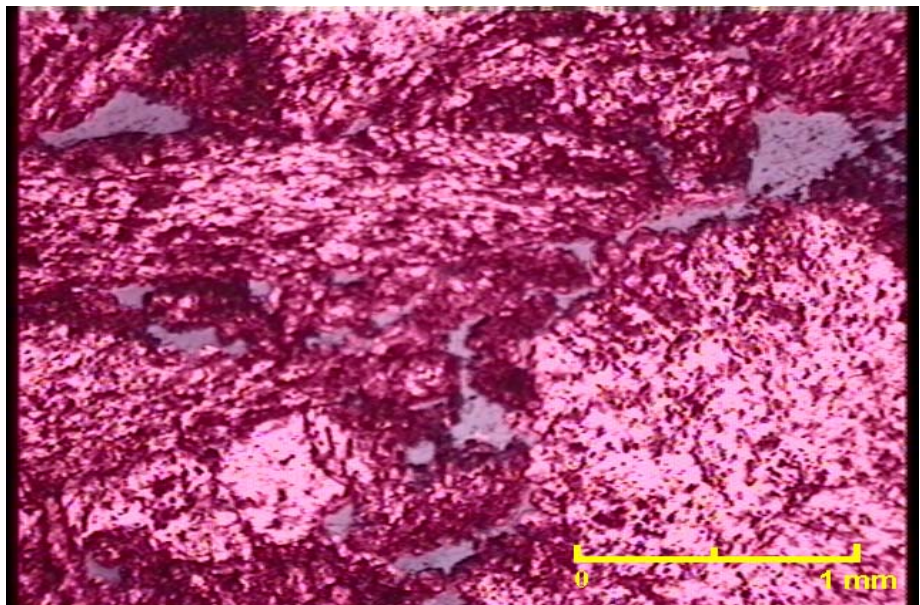


Figure 4-81: Horizontal thin-section of Mary Marie 4968.6-7 (Cores 3-4)

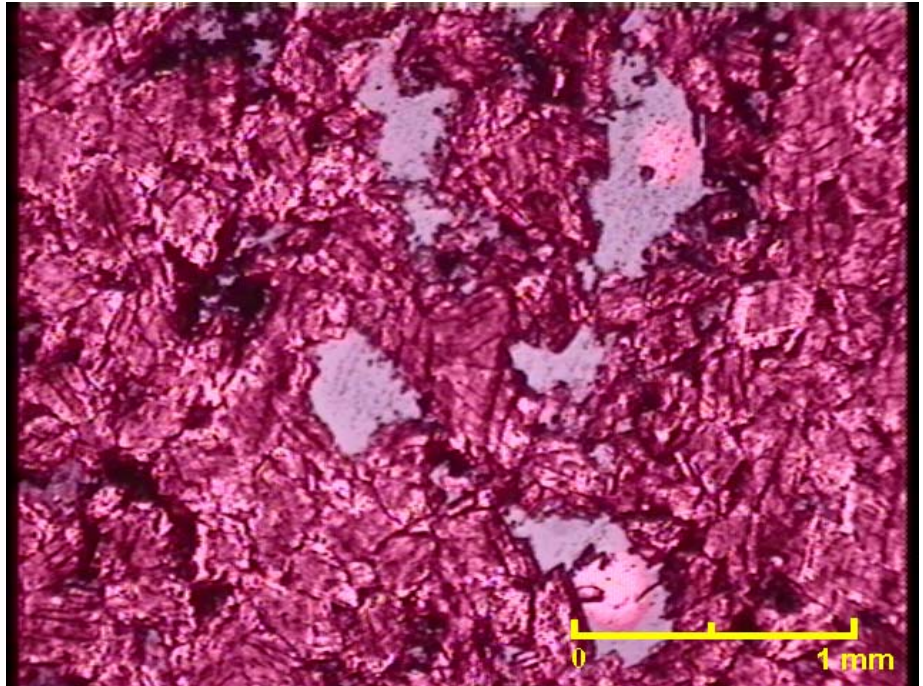


Figure 4-82: Horizontal thin-section of Wilkerson 4974.9 (Core 5)

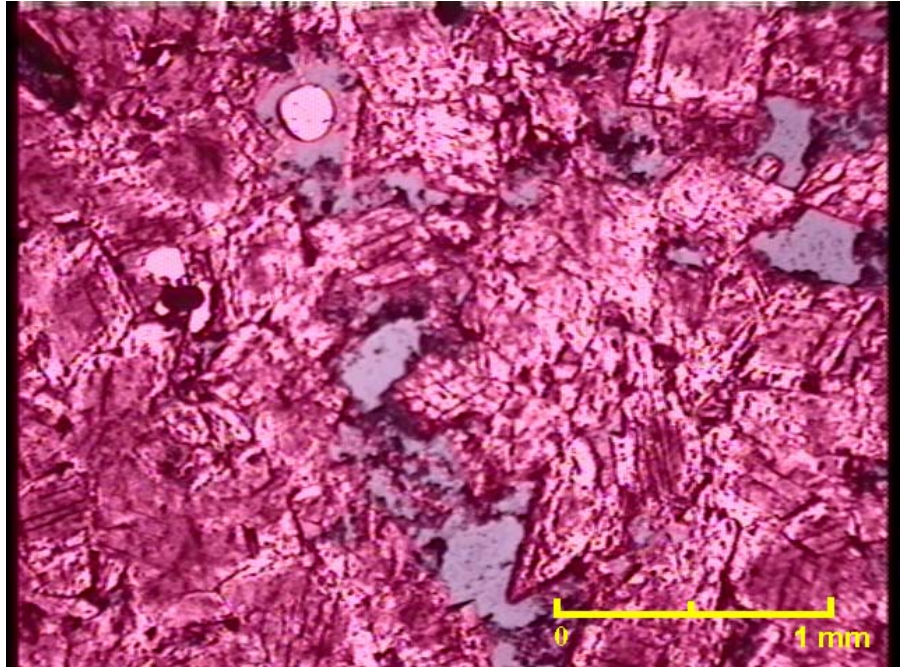


Figure 4-83: Vertical thin-section of Wilkerson 4974.9 (Core 5)

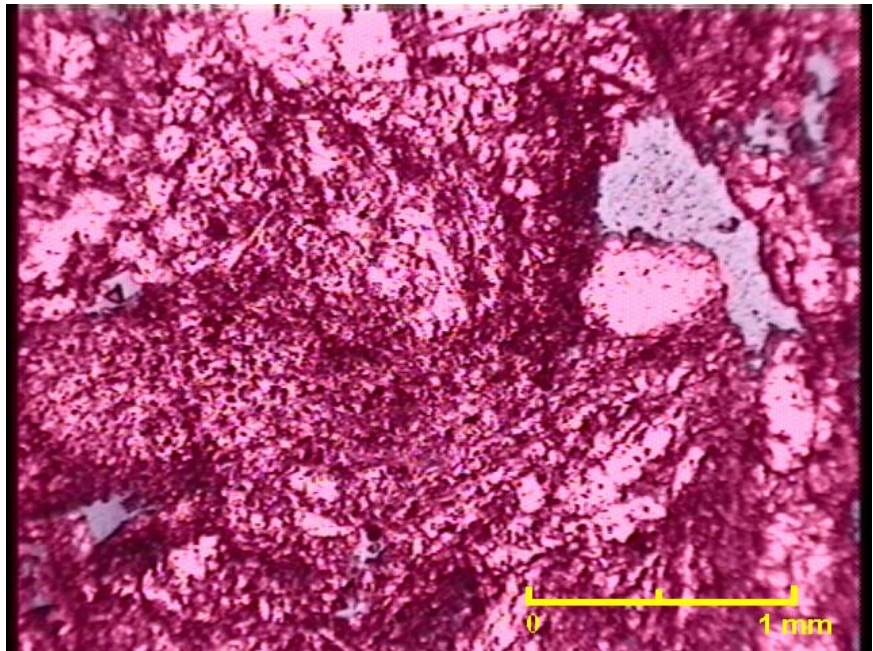


Figure 4-84: Horizontal thin-section of Carter 4995.2 (Core 6)

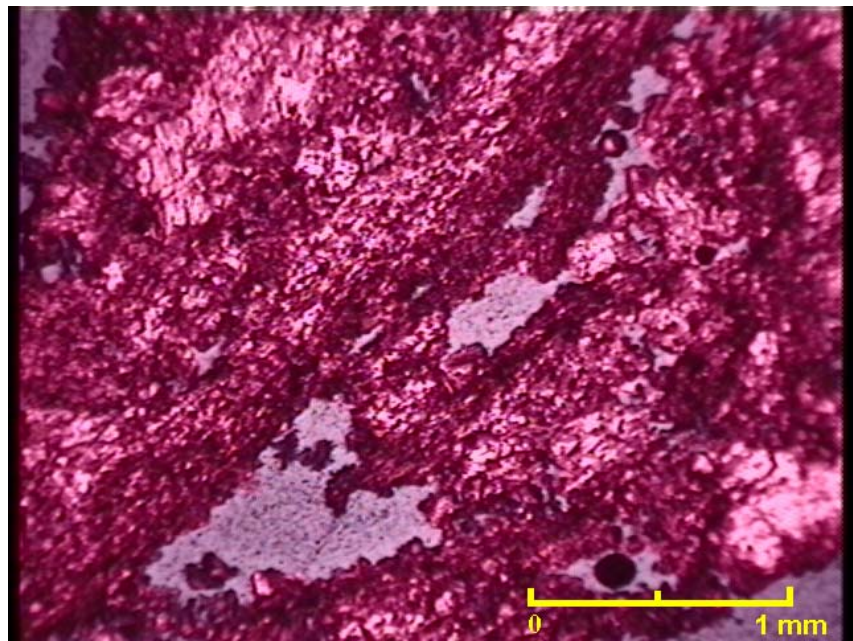


Figure 4-85: Vertical thin-section of Carter 4995.2 (Core 6)

4.3.3.2.5. Mercury Porosimetry

The mercury capillary pressure curves for cores 4, 5 and 6 are shown in **Figure 4-86**. The capillary pressure is the highest for the Mary Marie sample and the lowest for the Carter sample. It inversely correlates with the permeabilities of these samples. Higher mercury capillary pressure indicates smaller pore throats. Smaller pore throats lead to lower permeabilities. The capillary pressure curve for Mary Marie shows a bimodal pore throat distribution. This sample has significant microporosity.

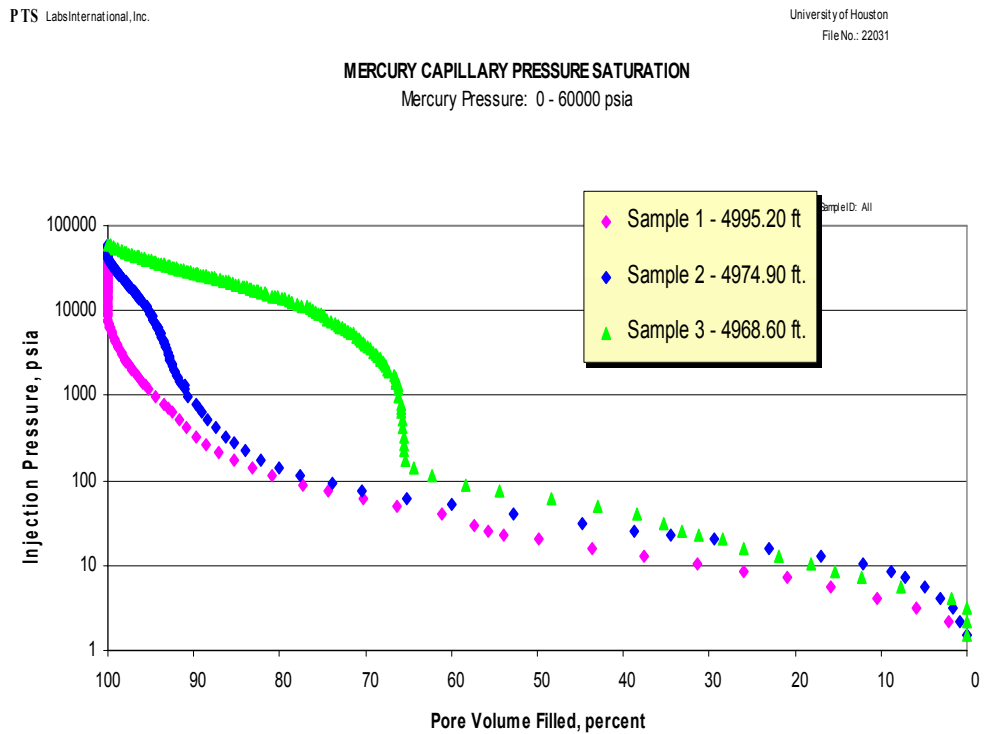


Figure 4-86: Mercury capillary pressure curves for Cores 4-6

Mixed- or oil- wettability is developed in rocks when originally brine filled rocks are invaded by oils with polar organics. Capillary pressure

during this invasion dictates the smallest pores oil can invade. Thus smaller pores remain occupied with brine and they remain water-wet. Thus one expects cores with more small pores and microporosity to be more water-wet than cores with larger pores. In these experiments, pore throat size increases from samples 4 to 5 to 6. Thus, water wettability decreases from samples 4 to 5 to 6 as demonstrated in Fig 16. The permeability of the core samples shows a linear correlation with the Amott wettability index.

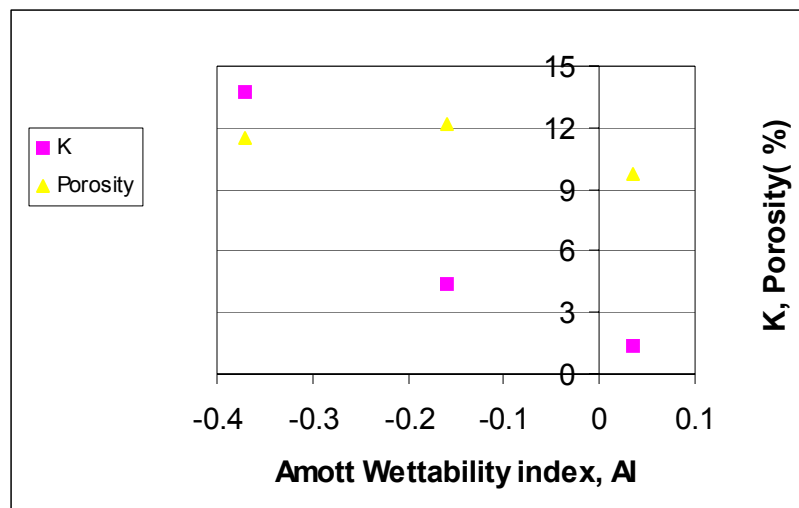


Figure 4-87: Correlation between absolute permeability, porosity and wettability

4.3.3.3. Conclusions

- Hunton rocks are found to be neutral wet to oil-wet.
- In rocks studied, oil wettability increases as absolute permeability and porosity increase.
- End point water relative permeability increases as oil wettability of rocks increase.

4.3.4. Flow Simulation Study

4.3.4.1. Model Characteristics

To build a model that could explain the primary production mechanism by which oil is being produced from the West Carney field, we first need to identify the unique production characteristics observed in the field. The anomalous behavior exhibited by the Hunton Formation is explained below.

- Water-oil ratio decreases over time - For most of the wells, when the well is completed, it produces large quantities of water with limited quantities of oil. Over time, the water production decreases and oil production increases resulting in decreasing water-oil ratio.
- Gas-oil ratio first decreases and then increases over time – For many wells, at the initial stages of production, the gas-oil ratio is very high. As the production continues, the gas-oil ratio will decrease over time. During the later stages of well production, the gas-oil ratio will increase again.
- Gas-oil ratio shows an increase for most wells when the wells are shut-in – When the well is shut in for workover, and is reopened, the gas-oil ratio will temporarily increase, and will slowly decrease over time. This is consistent with previous observation.
- In some wells, when the well is shut-in, instead of observing pressure buildup, pressure falloff is observed; normally, when a well is shut-in, it exhibits an increase in pressure over time, which can be used to determine reservoir properties. This decrease in pressure when the well is shut-in indicates back flow in the reservoir.
- Association between oil and water production – For most wells, oil production is related to the water rate. Some wells indicate good fluorescence and still are bad oil producers. They also produce less

water. While some other wells are very good producers and at the same time they produce large quantities of water even though they may not indicate very good fluorescence.

In this section we will discuss the characteristics of the model that could explain these unique characteristics in the field. In our model, we considered three-layers having gas, oil and water, which are present in three different layers. The top layer is the gas cap and the water is in the bottommost layer. We have considered the permeability of the water layer to be very high due to the presence of fractures in the reservoir. The layers are in vertical communication with each other and the hydrocarbon production is associated with the production of water layer. The explanations for our model are discussed below in detail.

4.3.4.1.1. Free Gas Cap

To understand the fluid characteristics in the field, we collected a fluid sample from Schwake Well (No. 1-10) located in SW quarter of Sec. 10-15N-2E. The API gravity of the oil is 43° indicating a light oil and the gas gravity is 0.84 indicating very rich gas. A well stream composition was created based on the existing gas-oil ratio and the individual composition of the liquid and gas streams, and was tested under constant composition expansion (CCE). The mixture exhibited a dew point of 7,000 psia. **Figure 4-88** shows the test results and it can be seen that the behavior is similar to a standard condensate reservoir with the percentage of liquid volume slowly increasing and then decreasing until it reaches zero value at about 7,000 psia. The mixture, thus, indicated that it is in two-phase region, but was originally a condensate fluid. Since we did not have the fluid sample at the original reservoir pressure, it is difficult to guess what

the physical state of the fluid was at initial conditions. The initial reservoir pressure in the field is less than 2,100 psia. Although it is hard to conclusively predict what type of initial condition existed in the reservoir, the PVT lab concluded, based on the API gravity of the liquid and the crude color of the residual liquid, that the most likely physical state is a gas cap with oil rim below it.

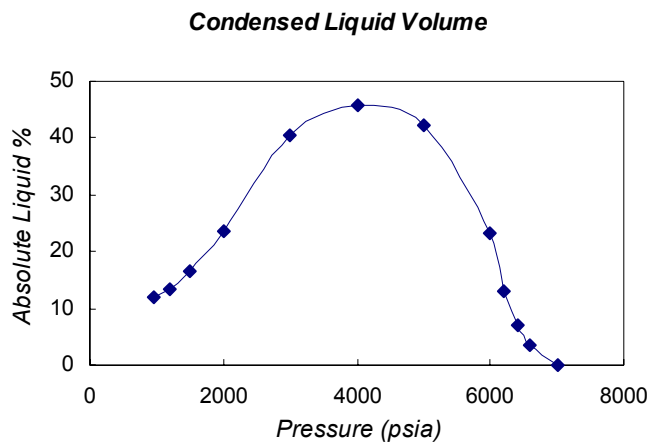


Figure 4-88: Condensed liquid volume in CCE experiment

The high gas-oil ratios observed in the field also indicate the presence of free gas cap in the reservoir. Most wells exhibit gas-oil ratios of more than 5,000 scf/stb, which is another indication of presence of free gas in the reservoir. **Figure 4-89** shows the GOR plot for well Danny (No.1-34), located at SE quarter of Sec. 34-16N-2E. Similar behavior has been observed in most of the other wells.

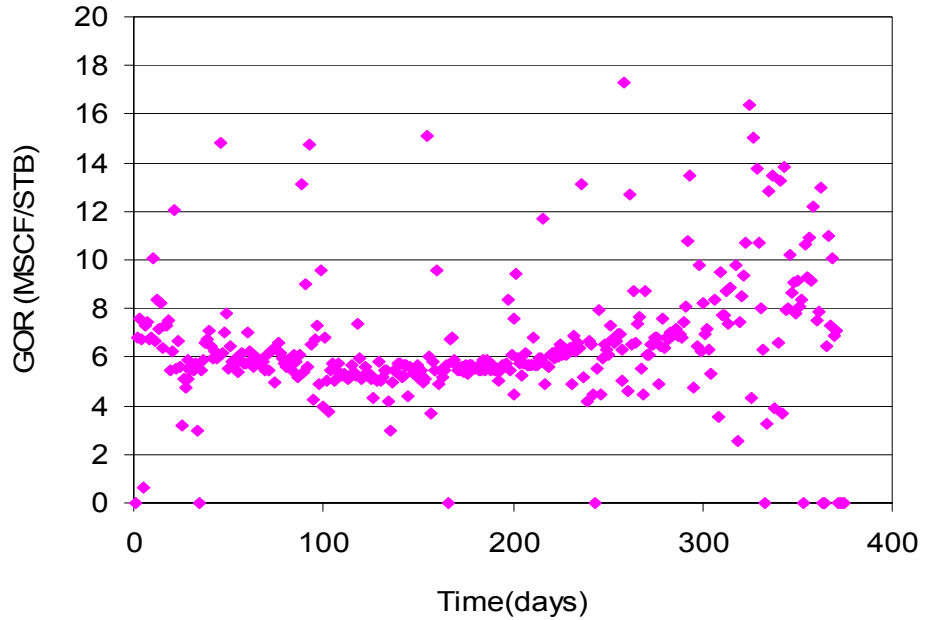


Figure 4-89: Gas-oil ratio for Danny #1 well

Another unique behavior observed in the wells in West Carney field is the increase in GOR when the well is shut-in. **Figure 4-90** shows the GOR for the Schwake well. It can be seen from the plot that the GOR has increased after 179 days and again after 256 days. This increase in GOR was observed when the well was shut-in and then opened after the workover job. The points are marked with blue color on the plot and the values of GOR are shown alongside. This increase in GOR after the well was shut-in indicates the presence of free gas, which has high mobility and thus results in more gas production when the well was opened again.

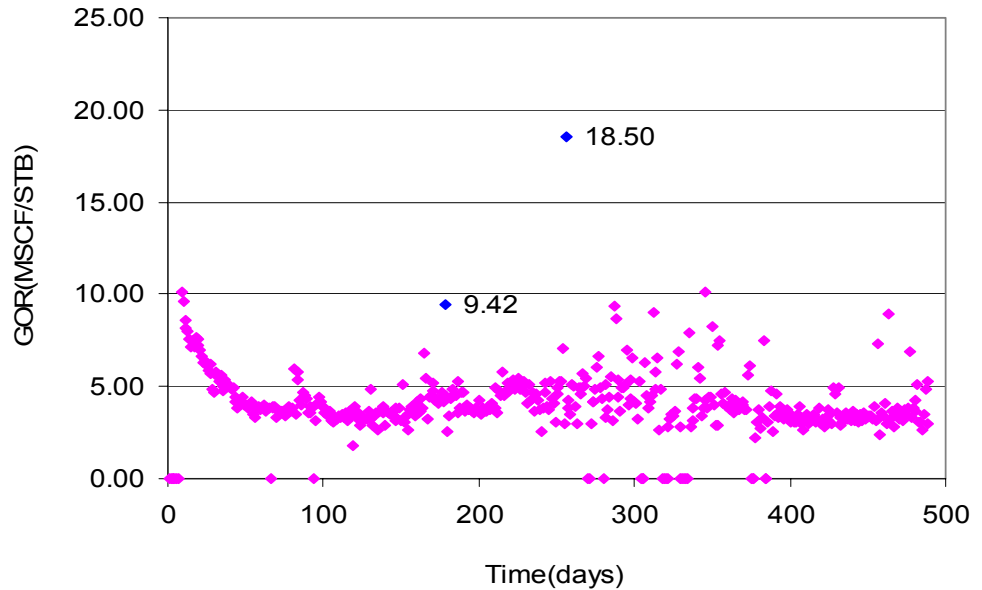


Figure 4-90: GOR plot of Schwake well

Whitson and Brule⁶ have also discussed the possibility of existence of gas cap under certain conditions. They have argued that if the initial reservoir pressure equals the measured dew point pressure of a reservoir gas sample, the gas is probably saturated at initial reservoir conditions, and equilibrium oil could exist at some lower elevation.

We have also studied reports from other fields that have been producing from the Hunton formation and which have shown some of the unique characteristics as exhibited by West Carney Field. One of the fields, West Edmund Hunton Lime Unit (WEHLU), has shown similarities with West Carney field. **Table 4-25** shows the comparison between WEHLU and West Carney Field. Engineering studies⁷ of WEHLU field have identified the presence of gas cap and an underlying oil rim. The hypothesis of existence of gas cap aided them in the reserve estimation process. They

could come up with more reasonable reserves, which matched with the field observations by considering the gas cap.

Table 4-25: Comparison between WEHLU and West Carney Field

	WEHLU	West Carney Field
API Gravity of oil	41° - 43°	41° - 43°
Gas Gravity @ 60 F	0.77 to 0.82	0.80 to 0.88
Fractures Present	Yes	Yes
Water Oil Ratio	N/A	decreases over time
Avg. Initial Reservoir Pressure	3100 psia	1500 psia
Payzone Thickness	30 - 60 ft	30 - 40 ft
Reservoir Depth (subsea)	5800 ft	4900 ft
Avg. Porosity excluding the fracture porosity	5.17%	5.00%
Permeability excluding the fractures and vugs	0 to few mD	0 to few mD

4.3.4.1.2. Presence of Fractures

Cores obtained from the wells have been studied and fractures have been observed in them (see **Section 4.2**). The permeabilities obtained from the cores have been, at some points, in excess of 1,000 mD, which confirms the presence of channels in the reservoir. CT scans have also shown fractures in the cores. Both vertical as well as horizontal fractures have been noticed.

Another indication of presence of fractures is the high water rates. Water rates in some of the wells have been very high compared to the permeability values observed at the wellbore. This also indicates that the water flows through the fractures. The sharp decline in the water rates also points toward the presence of water in the fractures. **Figure 4-91** shows the water rate for Danny #1 well. It can be observed from the plot that the initial water rate was more than 2,000 stb/day, but rapidly declines to about 1,000 stb/day in less than 300 days of production.

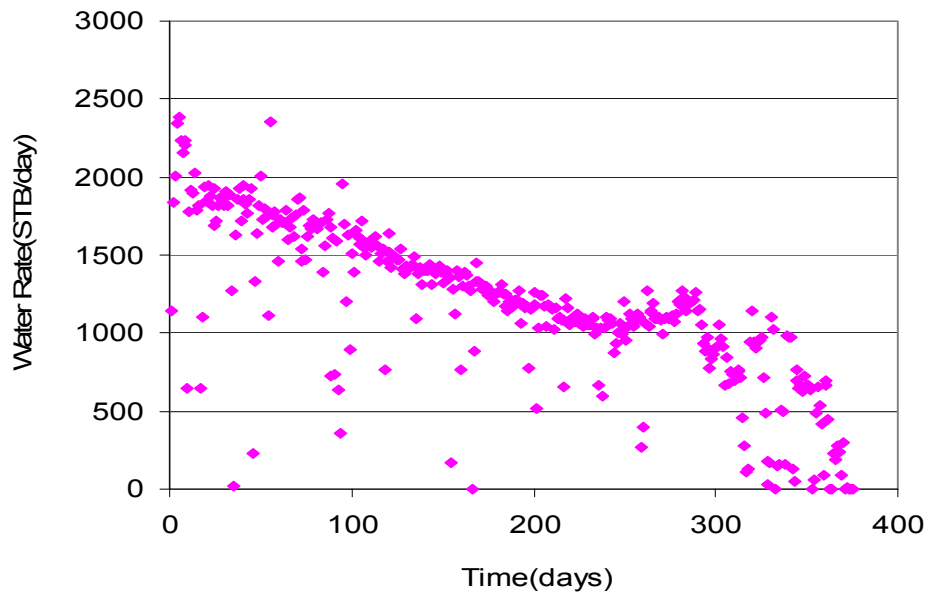


Figure 4-91: Water rate plot for Danny #1 well

Most of the wells have also shown high water-oil ratios at the start. The water cut in the wells, when they start producing, has been in excess of 90 % and then decreases over time. This is due to the increase in oil rate and decrease in water rate, another indication of movement of water through fractures. This implies that the water is draining faster than hydrocarbons. **Figure 4-92** shows the WOR plot for the Schwake well. The decline in water-oil ratio is very much visible for the Schwake well. A similar trend has been observed in other wells.

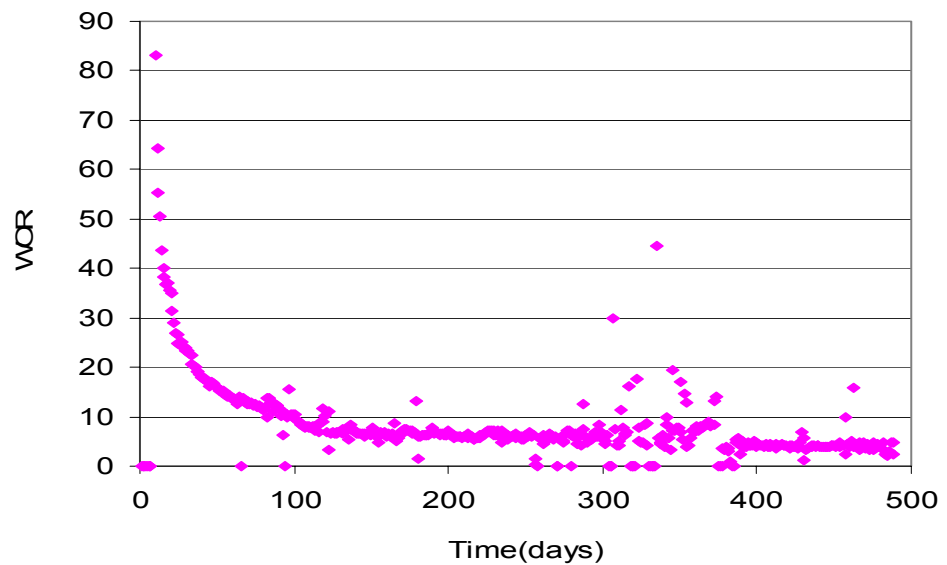


Figure 4-92: Water-oil ratio for the Schwake well

Another indication of fractures in the reservoir is the communication between the wells. Strong communication has been observed in some of the wells. As an example, the production from the Wilkerson #1 well started declining when the Wilkerson #2 well was put on production. The two wells are approximately 1200 feet apart. **Figure 4-93** shows the production behavior of these wells.

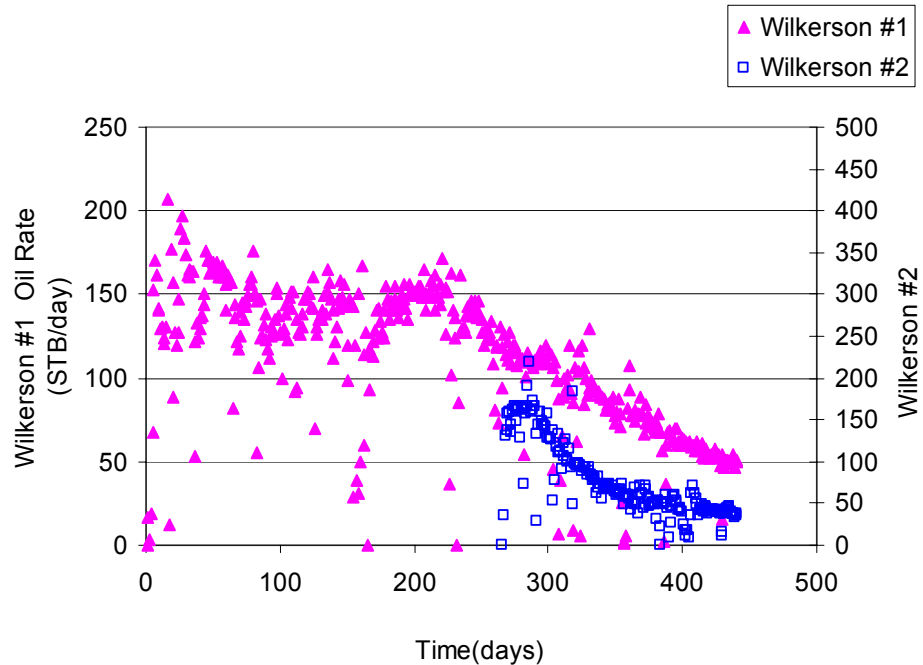


Figure 4-93: Effect of Wilkerson #2 on the production of Wilkerson #1

Well test data from some of the wells also indicates the presence of fractures. As discussed in the Core Log Correlation section, when the wells were shut-in for the pressure buildup test, they had gone on vacuum, indicating a back flow in the wells. Movement of water in the fracture system has also been observed in the WEHLU field. Water flooding in WEHLU has proved futile as the front bypasses the oil trapped in the matrix system, indicating movement of water in fracture system. Based on the opinion of Engineering Committee⁷, the water encroachment into the oil-filled reservoir came from a limited aquifer and that during 1947 and 1948 water production was substantially equal to the rate of water influx. In WEHLU field, first row offset wells changed from commercial oil production to nearly 100% water production within three to six weeks after beginning injection of water. The Engineering Subcommittee report

on WEHLU field established that the water moved through only a small percentage of the total reservoir pore volume.

4.3.4.1.3. Relationship between oil and gas production

The production behaviors of the wells indicate that the oil and gas coexist in the reservoir. All the wells that produce oil also produce gas and exhibit the same production trend. The possibility of existence of separate gas and oil pockets would not support the production behavior that is observed in the field. **Figure 4-94** shows the oil and gas production of Danny #2 well. Both, oil and gas, exhibit the same decline trend. Other wells also display the relation between oil and gas production. The plot between oil rate versus gas rate for all the wells in the field is shown in **Figure 4-95**. The trend clearly indicates that oil and gas exist together. Although hydrocarbons may be present in discontinuous pockets, if oil exists in a pocket, most likely, gas also co-exists along with oil. Thus, we consider that oil and gas co-exist in the model.

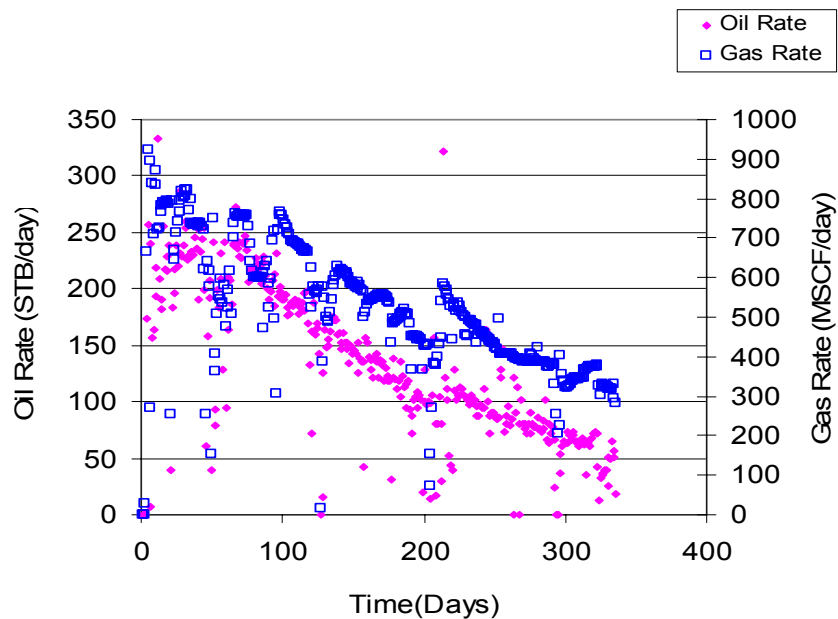


Figure 4-94: Oil and Gas rate plot for Danny #2 well

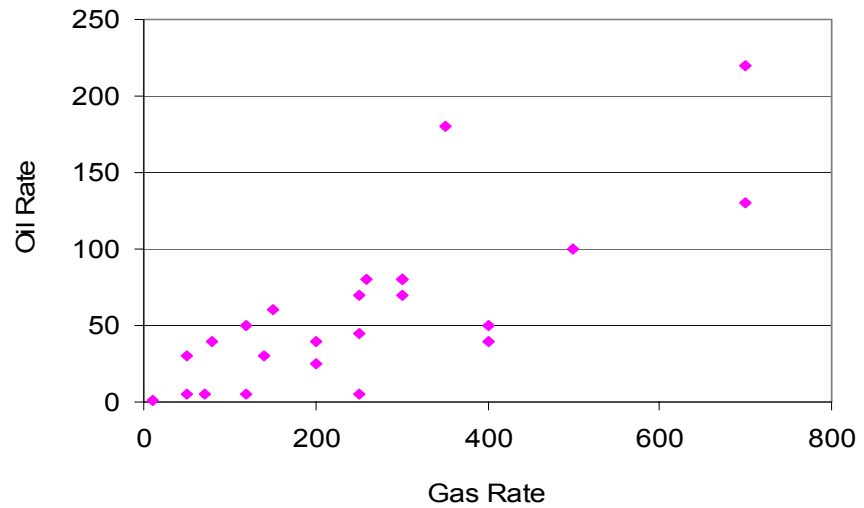


Figure 4-95: Relation between oil and gas rate for the wells

4.3.4.1.4. Limited Aquifer

To account for the high water production rates, water had to be included in our model. The initial pressure of all the newly drilled wells is observed in the field is plotted in **Figure 4-96**. It can be clearly seen that the pressure in the reservoir is declining.

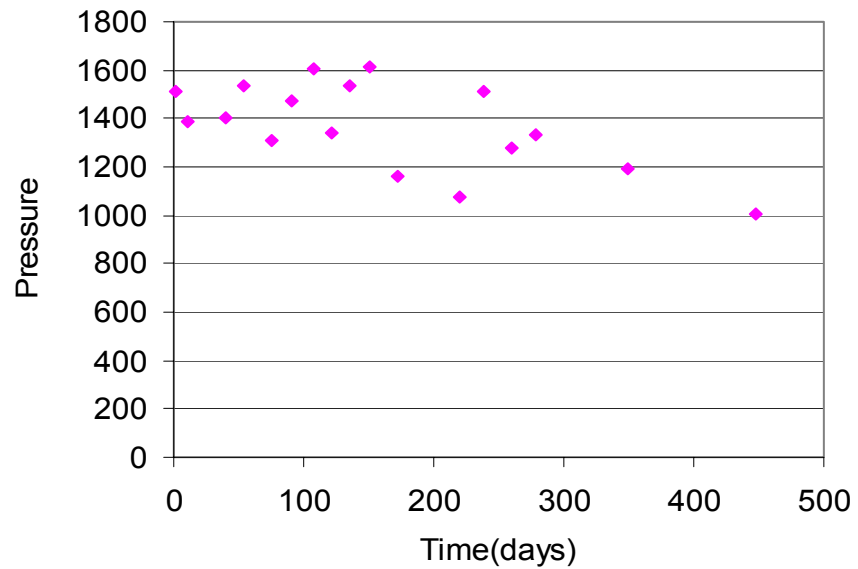


Figure 4-96: Bottomhole pressure of wells

The water rates in the field have also been declining, another indication of limited aquifer. The rates in the newly drilled wells have been less as compared to the surrounding wells that were drilled earlier. **Figure 4-97** shows the water rate for the McBride North well, located at NE quarter of Sec. 10-15N-2E, and the McBride South well, which is located at SE quarter of Sec. 10-15N-2E. Both the wells are located at the same section of the field and exhibit similar porosities. The initial water rate in the McBride South well is significantly less compared to the water rates in the McBride North well. McBride North started production before McBride South was drilled and thus confirms the diminishing water reserves in the field.

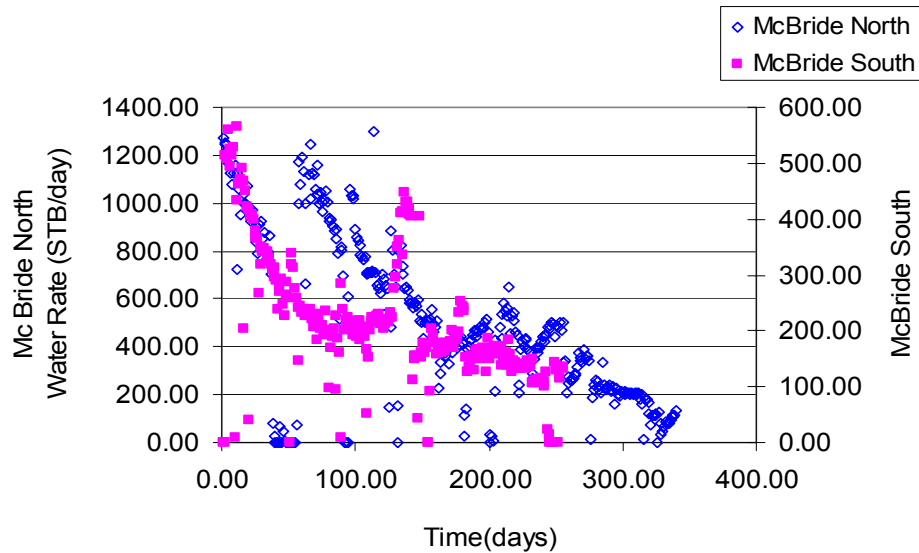


Figure 4-97: Water production for wells, McBride North and McBride South

4.3.4.1.5. Bulk of the hydrocarbon production is through water zone

We have discussed earlier that oil and gas coexist and show similar production trends. Some of the wells in this field have shown good fluorescence, but are bad oil producers. Water production from these wells is also low indicating the association between the oil and water production. For example, the Boone well shows good fluorescence but is not a very good oil producer. It also has less water production. Some other wells have not shown very good fluorescence and still have good oil production. The general trend in the field has been that if a well produces good quantities of oil then the water production from the well is also high. This behavior indicates the communication between the hydrocarbon and water bearing zones and that the bulk of the oil gets produced through the water zone. The oil production from the well is more if there is good communication between the oil and water layers and water layer has high permeability.

In our model, we incorporated a free gas cap and an underlying oil rim. To account for the high water rates, we added a water layer with high permeability at the bottom of the hydrocarbon zone. All the three-layers are in communication with each other and the bulk of the hydrocarbon production takes place through the water layer. This model has been able to reproduce most of the unique characteristics of the field and has resulted in good match for individual wells.

4.3.4.2. Analytical Model

Based on the field observations, which are discussed in the previous section, we first decided to make a simple analytical model. Although the reservoir produces significant amount of gas, we assumed that the reservoir model consists of two layers having inter-layer crossflow. The upper layer is the oil layer having zero horizontal permeability and the bottom layer is initially filled with water. The bottom layer has high horizontal permeability so that it would produce first, resulting in lowering of pressure. This model cannot be used for in-depth study of the field and has limitations. The model considers a single well draining 160 acres of area. Analytical models are used to study the general behavior as they are computationally fast and can provide an idea about the behavior. The purpose of making this model was to observe if this model could capture some of the unique production behavior exhibited by wells in the West Carney Field.

The model is graphically shown in **Figure 4-98**. The top layer is the oil layer having zero horizontal permeability but is in communication with the bottom layer through vertical permeability. The bottom layer is initially filled with water and it is in communication with the wellbore. When the well is first

drilled, production takes place from the bottom layer resulting in lowering of pressure in the layer, which leads to the migration of oil from the top layer into the bottom layer due to the pressure difference and gets produced along with water.

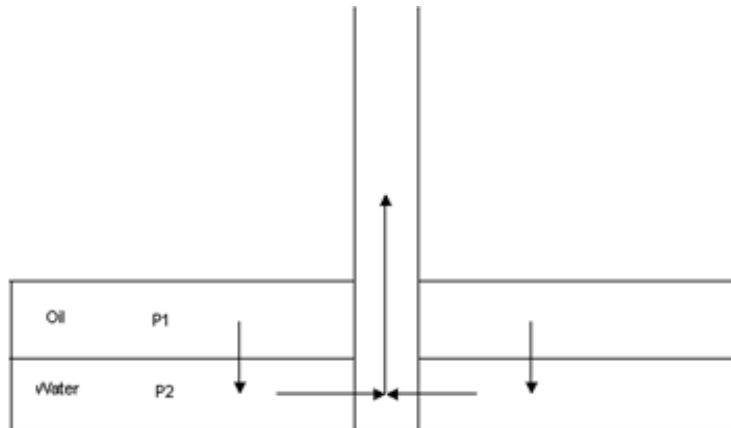


Figure 4-98: Two layer model

4.3.4.2.1. Model Assumptions

1. ρ_o and ρ_w are constant.
2. Water and oil formation volume factors are equal.
3. Viscosities of two-phases are assumed to be the same.
4. Both the oil and water layers are homogeneous. The oil layer's horizontal permeability is zero.
5. The relative permeabilities are linear functions of saturations,

$$k_{rw} = 1 - k_{ro}$$

Equation 4-25

or,

$$k_w = k k_{rw} = k(1 - k_{ro})$$
$$k_o = k k_{ro}$$

Equation 4-26

where k is the absolute permeability.

In our model, we assumed that the oil is present in the matrix, which is the layer 1 or the oil layer and water is mainly present in the fractures that we have represented by layer 2 or the water layer. To account for these we have defined two parameters:

Matrix storativity:

$$\omega = \frac{\phi_o c_o h_o}{\phi_w c_w h_w}$$

Fracture coefficient

$$\lambda = 12 \left(\frac{k_o h_o}{k_w h_w} \right) \left(\frac{r_w^2}{h_o^2} \right)$$

r_w = wellbore radius.

The dimensionless terms are defined as,

$$z_D = \frac{z}{h}$$

$$t_D = \frac{kt}{\phi\mu c_t A}$$

$$p_{Do}|_{t_D=0} = 0$$

Equation 4-27

$$\left. \frac{\partial p_{Do}}{\partial z_D} \right|_{z_D=0} = 0$$

$$p_{Do}|_{z_D=1} = p_{Dw}$$

where, h is the thickness of the layer.

p_{Do} and p_{Dw} are the pressures in the oil and water layers.

The boundary and initial conditions for this case are defined as,

$$\left. \frac{\partial p}{\partial z} \right|_{z=0} = 0$$

$$p(h, t) = P_2$$

Equation 4-28

$P_2 =$ Pressure of layer two.

$$p(z,0) = P_i$$

Equation 4-29

P_i = Initial Reservoir Pressure.

The detailed derivation of the final expression is provided by Marwah⁸. In dimensionless form, the solution for the oil layer can be written as,

$$\bar{p}_{Do} = \bar{p}_{Dw} \frac{\cosh(z_D \sqrt{3\omega u / \lambda})}{\cosh(\sqrt{3\omega u / \lambda})}$$

Equation 4-30

where the solution is written in Laplace space, which can be inverted into real space.

As can be seen from this derivation, the pressure in oil layer depends on the pressure in the bottom layer-which is a water layer. The equation for the water layer can be similarly derived. The dimensionless variables for the water layer are defined as,

$$r_D = \frac{r}{r_w}$$

$$t_D = \frac{kt}{\phi \mu c_t r_w^2}$$

$$p_{Dw} = \frac{P_i - p(r)}{P_i - p_{wf}}$$

Equation 4-31

where, r_w is the radius of the well.

and p_{wf} is the wellbore pressure.

The equation for the water layer is for the case when there is a constant bottomhole pressure. The boundary conditions for the bottom layer are,

$$\begin{aligned} \frac{\partial p}{\partial r} (@ r = r_e) &= 0 \\ p(r_w, t) &= p_{wf} \end{aligned}$$

Equation 4-32

The solution for water layer can be written as,

$$\bar{p}_{Dw} = \frac{K_1(\sqrt{uf(u)r_{eD}})I_0(\sqrt{uf(u)r_D}) + I_1(\sqrt{uf(u)r_{eD}})K_0(\sqrt{uf(u)r_D})}{u[K_1(\sqrt{uf(u)r_{eD}})I_0(\sqrt{uf(u)}) + I_1(\sqrt{uf(u)r_{eD}})K_0(\sqrt{uf(u)})]}$$

Equation 4-33

where, $f(u) = 1 + \frac{\sqrt{\lambda\omega}}{3u} \tanh(\sqrt{3\omega u / \lambda})$.

The solution for water layer is in Laplace space having Bessel functions and can be inverted using numerical inversion algorithm.

4.3.4.2.2. Results

A single well was considered in this case that drains the 160-acre area. The model has limitations and thus it cannot completely reproduce the field production data. The results from the model have been able to capture the production profile of the field. In our model, we considered a reservoir with an initial pressure of 1500 psia, and well production at a constant bottomhole pressure of 250 psia. We modeled different cases to study the sensitivity of the parameters on the production performance. The parameters that were modified include permeability, porosity and thickness of the two layers.

Figure 4-99 shows the water production rate obtained from the analytical model and also shows the actual rate from the Schwake well. In this case, we considered a permeability of 255mD and 1555mD in the two layers. The top layer has permeability only in the vertical direction while the bottom layer has only horizontal permeability. Thus, the permeability for layer 1 is the z-direction permeability. The porosities in the two layers were 0.075 and 0.025. As seen from the figure, the oil production rate first increases with time and after reaching a maximum value starts decreasing over time. This behavior has been seen in some of the early wells like Schwake. Later wells indicate oil production right from the beginning. The match between the model results and the field data is not good, but has been able to capture the production profile and the properties used in the model may not represent the actual observed parameters.

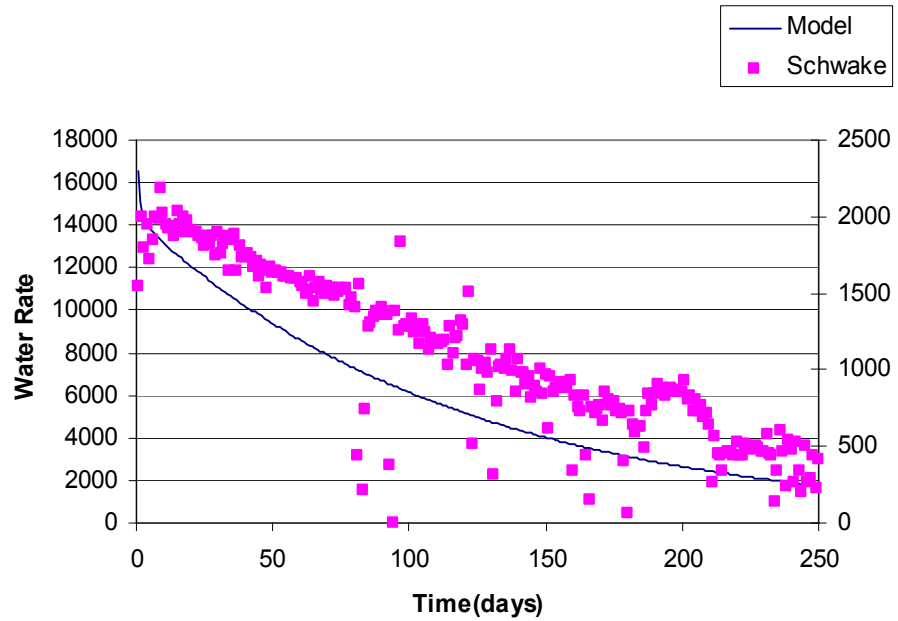


Figure 4-99: Water Production Rate

The effect of changing the horizontal permeability of the water layer is shown in **Figure 4-100**. In this case, we reduced the permeability of the water layer from 155 mD to 75 mD keeping all the other parameters same. The plot shows the results obtained from the model and the sensitivity of different parameters on the results. It can be seen that the profile from the model matches well with the actual field data though the values are higher.

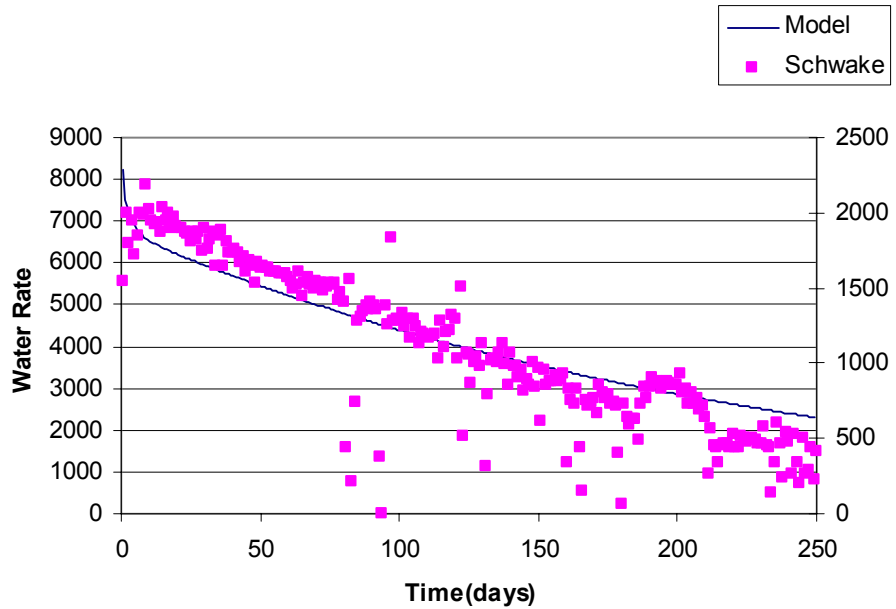


Figure 4-100: Water Production for Case 2

4.3.4.2.3. Limitations

The analytical model was derived based on the assumptions that there are only two phases and the relative permeability of the phases is a linear function of saturation. Due to the assumptions, the model has limitations and cannot be used for the matching the field data. The formation volume factor and the viscosity are considered to be same for the different phases in our model. The other limitation in the model is that the layers are considered to be homogeneous and the flow is unidirectional in them. Though the model has limitations, it has been able to reproduce some aspects of the production behavior observed in the field.

4.3.4.3. Flow Simulation Study

To extend the analytical model and remove some of the limitations of the analytical model, we also used a numerical simulator to study the behavior of

the field characteristics. We developed a three-layer model having gas, oil and water. The top layer is the gas layer, oil is present in the middle layer and the water is in the bottom layer. This is consistent with the PVT properties observation, according to which reservoir consists of an oil rim underneath a gas cap. In this model, all the three-layers are in communication with each other with water layer having very high permeability due to the fractures. The vertical permeability between the layers is also high due to the presence of vertical fractures. The typical production characteristics we want to reproduce from numerical model are as follows.

- Initial decline in gas-oil ratio.
- Association of oil production with that of water production.
- Decreasing water-oil ratio.
- Increase in gas-oil ratio after the well was shut in.

4.3.4.3.1. Single Well Model

We first developed a single well model that could reproduce these production characteristics based on the petrophysical properties observed in the field. The model is graphically shown in **Figure 4-101**.

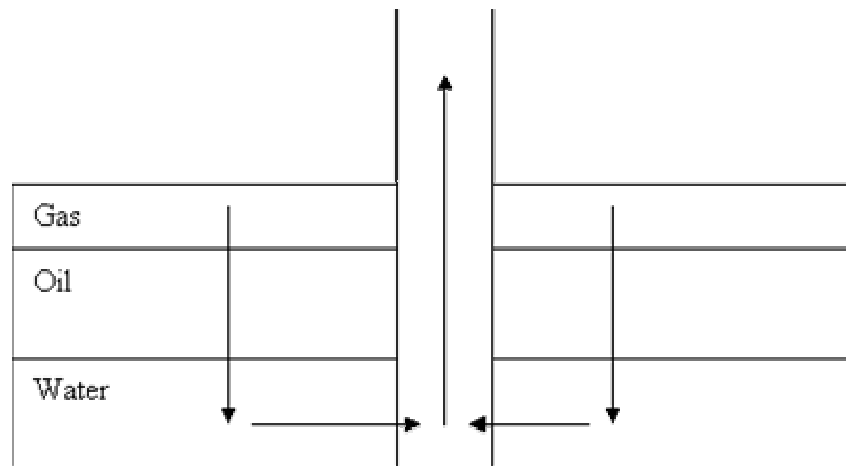


Figure 4-101: Three-layer model

For single well study, Schwake well was considered because of its unique production characteristics. The reasons for selecting Schwake well are listed below.

- Schwake well was one of the earliest wells to start production.
- It has unique hydrocarbon production behavior. The oil and gas production rates first increase with time and then starts decreasing.
- A bottomhole pressure gauge has been installed in this well, which gives real time pressure values. The availability of continuous pressure values help in normalizing the production data.
- High total liquid production.
- More traditional water rate decline.

Parameters used in the model were in accordance with the field values. **Table 4-26** lists the initial properties we used in our model to match the field behavior. In the single well model, we considered a well at the center of a 160 acre area. We divided this area into 32 by 32 by 3 grid blocks. Near the well, we used smaller grid sizes of 50 feet by 50 feet and the grid size away from the well is 75 feet by 75 feet. The grid size in the vertical direction is same as the layer thickness.

The Hunton formation thickness is on the order of 40 ft. Due to the lack of precise information, we assigned the thickness to the three-layers based on the production data. The reserve estimation and production data indicated that the around 75% of hydrocarbon is in the oil phase. In the model, a horizontal reservoir is considered without any inclination at a depth of 4960 feet and has an initial reservoir pressure of 1500 psia.

Relative permeability experiments have been performed on the cores obtained from the field. In addition to the relative permeability data obtained in the lab, we also assumed straight-line curves for the phases in

the water layer, which is a high permeability layer due to the presence of fractures. A different set of values was used for the hydrocarbon layers.

We used ECLIPSE software to perform flow simulation. E100, a black oil simulator, along with ancillary packages SIMOPT and SCHEDULE were used for this study.

Table 4-26: Input Data used for Single Well Simulation

Horizontal Permeability	Layer 1	0.1
	Layer 2	0.005
	Layer 3	100
Vertical Permeability	Layer 1	75
	Layer 2	75
	Layer 3	75
Porosity	Layer 1	1.60%
	Layer 2	3%
	Layer 3	6.50%
Thickness	Layer 1	6
	Layer 2	15
	Layer 3	21
Grid size	Near well	50 ft x 50 ft.
	Away from well	75 ft x 75 ft.
	Height	Same as layer thickness
Skin	Layer 1	0
	Layer 2	-3.5
	Layer 3	-3
Depth		4960 ft.
Bubble Point		1600 psia

In the forward simulation run, we used water rates from the Schwake well as the constraint. To obtain better results, we performed automatic history matching and have generated the properties match that gave us the good results. In doing the history matching, we have used permeabilities in the three-layers and also the pore volume as parameters. **Figure 4-102**, **Figure 4-103**, and **Figure 4-104** show the results obtained for Schwake well from the model. There is a good match between the simulated results

and the actual field production. Though there is some mismatch at initial time in the oil rate, this could be because of the relative permeability uncertainties. The limited knowledge about the relative permeability could have also been the reason for not getting a very good match.

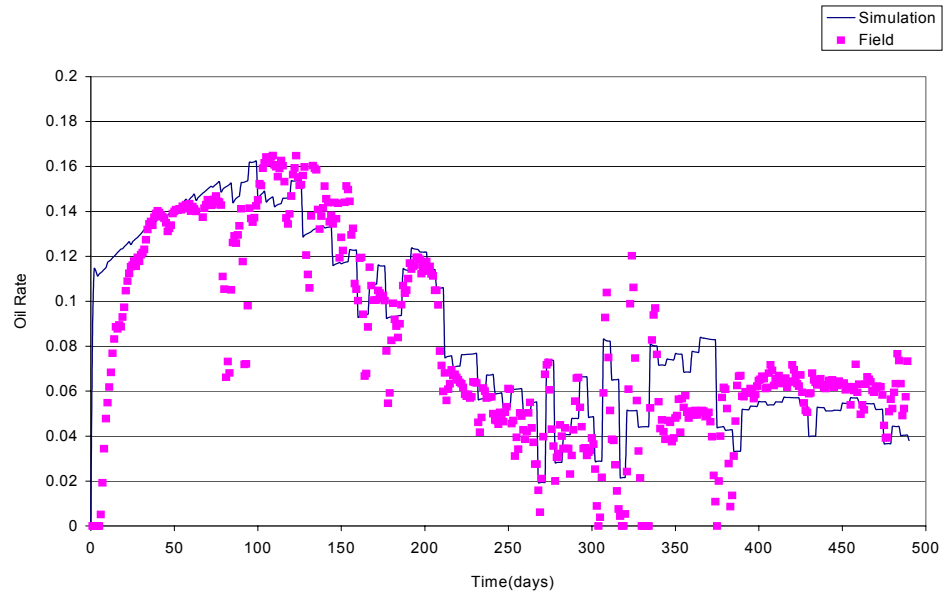


Figure 4-102: Oil rate match for Schwake well

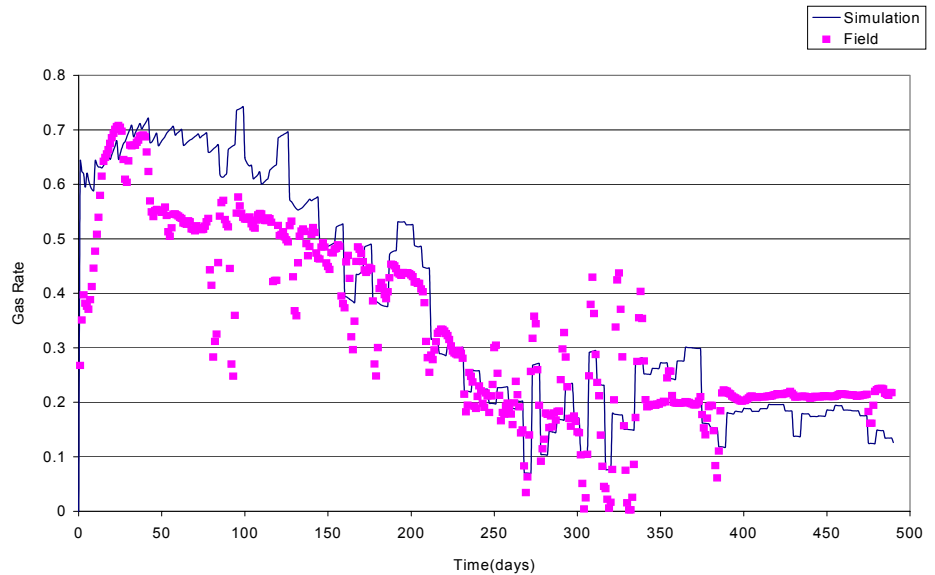


Figure 4-103: Gas rate for Schwake well

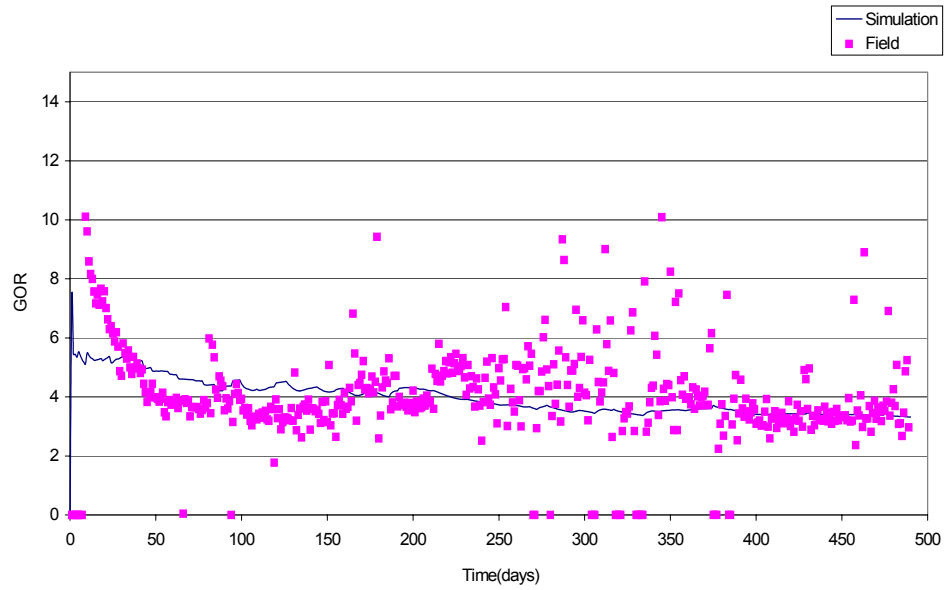


Figure 4-104: GOR for Schwake Well

for the gas rate. The oil and gas rates are normalized in order to standardize them. The actual values were divided by the change in pressure (ΔP).

Gas-oil ratio match is shown in **Figure 4-104**. The simulation has not been able to reproduce the rapid initial decline in the gas-oil ratio. The reason for this is the initial mismatch in the oil rates as discussed above. Apart from the initial mismatch there is a very good match between the simulation results and the field data. Although not shown, the simulation has been able to reproduce water cut as well as bottomhole pressure data reasonably well.

The results shown above were obtained after performing automatic history matching for the single well case. The rock properties were modified accordingly to obtain these results. The regional parameters were also changed in the study to obtain better results. The overall changes in the

properties were within the range of uncertainties (e.g., water layer permeability was changed from 100 md to 64 md). However, one important change which was significant was the drainage volume for the water zone. This zone was significantly bigger than what was originally estimated. This clearly indicates that water was drained beyond the 160 acre drainage area. This is consistent with our prior observations that water zones are interconnected through high permeability/fracture regions. Therefore, communication for water zone extends beyond the drainage area based on the well density. In effect, this confirmed our analysis that aquifer is well connected.

Although the model was able to reproduce most of the production characteristics, it was not able to reproduce the increase in GOR when the well is shut-in. It is believed that the only way we can reproduce this result is if we introduce another non-communicating gas layer in the model. In the next generation model, we will try to incorporate this additional feature.

4.3.4.3.2. Field-Wide Model

We also extended the single well model to the entire field to reproduce the production behavior of the wells. Marjo Operating Company's lease is divided into two parts by a major fault. One side of the field, the west side, has an initial pressure of around 1500 psia, while the other side, the east side, has an average pressure of only 500 psia. Most of the wells have been drilled on the west side of the fault and they have indicated good production characteristics. We, therefore, studied this side of the field in more detail. There have been restrictions in doing the multiple wells model due to the lack of all the desired data. We considered 18 wells on

the west side of the fault for study and there are 6 producing wells on the east side.

Based on the data from the wells, we generated the porosity and permeability maps for the field using interpolation. Due to simplicity of interpolated values, local variations may not have been properly captured that could affect the results. We also had limited information about the respective thickness of the three zones producing oil, gas and water. We used SIMOPT to perform the automatic history matching, and one of the parameters used in it was pore volume, which could account for the uncertainty in the thickness. The other parameter used in the SIMOPT was permeability of the three-layers in both horizontal and vertical direction.

The other limitation of the model was the unavailability of relative permeability values that could represent the fluid behavior. Relative permeability experiments are available for non-fractured cores, but not for fractures. We, therefore used two sets of relative permeability values, one set for the matrix system and the other for the fractures.

In doing the field-wide simulation, we divided the west side of the field into 51 by 105 grid blocks of 200 ft by 200 ft dimensions. The grid block depth is equal to the thickness of the layer. The porosity map that was generated using the interpolation technique was used in this case. Different skin factors were used for different wells based on the production characteristics of each well. The total Hunton thickness used in the model is 40 ft. The gas layer and water layer are 10 ft thick and the oil layer has a thickness of 20 feet. **Figure 4-105** shows the grid structure used for the study. The PVT properties used in the field model are same as the ones used for single well case.

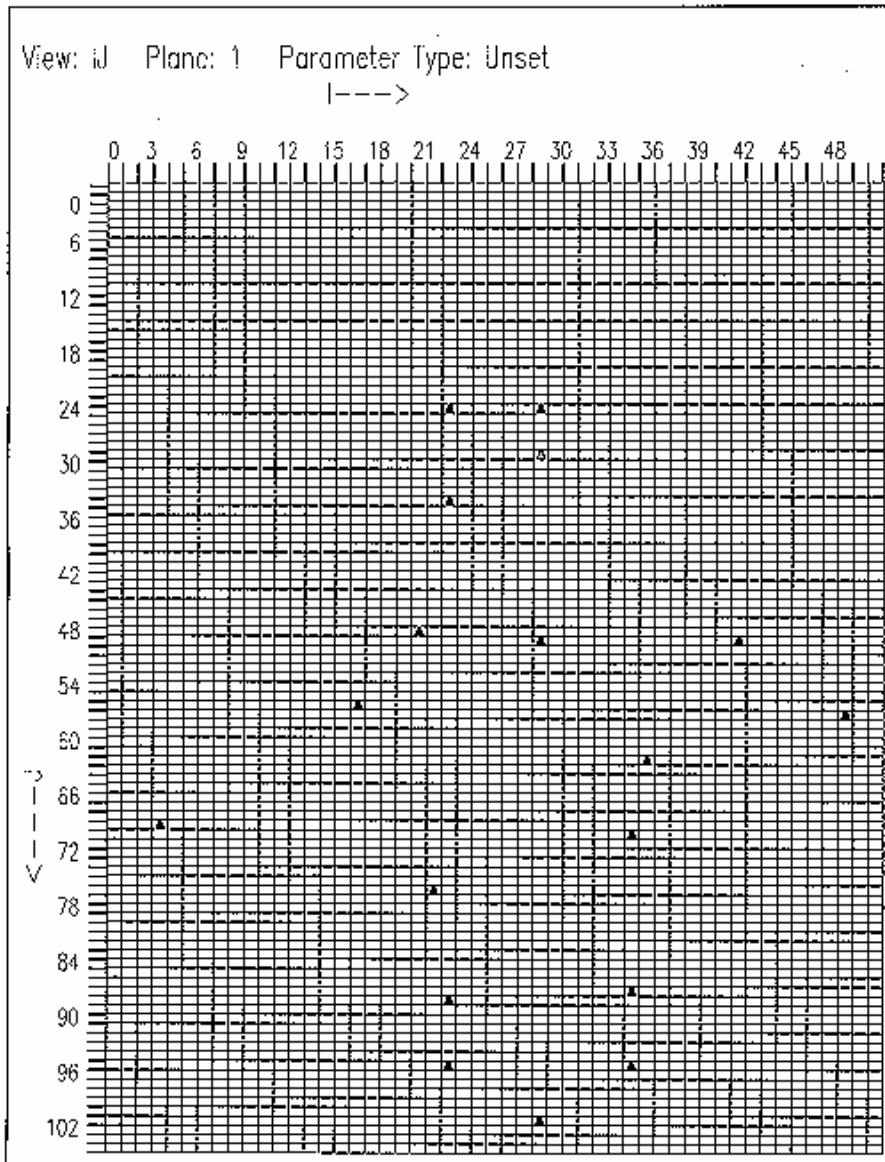


Figure 4-105: Grid structure and the Well locations

Figure 4-106 and **Figure 4-107** show the maps of oil and gas production rates for the entire field. The match appears reasonable.

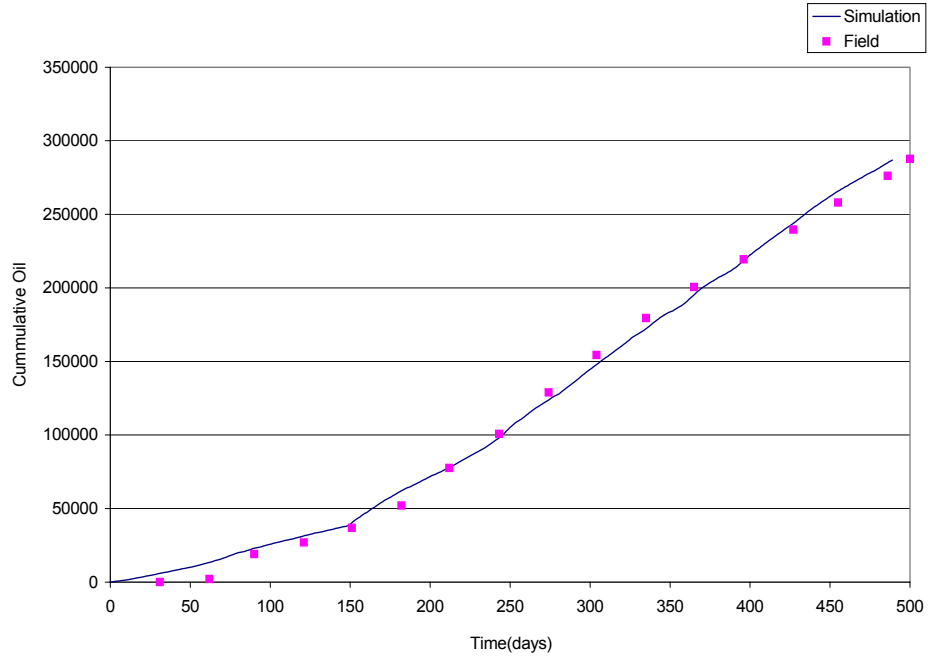


Figure 4-106: Cumulative oil production of the field

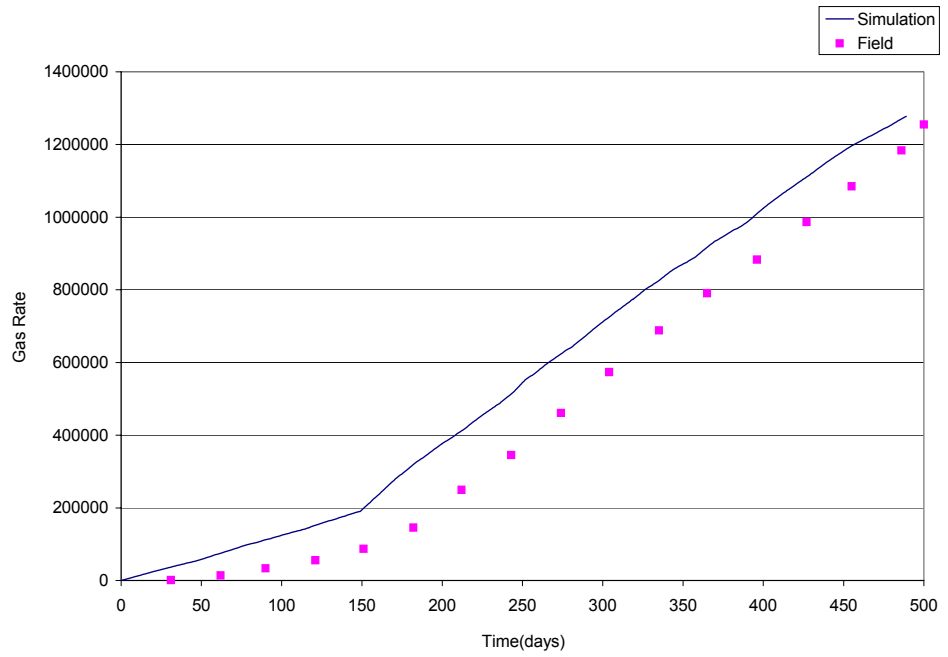


Figure 4-107: Cumulative Gas Production of the Field

Figure 4-108 shows the oil production rate for the Boone the well located at SE quarter of Sec. 4-15N-2E. It can be seen that there is a good match between the simulated results and the actual field data. The model has been able to properly capture the production profile of the well except for the very initial time period when the prediction from the simulation is higher than the field data. The noise in the simulated results is because we have tried to match the daily rates, and the constraint in the forward simulation is the water rate. The gas rate plot for Boone is shown in **Figure 4-109**. The simulation has over-predicted the results. That could be because of the uncertainty in the pore volume of free gas, which was included in the original model. However, the overall trends are captured well.

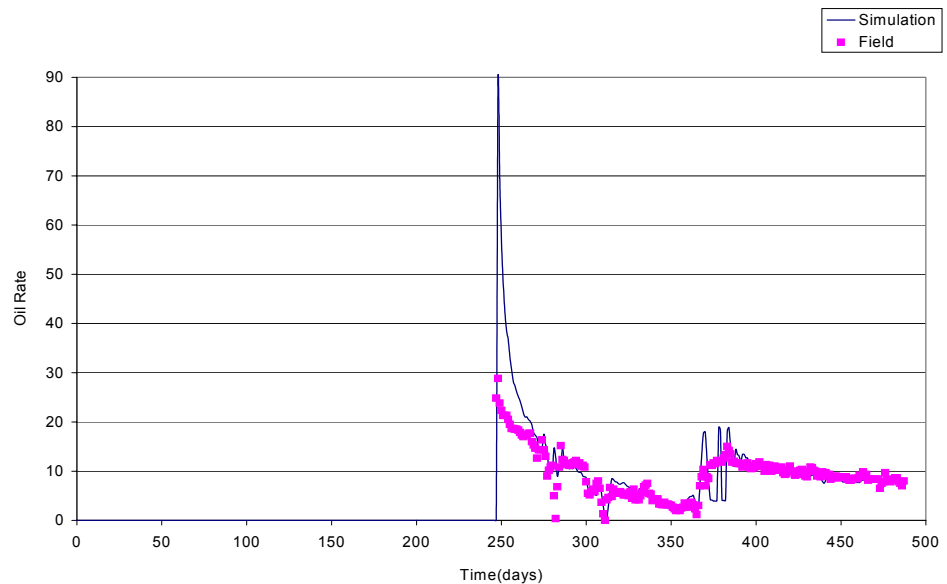


Figure 4-108: Oil Rate for the Boone well

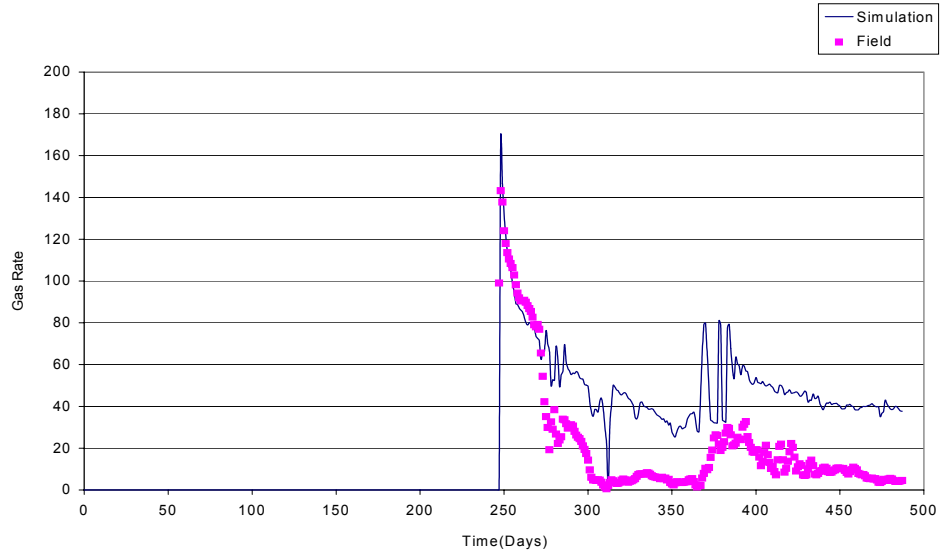


Figure 4-109: Gas Rate for the Boone well

Figure 4-110 shows the plot of GOR for Danny # 1. Again the match is reasonable indicating that important characteristics of the production data are preserved in the proposed model.

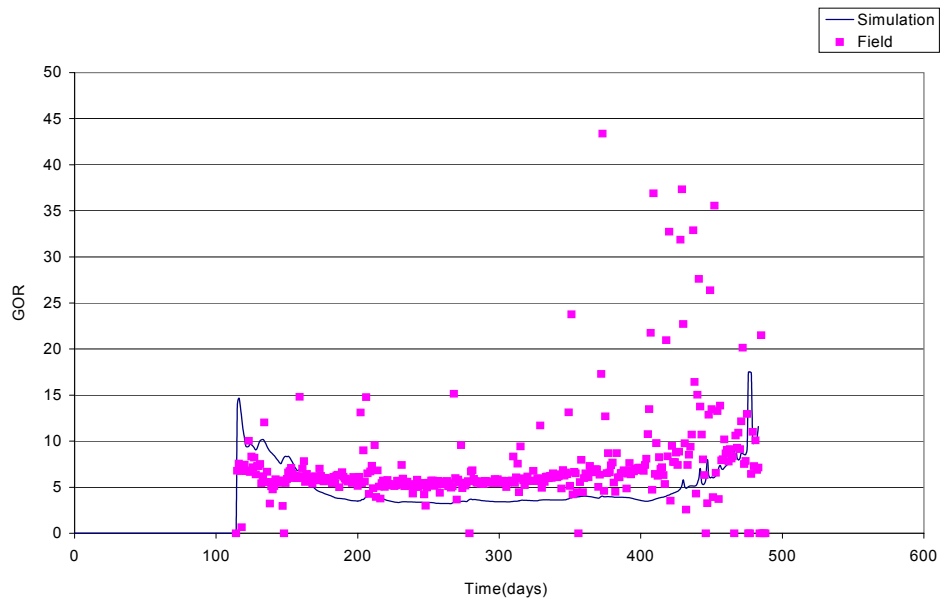


Figure 4-110: GOR plot of Well Danny #1

In general, the changes in the physical properties were reasonable for achieving the history match. We are encouraged by the success of this history matching result. Although our petrophysical properties model was simple, we were able to capture important characteristics of the production behavior. With improved geological and petrol-physical model as well as additional relative permeability data, we should be able to improve our history matching results. We intend to continue our efforts in the next budget period.

4.3.5. Excess Water Disposal

In the original proposal, we had decided that we would use downhole water separators to reduce the water handling costs. Downhole separators allow the water to be separated down hole and be injected into the formation below the oil producing formation. Since this field produces a lot of water, we thought that we would be able to save the cost of handling the surface water.

We provided the initial information to CFR, a company in Canada which specializes in down hole water separation. They conducted the economic analysis and provided us with results which showed that the technique would work and would be economically viable. The results were included in the original proposal to demonstrate that DOWS is a viable technology.

The two key elements which make the DOWS technology viable are the reduction in surface handling costs and an increase in the production after DOWS is installed. In the original model, CFR had assumed that the production in West Carney field would increase by 25 % after installation of DOWS.

After the contract was awarded, we started re-examining the calculations provided by CFR. We wanted to understand what would make the technology viable. After further reviewing the literature on DOWS, we realized that the primary reason for increase in production after installing the DOWS is the reduction in back pressure on the formation since there is no fluid in the tubing. We also noticed that in several field cases, the increase in production after installation of DOWS was minimal, and in some cases the production actually decreased. In West Carney field, Marjo Operating Company has made a concerted effort to keep the fluid levels down in the tubing. The wells are tested frequently, and, with the help of appropriate equipment, the fluid level is maintained close to the top of the formation. In light of this information, installation of DOWS would not increase the production from a well.

We used this information and re-run the economics and observed that installation of DOWS would be economically less beneficial than not installing it. We have enclosed the revised economics below. Clearly, the installation of DHOWS is not feasible based on this information.

	Case 1: Without DHOWS	Case 2: With DHOWS	Case 1-Case 2
NPV (M\$)	\$ 568.278	\$ 558.814	\$ 9.464
Np (Mbbbls)	81.478	78.998	2.480
Gp (MMscf)	244.434	236.993	7.441

One needs to be aware that the risk factors associated with installation of DOWS are not included in those calculations. Based on the field evidence so far, there are significant risk factors associated with design and implementation of the DOWS. We provided this new economic analysis to CFR and invited them to respond. They did not do so, in essence, accepting our economic evaluation. In light of adverse economic impact, we decided not to implement DOWS in this study.

In addition to using DOWS, we are also interested in applying compact separators to reduce the separation costs. Currently, DOE is funding a project at the University of Tulsa, which involves testing of compact separators for separating oil and water. Unfortunately, although significant progress has been made, we still do not have a technology mature enough to test it in actual field conditions. We are in constant communication with the principal investigators of the project and, as soon as the technology becomes available, we would like to be the first to install it in the field.

5. TECHNOLOGY TRANSFER

5.1. Overview

Mohan Kelkar and Lori Watts (The University of Tulsa)

An important aspect of this project is effective communication and technology transfer. We have explored several avenues to effectively transfer the technology. These include field trips, presentations and publications, a newsletter, and web page.

In order to explain the details of the project, we have taken several teams on field trips. These trips allowed students and various industry and government professionals to visit the field and appreciate its rapid development.

Project findings were published and presented at quarterly project team meetings and various public meetings as noted below.

Publications and Presentations

- Derby, J., Podpechan, J., and Andrews, J.: “U.S. Department of Energy Sponsored Study of West Carney Hunton Field, Lincoln and Logan County, Oklahoma: A Preliminary Report”, presented at the Tulsa Geological Society Meeting on November 13, 2001 and at the Oklahoma City Geological Society Meeting on January 23, 2002.
- Kelkar, M.: “Production from Hunton Formation: Engineering Perspective”, presented at New Mexico Institute of Technology, September 12, 2000, and at Texas A&M University, October 18, 2001.
- Marwah, V., Kelkar, M., and Keefer, B.: “Reservoir Mechanism for Hunton Formation Production”, SPE 75127 paper to be presented at the SPE/DOE

Thirteenth Symposium on Improved Oil Recovery, Tulsa, Oklahoma, April 13-17, 2002.

- Frederick, J., Kelkar, M., and Keefer, B.: “Production Type Curves for the Hunton Formation”, SPE 75248 paper to be presented at the SPE/DOE Thirteenth Symposium on Improved Oil Recovery, Tulsa, Oklahoma, April 13-17, 2002.
- Kho, T. and Kelkar, M.: “History Matching Using Triple Loop Procedure”, SPE 75220 paper to be presented at the SPE/DOE Thirteenth Symposium on Improved Oil Recovery, Tulsa, Oklahoma, April 13-17, 2002.
- Derby, J., Podpechan, J., and Andrews, J.: "Petroleum Geology of West Carney Hunton Field", to be published in the 2nd quarter 2002 edition of the Oklahoma City Geological Society's “The Shale Shaker”.

The 2001 annual newsletter, TUCRS Hunton News, was published during the second quarter of 2001. The first edition was mailed to over 5,000 small operators and generated much interest. We will begin work on the 2002 newsletter April 1st with a target publication date of May 1, 2002.

In addition, we continue to work to expand the functionality of the project web site. We are currently working with The University of Tulsa's webmaster to utilize new technology available update security controls. It is our goal to provide the most user-friendly security controls, while protecting the integrity of our project's data.

The look of the web site is changing, too. We are adding more color, graphics, and updated navigation buttons for easier viewing.

To view our web site, go to <http://www.tucrs.utulsa.edu>.

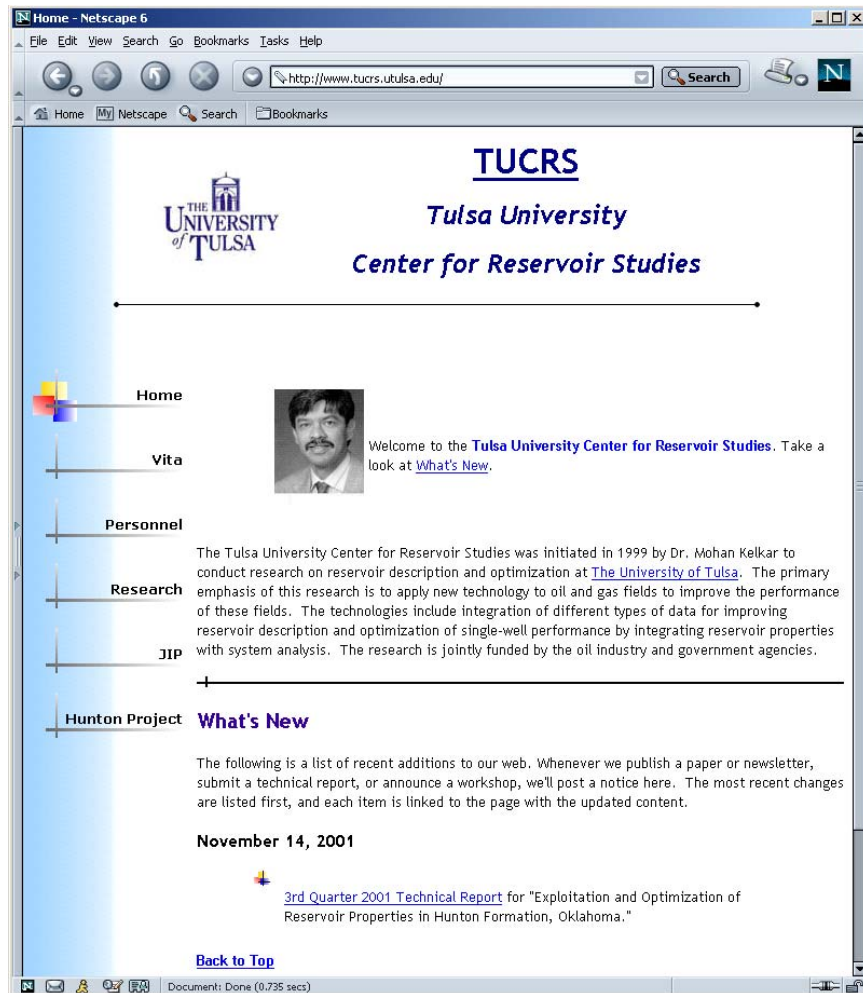


Figure 5-1: TUCRS home page

From The University of Tulsa Center for Reservoir Studies's (TUCRS) home page (**Figure 5-1**), click the "Hunton Project" button. This will take you to the Hunton Project home page (**Figure 5-2**), which contains non-restricted information available to the public, as well as the member login fields.

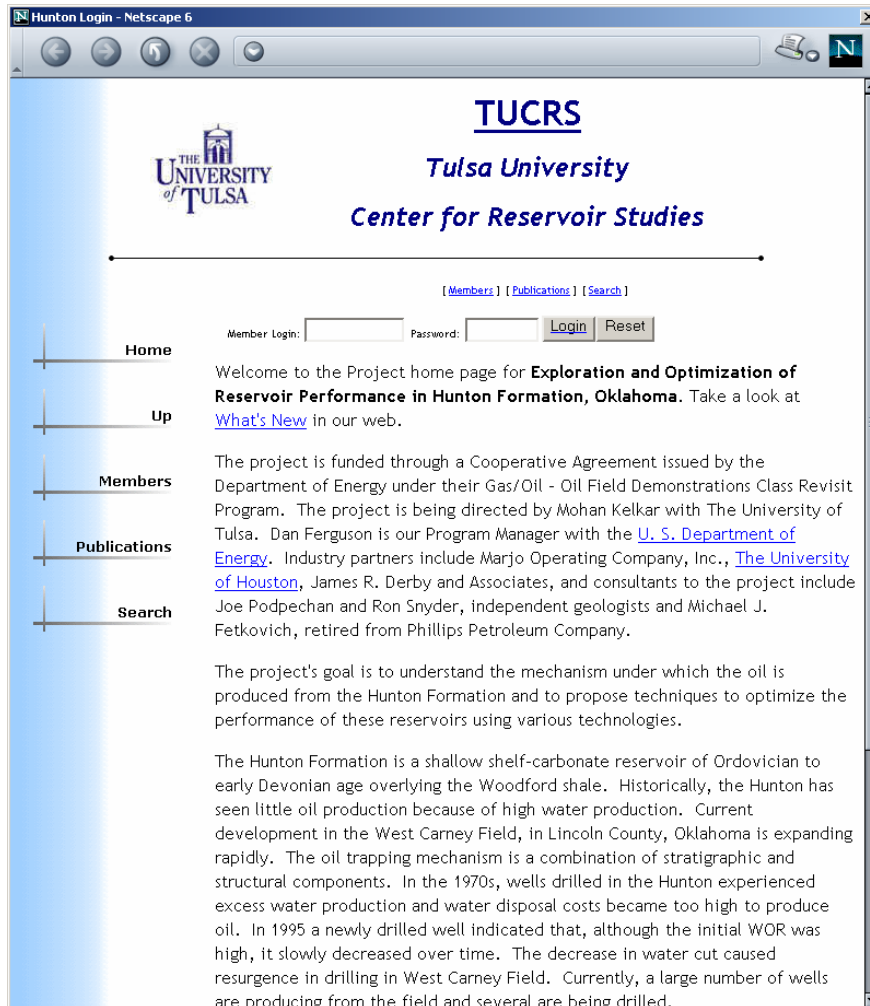


Figure 5-2: Hunton Project home page (non-restricted access)

Information available to the public from the Hunton Project page includes the following:

- **Members** – This page contains contact information for all the members of the DOE Hunton Project. (See **Figure 5-4** for example.)
- **Publications** – This page contains links to our project's status reports, publications and newsletters (non-restricted documents only). (See **Figure 5-6** for example.)
- **Search** - Use the search form to search for documents in this web containing specific words or combinations of words. (See **Figure 5-15** for example.)

To access information restricted to project members, enter your member login ID and password.

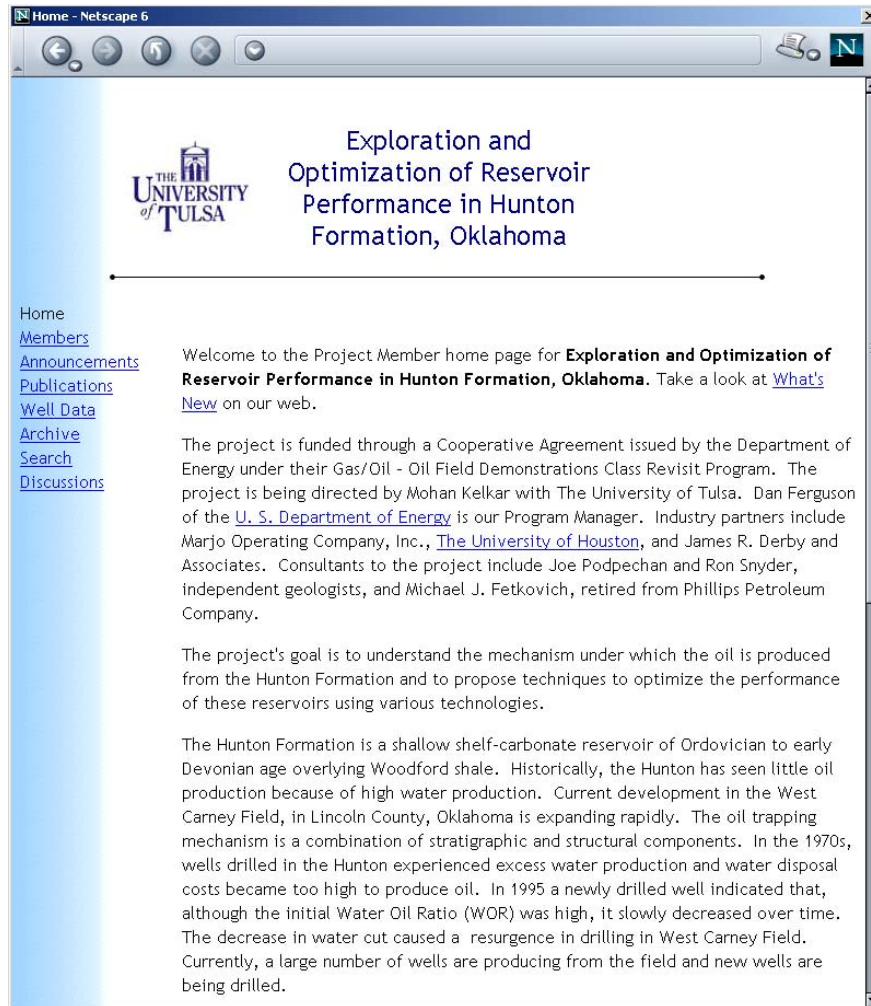


Figure 5-3: Hunton Project member home page

This page is restricted to members of the Exploration and Optimization of Reservoir Performance in Hunton Formation, Oklahoma project. From the Hunton Project member home page, you may access the following information:

5.2. Project Web Page

Lori Watts (The University of Tulsa)

5.2.1. Members

This page (**Figure 5-4**) contains contact information for all the members of the DOE Hunton Project. From here, you can send e-mail to project members or visit their personal home pages.

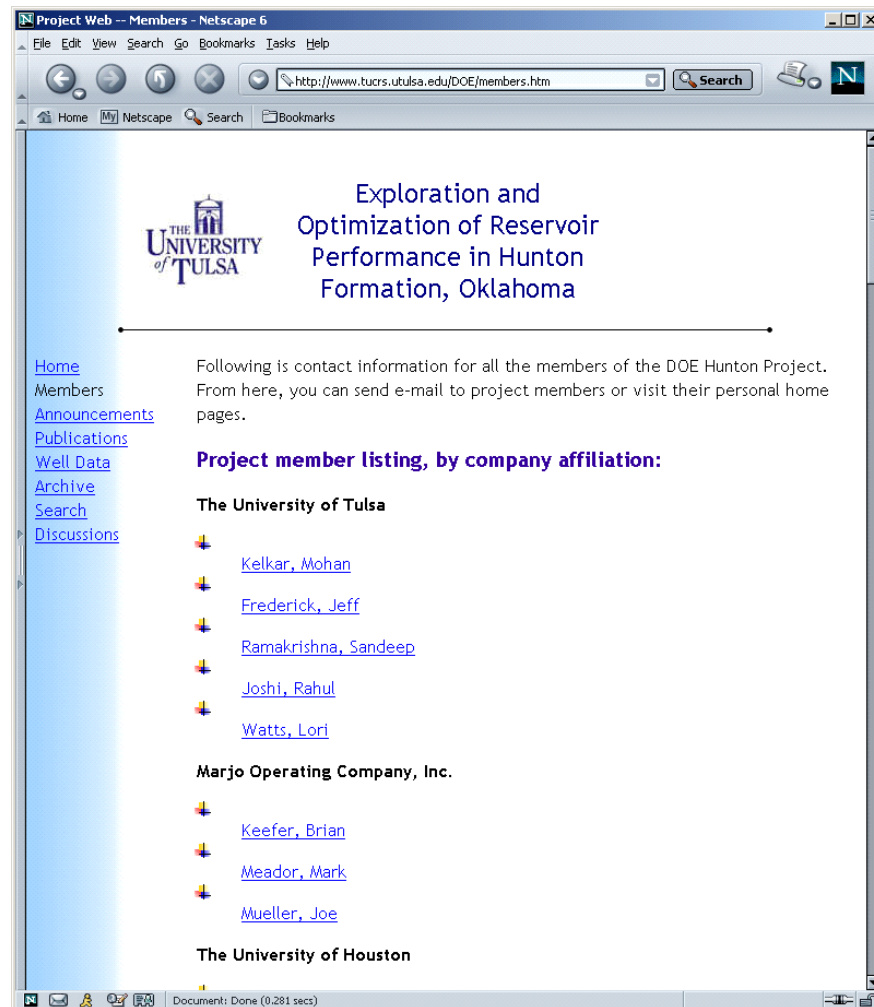


Figure 5-4: Hunton Project Members page

5.2.2. Announcements

This page (**Figure 5-5**) contains a list of scheduled project-related deliverables, events, and key milestones.

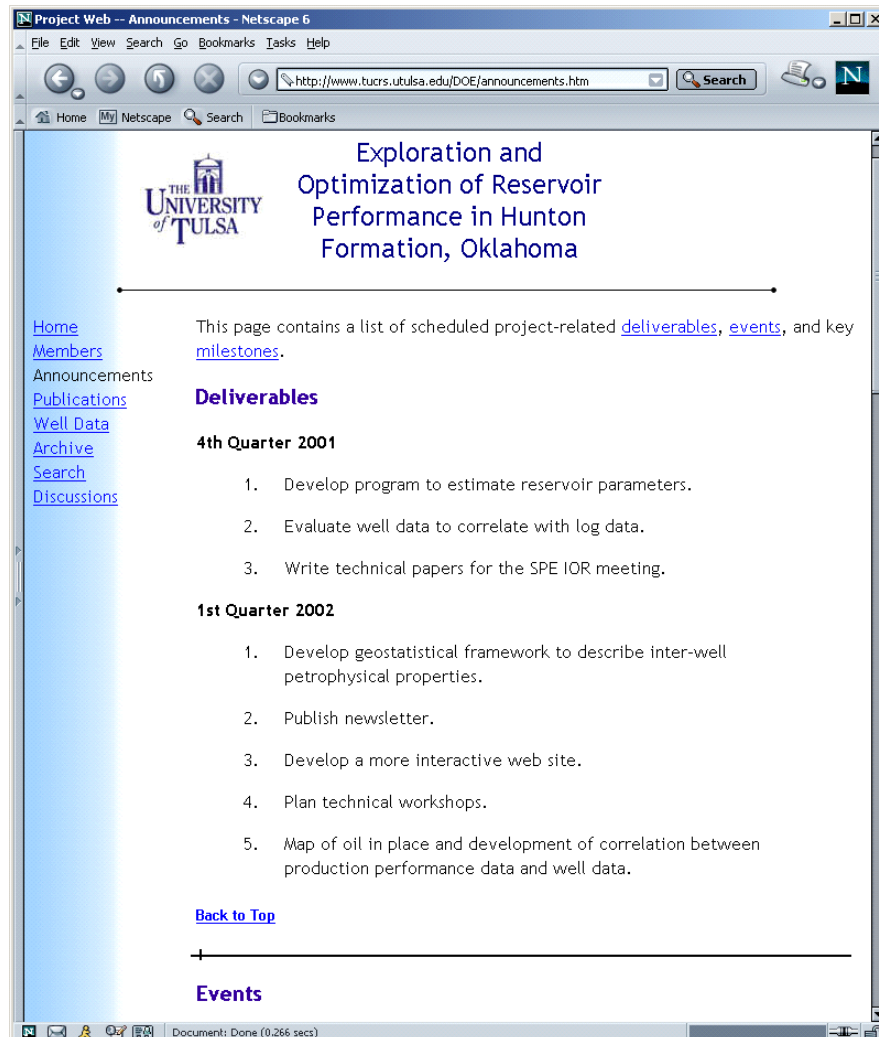


Figure 5-5: Hunton Project Announcements page

5.2.3. Publications

This page (**Figure 5-6**) contains links to published documents related to the project, but that are authored by non-project members. Subjects include Reservoir Engineering, Production Engineering and Geology.

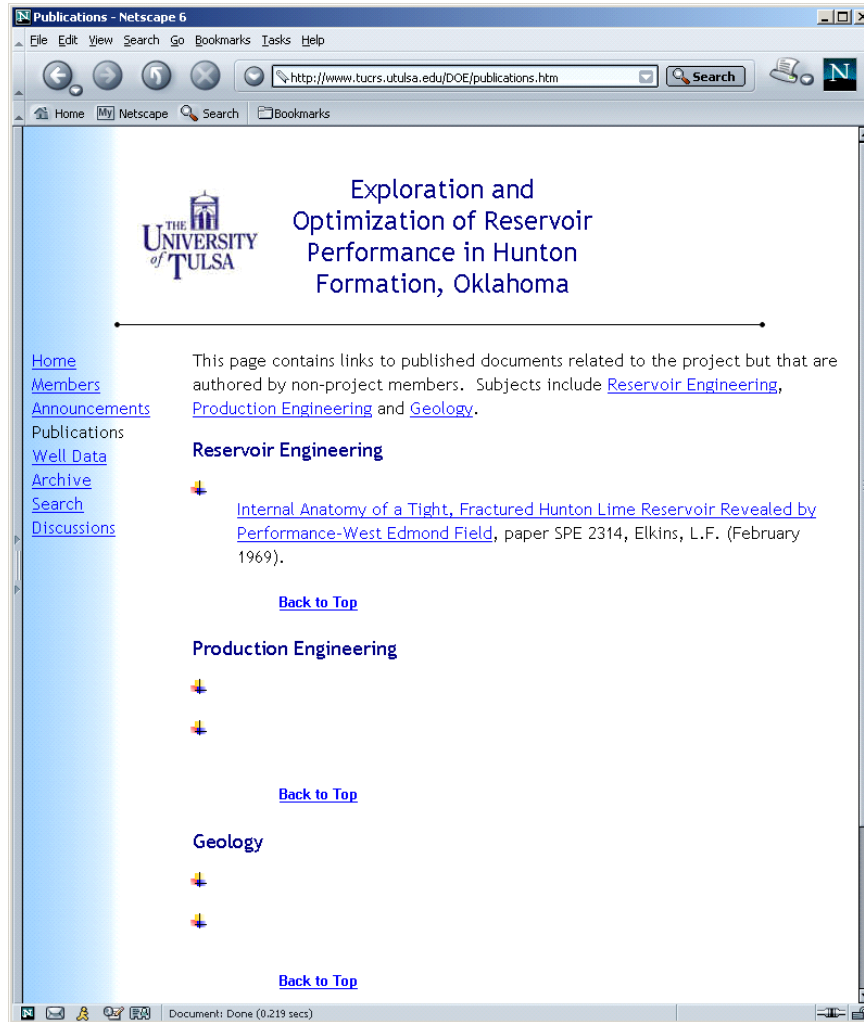


Figure 5-6: Hunton Project Publications page

5.2.4. Well Data

This page (**Figure 5-7**) contains the well data repository for the Exploration and Optimization of Reservoir Performance in Hunton Formation, Oklahoma project.

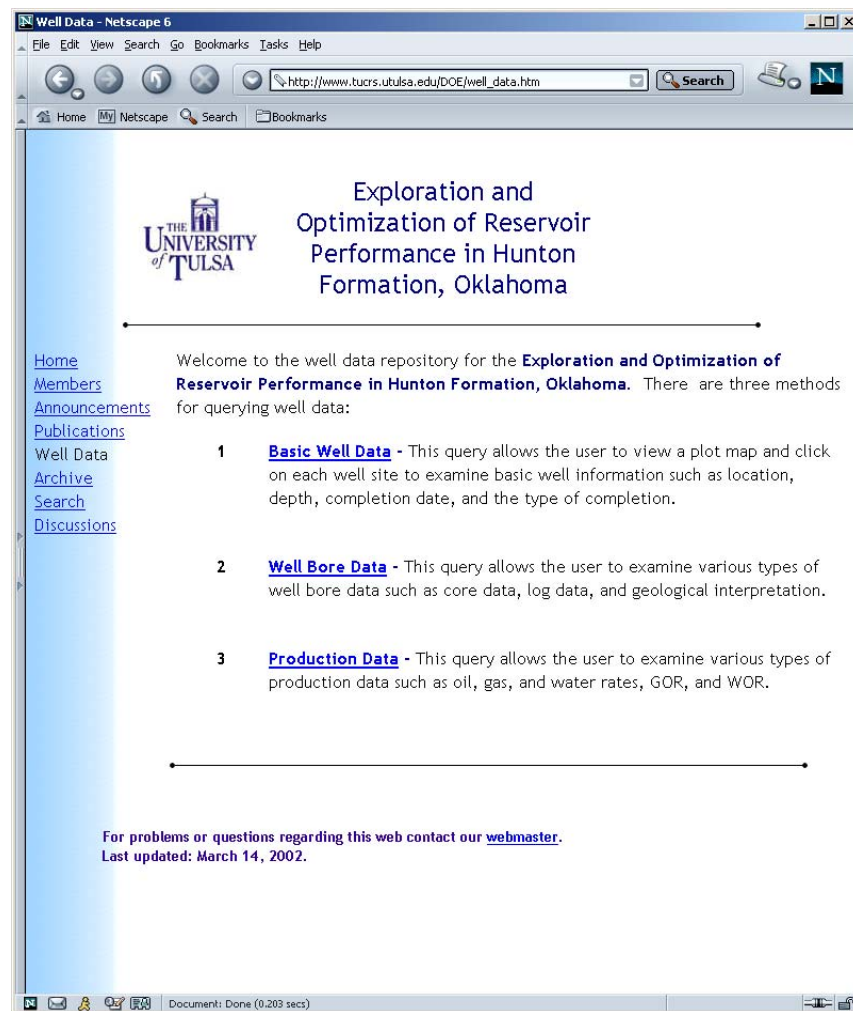


Figure 5-7: Hunton Project Well Data page

There are three methods for querying well data:

5.2.4.1. Basic Well Data

This query page (**Figure 5-8**) allows the user to view a plot map and click on each well site to examine basic well information (**Figure 5-9**) such as location, depth, completion date, and the type of completion.

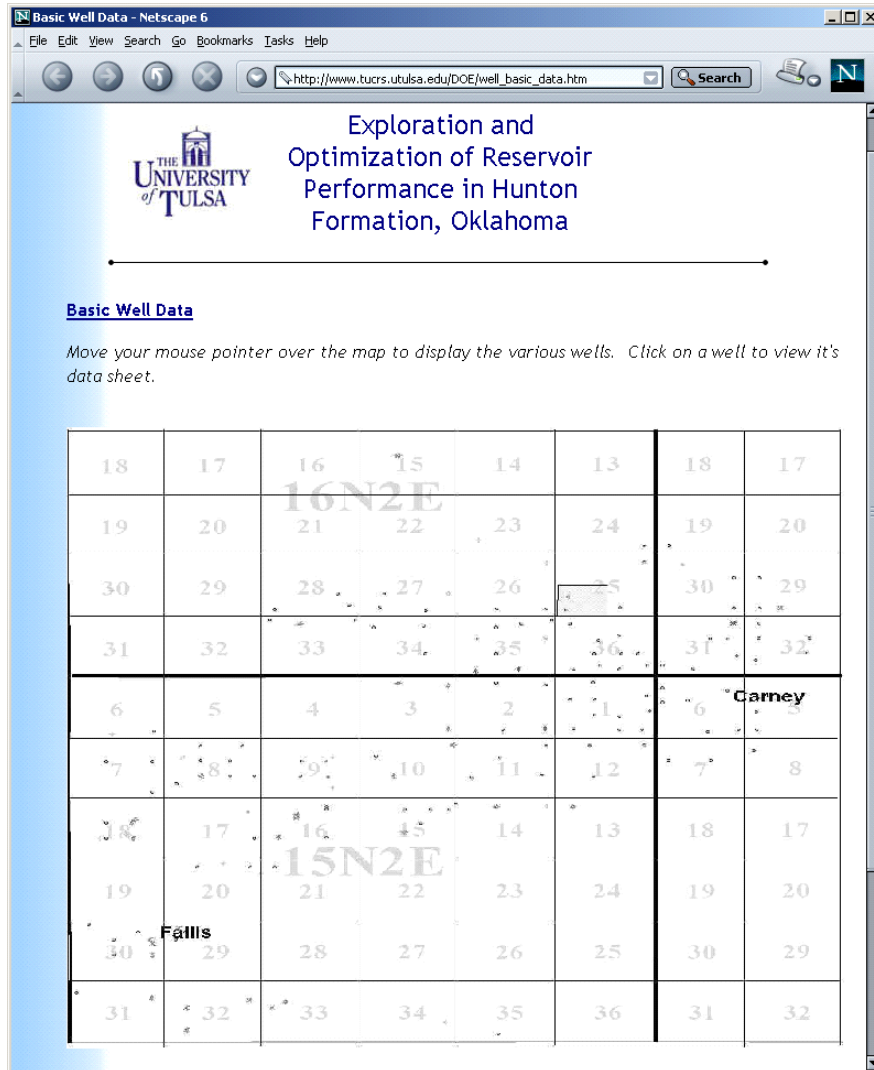


Figure 5-8: Hunton Project Basic Well Data page

Note: New software has been purchased which will allow our research assistants to plot and update the map as new wells are drilled. And since the wells will be plotted by longitude/latitude coordinates, the map will be more

accurate than the one currently available. The display and colors should also appear sharper.

Adobe Acrobat - [rwgfd2ec.pdf]

File Edit Document Tools View Window Help

Parkview #1-3 Data Sheet

Company Marjo Operating Co., Inc. Well Name _____ Parkview #1-3
 Area Name _____ Carney
 Loc. Sec. _____ C SE SE Sec. 3 Twp/Blk 15N Rng/Surv 2E County Lincoln State OK
 Field _____ NE Falls GL 1048 KB 1056 Datum Above GL 8
 Drilling Contractor _____ Akerman Drilling Completion Contractor _____ Genie Well Service

Completion Type
 Oil Gas Other

Tools	Date Commenced	Date Completed	Depth (ft)	
			From	To
Rotary	1/23/00	1/31/00	0	4981
Completion	2/7/00	2/14/00	4910	4987

TD: _____ 4987
 PBD: _____

CASING-CEMENT RECORD

HOLE		CASING				CEMENT			
Size	Depth	Set At	Size	Weight	Grade	Cond	#Sx	Type	Cmt Top
12 1/4	628	618	8 5/8	24	LS		300	A+3%ccc+1/4#sk Floccle	Surface
7 7/8	4981	4950	5 1/2	15.50	J55		125	H+5%KCl+0.4% FL62	4227
4 3/4	4987	OH							

LOGGING

PERFORATIONS
 Perforated Intervals _____ 4950-4987 OH
 Perforating Company _____ Type Gun _____ No. Shots/Ft _____

PRODUCING FORMATION(S)
 Producing Formation _____ Depth, Top of Formation _____
 Hunton 4965

FLOWING PRESSURES (psig) **SHUT-IN PRESSURES (psig)** **OTHER DATA**
 Tubing _____ Tubing _____ Choke Size (in) _____
 Casing _____ Casing _____ BHP (psig) 1685.64

DRILLING DATA

COMPLETION DATA
 Acidize w/ 10080 gal 15% NE-FE ret acid. AIR=38.4 BPM, AIP=1050#, ISDP=750#, 5"=650#, 10"=550#, 15"=400#
 Tubing: DN2150 pump, crossover, 152 jts tbg

TUBING **PACKER**
 Size 2 7/8 Type _____ 6.5 Grade J55 Type _____
 No. Jts 152 Depth 4874 SN Depth _____ Size _____ Set @ _____
 Avg Jt Length _____ 31.65
 Tubing Run Open Ended Yes No

RODS
 API Rod Designation: _____

PUMPING
 SPM _____ Stroke Length (in) _____

PUMPING EQUIPMENT
 Sub Surface Pump: Make _____ DN2150 Size _____
 Pumping Unit: Make _____ Size _____
 Prime Mover: Make _____ Size/HP _____

SPECIAL EQUIPMENT

119% 1 of 2 8.5 x 11 in

Figure 5-9: Well Data Sheet

5.2.4.2. Production Data

This query page (**Figure 5-10**) allows the user to select a specific well (**Figure 5-11**) from the drop-down list and examine various types of production data (**Figure 5-12**) such as oil, gas, and water rates, GOR, and WOR for the well selected.

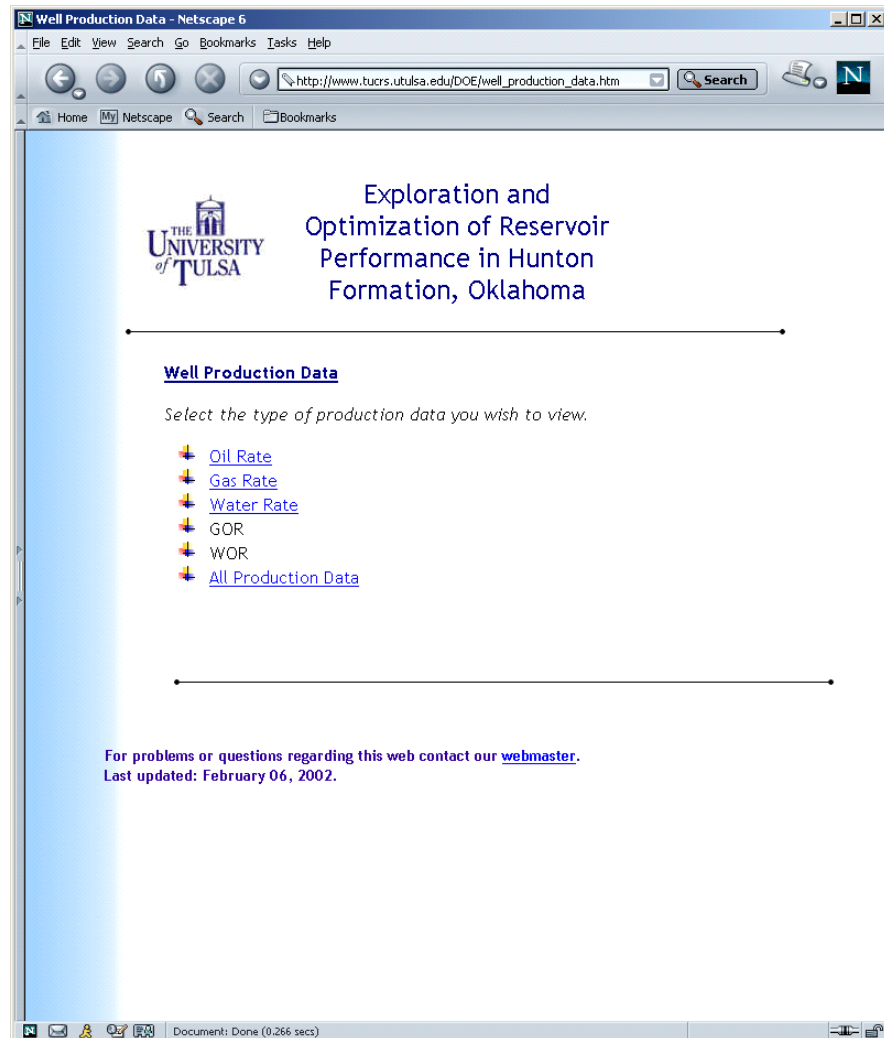


Figure 5-10: Hunton Project Well Production Data page

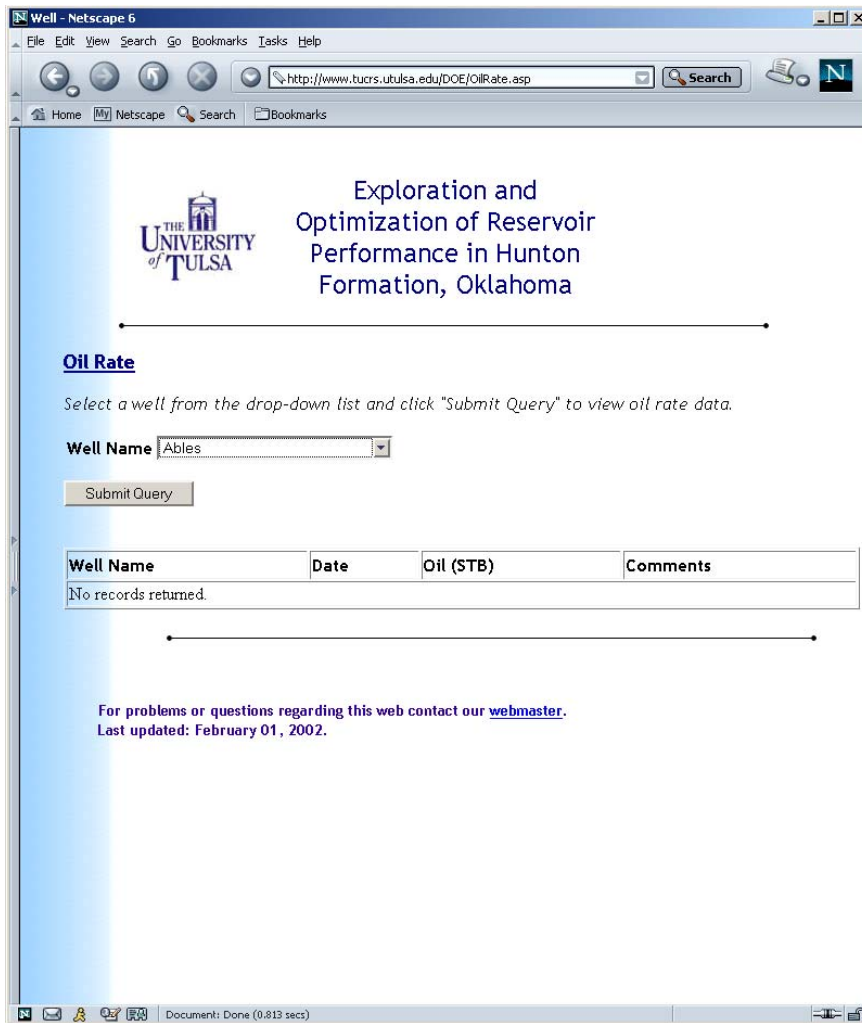


Figure 5-11: Hunton Project Well Production Data, Oil Rate page

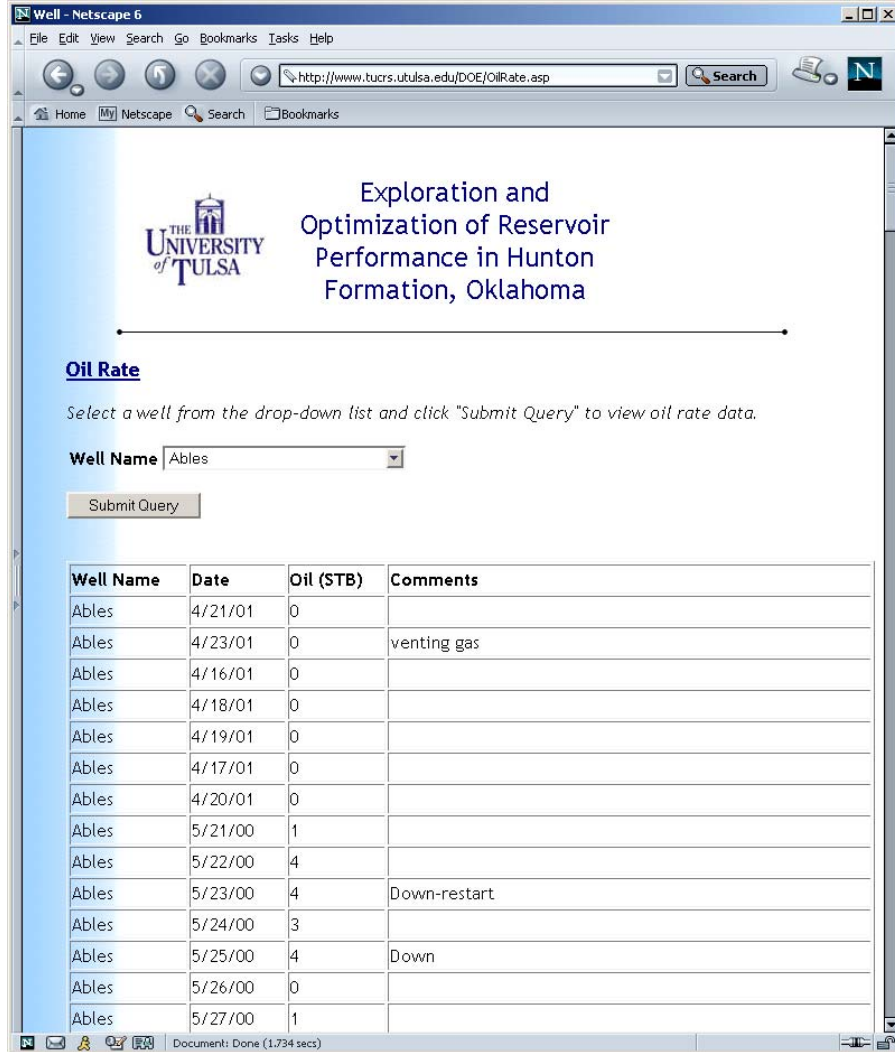


Figure 5-12: Hunton Project Well Production Data, Oil Rate page with query information displayed

5.2.4.3. Well Bore Data

This query page (**Figure 5-13**) operates the same as the Well Production Data page (**Figure 5-10**) and allows the user to examine various types of well bore data, such as core data, log data, and geological interpretation, for individual wells.

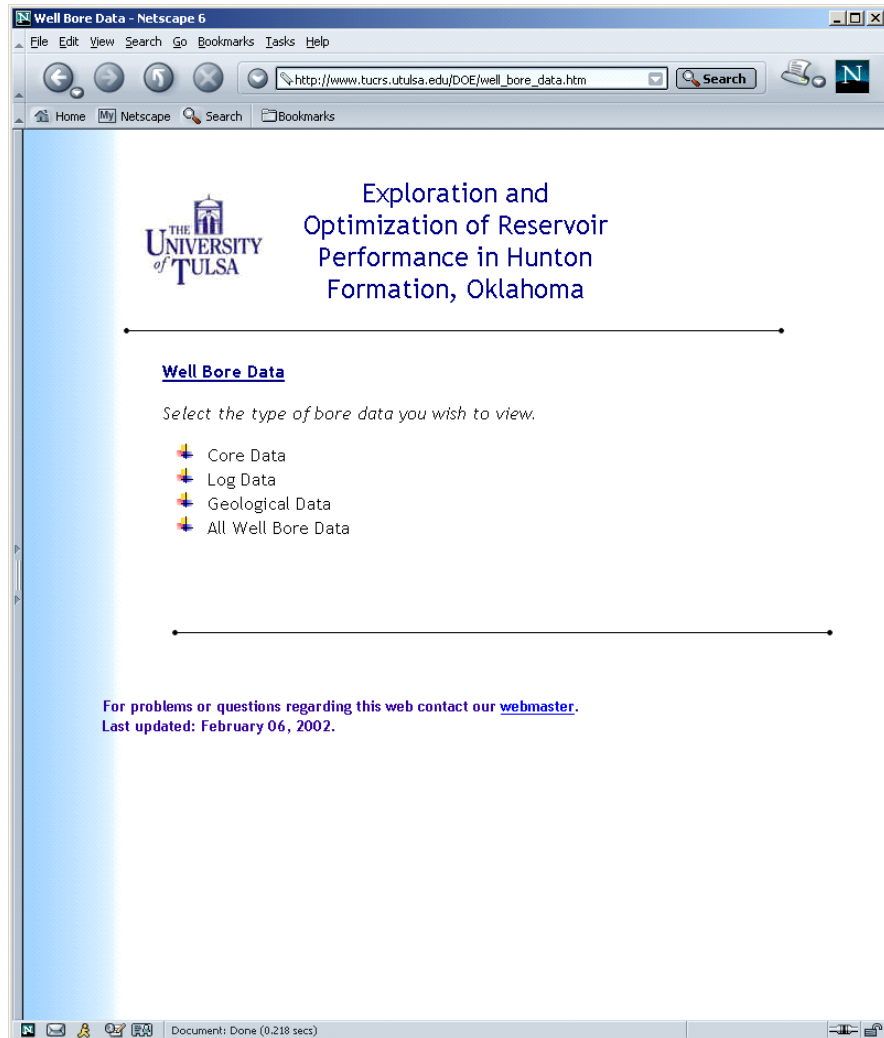


Figure 5-13: Hunton Project Well Bore Data page

5.2.5. Archive

This page (**Figure 5-14**) contains links to internal documents authored by project members, technical status reports, and database programs and components developed by the project team.

Each entry provides the document title or topic with a link to the document, author name(s), and the designated document format.

The screenshot shows a web browser window with the following content:

THE UNIVERSITY OF TULSA Exploration and Optimization of Reservoir Performance in Hunton Formation, Oklahoma

This page contains links to [internal documents](#) authored by project members, to [technical status reports](#) and database programs and components developed by the project team.

Each entry provides the document title or topic with a link to the document, author(s), and the designated document format.

Internal Documents

The following documentation may only be viewed by **internal** project members.

All documents are in .pdf format, unless noted otherwise, and require a free download of [Adobe Acrobat Reader](#) to view.

Large presentation packages have been compressed into one file (.zip) and require a free download of [WinZip](#) to unzip.

Document Title/Topic	Author	Back to Top
Project Meeting - February 8, 2002		
Agenda	Watts, Lori	
Carbonates: Wettability, Permeability from NMR Logging	Mohanty, Kishore	
Evaluation of Production Data to Estimate Reservoir Parameters	Frederick, Jeff	
Log Analysis Update	Ramakrishna, Sandeep & Joshi, Rahul	
Study of the West Carney Hunton Field: Lincoln & Logan County, Oklahoma: A Preliminary Report (.zip)	Podpechan, Joe & Derby, Jim	
Web Diagram	Watts, Lori	
Project Meeting - October 5, 2001		
Agenda	Watts, Lori	
Geological Analysis, Current Status	Ramakrishna, Sandeep	
Exploitation & Optimization of Reservoir Performance in Hunton Formation, Oklahoma	Kishore, Mohanty	
Decline Curve Analysis	Frederick, Jeff	
Primary Production Mechanism Assessment for Hunton Reservoir	Marwah, Vineet	

Figure 5-14: Hunton Project Archive page

5.2.6. Search

Use the search form to search (**Figure 5-15**) for documents in this web containing specific words or combinations of words.

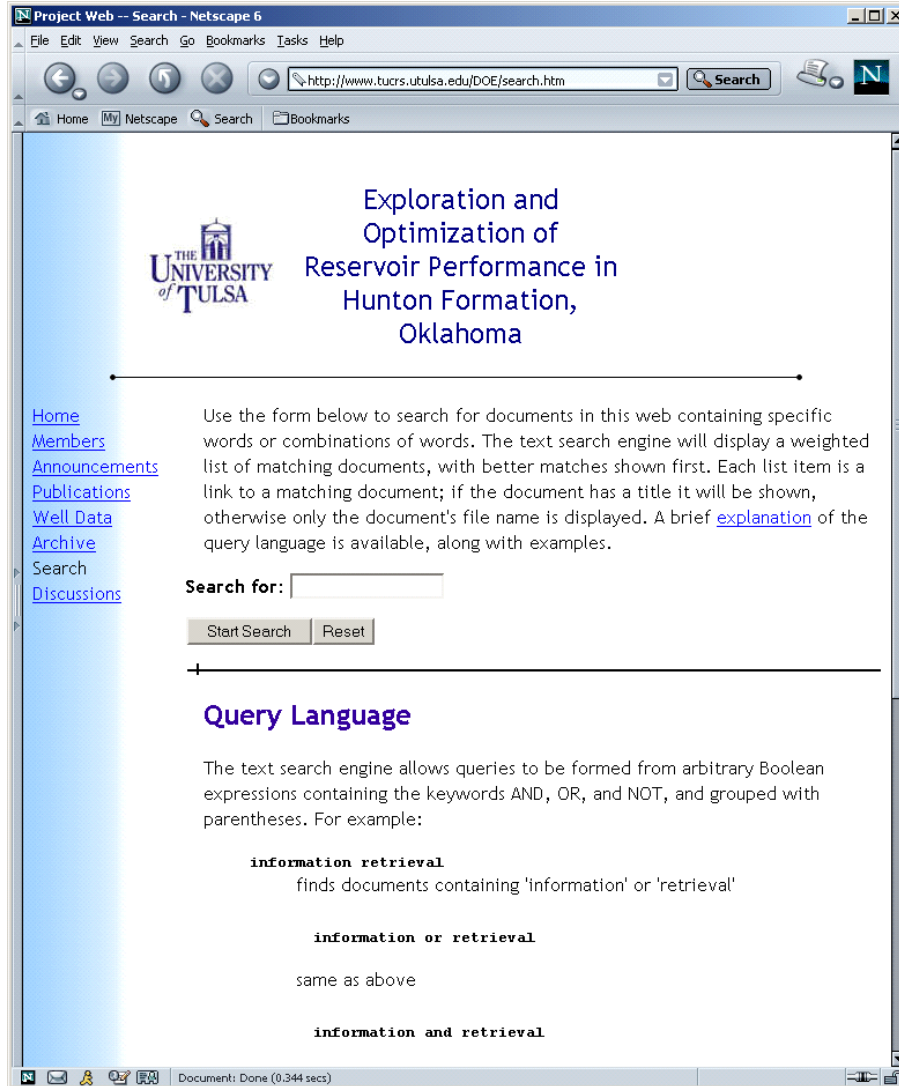


Figure 5-15: Hunton Project Search page

5.2.7. Discussions

This page (**Figure 5-16**) contains links to discussions for the project.

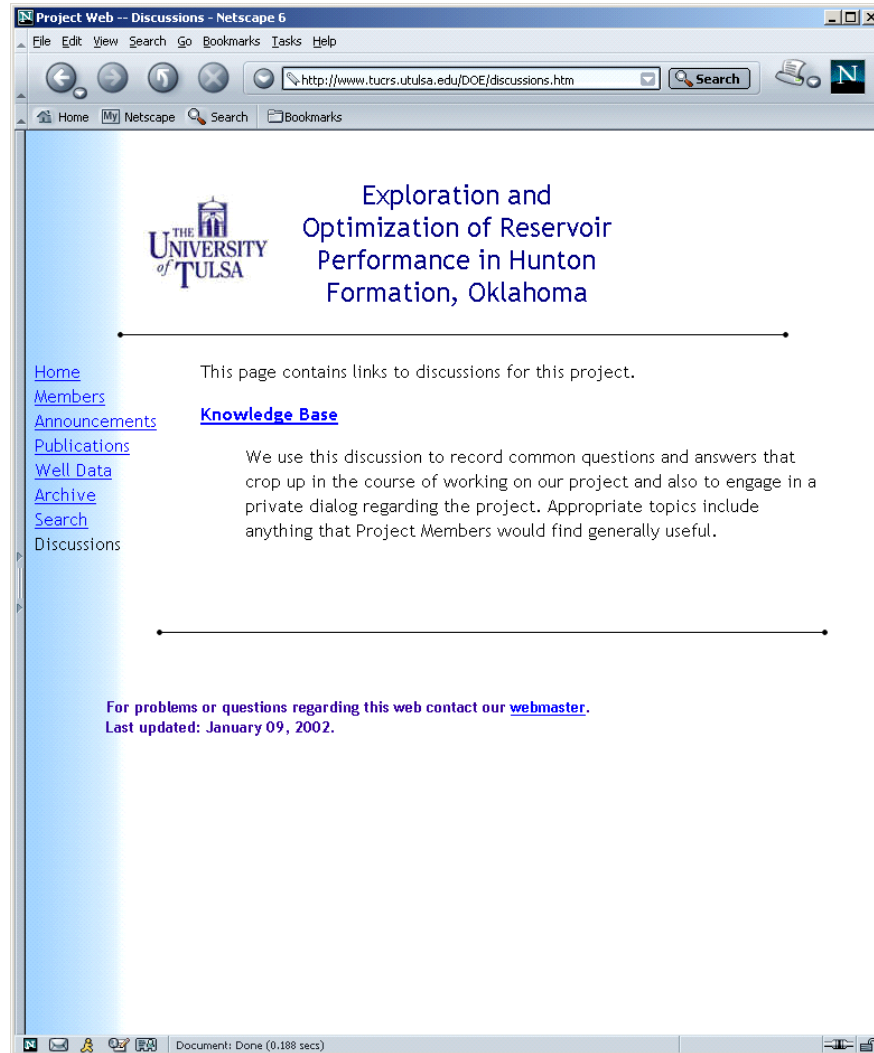


Figure 5-16: Hunton Project Discussions page

6. REFERENCES

1. Fritz, R. C., 1978, Structural Contour Map of Oklahoma on the Pennsylvanian Wapanucka Limestone: Unpublished Master of Science Thesis, Oklahoma State University.
2. Johnson, K. S, and others, 1988, Southern Midcontinent Region, *in* Sloss, L. L. (ed). Sedimentary cover-North American craton, U. S., The Geology of North America, Geological Society of America, Boulder, v. D-2, p. 307-359.
3. Jordan, L., 1965, Geologic Map and section of Pre-Woodford Rocks in Oklahoma: Oklahoma Geological Survey Map GM-9 (1965).
4. Comer, J.B., and Hinch, H.H., 1987, Recognizing and Quantifying Expulsion of Oil from the Woodford Formation and Age-Equivalent Rocks in Oklahoma and Arkansas: AAPG Bulletin, v. 71 (1987) p 844-858.
5. Stanley, T.M., 2001, Stratigraphy and Facies Relationships of the Hunton Group, Northern Arbuckle Mountains and Lawrence Uplift, Oklahoma: Oklahoma Geological Survey Guidebook 33, 73 p.
6. Jordan, L., 1962, "Geologic Map and Section of Pre-Pennsylvanian Rocks in Oklahoma," Oklahoma Geological Survey Map GM-5 (1962).
7. Levorsen, A.I., 1967, Geology of Petroleum, W.H Freeman Co, San Francisco, California (1967) p 724.
8. Amsden, T.W., 1980, Hunton Group (Late Ordovician, Silurian, and Early Devonian) in the Arkoma Basin of Oklahoma: Oklahoma Geological Survey Bulletin 129, 136 p., 16 pl..
9. Rottmannn, Kurt, E.A. Beaumont, R.A. Northcutt, Zuhair Al-Shaieb, Jim Puckett, and Paul Blubaugh, 2000, Hunton Play in Oklahoma (including Northeast Texas Panhandle): Oklahoma Geological Survey Special Publication 2000-2, 131 p., 6 pls.
10. Barrick, J. E., 2001, Conodont biofacies and biostratigraphy of Silurian strata of the Hunton Group in Oklahoma, and equivalent units in west Texas and eastern New Mexico, *in* Johnson, K.S. (ed.), Silurian, Devonian, and Mississippian geology and

- petroleum in the southern Midcontinent, 1999 Symposium: Oklahoma Geological survey Circular 105, p. 169.
11. Jeppsson, L., 1998, Silurian Oceanic Events: Summary of General Characteristics: *in* Landing, E. and Johnson, M., (eds.), *Silurian Cycles: Linkages of Dynamic Stratigraphy with Atmospheric, Oceanic, and Tectonic Changes*, New York State Museum Bulletin 491 (1998) pp 239-257.
 12. Comer, J.B., 1992 Organic Geochemistry and Paleogeography of Upper Devonian Formations in Oklahoma and Northwestern Arkansas, Oklahoma Geological Survey Circular 93, p. 70-93, *in* Johnson, K.S., and Cardott, B.J., (eds) 1992, *Source Rocks in the Southern Midcontinent, 1990 Symposium: Oklahoma Geological Survey Circular 93* (1992) pp 352.
 13. Lucia, F. J., 1995, Rock Fabric/Petrophysical Classification of Carbonate Pore Space for Reservoir Characterization, *AAPG Bulletin*, v. 79, no. 9, p 1275-1300.
 14. Johnson, M.E., Y.I. Tesakov, N. N. Predtetchensky, and B.G. Baarli, 1997, Comparison of Lower Silurian shores and shelves in North America and Siberia: *Geological Society of America Special Paper 321*, p. 23-45.
 15. Johnson, M. E., 1987, Extent and Bathymetry of North American Platform Seas in the Early Silurian: *Paleoceanography*, v. 2, no. 2, p. 185-211 (April, 1987).
 16. Loucks, R.G., 1999, Paleocave Carbonate Reservoirs: Origins, Burial-Depth Modifications, Spatial Complexity, and Reservoir Implications : *AAPG Bulletin* , Vol. 83, no. 11 , Pages 1795 - 1834 .
 17. Ripley, B.D., *Modern Applied Statistics with S-Plus*, Springer-Verlag, New York, (1994) 301.
 18. Lee, S.H. and Datta-Gupta, A., “Electrofacies Characterization and Permeability Predictions in Carbonate Reservoirs: Role of Multivariate Analysis and Nonparametric Regression,” SPE 56658 paper presented at the 1999 SPE Annual Technical Conference and Exhibition, Houston, Texas, October 3-6.
 19. Doveton, J., “Pfeffer: Petrofacies Evaluation of Formations for Engineering Reservoirs”, The University of Kansas. (July 2001).

20. Agarwal, R.G. *et al.*, “Analyzing Well Production Data Using Combined-Type-Curve and Decline-Curve Analysis Concepts,” SPEREE (Oct. 1999) 478.
21. Myers, G.E., *Analytical Methods in Conduction Heat Transfer*, second edition, AMCHT Publications, Madison, WE (1998).
22. Stehfest, H., “Numerical Inversion of Laplace Transforms,” *Algorithm 368, Communications of ACM* (Jan. 1970) 13, No. 1, 47-49.
23. Carvalho, R.S. *et al.*, “Robust Procedures for Parameter Estimation by Automated Type-Curve Matching,” paper SPE 24732 presented at the 1992 SPE Annual Technical Conference and Exhibition, Washington D.C., Oct. 4-7.
24. Carvalho, R.S. *et al.*, “Simple Procedures for Imposing Constraints for Nonlinear Least Squares Optimization,” paper SPE 29582 presented at the 1995 SPE Rocky Mountain Regional/Low-Permeability Reservoirs Symposium, Denver, March 20-22.
25. Whitson, C.H. and Brule, M.R., *Phase Behavior*. SPE Monograph Series, Richardson, Texas, Volume 20, 2000.
26. “Analysis of Reservoir Performance, Operating Costs and Future Operating Program”, West Edmund Hunton Lime Unit, Sohio Operating Company, Oklahoma City, OK, June 1953.
27. Marwah, V., *Primary Production Mechanism Assessment for Hunton Reservoir*, M.S. Thesis, The University of Tulsa (December 2001).
28. Dunham, R. J., Classification of carbonate rocks according to depositional texture, *in* W.E. Ham, ed., *Classification of carbonate rocks—a symposium: AAPG Memoir 1*, p. 108-121.
29. Archie, G.E., 1952, Classification of carbonate reservoir rocks and petrophysical considerations: *American Association of Petroleum Geologists (AAPG) Bulletin*, v. 36, no. 2, p. 278-298
30. Choquette, P.W., and L. C. Pray, 1970, Geological nomenclature and classification of porosity in sedimentary carbonates: *AAPG Bulletin*, v. 54, no. 2, p. 207-250.

31. Lucia, F.J., 1983, Petrophysical parameters estimated from visual descriptions of carbonate rocks: A field classification of carbonate pore space: Jour. Petroleum Technology, March, 1983, p. 629-637.

7. APPENDICES

7.1. Geologic Appendix

James R. Derby (Derby & Associates, Inc.), Joe Podpechan and Jason Andrews (Independent Geologists), and Sandeep Ramakrishna (The University of Tulsa)

7.1.1. Structural Map of West Carney Hunton Field, showing location of cross-sections

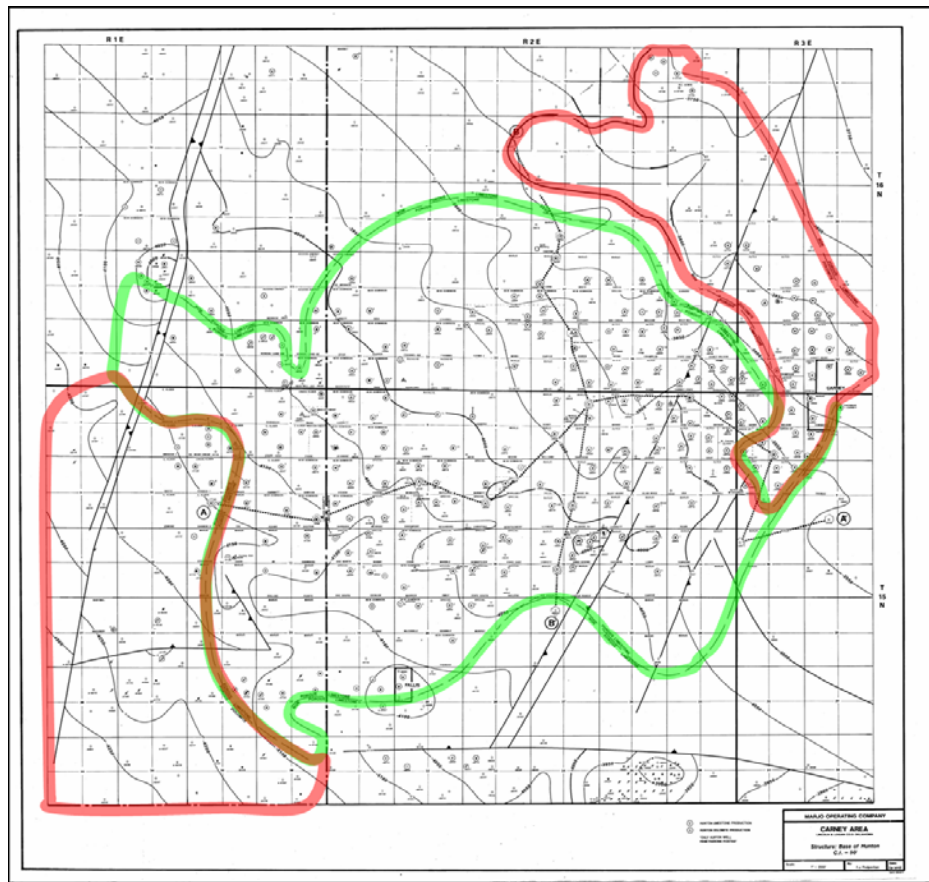


Figure 7-1: Structural Map of West Carney Hunton Field, showing location of cross-sections

7.1.2. Hunton Isopach Map of West Carney Hunton Field, showing location of cross-sections

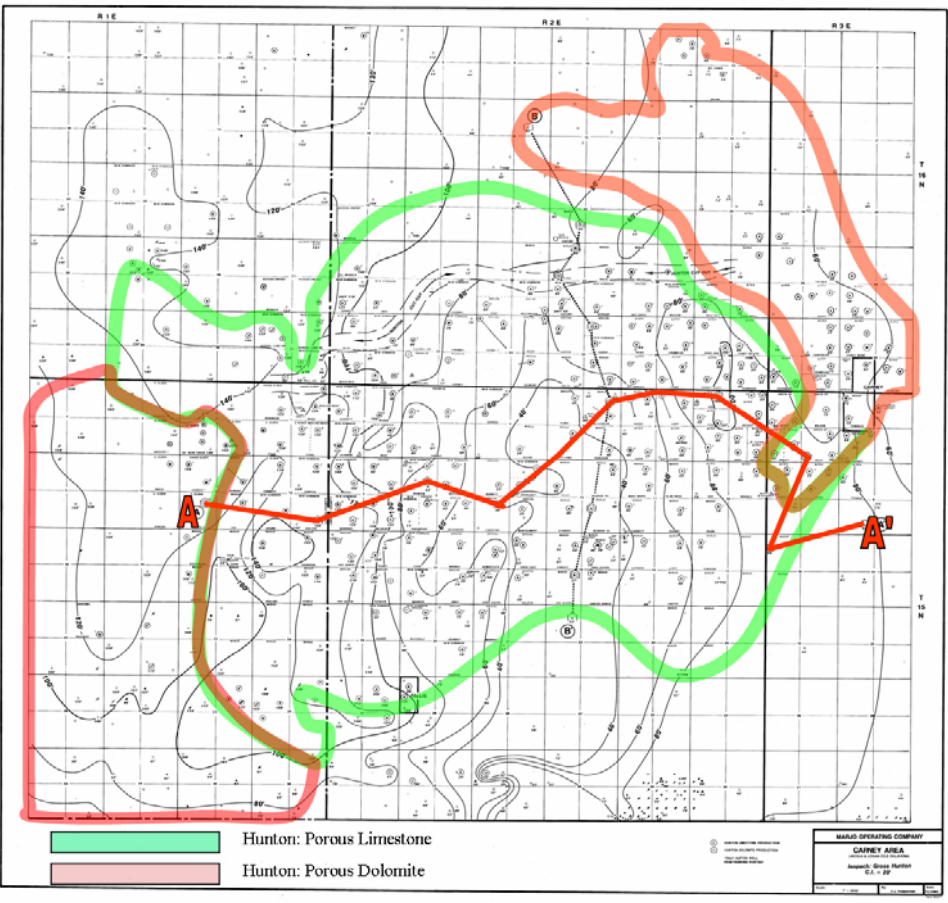


Figure 7-2: Hunton Isopach Map of West Carney Hunton Field, showing location of cross-sections

7.1.3. Location of Well Cores in and near West Carney Hunton Field, on Hunton Isopach Map

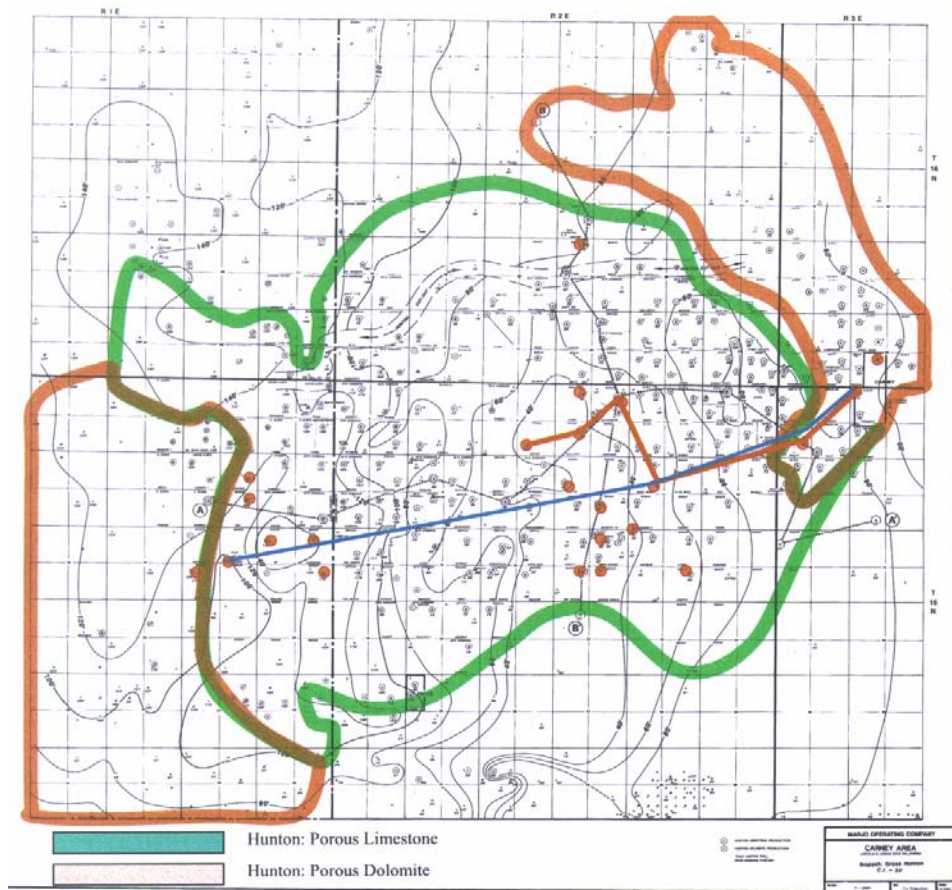


Figure 7-3: Location of Well Cores in and near West Carney Hunton Field, on Hunton Isopach Map

7.1.4. E – W Hunton Well-log Cross-section of West Carney Hunton Field

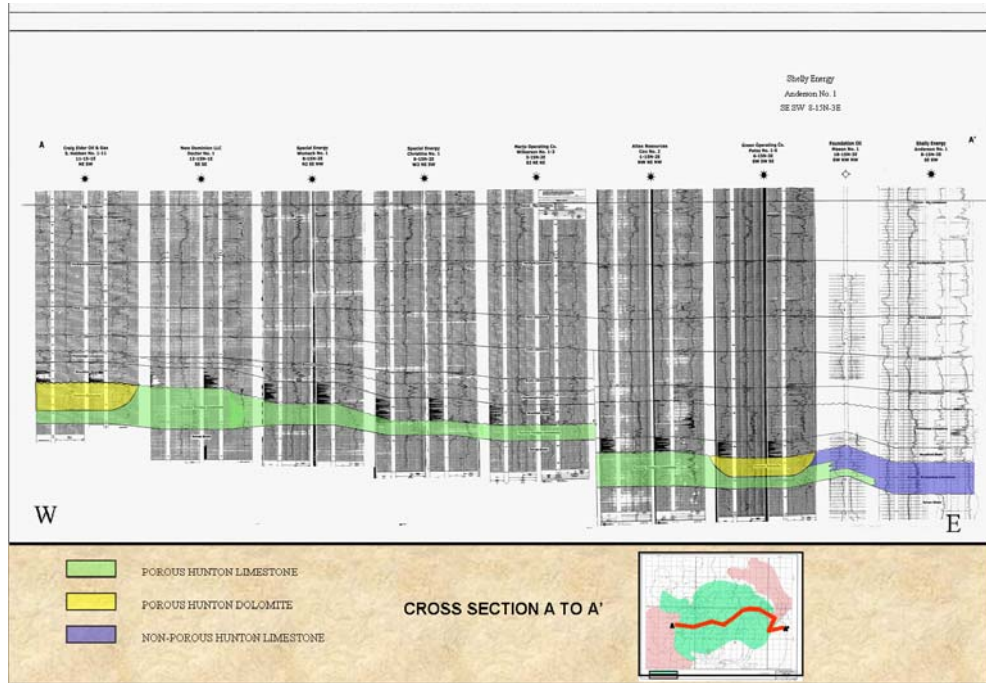


Figure 7-4: E – W Hunton Well-log Cross-section of West Carney Hunton Field

7.1.5. N – S Hunton Well-log Cross-section of West Carney Hunton Field

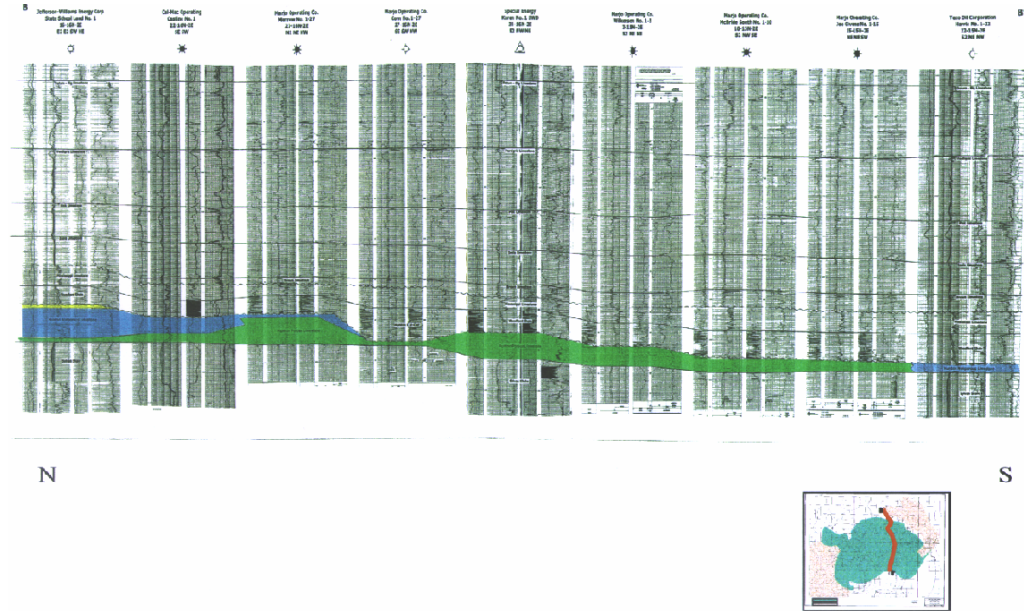


Figure 7-5: N – S Hunton Well-log Cross-section of West Carney Hunton Field

7.1.6. Table of Wells Cored

Table 7-1: Table of Wells Cored

DOE/TU West Carney Hunton Project															
TABLE OF WELLS CORED: Thickness, Core/Log adjustment, Data															
X = top or base of Hunton not cored;; (footage) = top or base of core; <i>italicized depth</i> is "core depth" of fm top or base picked on logs															
		Hunton Top		Core/log	Hunton Base		Thickness	Status & Data. * = Completed						Lithology	
		Core	Log	adj.	Core	Log		Wk	TS	PC	SEM	Cono	UH		Wett
1	5705 - Mary Marie 1-11	4961	4944	17	5003.5		42.5	C	33	C	4	14*	10	4	Ls/ 2'dol
2	5712 - Wilkerson 1-3	4953.4	4937.5	15.8	4999.8	4984	46.4	C	17*	C	1		8	1	Ls/ 2'dol
3	5733 - Toles 1	4964	X	na	5003.7	X	39.7	C	8*	C					Ls/ 2'dol
4	5818 - Henry 1-3	X (4966)	4958	7.5	X (4996.6)		30.6+	C		C					Ls/5' dol/lis
5	5838 - Danny 2-34	X (4930)	4918	10.8	4984.3		54.3+	C		C			4	1	Ls
6	5874 - Joe Givens 1-15	5017.8	5010	9	5044		26.2	C		C					Ls/ 0.1' dol
7	5887 - Williams 1-3	4943.5	4934	9.5	4983.7	4974	40.2	C		C			8		Ls/ 5' dol
8	5899 - McBride South 1-10	X (4962)	4947	13.3	4996.2	4983	34.3	C	1*	C		1*	4		Ls/dol/lis
9	5913 - Boone 1-4	X (5037)	5028	6.5	5066.5	5060	29.5+	C	6*	C		6*	4	1	Ls/ dol Ls/ 4' dol
10	5934 - Carter 1-14	X (4940)	4927	13.3	4995.8	4983	56.1	C	16	C		18*	4	2	1'dol/ Ls/ 2'dol
11	5943 - Anna 1	4967.1	4947	20.1	5004.7	4985	37.6	C	10	C					Dol
12	5992 Carney Townsite 2-5	X (4906)	4907	1.3	X (4966); 4979.3L	4978	60 cored; 73.3 log	C	8*	C		10	4		Dol/Ls
13	6011 - Bailey 2-6	X(4876)	4875	-2.8	X(4934)	4964	58 cored; 89 log	C	20	C		12			14' Dol/Ls
14	6029 - Kathryn	X(4994)	4990	2.5	5030.5	5028	36.5 core 38 log								Ls/Dol/Ls/Dol
15	Geneva						9 ft cored		1						Ls(Cri pkstn)
16	6051-Carter Ranch	5006	5000	6	5035.1	5030	29.1 cored	C	5	C					
17	6061-Carney Ext SWDW	5042.7	5039.2	3.5	X(5131); =5156 L	5151	88.7 core 112 log	IP	15			10			Ls
18	6088-Cal 1-11	X(5034)	5025	4.2	5135.8	5134	101.8core 108.5L								
19	6100-Mark Houser 1-11	X(4961)	4940		X(5077.6)	5066	116.6core 126L								
20	6112-JB 1-13	4971.9	4964.5		X(5058.8)	5120	86.9 core 155.5L								
21	6131-Saunders 1-13	4917.3	4911		X(4940.5)	5053	23.2 core 142L								
22	6143-Points 1-13	4989.5	4978	11.5	X(5107)	5096	117.5core 118								Ls
23	Mercer 1-28	X(4527)	4526		X(4583)	4606	56 cored 80L	IP							
24	6209-Griffen 1-14	X (5082)	5077	5	X(5142); 5191.5	5186.5	60 cored 109.5L	IP				14			Ls/dol/limy dol
25	Morrow	X(4905)	4886		4956.4	4956	51.9 cored 69L								
26	Chandler SWDW	X(4810)	4797.5		X(4869.8)	4865	59.8 core 68L								
27	Stevenson	X(5143)	5101		X(5167.6)	5186	24.6 core 42.5L								

Wk = Work status (Core description), PC = Porosity Codes, Core description, Pore codes: C = Completed; IP = In Process.
 TS = Thin Sections,# made, * described ; SEM = Scanning Electron Microscopy, Cono = Conodont micropaleontology, # of samples, * completed
 UH = Core Plug samples at Univ. Houston; Wett = Wettability Analysis,
 Numbers in front of Well Name is StimLab well Identification Number

7.1.7. Introduction to Core Description and Explanation of Terminology

All wells cored by Marjo for this study are listed in **Table 4-4** in the text. **Table 4-4** also shows which wells have been described, the thickness of Hunton cored, and the different types of analyses performed on the core. Appendix **Section 7.1.8** contains the description of the fourteen (14) cores described to date. Each core description contains two parts: first a conventional description of discrete intervals of natural sedimentological significance, and secondly a three-part description describing the Karst Features, Stylolites, and Fractures separately.

Cores are described from slabbed core surfaces with aid of hand lenses and binocular microscope. Commonly the core is polished to better reveal rock textures . A standardized descriptive format, in an Excel Spreadsheet, is utilized. A standard verbal description is accompanied by 7 data columns described below. Our goal is to describe the natural sedimentological units, while attempting to make those units thick enough to be recognizable in the response of petrophysical well logs.

Lith (lithology) : The dominant rock type: limestone, dolomite, sandstone, shale.

Fabric : Terminology is the Rock-Fabric classification of Dunham, 1962²⁸. Grainstone and Packstone denotes grain-supported rocks; grainstones having no mud, whereas packstones have significant mud matrix. Wackestones (>10% grains) and Mudstones (< 10% grains) are mud-supported rocks. Lucia's, 1995¹³ important distinction between Grain dominated and Mud dominated Packstones has not been encountered yet, as all packstones seen in West Carney Hunton Field cores are grain dominated. However dissolution of mud matrix in packstones and wackestones is an important component of the porosity in the West Carney Hunton Field cores.

Pore Types : This column uses the pore classification of Lucia, 1995¹³, shown below, with the occasional use of PP for pinpoint porosity . Pin point porosity is a general term for discrete fine pores of uncertain origin; typically they are microvugs formed by dissolution of mud or fossil fragments (molds).

Av Pore % : Average porosity through the interval from core analysis adjusted by rock and thin-section data.

% TV : Touching vug porosity, typically interconnected vugs, solution-enhanced fractures, and interconnected fossil molds. (see Lucia's explanation below). TV% is included in the AvPore% number, so TV% is always less than or equal to total percent porosity.

Chalky : Presence (Y) , absence (N), or slight amount (**sli**) is noted, as used by Archie, 1952²⁹, for dull or earthy appearing rock, composed of fine crystals, not tightly interlocking, usually soft or friable. Chalky limestone (as opposed to true chalk) is generally believed to result from extensive fresh-water dissolution and recrystallization. In other areas, chalky sediments commonly have high (but microscopic) porosity. In West Carney Hunton Field core analysis commonly shows that intervals with chalky appearance have low porosity.

Facies : In this column we put the number code for the lithofacies type described in **Table 4-5** in the text and in the appendix Explanation of coding of Porosity and Facies types. Since an interval may include a variety of lithofacies, the dominant lithofacies is denoted.

Shown below the Pore-type classification of carbonate rocks published by Lucia (1995)¹³, in which he also includes his abbreviations defined in a 1983 paper and

those used by Choquette and Pray in 1970³⁰. The 1983 abbreviations are used in this study.

Table 7-2: Pore-type classification of carbonate rocks (Lucia, 1995)¹³

Term	Abbreviations	
	Lucia (1983)	Choquette and Pray (1970)
Interparticle	IP	BP
Intergrain	IG	-
Intercrystal	IX	BC
Vug	VUG	VUG
Separate vug	SV	-
Moldic	MO	MO
Intraparticle	W/P	WP
Intragrain	WG	-
Intracrystal	WX	-
Intrafossil	WF	-
Intragrain		
Microporosity	μ G	-
Shelter	SH	SH
Touching Vug	TV	-
Fracture	FR	FR
Solution-Enlarged Fracture	SF	CH*
Cavernous	CV	CV
Breccia	BR	BR
Fenestral	FE	FE

*Channel

From Lucia, 1995¹³: Pore-type terminology and abbreviations used in this paper compared to abbreviations used in Lucia (1983)³¹ and Choquette and Pray (1970)³⁰



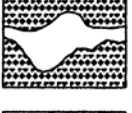
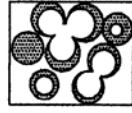
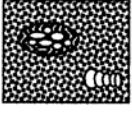
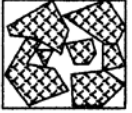
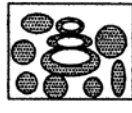
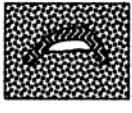




VUGGY PORE SPACE			
SEPARATE-VUG PORES (VUG-TO-MATRIX-TO-VUG CONNECTION)		TOUCHING-VUG PORES (VUG-TO-VUG CONNECTION)	
GRAIN-DOMINATED FABRIC		MUD-DOMINATED FABRIC	GRAIN- AND MUD-DOMINATED FABRICS
EXAMPLE TYPES		EXAMPLE TYPES	EXAMPLE TYPES
PERCENT SEPARATE-VUG POROSITY	Moldic pores 	Moldic pores 	Cavernous 
	Composite moldic pores 	Intrafossil pores 	Breccia 
	Intrafossil pores 	Shelter pores 	Fractures 
	Intragranular microporosity 		Solution-enlarged fractures 
			Fenestral 

Figure 7-6: Geological and petrophysical classification of vuggy pore space based on vug interconnection. The volume of separate vug pore space is important for characterizing the petrophysical properties. From Lucia, 1995¹³

7.1.8. Core Descriptions of Individual Wells

Table 7-3: Core Description, Marjo Anna 1-15

CORE DESCRIPTION MARJO ANNA 1-15, SEC.15, T15N, R2E LINCOLN COUNTY, OKLAHOMA										
Depth		Lith	Fabric	Pore Types	Av Pore %	% TV	Chalky	Facies	Description	
From	To									
4967 Top of Core										
		Woodford Shale	(not cored) Shale	nil	nil					
		Misener Sandstone (0.5 ft cored)	SS	nil	nil					
4967.15 Hunton Limestone (37.6)										
4967.15	4972.8	Ls	pkstn	Vug, IG	7	5	Y	7	Ls, Partly dolomitized, lt to med gy, big pent brac facies with karst infill of carbonate silt and very fine quartz sand. Some vuggy porosity.	
4972.8	4978.6	Ls	pkstn/wkstn	Vug, IG	9	5	Y	7	Ls, Partly dolomitized, yellowish gy 5Y7/2 to lt gy, coarse brac pkstn with thin interbeds of sparse fossil wkstn, thick shelled big pent brac, sli SF and karst infill	
4978.6	4979.7	Ls	pkstn	SF	4	4	N	15	Ls, Partly dolomitized, yellowish gy to lt gy, very coarse brac pkstn with thin bed of fine grnstn, very large thin shelled brac	
4979.7	4989.8	Ls	pkstn/wkstn	Coarse IG, Vug	8	3	N	7	Ls, Partly dolomitized, yellowish gy to lt gy, coarse pent brac pkstn with sparse thin intervals of wkstn, widely scattered vugs, part with carbonate silt karst infill and occasional SF	
4989.8	4996.6	Dol	pkstn	IG, Vug, SF	10	7	sli	7	Dol, yellowish gy, rarely lt gy, coarse pent brac pkstn and thin intervals of sparse fossil wkstn, locally vuggy porosity in brac shelters and also MO porosity by dissolution of pent brac	
4996.6	5001.6	Dol	Mdstn/wkstn	SF, Vug, IG	6	3	N	10	Dol, lt to med gy, rarely yellowish gy, sparse fossil wkstn and mdstn with two thin beds of brac coquina. Includes thin intervals of thin bedded to laminated recrystallized mdstn with very sparse fossils. @ 4998.4 is dissolution breccia with Terra Rossa, probably a microkarst breccia but possibly a palaeosol	
5001.6	5004.1	Ls	grnstn/wkstn	SF, Vug	6	5	N	12	Ls, Partly dolomitized, v lt gy, finely recrystallized fine grnstn, fabric obscured by recrystallization, possibly burrow mottled	
5004.1	5004.7	Ls	pkstn	SF	3	3	N	6	Ls, coarse fossil pkstn with sparse big brac and basal 0.2 ft contains laminated carbonate silt, apparent karst cavity fill	
5004.7	5005.3	Dol	mdstn	ixln	3	-	-	1	Dol, argillaceous greenish gy to lt olive gy 5GY 5/1, slightly fractured, pyritic, burrow mottled, sharp irregular upper contact	

Table 7-4: Core Description, Marjo Bailey 2-6

CORE DESCRIPTION										
MARJO BAILEY 2-6, SEC.6, T15N, R3E										
LINCOLN COUNTY, OKLAHOMA										
Depth		Lith	Fabric	Pore Types	Av Pore %	TV	Chalky	Facies		Description
From	To									
4876 Top of Core										
Woodford Shale (not cored)										
		Shale		nil	nil					
Misener Sandstone (not cored)										
		SS		nil	nil					
4876 Hunton Limestone (58.15)										
										Dol, fine to med xln, lt gy N7 to yellowish gy 5Y 7/2, strongly rexln, originally cri brac pkstn and grnstm. Crudely interbedded, tightly cemented zones and zones of abundant moldic and vuggy porosity, vertically solution enhanced frac connect karst solution cavities .05 by .01 ft, filled with coarse to med quartz sand and phosphate grains, certainly misener.
4876	4880.45	Dol	xln	ΓV,SF,MO,D	11	7	N	6		
4880.45	4881.95	Ls	pkstn	IG, Vug	4	0	N	4		Ls, partly dolomitized, med cri pkstn, finely xln dol in part, pinkish gy 5 YR 8/1, porosity is dissolved intergranular matrix
4881.95	4889.8	Dol	pkstn	SF, Vug, Mo	5	4	N	9		Dol, fine to med xln, color a/a, fine to med cri coral pkstn, sparse brac and bryzoans. Mostly tight with thin zones of abundant moldic porosity, obscured dolomitization but probably coral layers
4889.8	4891.4	Ls	pkstn	SF, SV	2.5	2	N	8		Ls, partly dolomitized, v lt gy to med gy N6 - N8, med to coarse coral-cri-brac-bryzoan-trilobite pkstn, strongly rexln, much coarse pore filling spar
4891.4	4899.75	Ls	grnstm	SF, Vug	1.5	1.5	N	3		Ls, pinkish gy with mottles and crude banding of moderately reddish orange 10 R 6/5 wich are Terra Rossa, brac grnstm and pkstn mostly small brac facies with the big pent brac facies present 4892.5 to 4893.5, porosity is dominantly SF
4919.3	4926.3	Ls	pkstn	Vug, fine matrix	2	1	N	6		Ls, color a/a, mixed brac cri facies, locally v large thin shelle brac, abundant karst mosaic frac and dissolution with karst infill of v fine laminated carbonate silt. At the top of the interval and locally throughout are large cavities filled with coarse calcite. From 4924 to base is Terra Rossa and possible palaeosol horizons
4926.3	4928.7	Ls	pkstn	Vug	3	3	N	7		Ls, color a/a to lt gy, coarse brac pkstn, large vugs and solution frac in upeer 1.5 ft
4928.7	4934.15	Ls	pkstn	SF, IG	2	1	N	6		Ls, lt to med gy, med gm brac cri pkstn, locally dense dark gy matrix, possibly carbonate silt

Table 7-5: Core Description, Marjo Boone 1-4

CORE DESCRIPTION MARJO BOONE 1-4, SEC. 4, T15N, R2E LINCOLN COUNTY, OKLAHOMA										
Depth		Lith	Fabric	Pore Types	Av Pore %	% TV	Chalky	Facies		Description
From	To									
Woodford Shale		Shale		nil	nil					not cored
Misener Sandstone		SS		nil	nil					not cored
5037.0		Hunton Limestone (29.5)								TOP OF CORE
5037.0	5042.8	Ls	pkstn	SF,IG,IP	3	2	N	6		c to med cri-brac pkstn, pinkish gy (5YR 8/1), tightly cemented with closely spaced SF, especially in top two feet, slight karst breccia, karst cavities filled with silt sized carbonates, sparse large brac and cri
5042.8	5045.8	Ls	pkstn	MO,IG	2	1	N	9		c cri coral pkstn, pinkish gy, tightly cemented with moldic porosity in favositid corals.
5045.9	5047.9	Ls	grnstn	IG, IXLN	8	-	N	9		c coral cri grnstn, yellow gy to v pale orange (10YR 8/2), with sparse large MO vugs in favositid and rugose corals, partially dolomitized, good IG porosity
5047.9	5051.7	Ls	grnstn	IG,IXLN	8	1	sli	5		partly dolomitized, c cri grnstn, v pale orange, sli oil stain, with large karst cavities filled with fine carbonate silt upto 0.2 ft wide x 0.3 high. Sli SF, sli chalky, grades to unit below
5051.7	5056.2	Ls	grnstn	IG,MO,IXLN	7	1	Y	4		partly dolomitized, f cri grnstn with sparse large cri grains, v pale orange with oil stains, sparse corals with MO porosity, lower 2 ft with thin current bedding, very sparse large brac. Cleanly washed intra sparite
5056.2	5059.7	Ls	grnstn	IG,sli MO	6	-	N	6		partly dolomitized, c cri brac coral grnstn, v pale orange to pinkish gy, with v large pent brac (5056 to 5057), increasingly tightly cemented towards base
5059.7	5062.2	Ls	grnstn	IG	2	-	N	5		c cri grnstn, not dolomitic, pinkish gy to moderately orange pink 10 R 7/4 , sparse brac, sparse vertical frac completely filled with carbonate silt (karst ?), sli vertical frac, crystalline
5062.2	5066.5	Dol	XLN	IXLN,MO,SF	9	3	N	6		Dol, recrystallized, cri brac coral grnstn, pinkish gy to gysh orange, with large MO porosity around bracs and corals, partly connected by solution enhanced frac, basal 0.1 ft is laminated dolomite with felted texture, possible replacement of anhydrite
TOP SYLVAN ?										
5066.5	5067.9	Dol	mdstn	-	-	-	-	11		Top of Sylvan ? Dol, argillaceous, gmsh gy, abrupt contact at the top, marked by 3 mm of pyrite. Burrow mottled, indistinct bedding, increasing fissile downward.

Table 7-6: Core Description, Marjo Carney Townsite 2-5

CORE DESCRIPTION										
MARJO CARNEY TOWNSITE 2-5, SEC. 5, T15N, R2E										
LINCOLN COUNTY, OKLAHOMA										
Depth		Lith	Fabric	Pore Types	Av Pore %	% TV	Chalky	Facies	Description	
From	To									
Woodford Shale		Shale		nil	nil				not cored	
Misener Sandstone		SS		nil	nil				not cored	
4906.0		Hunton Limestone (60 ft)								
4906.0	4907.0	Dol	XLN	IX,SF	9	2	N	2	Dol, limy, f xln , v pale orange 10 YR 8/2, equant subhedral crystals, faint foss allochems, vertical frac	
4907.0	4910.0	Ls	XLN pkstn	IX, SF	11	3	N	4	Ls, strongly dolomitic gysh orange 10YR 7/3, fine to med foss pkstn with minor wkstn, vague thin bedding, allochems largely fine cri grains, sparse large cri & small brac, sli MO & SV porosity, prominent vertical SF 4907 to 4908.3 with associated large vu	
4910.0	4912.0	Dol	XLN	IX,SF	12	1	N	4	Dol, limy, gysh orange, dolomitized f cri pkstn & wkstn, SF 4910 to 4910.6 & associated minor vuggy porosity. Thin horizontal zones of dense rexln matrix possibly are rexln stylolite zones	
4912.0	4916.0	Ls	grnstn	IX, SV	10.5	-	N	5	Ls, strongly dolomitized, gyish orange, med cri brac grnstn? With numerous coarse cri grains & sparse small brac	
4916	4927	Dol	XLN pkstn	IX,SF	13	2	N	4	Dol limy gysh orange, dolomitized f cri pkstn with thin intervals of moderately abundant small brac fragments, irregularly thin bedded, apparently grainsize sorted, numerous sub horizontal tightly cemented layers or possibly rexln stylolites. Scattered fo	
4927	4940.3	Ls	pkstn/grnstn	IG,SF,MO	10	3	N	4	Ls, strongly doltzd, gysh orange, f to c cri pkstn, grnstn with 3 ft of mixed cri brac pkstn 4931 to 4934. Large vugs associated with SF & minor mosaic breccia scattered through the interval. Also contains thin intervals of karst solution cavities filled	
4940.3	4941	Dol	pkstn	SF,Vug,IX	6.9	5	N	4	Dol, limy, gysg orange to lt gy, f cri pkstn with tight cemented zones a/a, SF with large xln vuggy porosity and 3 karst cavities filled with carbonate silt	
4941	4943.7	Ls	pkstn/wkstn	IG, Mo	4	1	N	4	Ls, lt gy to pinkish gy 5 YR 8/1, f to med cri pkstn/wkstn thin inetrvls of MO and sli SF porosity in wkstn layers, numerous calcite filled frac & silt filled karst fissures	
4943.7	4944.6	Dol	mdstn	IX, Sf	6	2	N	11	Dol, limy pinkish gy mottled med gy, f mdstn , probably sabkha mdstn	

Table 7-7: Core Description #1, Marjo Carter 1-14

CORE DESCRIPTION MARJO CARTER 1-14, SEC.14, T15N, R2E LINCOLN COUNTY, OKLAHOMA										
Depth		Lith	Fabric	Pore Types	Av Pore %	% TV	Chalky	Facies	Description	
From	To									
Woodford Shale		Shale		nil	nil				not cored	
Misener Sandstone		SS		nil	nil				not cored	
4940.0 Hunton Limestone (55.8)										
4940.0	4941.3	Dol	XLN	IX,Vug	7	2	N	6	Dol, lt olive gy 5Y6/1, f xln with slight dissolution vugs, appears burrow mottled, abundant stylolites, silt filled fractures	
4941.3	4942.0	Ls	grnstr	IG	5	-	N	6	Ls, yellowish gy 5 Y 8/1, med cri brac grnstr, sparse large brac, collapsed (leached) grnstr fabric	
4942.0	4950.2	Ls	grnstr/pkstr	TV,IG	9	2	sli	7	Ls, yellowish gy, c brac grnstr/pkstr, large pent brac coquina with partially collapsed (dissolved) fine grnstr fabric and abundant vuggy porosity, vugs commonly dissolution of inter brac matrix	
4950.2	4952.2	Ls	grnstr	IG, FR	3	1	N	6	Ls, pinkish gy, 5Y8/1, c brac cri grnstr, porosity occluded by syntaxial overgrowth, slight frac	
4952.2	4955.3	Ls	grnstr	IG,SV	5	-	N	6	Ls, sli dolomitic, yellowish gy, med to c cri brac grnstr with sparse large vugs	
4955.3	4958.4	Ls	grnstr	IG,SF	2	1	N	5	Ls, pinkish gy, c cri grnstr with v sparse brac, vertical frac mostly calcite filled, locally mottled med gy, karst stained?	
4958.4	4960.0	Ls	grnstr	IG	3	-	N	5	Ls, sli dolomitic, pinkish gy, c cri grnstr with sparse med brac fragments, tightly cemented	
4960.0	4962.1	Ls	grnstr	IG,SV	2	-	N	5	Ls, pinkish gy, c cri grnstr with scattered large vugs	
4962.1	4976.6	Ls	grnstr	IG,TV	3	1	N	6	Ls, pinkish gy v c brac cri grnstr, partly heavily leached and vuggy	
4976.6	4979.7	Ls	grnstr	IG,SF	2	1	N	5	Ls, lt gyish orange pink 5YR 8/2, c cri grnstr with sparse solution frac and minor small vugs. 4978.7 mto 4979.3 karst mosaic breccia with sediment filled cavity 0.1X 0.1 ft laminated carbonate silt. Mostly tightly cemented	
4979.7	4983.0	Ls	grnstr	IG,TV	2	1	N	3	Ls, pinkish gy c brac grnstr, small to med bracs and sparse v large cri in dense grnstr matrix, sparse vugs	

Table 7-8: Core Description #2, Marjo Carter 1-14

CORE DESCRIPTION MARJO CARTER 1-14, SEC.14, T15N, R2E LINCOLN COUNTY, OKLAHOMA									
Depth		Lith	Fabric	Pore Types	Av Pore %	% TV	Chalky	Facies	Description
From	To								
4983.0	4987.2	Ls	grnstrn	IG,TV	6	1	N	6	Ls, sli dolomitic, pinkish gy to med lt gy, c to med brac cri grnstrn, vuggy with some baroque dolomite vug fill, one large coral @ 4985.4
4987.2	4988.8	Ls	grnstrn	IG,Vug	5	-	N	6	Ls, pinkish gy, c brac cri grnstrn , sparse separate vugs
4988.8	4994.1	Ls	grnstrn	IG	7	1	Y	6	Ls, dolomitic in parts, pinkish gy to v lt gy, f cri grnstrn & f cri brac grnstrn, dolomitic below 4991, good IG porosity, karst dissolution 4989.7 to 4990 with carbonate silt infill
4994.1	4995.8	Dol	grnstrn	IG,IX,TV	10	5	N	12	Dol, med ltgy to lt brnsh gy, med to f crystalline dolomictic grnstrn, locally dolomitic mdstrn with two zones of well developed interconnected vuggy posority @ 4994.9 & 4995.3, includes zones that resemble sabkha dolomite as well as basal 0.3 ft appears
Sylvan Shale (4.1 ft cored)									Unconformity (Irregular surface, about 1 cm relief, short sediment-filled fractures)
4995.8	4999.9	Dol	IX	-	4	-	N	1	Dol, argillaceous lt grnsh gy, pyritic, burrow mottled, upper contact is irregular but sharp and contains short vertical fracture filled with material from overlying Hunton, an unconformity.
Note : slabbed only to 4997.2									

Table 7-9: Core Description #1, Marjo Carter Ranch 2-15

CORE DESCRIPTION										
MARJO CARTER RANCH 2-15, SEC.15, T15N, R2E										
LINCOLN COUNTY, OKLAHOMA										
Depth		Lith	Fabric	Pore Types	Av Pore %	TV	Chalky	Facies		Description
From	To									
5006 Top of Core										
Woodford Shale (not cored)										
		Shale		nil	nil					
Misener Sandstone (not cored)										
		SS		nil	nil					
Hunton Limestone (29.1 ft)										
5006	5009.4	Ls	pkstn	SF, Vug, IG	4	2	-	7		Ls, pinkish gy, mottled dk gy, coarse pent brac pkstn, strongly effected by karst dissolution of fine matrix. Much dk gy karst sediment infill, fine sand to clay partly carbonate cemented. Base is gradational.
5009.4	5010	Ls	ndstn / wkst	SF, Vug	2	1	-	11		Ls, partly dolomitized, pinkish gy to med lt gy, carbonate mdstn with a thin interval of 0.2 ft of big thin shelled brac (facies 15 , wkstn) with vispy laminae outlining sub horizontal burrow mottles. The gy part is partially dolomitized and leached with micr vug porosity
5010	5015.8	Ls	pkstn	SF, Vug, IG	3	1	-	7		Ls, pinkish gy, mottled dk gy, coarse pent brac coquina, partly tightly cemented with fine matrix, partly heavily karsted with abundant karst infill> In part mosaic breccia of partly cemented large brac with abundant karst infill of fine quartz sand and laminated carbonate silt. @ 5011 to 5012 is good micro vuggy porosity resembling IG porosity by dissolution of fine matrix.
5015.8	5016.1	Dol	mdstn	SF	2	1	-	11		Dol, med lt gy, limy burrow mottled mdstn with karst dissolution filled with fine sand
5016.1	5017	Dol	pkstn	SF, Vug	2	1	-	7		Dol, med lt gy to pinkish gy , coarse pent brac pkstn with fine sand filled karst dissolution fractures and slight sand filled MO porosity
5017	5020.1	Ls	pkstn	SF, Vug	2	1	-	7		Ls, Pinkish gy with med gy mottles, coarse pent brac pkstn with thin fine grnsth intervals. In part strong karst dissolution with large vugs filled with brownish grey clay.
5020.1	5022.6	Ls	pkstn	SF, Vug, IG	8	5	sli	7		Ls, partially dolomitized, very pale orange 10 YR 8/2, coarse pent brac pkstn, upper part strongly dissolved with vugs and solution fractures, but very little karst infill. Lwoer part largely fine matrix porosity by dissolution, fine grains.
5022.6	5026.8	Dol	ndstn, wkstn	IG, Vug, SF	6	1	-	10		Dol, lt brownish gy 5 YR 6/1, sparsely fossileferous dolomitized mdstn with thin intervals of big thin shelled brac (15 facies wkstn). Thin intervals, very heavily leached with both micro vuggy and macro vuggy porosity upto 15%

Table 7-10: Core Description #2, Marjo Carter Ranch 2-15

CORE DESCRIPTION MARJO CARTER RANCH 2-15, SEC.15, T15N, R2E LINCOLN COUNTY, OKLAHOMA										
Depth		Lith	Fabric	Pore Types	Av Pore %	TV	Chalky	Facies	Description	
From	To									
5026.8	5032.3	Dol	stn/wkstn/pli	Vug, SF, M	10	3	-	10	Dol, lt brownish gy to very pale orange, strongly dolomitized and leached sparse fossil wkstn with thin zone of abundant fossils heavily leached, probably the small brac pkstn	
5032.3	5033.4	Ls	grnstn	IG, SF	9	1	sli	12	Ls, partly dolomitized, yellowish gy 5Y 8/1, fine grnstn, burrow mottled with solution frac in lower part and slight karst infill	
5033.4	5034.1	Ls	grnstn	SF, MO, IG	9	2	sli	8	Ls, partly dolomitized, yellowish gy, fine grnstn with large coral (Favosities) colony, fractured and partly destroyed by dolomitization, karst cavity 0.1 ft high * 0.2 ft wide and minor solution fractures filled with dk gy very fine sand	
5034.1	5035.1	Ls	grnstn	Sf, Mo	3	1	-	3	Ls, pinkish gy, med fossil grnstn with small brac mostly tightly cemented, grades down into a sparse fossil wkstn, sharp basal contact	
5035.1	5036	Dol	xln						maybe sylvan	

Table 7-11: Core Description, Marjo Danny 2-34

CORE DESCRIPTION MARJO DANNY 2-34, SEC. 34, T16N, R2E LINCOLN COUNTY, OKLAHOMA										
Depth		Lith	Fabric	Pore Types	Av Pore %	TV	Chalky	Facies		Description
From	To									
Woodford Shale		Shale		nil	nil					not cored
Misener Sandstor		SS		nil	nil					not cored
4930.0 HUNTON LIMESTONE (54.3 feet cored, top not cored)										
4930.0	4954.5	Ls	pkstn/wkstn	SF,MO-TV, IG	4	3	N	7		LS, c pkstn w thin intervals of f wkstn, abundant large pent brac in pkstn, pinkish gy to lt gy, strongly karsted with sand infill, terra rossa @ 4931.2 & 4944.4
4954.5	4961.4	Ls	wkstn	SF	3	3	sli	10,7		LS, f wkstn w sparse pent brac, lt gy, one interval of abundant brachs from 4958.3 to 4959.4
4961.4	4965.6	Ls	pkstn/wkstn	SF,SLI MO	6	5	Y	10		LS, f pkstn / c wkstn w v abundant large pent brach (brachs do not create a grn supported matrix)
4965.6	4971.0	Ls	wkstn	SF,STY, MV	6	5	Y	3		LS, sparse brac wkstn, pinkish gy to lt gy, dense mud matrix w sparse large pent brac, sty & vertical fractures
4971.0	4973.3	Ls	f grnstn	IG,SV, MO,STY	9	1	Y	5		LS, f foss grnstn w scattered large brac incl <i>Virginia?</i> , v pale orange (buff), fining upward to overlying wkstn
4973.3	4977.0	Ls	grnstn	IG,SV,SF,MV	7	1	sli	5		LS, v c cri grnstn, pinkish gy, clean biosparite
4977.0	4984.3	Ls	grnstn	IG,SV, MO,MV	4	0	sli	5		LS, c to med cri grnstn, pinkish gy to lt gy, mostly clean biosparite, sparse large vugs, basal contact sharp, abundant cri, sparse corals
SYLVAN SHALE (5.7 ft cored)										
4984.3	4985.8	Dol	mdstn	IX	4	0	N	1		DOL, silt size, grnish gy, burrowed, pyritic
4985.8	4990.0	Shale	sh	-	-	-	-	13		SHALE, grnsh gy, large pyrite nodules, thin lenses of lt gy silt
4990.0		BASE OF CORE								

Table 7-12: Core Description, Marjo Henry 1-3

CORE DESCRIPTION MARJO HENRY 1-3, SEC. 3, T15N, R2E LINCOLN COUNTY, OKLAHOMA										
Depth		Lith	Fabric	Pore Types	Av Pore %	% TV	Chalky	Facies	Description	
From	To									
Woodford Shale		Shale		nil	nil				not cored	
Misener Sandstone		SS		nil	nil				not cored	
4966.0		Hunton Limestone (30.6)							TOP OF CORE	
4966.0	4973.0	Ls	grnstrn	TV,SF	4	3	N	7	Ls, pinkish gy 5YR 8/1, mottled to dk gy, c pent brac coquina with fine grnstrn matrix. Heavily altered by karsting with mosaic and collapsed breccia, solution cavities filled with dk gy fine sand, gyish orange silt. Abundant vugs and frac and thin interva	
4973.0	4981.5	Ls	grnstrn	TV,SF	3	3	N	7	Ls, a/a with scattered white chert replacing large brac and Ls clasts	
4981.5	4986.2	Ls	grnstrn	TV,SF	2	2	N	7	Ls, a/a no chert	
4986.2	4990.7	Ls	grnstrn	IG,FR	1	-	N	7	Ls, pinkish gy 5 YR 8/1, c pent brac grnstrn with fine grnstrn matrix, mostly intact rock with minor karst dissolution (4988.5 to 4990) with dk sand infill	
4990.7	4993.0	Ls	grnstrn	IG,TV	5.5	2	N	7	Ls, lt olive gy 5Y 7/1, c pent brac grnstrn with fine grnstrn matrix, good secondary IG porosity and minor vuggy porosity	
4993.0	4995.1	Dol	grnstrn	IX,TV	7	2	N	7	Dol, buff, lt gyish orange 10YR 7/3, c brac grnstrn, dolomitized with scattered vugs, largely dissolved brac cavity fill	
4995.1	4996.6	Dol	grnstrn	IX, SF	8.5	1	N	12	Dol, buff above, lt olive gy below 4996.1, fine grnstrn, dolomitized to med crystalline matrix, abrupt color contact @ 4996.1 at irregular stylolite, contains sparse small brac	
4996.6									BASE OF CORE	

Table 7-13: Core Description, Marjo Joe Givens 1-15

CORE DESCRIPTION										
MARJO JOE GIVENS 1-15, SEC.15, T15N, R20E										
LINCOLN COUNTY, OKLAHOMA										
Depth		Lith	Fabric	Pore Types	Av Pore %	% TV	Chalky	Facies		Description
From	To									
Woodford Shale		(1.6ft cored)								
5013.0	5014.6	Shale		nil	nil				13	Shale, dk gy N3, fissile, carbonaceous, pyritic
Misener Sandstone		(3.2 ft thick)								
5014.6	5017.2	Sh, SS		nil	nil				13	Shale, aa, with thin beds and laminae of f.gr. Ss, loc. Pyritic
5017.2	5017.8	SS							14	Basal 1.5 cm (0.05') laminated SS, broken by collapse into underlying karst cavern.
Hunton Limestone		(26.2 ft. thick)								
TOP OF CORE										
5018.8	5023.1	Ls	Grnstrn, Pkstr	TV, SF, IG	5	3	N		6	Limestone, pinkish gray 5YR8/1 with patchy dk gray f. ss infill. Grainstone of large pentamerid brachiopods, interbedded with dense brach-crinoid packstone(?). Partly dissolved by micro karst to chaotic breccia. Misener sand infill in open vertical fractures, vugs, and interclast voids. Intergrain porosity in fg ss infill. Coarse calcite crystals in vugs. common vertical fracturing, partly healed. Scattered favositid corals.
0.0	5032.4	Ls	Grnstrn	SF, IG	3	2	N		6	Ls, aa, less brecciated, less sand infill. Coarse large pentamerid brach grainstone, with sparse large crinoids, large trilobites (5027.1), and favositid corals (5028.1). Mostly dense tight rock with large sand-filled fissures, oil-stained.
0	5038.6	Ls	Grnstrn, Pkstr	TV, SF, IG	4	2	N		6	Ls, aa, crinoid -brach grainstone, largely dissolved by karsting to chaotic breccia of individual crinoids and brachs, infilled by vfg-fg sand, oil stained.
5038.6	5043.9	Ls	Grnstrn, Pkstr	SF, IG	2	1	N	4, 6, 3		Ls, pinkish-gy, coarse brach grainstone (<i>Stricklandia?</i> , orthids?) with interbeds of dense fine brach pkstrn(?). Thin karst chaotic breccias with sand infill, gradational contacts.
5043.9	5044	Dol	Xln	IX	4	0	N		2	Dolomite, calcitic, variegated brownish gray, crinkly laminae, indefinite contacts above and below.
Sylvan Shale		(3.2 ft cored)								
5044	5046	Dol	Mdstn		nil	0			1	Dolomite mudstone, argillaceous, greenish gray, 5GY6/1, abund pyrite throughout, terra rosa near top.
5046	5047.2	Sh							13	Shale, greenish gray, dolomitic, blocky, pyritic, burrow mottled.
5047.2										BASE OF CORE

Table 7-14: Core Description #1, Marjo Mary Marie 1-11

CORE DESCRIPTION										
MARJO MARY MARIE 1-11, SEC. 11, T15N, R2E										
LINCOLN COUNTY, OKLAHOMA										
Depth		Lith	Fabric	Pore Types	Av Pore %	TV	Chalky	Facies		Description
From	To									
Woodford Shale										
4960.0	4960.7	Shale		nil	nil				13	Shale, dk gy N3, fissile, carbonaceous, pyritic
Misener Sandstone										
4960.7	4961.0	SS		nil	nil				14	SS, med. Gy, vfg, calc, large brachiopods & fragments (Disconformity: erosional surface)
Hunton Limestone										
4961.0	4965.5	Ls	Pkstn, Grmstn	IG	<2	0			6	Ls, pinkish gy (5YR8/1)-lt brn gy (5Yr6/1), brachiopod-crinoid pkstn & grmstn. Karst: dissol breccias tightly cemented, Misener SS cavern fill in top 4 ft. Tight.
4965.5	4971.6	Ls	Pkstn	PP,MO,TV	7	3			7	Ls, v pale orange 10YR8/2, c. brach pkstn. PP porosity probably dissolution of mud matrix. Abund. Lg pentamerid brachs. Coral at 4970.5
4971.6	4973.6	Ls	Pkstn	IG	<2	0			7	Ls, aa, pinkish gy, tightly cemented
4973.6	4975.3	Ls	Pkstn	TV:SF, MO	4	4			7	Ls, aa., large solution enhanced fractures, partly connecting moldic pores.
4975.3	4983.6	Ls	Pkstn	PP, SV	<2	0			7	Ls, aa, tightly cemented, locally pin-point (IG?) porosity. Thin beds of large brachs with moldic separate vugs (SV). Strongly karsted (partly dissolved) and infilled with geopedal mud; sli terra rosa.
4983.6	4988.4	Ls	Pkstn	PP, M0, SF	5	2			7	Ls, aa to v.pale orange 10YR6/2, fine to coarse brach pkstn. Much PinPoint (probably intergranular) porosity, minor moldic and solution-enhanced fractures.
4988.4	4994.2	Ls	Grnst	SV, MO	1	0			7	Ls, aa, large pentamerid brachs in v. fgr collapsed grainstone matrix. Many vertical fractures completely cemented. Separate moldic vugs.
4994.2	5001.6	Ls	Grnst	IX, SV	<1	0			6	Ls, pinkish gy, vfg mixed crinoidal and brachiopod grainstone, leached collapsed grains uniformly tightly cemented. <1% porosity except in basal foot which has 2% pinpoint separate vug (?moldic) porosity. Very rare large brachiopods. Basal 0.12 ft. is greenish gray 5GY6/1 fine packstone with sharp basal contact on a dissolution surface. Probably a sequence boundary.
5001.6	5003.5	Ls, dolo	Pkstn, Grmstn	IX, IG	5	0			6	Ls, v pale orange, part dolomitized. Mostly crinoidal/ brachiopod packstone and grainstone, in part dolomitized to uniform fine crystalline mosaic. Small pentamerid brachiopods in a fine to medium grained matrix, locally with abundant mud. All porosity is secondary, as dissolved mud matrix, dissolved crystals & fossil grains. Slight healed vertical fractures. Basal 0.2 ft is vfg grainstone with no brachiopods. Sharp basal contact on erosional surface.

Table 7-15: Core Description #2, Marjo Mary Marie 1-11

CORE DESCRIPTION										
MARJO MARY MARIE 1-11, SEC. 11, T15N, R2E										
LINCOLN COUNTY, OKLAHOMA										
Depth		Lith	Fabric	Pore Types	Av Pore %	TV	Chalky	Facies		Description
From	To									
5003.5		Sylvan Shale								(Disconformity: erosional surface)
5003.5	5006.0	Dol	Mdstn	IX	-			1		Dol, argillaceous, greenish-gray, burrow-mottled, pyritic. Top 1 ft closely fractured, abund pyrite throughout, terra rosa near top. Gradational into shale below by apparent decreasing dolomite content.
5006.0	5016.0	Shale			nil	0		13		Shale, greenish gray, 5GY6/1, pyritic. Slightly dolomitic or silty, partly burrowed.

Table 7-16: Core Description, Marjo McBride South 1-10

CORE DESCRIPTION										
MARJO MCBRIDE SOUTH 1-10, SEC. 10, T15N, R2E										
LINCOLN COUNTY, OKLAHOMA										
Depth		Lith	Fabric	Pore Types	Av Pore %	TV	Chalky	Facies		Description
From	To									
4968.0	4970.1	Ls	grnstrn	IG, Vugs	2	1	N	7		Ls, lt pinkish gy to ly gy, c pent brac grnstrn with fine grn carbonate matrix, tightly cemented at top with increasing karst dissolution and fine quartz sand infill to the base. 30 degree incline sharp contact with dolomite at 4970.1
4970.1	4971.9	Dol	grnstrn	IX, Vug	7	3	N	7		Dol, lt olive gy, c pent brac grnstrn with med crystalline dolomitic matrix grading downward into partially dolomitized Ls a/a.
4971.9	4983.1	Ls	grnstrn	IG, Vug	2	1	N	7		Ls, lt pinkish gy to med gy (in karsted sediments), c pent brac grnstrn with fine grn carbonate matrix, mostly v tightly cemented with zones of karst dissolution, vuggy porosity and karst solution frac filled with med gy quartz sand
4983.1	4990.3	Ls	pkstrn/wkstrn	IG, Vug	2	1	N	6		Ls, lt pinkish gy to med gy (in karsted sediments), c pent brac pkstrn with moderate to abundant cri material, mostly v tightly with zones of karst dissolution, vuggy porosity and karst solution frac filled with med gy fine quartz sand. Thin interbeds of s
4990.3	4994.3	Ls	grnstrn	IG, FR	3	2	N	3		Ls, lt pinkish gy, v fine brac grnstrn, tightly cemented with widely scattered large brac, includes thin section zones of karst mosaic breccia with minor med gy infill, leached IG porosity associated with karst zones
4994.3	4996.3	Ls	grnstrn	IG, FR	4	1	N	6		Ls, lt brnsh gy 5 YR7/1, v c large brac cri grnstrn with v c grn matrix, partially dissolved by karst, but all vugs and cavities are filled with dk gy carbonate silt and very fine qtz sand, v sharp contact with Sylvan below, includes cri grns up to 1 inch
TOP SYLVAN (1.7 ft)										
4996.3	4998.0	Dol	mdstrn	IG	5	-	N	1		Dol, grnsh gy 5 GY 6/1, argillaceous with wispy laminae and burrow mottles suggesting moderately disturbed bedding, scattered irregular pyritic zones

Table 7-17: Core Description #1, Marjo Toles 1-10

CORE DESCRIPTION MARJO TOLES 1-10, SEC. 10, T15N, R2E LINCOLN COUNTY, OKLAHOMA										
Depth		Lith	Fabric	Pore Types	Av Pore %	TV	Chalky	Facies	Description	
From	To									
Woodford Shale		Shale		nil	nil				not cored	
Misener Sandstone		SS		nil	nil				not cored	
4964.0 Hunton Limestone (39.7 feet cored)										
4964.0	4973.8	Ls	Pkstn, Grnstn	IP, BR, SF	3.0	2.0	N	6,7	Limestone, pinkish gray 5YR8/1 with patches & stringers of dark gray matrix, coarse crinoid-brachiopod packstone and grainstone. Leached skeletal grains gives compacted fabric, partly dissolved by micro karst. Misener sand infill in open semi-horizontal vugs & sparse solution-enlarged fractures. Vugs largely leached mudstone matrix & brach shelter infill. Coarse calcite crystals in vugs. Karst collapse breccia mostly clast supported (cave floor); thin intervals of high (5-10%) vuggy porosity. Abundant large strophomenid brachiopods & large crinoids.	
4973.8	4983.0	Ls	Grnstn	SV, Fr, SF	4.0	2.0	Y	4,5	Ls, aa to white, med gr crinoid grainstone, mostly recrystallized. Abund small separate vugs. Vert & inclined fractures (cave roof?) with slight movement, solution-enlarged fractures with Woodford clay infill. Sparse v.lg crinoids (to 1.5"), sparse thin layers of brachiopods.	
4983.0	4984.5	Ls	Grnstn	SV, Mo, SF	6.0	3.0	Y	6.0	Ls, aa to lt brn gy, dk gy along fractures, stylolites, and in vugs; coarse brach-crinoid grainstone, compacted, leached, large moldic brach vugs. Dissol breccia at top. Zones of abundant microvugs, apparently interconnected molds.	
4984.5	4987.1	Ls	Grnstn	IX, V, Fr	5.0	1.0	Y	4.0	Ls, aa, fine crinoid grainstone, strongly recrystallized, num microvugs & sparse large vugs. 1 lg sed-filled vug.	
4987.1	4991.0	Ls	Grnstn	V, Imo, Fr	10.0	4.0	Y	7,9	Ls, aa, much dk gy sed infill & stain, v.coarse crinoid-brach grainstone, large coral (Favosites?) in basal 0.5 ft. Strongly leached, abund large vugs, mostly clay-sediment infilled, inside brachs & corals, abund moldic microvugs. Partly recrystallized to coarse spar. Top contact probably a dissolution (cave roof) contact.	
4991.0	4996.6	Ls	Grnstn	SF, SV, Mo	3.0	1.0	P	5,8	Ls, pk-gy, f.-c. crinoid grainstone (sparrite), partly compacted with fitted grains. Rare brachs, corals, bryozoan & stromatoporoid fragments. Tightly cemented, strongly recrystallized IP, SFs with dk-gy Woodford ? fill.	

Table 7-18: Core Description #2, Marjo Toles 1-10

CORE DESCRIPTION MARJO TOLES 1-10, SEC. 10, T15N, R2E LINCOLN COUNTY, OKLAHOMA										
Depth		Lith	Fabric	Pore Types	Av Pore %	TV	Chalky	Facies	Description	
From	To									
4996.6	4998.3	Ls	Pkstn	SF, Vug	2.0	0.0	N	5,6	Ls, pk gy, f-med crinoid-brach packstone, with thin grainstones; foss allochems <3mm.	
4998.3	5001.8	Ls	Grnstn	SF, IX, Vug	3.0	2.0	N	5,6	Ls, pk-gy, c crinoid-brach grainstone, part recrystall., fractured, vuggy, both partly clay-filled. Sharp upper boundary at corrosion surface, poss seq boundary	
5001.8	5003.7	Dol	Grnstn/XlIn	IX, Mo, Fr	4.0	1.0	N	5.0	Dol, lt olive gy (5Y 6/1) to green-gy ((5GY 6/1), c. grainstone with large brachs to fine grainstone to med xln dol. Moldic pores around large brachs.	
5003.7	Sylvan Shale (0.6 ft cored)									
5003.7	5004.4	Dol	Mdstn	IX	3.0	0.0	N	1.0	Dolomite, greenish gray (5GY6/1), mudstone, argillaceous, pyritic, burrow mottled.	
5004.4	Base of Core									

Table 7-19: Core Description #1, Marjo Wilkerson 1-3

CORE DESCRIPTION MARJO WILKERSON 1-3, SEC. 3, T15N, R2E LINCOLN COUNTY, OKLAHOMA											
Depth		Lith	Fabric	Pore Types	Av Pore %	TV	Chalky	Facies	Description		
From	To										
Shale (2.43 ft cored)											
4950	4952.43	Shale		nil	nil			13	Shale, dk gy N3, fissile, carbonaceous, pyritic		
Sandstone (0.99 ft)											
4952.43	4952.42	SS		nil	nil			14	SS, med-dk Gy, vfg-fig, calc, abund large brachiopods & fragments, sharp upper contact. ---Disconformity: erosional surface---		
Hunton Limestone (46.38 ft)											
4953.42	4958	Ls	Pkstn, Grmstn	IG,BR,SF	6	3	Y	7	Limestone, pinkish gray 5YR8/1 with patchy dark gray matrix, brachiopod packstone and grainstone. Leached skeletal grains gives collapsed fabric, partly dissolved by micro karst. Misener sand infill in open vertical fractures and vugs. Vugs largely leached mudstone matrix. coarse calcite crystals in vugs. collapse breccia 4954.5-56. Abundant large strophomenid brachiopods. common vertical fracturing.		
4958	4960	Ls	Pkstn	PP, SV, MO	3	0	Y	7	Ls, aa, little sand infill, mostly tightly cemented, isolated moldic vugs		
4960	4962.6	Ls	Pkstn	SF, MO	5	2	Y	7	Ls, aa, brach packstone. Short vertical fractures, open, solution-enlarged. Many vugs surrounding brachiopod shells, moldic on outer (primary) shell		
4962.6	4965.3	Ls	Pkstn	SF,MO	3.5	1	P	7	Ls, aa, brach packstone. Mostly tight matrix. Solution enlarged and moldic (SF,MO) porosity sparse. Coral at 66.7'. Coarse crystalline calcite layer (0.1') @ 65.1, ? cavern fill.		
4965.3	4967	Ls	Pkstn, Grmstn	SF, MO	4.5	3	P	7	Ls, aa, brach packstone and grainstone, decreasing mud matrix. Touching vugs common, vertical open fractures crystal-lined. Thin zone of 8% TV porosity at 4966-66.4'.		
4967	4973.5	Ls	Grmstn	SV:MO	1.5	0	N	7	Ls, aa, brach grainstone, large Pentamerids less abundant. Mostly tightly cemented with sparse separate moldic vugs. Recrystallized to dense spar at 4971.5-71.7, ?cavern fill.		
4973.5	4975.8	Ls	Pkstn	IG,MO,SF	10	2	Y	7	Ls, v pale orange 10YR8/2, leached vuggy brach packstone. Good secondary intergranular porosity due to dissol of mud matrix, good moldic vugs, mod. fractures		
4975.8	4978.7	Ls	Pkstn	MO	1.5	0	N	6	Ls, pinkish gy, crinoidal & brach packstone, tighly cemented. Rare moldic vugs. Large crinoid at 4978.5		
4978.7	4981.7	Ls	Grmstn	IX?, MO	1	0	N	6	Ls, aa, mixed crinoidal & brach fine grainstone, tighly cemented. Sparse large brachs & large crinoids,		

Table 7-20: Core Description #2, Marjo Wilkerson 1-3

CORE DESCRIPTION MARJO WILKERSON 1-3, SEC. 3, T15N, R2E LINCOLN COUNTY, OKLAHOMA										
Depth		Lith	Fabric	Pore Types	Av Pore %	TV	Chalky	Facies	Description	
From	To									
4981.7	4992.7	Ls	Grnsth	IG, MO	2	0	N	6.5.4	Ls, grayish orange pink 5YR7/2, crinoidal grainstone ("pink encrinite" of workers), fine to vfg, with sparse large crinoids & sparse thin layers of small brachiopods. Trace of ooids. Leached, collapsed grainstone, about 5% mud matrix. Porosity largely intergranular, due to leaching of mud matrix, with 1% microporosity in mud. Thin layers of moldic porosity up to 3%. Bottom 1' has 4% porosity, moldic & fine fractures. [4985.2-86.2 is brachiopod ppksth, vuggy; appears out of place. Probably Misplaced Core!]	
4992.7	4994.9	Ls	Grnsth	IG	1.8	0	N	5	Ls, aa, tightly cemented, terra rosa; stylolite base; ?depositional boundary	
4994.9	4997.9	Ls	Grnsth	IG, MO	8	0	P	6	Ls, aa, brach/crinoid grnsth, coarse grained. Rare corals, abund. large Pentamerid brachs (diff. Species from above). Sparse mud matrix, leached to fine Separate Vugs in intergranular space. Basal 0.3' is dark muddy grainstone, stylolitic. Possible Sequence boundary. Dolomite and dolomitic limestone, lt olive gy 5Y6/1, dolomitized brach/crinoid grainstone. Excellent intercrystalline porosity, and moldic porosity on primary (outer) layer of large pentamerid brachs. Abrupt contact at base. Basal 0.2' is fine-grained grainstone, possibly oolitic (Need TS). Possibly Keel Oolite unit reported by Amsden in the Kirkpatrick 1 Blevins in 7-17N-4W, Logan Co, OGS Bull. 129.	
4997.9	4999.8	Dol	Grnsth	IX, MO	10	1	P	3	---Disconformity: erosional surface---	
4999.8	Sylvan Shale (4.4 ft cored)									
4999.8	5004.2	Dol	Mdstn	IX		0		1	Dol, argillaceous mudstone, greenish gray, 5GY6/1, top is erosional surface, abund pyrite throughout, terra rosa near top	

Table 7-21: Core Description, Marjo Williams 1-3

CORE DESCRIPTION MARJO WILLIAMS 1-3, SEC.3, T15N, R2E LINCOLN COUNTY, OKLAHOMA										
Depth		Lith	Fabric	Pore Types	Av Pore %	TV	Chalky	Facies		Description
From	To									
4942 Top of Core										
Woodford Shale (0.2ft)										
4942	4942.2	Shale		nil	nil				13	Shale, brownish black, fissile, highly clacareous, pyritic
Misener Sandston (1.3ft)										
4942.2	4943.5	SS		nil	nil				14	Sand stone, brownish black to med gy gy, shaly, thin beds and laminae of very fine qtz sand and fissile shale. Basal contact is sharp, very irregular and sand extends deep into fractured fissures in underlying hunton
4943.5 Hunton Limestone (40.3)										
4943.5	4944	Ls	pkstn	SF	1	1	-		7	Ls, partly dol, med gy, mottled lt gy, pent brac coquina with solution fractures and vugs, filled with dk misener sediments occluding porosity.
4944	4949.2	Ls	pkstn	VUG, SF	1.5	1	-		7	Ls, pksh gy 5YR 8/1 to med lt gy near top, coarse pent brac pkstn, mostly very tightly cemented, minor karst infill of vuggy cavities.
4949.2	4954	Ls	pkstn	VUG, SF	3.5	3	-		7	Ls, pkstn, pinkish gy to mottled med lt gy, coarse pent brac coquina, partly tightly cemented pkstn, partly with well developed vuggy porosity filled with misener clay and silt.
4954	4959.5	Ls	pkstn	SF	1.5	1	-		7	Ls, pkstn, pinkish gy with med gy mottles, coarse pent brac coquina, about 60% with intra brac matrix absent, voids totally filled with misener clay and silt. About 40% tightly cemented with carbonate mud and fine grains
4959.5	4973.2	Ls	pkstn	SF, VUG	2	1	-		7	Ls, pkstn, lt pinkish gy to med dk gy, coarse pent brac coquina, mostly pkstn with thin intervals of mdstn/wkstn, @4967.6-7, 4972.2-.5. <uch mostly karst dissolution, large SF upto .1 ft across and inter-clast voids filled with misener or woodford dk brown clay and silt. Porosity largely occluded by karst infill.
4973.2	4975.4	Ls	wkstn	SF	2	1	-		15	Ls, pinkish gy, large thin brac wkstn to sparsely fossil mdstn, discontinuous VIH SF, partially healed
4975.4	4976.8	Ls	pkstn	VUG, SF	4	2	-		7	Ls, med gy to pinkish gy, coarse pent brac pkstn with abundant karst infill in interclasts spaces, in part fine silty sand
4976.8	4978.2	Ls	grnstn	SF	1.5	1.5	-		12	Ls, lt gy to pinkish gy, very fine grnstn with very sparse large fossils and open V SF
4978.2	4982.3	Dol	pkstn	lxln, VUG	7.5	1	sli		7	Dol, yellowish gy to ly gy, coarse pent brac pkstn, top 0.7ft is partially dolomitized brac wkstn, includes thin intervals of fine to med grnstn
4982.3	4983.8	Dol	grnstn	lxln	7	-	-		12	Dol, yellowish gy to greyish orange pink 5YR7/2, fine to med grnstn, burrow mottled, bottom 0.1 ft is med gy, laminated, pyritic, sharp contact with sylvan @ 4983.8
TOP SYLVAN										
4983.8	4987.5	Dol	mdstn	lxln	5	-	-		1	Dol, argillaceous, grnsh gy to lt olive gy, pyritic, burrow mottled, increasing in argillaceous content downward

7.1.9. Explanation of Coding of Porosity and Facies Type

A data table for each well presented is given below in **Section 7.1.10**. The data includes the following for each core sample analyzed by Stim-Lab:

- The footage interval analyzed
- The mid-depth of that interval, for purposes of comparing core data to well-log response.
- Porosity (ϕ)
- Grain density: Since Hunton rocks are nearly 100% carbonate, grain density can be converted into limestone/dolomite ratios. The densities are highlighted to discriminate limestone vs. partially dolomitized limestone vs. dolomite.
- Pore-type code (See table below)
- Facies code (See table below)
- Stratigraphic position: Expressed as footage above or below the Hunton/Sylvan contact.
- Comments, including a brief description of a thin section.

7.1.9.1. Table of Porosity Types and Codes

Limestones (grain density 2.71 to <2.73):

1. Interconnected Vuggy porosity

Vug or MO with IG, SF or other connection, TV general, Vug general.
Not vugs with tight matrix.

2. Coarse Matrix porosity

Inter-particle (IP), IG or IX of coarse-grained rock, > .25 mm particle size.
Many include dissolution porosity that is inter-particle micro vugs
(dissolution of spar or matrix).

3. Fine Matrix porosity

Inter-particle (IP), IG or IX of medium to fine-grained rocks, < .25 mm
particle size. Includes fine non touching vugs and non touching fine
Moldic (MO) porosity along with intra-particle porosity

4. Fracture

FR or SF without significant matrix or vugs.

For this study, includes solution-enhanced fractures with sand in-fill.

Dolomite (> 50% dolomite; grain density 2.79 or higher):

5. Vuggy (vug) or Moldic (MO) in coarse crystalline (IX) matrix (> .25 mm)

6. Coarse crystalline with Inter-crystalline porosity (IX) (> .25 mm)

7. Medium to fine crystalline (IX) (.25 mm to .02 mm)

8. Fracture FR or SF without significant matrix porosity

**Partly Dolomitized Limestone (10 – 50 % dolomite; grain density 2.73-
2.78):**

9. Interconnected Vuggy porosity

Vug or MO with IG, SF or other connection, TV general, Vug general.

Not vugs with tight matrix.

10. Coarse Matrix porosity

Inter-particle (IP), IG or IX of coarse-grained rock, > .25 mm particle size.
May include dissolution porosity that is inter-particle micro vugs (dissolution of spar or matrix).

11. Fine Matrix porosity

Inter-particle (IP), IG or IX of medium to fine-grained rocks, < .25 mm particle size. Includes fine non touching vugs and non touching fine Moldic (MO) porosity along with intra-particle porosity

12. Fracture

FR or SF without significant matrix or interconnected vuggy porosity.

For this study, includes solution-enhanced fractures with sand in-fill.

For the Tables in **Section 7.1.10**, the description of the grain density is as follows:

Shaded values (2.73 to 2.78) represent partially dolomitized limestone, bold values (>2.78) represent dolomite and others are limestone (<2.73).

Table 7-22: Table of Facies Codes

Numeric codes for 14 identified Lithofacies

1. Argillaceous Dolomite (Greenish-gray, resembles
Sylvan Fm)
2. Crystalline Dolomite (No fossils or allochems
identifiable)
3. Small Brachiopod Grainstone/Packstone/Wackestone
4. Fine Crinoid Grainstone/Packstone/Wackestone
5. Coarse Crinoid Grainstone/Packstone
6. Mixed Crinoid-Brachiopod
Grainstone/Packstone/Wackestone
7. Big Pentamerid Brachiopod Coquina
8. Coral and Diverse Fauna
9. Coral and Crinoid Grainstone-Wackestone
10. Sparse Fossil Wackestone
11. Mudstone, carbonate
12. Fine- Medium Grainstone
13. Shale (Woodford, Sylvan)
14. Fine Sandstone (Misener SS)

7.1.10. Tables of Core Porosity, Grain Density, Porosity and Facies Codes of Individual Wells

Table 7-23: Marjo Anna Porosity and Facies Codes

Marjo Anna Porosity and Facies codes										
Core #	From	To	Mid-Depth	Phi	Grain Density	Pore Code	Facies Code	strat position	Thin Section	
			Core Depth	CORE PHI						
1	4967.3	to	68	4967.65	3.5	2.76	9	7	37.4	
2	4968	to	68.6	4968.3	5.9	2.77	9	7	36.7	
3	4969	to	69.6	4969.3	8.2	2.75	9	7	35.7	
4	4970.5	to	71	4970.75	7	2.74	9	7	34.2	
5	4971	to	71.6	4971.3	9.5	2.77	9	7	33.7	
6	4972	to	72.7	4972.35	7.1	2.78	9	7	32.7	
7	4973	to	73.6	4973.3	8.2	2.78	10	7	31.7	
8	4974.3	to	75	4974.65	7.1	2.73	10	7	30.4	
9	4975	to	75.7	4975.35	7.2	2.72	9	7	29.7	
10	4976.3	to	76.9	4976.6	11.2	2.75	9	7	28.4	
11	4977.3	to	78	4977.65	9.8	2.77	10	7	27.4	
12	4978	to	78.7	4978.35	7.4	2.77	9	7	26.7	
13	4979	to	79.5	4979.25	4.4	2.77	10	15	25.7	
14	4980	to	80.6	4980.3	9.2	2.76	10	7	24.7	
15	4981	to	81.6	4981.3	9.3	2.75	9	7	23.7	
16	4982.5	to	83	4982.75	4.9	2.76	10	7	22.2	
17	4983	to	83.6	4983.3	9.1	2.76	10	7	21.7	
18	4984	to	84.6	4984.3	9.4	2.79	6	7	20.7	
19	4985	to	85.6	4985.3	5.3	2.79	6	7	19.7	
20	4986	to	86.6	4986.3	7.3	2.77	10	7	18.7	
21	4987	to	87.7	4987.35	8.1	2.78	9	7	17.7	
22	4988.3	to	89	4988.65	4.2	2.79	5	7	16.4	
23	4989	to	89.7	4989.35	6	2.75	10	7	15.7	
24	4990.4	to	91	4990.7	5	2.79	5	7	14.3	
25	4991	to	91.6	4991.3	6.1	2.8	5	7	13.7	
26	4992.3	to	93.9	4993.1	4.9	2.79	6	7	12.4	
27	4993.5	to	94	4993.75	9.4	2.81	6	7	11.2	
28	4994.3	to	95	4994.65	12.3	2.82	5	7	10.4	
29	4995.5	to	96	4995.75	13.2	2.83	5	7	9.2	
30	4996.3	to	96.8	4996.55	11.7	2.85	5	7	8.4	
31	4997.3	to	98	4997.65	4	2.82	5	7	7.4	
32	4998	to	98.6	4998.3	5.2	2.85	5	10	6.7	
33	4999.4	to	99.8	4999.6	5.7	2.87	5	10	5.3	
34*	5000.8			5000.8	9.5	2.84	5	10	3.9	
35	5001.1	to	1.8	5001.45	9.1	2.82	5	10	3.6	
36	5002	to	2.3	5002.15	6.4	2.78	12	12	2.7	
37	5003.4	to	4	5003.7	2.3	2.76	11	12	1.3	
38	5004	to	4.6	5004.3	7.8	2.9	4	6	0.7	Not dolomite , good fossil Ls, tight
39	5005	to	5.3	5005.15	3.5	2.86			-0.3	Sylvan

Strat Position is footage above or below (-) the Hunton/Sylvan contact at 5004.7, core depth

Table 7-24: Bailey 2-6 Porosity and Facies Codes

Bailey 2-6										
Core #	From	To	Mid-Depth	Phi		Pore Code	Facies Code	Strat Position	Thin Section	
			Core Depth	CORE PHI	grain density					
1	4876.0	to	4876.5	4876.25	8.81	2.84	7	6	85.2	* 76.3 mo or vuggy with dol, f xln dol
2	4877.5	to	4877.8	4877.65	11.30	2.85	5	6	83.7	
3	4878.0	to	4878.4	4878.2	16.26	2.84	5	6	83.2	*78.3 Dol cavity fill, SF, vug
4	4879.0	to	4879.3	4879.15	10.58	2.84	5	6	82.2	
5	4880.0	to	4880.5	4880.25	5.69	2.79	5	4	81.2	
6	4881.2	to	4881.9	4881.55	4.21	2.75	10	4	80	* cri pkstn 81.2
7	4882.8	to	4883.0	4882.9	5.46	2.80	5	9	78.4	
8	4883.0	to	4883.6	4883.3	4.72	2.79	5	9	78.2	
9	4884.3	to	4885.0	4884.65	8.66	2.83	5	9	76.9	
10	4885.0	to	4885.5	4885.25	10.42	2.84	5	9	76.2	
11	4886.5	to	4887.0	4886.75	2.51	2.81	8	9	74.7	
12	4887.0	to	4887.3	4887.15	1.92	2.80	8	9	74.2	*4887.2
13	4888.5	to	4889.0	4888.75	1.61	2.83	8	9	72.7	
14	4889.0	to	4889.3	4889.15	1.58	2.79	8	8	72.2	
15	4890.4	to	4891.0	4890.7	2.71	2.75	12	8	70.8	
16	4891.4	to	4892.0	4891.7	2.64	2.75	12	3	69.8	* br-cri gmstn
17	4892.3	to	4893.0	4892.65	1.22	2.70	4	7	68.9	
18	4893.5	to	4894.0	4893.75	2.21	2.71	1	7	67.7	
19	4894.0	to	4894.6	4894.3	1.67	2.71	1	3	67.2	
20	4895.3	to	4896.0	4895.65	0.96	2.71	4	3	65.9	
21	4896.0	to	4896.4	4896.2	0.80	2.70	4	3	65.2	
22	4897.2	to	4898.0	4897.6	0.86	2.71	4	3	64	
23	4898.2	to	4899.0	4898.6	1.04	2.71	4	3	63	
24	4899.3	to	4900.0	4899.65	0.86	2.71	4	3	61.9	*4899.1 small br, br/cri
25	4900.1	to	4900.5	4900.3	1.31	2.73	12	3	61.1	
26	4901.3	to	4901.9	4901.6	0.85	2.71	3	3	59.9	
27	4902.0	to	4902.5	4902.25	1.04	2.71	3	6	59.2	
28	4903.3	to	4903.9	4903.6	0.86	2.71	3	6	57.9	
29	4904.4	to	4950.0	4927.2	0.87	2.71	3	6	56.8	
30	4905.3	to	4906.0	4905.65	0.68	2.71	3	6	55.9	
31	4906.0	to	4906.5	4906.25	0.86	2.72	3	6	55.2	
32	4907.3	to	4907.9	4907.6	0.69	2.71	3	6	53.9	
33	4908.0	to	4908.5	4908.25	0.78	2.71	3	6	53.2	
34	4909.2	to	4909.8	4909.5	0.82	2.71	3	6	52	
35	4910.1	to	4910.7	4910.4	0.87	2.71	3	6	51.1	
36	4911.3	to	4912.0	4911.65	0.93	2.71	3	6	49.9	
37	4912.0	to	4912.4	4912.2	0.89	2.70	3	6	49.2	
38	4913.0	to	4913.3	4913.15	0.88	2.72	4	6	48.2	
39	4914.4	to	4914.9	4914.65	1.24	2.71	3	7	46.8	
40	4915.0	to	4915.6	4915.3	2.15	2.71	1	7	46.2	* 4915.3 BB with shelter mud filled, SV
41	4916.0	to	4916.7	4916.35	0.93	2.71	3	7	45.2	*4916.3
42	4917.2	to	4917.8	4917.5	1.38	2.72	3	7	44	
43	4918.0	to	4918.6	4918.3	1.54	2.73	12	7	43.2	huge SF, coarse xln, sequence bndry?
44	4919.4	to	4919.9	4919.65	1.12	2.72	3	6	41.8	
45	4920.3	to	4920.9	4920.6	1.14	2.71	3	6	40.9	*4920.3
46	4921.0	to	4921.6	4921.3	1.72	2.71	1	6	40.2	vuggy, part mud filled
47	4922.0	to	4923	4922.5	2.02	2.71	1	6	39.2	
48	4923.0	to	4924	4923.5	3.03	2.71	1	6	38.2	* br, laminated karst mud infill
49	4924.3	to	4925	4924.65	1.76	2.72	3	6	36.9	
50	4925.3	to	4926	4925.65	3.05	2.74	9	6	35.9	
51	4926.0	to	4927	4926.5	2.87	2.74	9	7	35.2	
52	4927.3	to	4928	4927.65	2.16	2.72	1	7	33.9	*4927.4, *4927.8
53	4928.0	to	4929	4928.5	1.51	2.71	4	7	33.2	
54	4929.7	to	4930	4929.85	2.01	2.71	4	6	31.5	
55	4930.5	to	4931	4930.75	2.55	2.71	3	6	30.7	* small br wk/pk
56	4931.3	to	4932	4931.65	1.74	2.70	4	6	29.9	
57	4932.0	to	4933	4932.5	1.53	2.71	4	6	29.2	* 4932 fine brac facies
58	4933.2	to	4934	4933.6	1.67	2.70	4	6	28	

Table 7-25: Boone 1-4 Porosity and Facies Codes

Marjo Boone 1-4 Porosity and Facies codes									
Core #	From	To	Mid-Depth	Phi	Grain Density	Pore Code	Facies Code	strat position	Thin Section
			Core Depth	CORE PHI					
1	5037.1	to	38	5037.55	3.1	2.72	4	6	29.4
2	5038.3	to	39	5038.65	3.7	2.71	4	6	28.2
3	5039.1	to	39.9	5039.5	4.7	2.71	2	6	27.4
4	5040.1	to	40.9	5040.5	3.1	2.71	2	6	26.4
5	5041	to	41.4	5041.2	2.2	2.71	2	6	25.5
6	5042	to	42.9	5042.45	1.6	2.71	3	6	24.5
7	5043	to	43.9	5043.45	2.8	2.71	3	9	23.5
8	5044	to	44.6	5044.3	2.3	2.71	3	9	22.5
9	5045	to	45.8	5045.4	0.7	2.71	2	9	21.5
10	5046.1	to	47	5046.55	7.4	2.74	10	9	20.4
11	5047	to	47.9	5047.45	7.9	2.76	10	9	19.5
12	5048	to	48.6	5048.3	9.9	2.76	10	5	18.5
13	5049.3	to	50	5049.65	10.4	2.75	10	5	17.2
14	5050	to	50.6	5050.3	6.9	2.73	10	5	16.5
15	5051	to	51.8	5051.4	6.8	2.73	10	5	15.5
16	5052	to	52.8	5052.4	5.5	2.73	10	4	14.5
17	5053.2	to	54	5053.6	6.3	2.76	10	4	13.3
18	5054	to	54.8	5054.4	5.9	2.76	10	4	12.5
19	5055	to	55.5	5055.25	9.2	2.74	10	4	11.5
20	5056	to	56.8	5056.4	10.6	2.72	2	6	10.5
21	5057	to	57.6	5057.3	9	2.75	10	6	9.5
22	5058.5	to	59	5058.75	5.1	2.78	10	6	8
23	5059	to	59.7	5059.35	4.4	2.78	10	4	7.5
24	5060.3	to	61	5060.65	1.5	2.7	2	5	6.2
25	5061	to	61.8	5061.4	1.1	2.71	2	5	5.5
26	5062.2	to	63	5062.6	5.6	2.73	10	4	4.3
27	5063	to	63.9	5063.45	7.8	2.79	5	6	3.5
28	5064	to	64.3	5064.15	9.3	2.8	5	6	2.5
29	5065.7	to	66	5065.85	13.1	2.88	5	6	0.8
30	5066	to	66.4	5066.2	8.1	2.85	5	4	0.5
31	5067.1	to	67.3	5067.2	4.3	2.96	5	1	-0.6
32	5067.9							1	

Strat Position is footage above or below (-) the Hunton/Sylvan contact at 5066.5, core depth

Table 7-26: Carney Townsite 2-5 Porosity and Facies Codes

Marjo Carney Townsite 2-5 Porosity and Facies codes										
Core #	From	To	Mid-Depth	Phi	Grain Density	Pore Code	Facies Code	strat position	Thin Section	
			Core Depth	CORE PHI						
1	4906.1	to	6.9	4906.5	9.1	2.8	7	2	73.2	limy Dol, equant f xln, no allochems
2	4907.5	to	8	4907.75	11	2.78	10	4	71.8	
3	4908.3	to	9	4908.65	11.2	2.75	10	4	71	
4	4909.3	to	10	4909.65	11.7	2.78	10	4	70	
5	4910.3	to	11	4910.65	12.6	2.81	7	4	69	
6	4911.3	to	12	4911.65	11.7	2.8	7	4	68	
7	4912.3	to	13	4912.65	10.3	2.76	10	6	67	
8	4913.3	to	14	4913.65	10.5	2.77	10	6	66	
9	4914.3	to	15	4914.65	9.9	2.76	10	6	65	
10	4915.3	to	16	4915.65	10.8	2.78	10	6	64	
11	4916.3	to	17	4916.65	11.5	2.79	7	6	63	Dolomitized med cri wkstn, dissolved porosity, limy Dol
12	4917.5	to	18	4917.75	12.4	2.8	7	4	61.8	
13	4918.3	to	19	4918.65	11.7	2.78	11	4	61	
14	4919	to	19.7	4919.35	12.4	2.82	7	4	60.3	
15	4920.3	to	21	4920.65	12.3	2.8	7	6	59	
16	4921	to	21.7	4921.35	14.1	2.81	7	6	58.3	
17	4922	to	22.6	4922.3	12.8	2.83	7	6	57.3	
18	4923	to	23.6	4923.3	14	2.8	7	4	56.3	
19	4924.3	to	25	4924.65	14.5	2.81	7	4	55	Dolomitized med cri pkstn, limy Dol
20	4925.1	to	25.7	4925.4	13.2	2.82	7	4	54.2	
21	4926	to	26.8	4926.4	11.7	2.82	7	4	53.3	
22	4927.1	to	27.8	4927.45	11.2	2.76	9	4	52.2	
23	4928.3	to	29	4928.65	10.7	2.74	10	5	51	
24	4929.3	to	30	4929.65	11	2.76	9	5	50	
25	4930.3	to	31	4930.65	8.6	2.73	9	5	49	
26	4931.3	to	32	4931.65	9.1	2.73	10	6	48	sli dol LS, med cri brac pkstn
27	4932.2	to	32.9	4932.55	10.4	2.73	9	6	47.1	
28	4933.3	to	34	4933.65	10.1	2.76	9	6	46	
29	4934.3	to	35	4934.65	11	2.78	10	4	45	
30	4935	to	35.7	4935.35	11.6	2.76	10	4	44.3	
31	4936.3	to	37	4936.65	10.9	2.77	10	4	43	
32	4937	to	37.6	4937.3	11.4	2.78	9	4	42.3	
33	4938.3	to	39	4938.65	10.5	2.79	10	4	41	
34	4939.4	to	40	4939.7	9.8	2.8	10	4	39.9	
35	4940.2	to	40.9	4940.55	6.9	2.79	5	4	39.1	
36	4941.4	to	42	4941.7	4.2	2.77	1	4	37.9	
37	4942.4	to	43	4942.7	4	2.7	2	4	36.9	
38	4943	to	43.3	4943.15	3.6	2.71	2	4	36.3	
39	4944	to	44.3	4944.15	6.4	2.81	7	11	35.3	
40	4945.3	to	46	4945.65	2.5	2.71	3	4	34	
41	4946	to	46.7	4946.35	3	2.74	4	12	33.3	4946.4-6 dolomite Ls, r xl/2 grmatn, Fr 4946.8-9 limy dol, r xl/2 pkstn/wkstn, SV
42	4947.3	to	48	4947.65	7.1	2.8	11	10	32	
43	4948	to	48.6	4948.3	12	2.84	8	10	31.3	
44	4949	to	49.3	4949.15	3.9	2.76	11	4	30.3	
45*	4950.1	to	51	4950.55	6.2	2.84	7	10	29.2	
46*	4951.1	to	52	4951.55	2.1	2.76	11	11	28.2	
47	4952.5	to	52.8	4952.65	5.6	2.78	9	4	26.8	
48*	4953.1	to	54	4953.55	5.4	2.77	9	4	26.2	
49*	4954.9	to	55	4954.95	5	2.81	7	11	24.4	
50*	4955.1	to	56.3	4955.7	4.4	2.81	7	4	24.2	
51*	4956	to	57	4956.5	2	2.77	11	11	23.3	
52*	4957.5	to	58	4957.75	1.3	2.71	3	4	21.8	
53*	4958.1	to	59	4958.55	0.9	2.71	3	10	21.2	
54*	4959.1	to	60	4959.55	1.3	2.71	3	3	20.2	
55*	4960.1	to	61	4960.55	2	2.72	3	3	19.2	LS, med-f collapsed grnstn, fine brac
56	4961.3	to	62	4961.65	2.7	2.71	3	9	18	
57	4962	to	62.5	4962.25	2.2	2.71	3	6	17.3	
58	4963.5	to	64	4963.75	1.2	2.71	3	5	15.8	
59	4964	to	64.7	4964.35	0.9	2.72	3	6	15.3	med-c cri brac-ost grnstn, karst dissolved
60*	4965.1	to	66	4965.55	0.9	2.71	3	6	14.2	

Strat Position is footage above or below (-) the Hunton/Sylvan contact at 4978 feet, core depth. Core depth appears to equal log depth.

Table 7-27: Carter 1-4 Porosity and Facies Codes

Marjo Carter 1-4 Porosity and Facies codes										
Core #	From	To	Mid-Depth	Phi	Grain Density	Pore Code	Facies Code	strat position	Thin Section	
			Core Depth	CORE PHI						
1	4940.2	to	40.9	4940.55	6.7	2.85	7	6	55.6	* fine xln Dol. IX + dissolved IX
2	4941.4	to	42	4941.7	5.6	2.71	2	6	54.4	** a) med grnstrn, collapsed ~ .5 mm, 0 porosity. B) c grnstrn
3	4942.3	to	43	4942.65	9.3	2.71	1	7	53.5	
4	4943.1	to	43.7	4943.4	11	2.7	1	7	52.7	
5	4944.4	to	45	4944.7	6.7	2.71	1	7	51.4	
6	4945	to	45.6	4945.3	9.1	2.7	1	7	50.8	* c brac pkstrn, matrix dissolved, IG porosity
7	4946	to	46.4	4946.2	10.3	2.7	1	7	49.8	
8	4947.3	to	48	4947.65	7.3	2.71	1	7	48.5	
9	4948.3	to	49	4948.65	9.1	2.7	1	7	47.5	
10	4949.5	to	50	4949.75	6.1	2.7	2	7	46.3	
11	4950.4	to	51	4950.7	3.8	2.71	2	6	45.4	* c brac cri grnstrn, syntax overgrowth
12	4951	to	51.6	4951.3	2.9	2.71	2	6	44.8	
13	4952.3	to	53	4952.65	6.6	2.74	10	6	43.5	
14	4953	to	53.6	4953.3	2.3	2.72	2	6	42.8	
15	4954	to	54.6	4954.3	4.8	2.73	10	5	41.8	
16	4955.3	to	56	4955.65	2.5	2.72	2	5	40.5	* c cri grnstrn, syntax overgrowth, IG porosity, karst silt
17	4956	to	56.6	4956.3	2.3	2.71	4	6	39.8	
18	4957	to	57.6	4957.3	1.6	2.72	2	5	38.8	
19	4958	to	58.7	4958.35	1	2.72	2	5	37.8	
20	4959.3	to	60	4959.65	3.8	2.75	10	5	36.5	
21	4960.4	to	61	4960.7	2.6	2.71	2	5	35.4	
22	4961.3	to	62	4961.65	2.1	2.7	2	5	34.5	* c cri grnstrn, syntax overgrowth, tight
23	4962	to	62.6	4962.3	4.3	2.71	1	6	33.8	* c cri brac grnstrn, leached, vuggy
24	4963.3	to	64	4963.65	2.6	2.71	2	6	32.5	
25	4964	to	64.6	4964.3	2.1	2.71	2	6	31.8	
26	4965.3	to	66	4965.65	1.6	2.72	2	6	30.6	
27	4966	to	66.6	4966.3	2.4	2.71	2	6	29.8	
28	4967.3	to	68	4967.65	1.7	2.71	2	6	28.5	
29	4968.8	to	69	4968.9	2.9	2.72	1	6	27	
30	4969	to	69.6	4969.3	4.9	2.72	1	6	26.8	
31	4970.5	to	71	4970.75	2.6	2.72	2	6	25.3	
32	4971	to	71.6	4971.3	1.5	2.71	2	6	24.8	
33	4972.4	to	73	4972.7	1.9	2.71	2	6	23.4	
34	4973.3	to	74	4973.65	1	2.71	2	6	22.5	
35	4974.6	to	74.6	4974.6	1.5	2.71	4	6	21.2	
36	4975	to	75.7	4975.35	1.3	2.71	2	6	20.8	* c cri brac grnstrn, tight, syntax overgrowth
37	4976	to	76.6	4976.3	1.4	2.71	2	6	19.8	
38	4977.3	to	78	4977.65	1.2	2.7	2	5	18.5	* (4976.8) c cri grnstrn, tight, syntax overgrowth
39	4978	to	78.6	4978.3	1.7	2.7	2	5	17.8	
40	4979.6	to	80	4979.8	0.9	2.71	2	5	16.2	
41	4980.1	to	80.7	4980.4	0.9	2.71	2	6	15.7	
42	4981.3	to	82	4981.65	2.2	2.73	10	3	14.5	
43	4982	to	82.7	4982.35	2.6	2.71	2	3	13.8	
44	4983	to	83.5	4983.25	5.7	2.75	10	3	12.8	
45	4984	to	84.6	4984.3	5.4	2.76	10	6	11.8	*2x2 slide, Doltzd c m cri brac grnstrn, sli baroque Dol
46	4985	to	85.6	4985.3	6.1	2.75	9	6	10.8	
47	4986	to	86.6	4986.3	6	2.75	10	6	9.8	
48	4987.4	to	87.9	4987.65	5.4	2.7	1	6	8.4	
49	4988	to	88.6	4988.3	4.2	2.71	2	6	7.8	
50	4989	to	89.6	4989.3	4.6	2.71	3	4	6.8	
51	4990	to	90.6	4990.3	6	2.72	3	4	5.8	
52	4991.3	to	92	4991.65	10.3	2.73	11	6	4.5	* f cri brac grnstrn, good IG porosity
53	4992	to	92.6	4992.3	11.4	2.73	11	6	3.8	
54	4993	to	93.7	4993.35	5.2	2.73	11	6	2.8	
55	4994	to	94.4	4994.2	1.1	2.8	11/7	6/12	1.8	* Ls, f cri brac grnstrn / f Dol grnstrn, IG, IX porosity (4994.1)
56	4995	to	95.5	4995.25	11.6	2.89	7	12	0.8	* med-f xln Dol grnstrn, good IX porosity, f xln baroqued Dol
57	4996.3	to	97	4996.65	4.6	2.94	7	1	-0.5	
58	4998.2								-2.4	* v f argill dol mdstrn
	4999.9								-4.1	

Strat Position is footage above or below the Hunton/Sylvan contact at 4995.8, core depth.

Table 7-28: Carter Ranch 2-5 Porosity and Facies Codes

Marjo Carter Ranch 2-5 Porosity and Facies codes									
Core #	From	To	Mid-Depth	Phi	Grain Density	Pore Code	Facies Code	strat position	Thin Section
			Core Depth	CORE PHI					
1	5006.4	7.0	5006.7	2.2	2.72	4	7	28.7	
2	5007.0	7.6	5007.3	3.6	2.71	4	7	28.1	
3	5008.0	8.7	5008.35	5.4	2.70	2	7	27.1	Dissolution of grains in fine matrix
4	5009.0	9.7	5009.35	1.3	2.72	4	11	26.1	
5	5010.0	10.7	5010.35	2.2	2.71	4	7	25.1	
6	5011.3	12.0	5011.65	4.7	2.70	3	7	23.8	
7	5012.3	13.0	5012.65	1.9	2.71	4	7	22.8	
8	5013.3	14.0	5013.65	1.7	2.71	4	7	21.8	
9	5014.0	14.7	5014.35	2.5	2.70	4	7	21.1	
10	5015.0	15.5	5015.25	1.5	2.70	4	7	20.1	
11	5016.0	16.7	5016.35	1.8	2.79	8	7	19.1	
12	5017.0	17.6	5017.3	0.9	2.71	4	7	18.1	
13	5018.3	19.0	5018.65	1.1	2.71	4	7	16.8	
14	5019.0	19.5	5019.25	2.2	2.71	4	7	16.1	
15	5020.3	21.0	5020.65	9.2	2.74	9	7	14.8	
16	5021.5	22.0	5021.75	7.4	2.78	7	7	13.6	
17	5022.4	23.0	5022.7	5.7	2.75	11	7	12.7	
18	5023.3	24.0	5023.65	6.2	2.82	6	10	11.8	
19	5024.4	25.0	5024.7	7.4	2.80	6	10	10.7	
20	5025.0	25.4	5025.2	4.1	2.79	7	15	10.1	
21	5026.0	26.6	5026.3	5.4	2.82	7	10	9.1	
22	5027.3	28.0	5027.65	12.7	2.82	6	10	7.8	
23	5028.2	28.6	5028.4	8.8	2.84	5	10	6.9	
24	5029.2	29.5	5029.35	6.6	2.83	5	3	5.9	
25	5030.3	30.5	5030.4	8.6	2.83	5	10	4.8	
26	5031.8	32.0	5031.9	5.8	2.84	7	10	3.3	
27	5032.2	32.7	5032.45	8.9	2.78	7	12	2.9	
28	5033.0	33.5	5033.25	9.0	2.74	10	12	2.1	
29	5034.1	34.5	5034.3	2.9	2.72	4	3	1.0	
30	5035.3	36.0	5035.65	3.9	2.87	7	1	-0.2	Sylvan
Strat Position is footage above or below (-) the Hunton/Sylvan contact at 5035.1, core depth									

Table 7-29: Danny 2-34 Porosity and Facies Codes

Marjo Danny 2-34 Porosity and Facies codes									
Core #	From	To	Mid-Depth Core Depth	Phi CORE PHI	Grain Density	Pore Code	Facies Code	strat position	Thin Section
1	4930.2	to	30.9	4930.55	4.1	2.73	9	7	54.1
2	4931.2	to	31.5	4931.35	2.4	2.72	4	7	53.1
3	4932	to	32.6	4932.3	1.5	2.72	4	7	52.3
4	4933.3	to	34	4933.65	1.8	2.71	4	7	51
5	4934	to	34.2	4934.1	1.7	2.72	4	7	50.3
6	4935	to	35.2	4935.1	1.7	2.71	3	7	49.3
7	4936	to	36.2	4936.1	3.3	2.72	1	7	48.3
8	4937	to	37.6	4937.3	2.7	2.72	1	7	47.3
9	4938	to	38.6	4938.3	1.1	2.71	1	7	46.3
10	4939.3	to	40	4939.65	6.1	2.73	9	7	45
11	4940.2	to	41	4940.6	5.2	2.73	9	7	44.1
12	4941.2	to	42	4941.6	1.4	2.71	4	7	43.1
13	4942.5	to	43	4942.75	2	2.72	1	7	41.8
14	4943	to	43.5	4943.25	2.9	2.73	12	7	41.3
15	4944.3	to	45	4944.65	2.6	2.73	12	7	40
16	4945.3	to	46	4945.65	5.8	2.73	9	7	39
17	4946.2	to	46.9	4946.55	4.7	2.73	9	7	38.1
18	4947	to	47.4	4947.2	3.8	2.72	1	7	37.3
19	4948	to	48.4	4948.2	2.9	2.72	1	7	36.3
20	4949.3	to	50	4949.65	1.6	2.72	4	7	35
21	4950	to	50.7	4950.35	1.6	2.71	4	7	34.3
22	4951.3	to	52	4951.65	5.4	2.71	1	7	33
23	4952.3	to	53	4952.65	4.1	2.72	1	7	32
24	4953.3	to	53.7	4953.5	2.8	2.72	1	7	31
25	4954	to	54.7	4954.35	2.8	2.72	1	7	30.3
26	4955.3	to	56	4955.65	1	2.72	3	10	29
27	4956	to	56.6	4956.3	0.9	2.72	3	10	28.3
28	4957	to	57.6	4957.3	1.1	2.72	3	10	27.3
29	4958.3	to	59	4958.65	3	2.71	1	7	26
30	4959	to	59.7	4959.35	3.5	2.72	1	7	25.3
31	4960.6	to	61	4960.8	3.2	2.73	12	10	23.7
32	4961.3	to	62	4961.65	4.1	2.71	1	7	23
33	4962.1	to	62.7	4962.4	7	2.71	4	7	22.2
34	4963.3	to	64	4963.65	8.3	2.71	4	7	21
35	4964.3	to	65	4964.65	2.5	2.71	4	7	20
36	4965.1	to	65.8	4965.45	2.6	2.72	4	7	19.2
37	4966.4	to	67	4966.7	2.9	2.72	4	10	17.9
38	4967	to	67.7	4967.35	3	2.71	4	10	17.3
39	4968	to	68.6	4968.3	5.5	2.72	4	10	16.3
40	4969.1	to	69.9	4969.5	5.8	2.71	4	10	15.2
41	4970.3	to	71	4970.65	5.1	2.71	4	10	14
42	4971	to	71.4	4971.2	7.2	2.71	3	3	13.3
43	4972.3	to	73	4972.65	11.3	2.71	3	3	12
44	4973	to	73.7	4973.35	8.3	2.7	2	5	11.3
45	4974.2	to	74.9	4974.55	2.6	2.71	2	5	10.1
46	4975.3	to	76	4975.65	8.3	2.71	2	5	9
47	4976.3	to	77	4976.65	6.5	2.72	2	5	8
48	4977	to	77.4	4977.2	4.6	2.71	2	5	7.3
49	4978.3	to	79	4978.65	4.5	2.71	2	5	6
50	4979	to	79.7	4979.35	3.2	2.71	2	5	5.3
51	4980.3	to	81	4980.65	3.6	2.7	2	5	4
52	4981.3	to	82	4981.65	3.1	2.7	2	5	3
53	4982.3	to	83	4982.65	1.5	2.71	2	5	2
54	4983.3	to	84	4983.65	2.3	2.71	2	5	1
55	4984.3	to	85.8	4985.05	4	2.91	7	1	0
56	4985.8	4990						13	-1.5

Strat Position is footage above or below (-) the Hunton/Sylvan contact at 4984.3 ft., core depth.

Table 7-30: Henry 1-3 Porosity and Facies Codes

Henry 1-3 Porosity and Facies codes											
Core #	From	To	Mid-Depth Core Depth	Phi CORE PHI	Grain Density	Pore Code	Facies Code	strat position	Thin Section		
1	4966.4	to	4966.9	4966.65	3	2.71	1	7	38.1		
2	4967.1	to	4967.9	4967.5	2.6	2.72	4	7	37.4		
3	4968.4	to	4969.0	4968.7	3.3	2.71	1	7	36.1		
4	4969.3	to	4969.8	4969.55	1.1	2.72	4	7	35.2		
5	4970.4	to	4971.0	4970.7	3.9	2.72	1	7	34.1		
6	4971.0	to	4971.8	4971.4	2.8	2.72	4	7	33.5		
7	4972.7			4972.7	3.4	2.71	4	7	31.8		
8	4973.1	to	4973.8	4973.45	3.2	2.71	4	7	31.4		
9	4974.7	to	4975.0	4974.85	2.2	2.72	1	7	29.8		
10	4975.0	to	4975.8	4975.4	3.6	2.71	1	7	29.5		
11	4976.1	to	4976.8	4976.45	5.9	2.72	1	7	28.4		
12	4977.2	to	4978.0	4977.6	3.2	2.72	1	7	27.3		
13	4978.3	to	4979.0	4978.65	1.8	2.72	3	7	26.2		
14	4979.3	to	4980.0	4979.65	2.8	2.72	1	7	25.2		
15	4980.3	to	4981.0	4980.65	3.6	2.72	1	7	24.2		
16	4981.4	to	4981.6	4981.5	2.8	2.71	1	7	23.1		
17	4982.3	to	4983.0	4982.65	3.5	2.72	1	7	22.2		
18	4983.3	to	4984.0	4983.65	1.2	2.71	4	7	21.2		
19	4984.3	to	4985.0	4984.65	0.9	2.72	3	7	20.2		
20	4985.2	to	4986.0	4985.6	1.4	2.71	3	7	19.3		
21	4986.8	to	4987.0	4986.9	0.7	2.72	4	7	17.7		
22	4987.0	to	4987.7	4987.35	1.1	2.71	3	7	17.5		
23	4988.0	to	4988.7	4988.35	1.3	2.72	3	7	16.5		
24	4989.3	to	4990.0	4989.65	1	2.72	3	7	15.2		
25	4990.2	to	4991.0	4990.6	3.1	2.72	3	7	14.3	leached f grmstn matrix, c br coq	
26	4991.0	to	4991.7	4991.35	6.5	2.72	3	7	13.5	aa	
27	4992.3	to	4993.0	4992.65	6.2	2.73	1	7	12.2		
28	4993.0	to	4993.7	4993.35	7.8	2.77	9	7	11.5	dolomitic lst, good IX + vugs	
29	4994.3	to	4994.9	4994.6	6.4	2.83	10	7	10.2		
30	4995.0	to	4995.3	4995.15	10.2	2.8	6	12	9.5	fine gr grmstn, doltzd	
31	4996.2			4996.2	7.3	2.84	6	12	8.3		
	4996.6		Base of core						7.9		
			Base of Hunton, contact with Sylvan, is at 4997 log depth, which = 5004.5 Core Depth								
			Strat Position is footage above or below (-) the Hunton/Sylvan contact at 5004.5 ft., core depth.								

Table 7-31: Joe Givens #1-15 Porosity and Facies Codes

Marjo Joe Givens #1-15 Porosity and Facies codes											
Core #	From	To	Mid-Depth Core Depth	Phi CORE PHI	Grain Density	Pore Code	Facies Code	strat position	Thin Section		
	5013										
	5014.6										
	5017.2					3					
	5017.8					1		26.2	top of hunton		
1	5018.4	to	19	5018.7	5.7	2.71	1	3	25.6		
2	5019.5	to	20	5019.75	2.5	2.72	1	1	24.5		
3*	5020.3			5020.3	1.6	2.72	4	1	23.7		
4	5021.4	to	22	5021.7	2.8	2.7	4	1	22.6		
5	5022.4	to	23	5022.7	1.9	2.7	4	4	21.6		
6	5023.3	to	23.7	5023.5	1.7	2.72	4	4	20.7		
7	5024.6	to	25	5024.8	1.1	2.71	4	4	19.4		
8	5025.6	to	26	5025.8	1.2	2.7	4	4	18.4		
9	5026	to	26.5	5026.25	1	2.7	4	4	18		
10*	5027.7			5027.7	1.4	2.71	4	4	16.3		
11	5028.3	to	29	5028.65	0.8	2.71	4	4	15.7		
12	5029.3	to	30	5029.65	0.6	2.71	4	4	14.7		
13	5030.4	to	31	5030.7	1.9	2.71	4	4	13.6		
14	5031	to	31.7	5031.35	1.6	2.7	4	4	13		
15	5032.3	to	33	5032.65	1.7	2.71	4	4	11.7		
16	5033.3	to	34	5033.65	2.9	2.7	4	4	10.7		
17	5034	to	34.6	5034.3	2.2	2.71	4	4	10		
18	5035.3	to	36	5035.65	2.9	2.7	4	4	8.7		
19	5036.4	to	36.7	5036.55	3.7	2.71	4	4	7.6		
20	5037.3	to	38	5037.65	2.2	2.71	4	4	6.7		
21	5038.3	to	39	5038.65	1.9	2.7	4	4	5.7		
22	5039	to	39.7	5039.35	1.4	2.71	4	4	5		
23	5040.3	to	41	5040.65	0.8	2.71	3	4	3.7		
24	5041.6	to	42	5041.8	1.3	2.7	3	4	2.4		
25	5042.2	to	43	5042.6	1.3	2.71	2	3	1.8		
26*	5043.7			5043.7	2.2	2.72	2	3	0.3		
	5044		46	5045			7	2	0		
	5046		47.2	5046.6				2	-2		
	5047.2							7	-3.2		
			Strat Position is footage above or below (-) the Hunton/Sylvan contact at 5044 ft., core depth.								

Table 7-32: Mary Marie Porosity and Facies Codes

Marjo Mary Marie Porosity and Facies codes									
Core #	From	To	Mid-Depth Core Depth	Phi CORE PHI	Grain Density	Pore Code	Facies Code	strat position	Thin Section
1	4960						13	43.5	
2	4960.7						14	42.8	
3	4961						6	42.5	
4	4961.5	to	61.8	4961.65	1.7	2.71	2	6	42
5	4962	to	62.7	4962.35	1	2.7	2	6	41.5
6	4963.1	to	63.9	4963.5	0.8	2.71	2	6	40.4
7	4964.3	to	64.9	4964.6	1	2.7	2	6	39.2
8	4965.2	to	65.6	4965.4	1.6	2.7	2	7	38.3
9	4965.7	to	66	4965.85	6.1	2.71	2	7	37.8
10	4966	to	66.3	4966.15	6.2	2.7	2	7	37.5
11	4966.6	to	67	4966.8	4.5	2.71	2	7	36.9
12	4967	to	67.4	4967.2	7.3	2.69	2	7	36.5
13	4968.2	to	69	4968.6	8.1	2.69	1	7	35.3
14	4969	to	69.3	4969.15	7.3	2.7	2	7	34.5
15	4970	to	70.4	4970.2	5.8	2.69	1	7	33.5
16	4971.2	to	71.9	4971.55	2.8	2.7	1	7	32.3
17	4972.2	to	73	4972.6	1.9	2.71	2	7	31.3
18	4973	to	73.4	4973.2	1.2	2.7	2	7	30.5
19	4973.6	to	74	4973.8	4.6	2.72	1	7	29.9
20	4974.3	to	75	4974.65	2.9	2.72	4	7	29.2
21	4975.3	to	75.6	4975.45	0.9	2.7	3	7	28.2
22	4976.3	to	77	4976.65	0.8	2.71	3	7	27.2
23	4977	to	77.7	4977.35	0.9	2.71	3	7	26.5
24	4978.2	to	79	4978.6	0.8	2.72	3	7	25.3
25	4979.2	to	79.7	4979.45	1.7	2.71	4	7	24.3
26	4980	to	80.6	4980.3	1	2.71	3	7	23.5
27	4981	to	81.7	4981.35	2	2.71	3	7	22.5
28	4982.2	to	83	4982.6	1.1	2.71	3	7	21.3
29	4983	to	83.7	4983.35	2.2	2.72	3	7	20.5
30	4984.4	to	84.8	4984.6	5.7	2.7	1	7	19.1
31	4985.3	to	85.8	4985.55	3.2	2.71	1	7	18.2
32	4986	to	86.5	4986.25	5	2.7	3	7	17.5
33	4987.4	to	87.8	4987.6	4.5	2.71	1	7	16.1
34	4988.3	to	88.8	4988.55	2.3	2.71	3	7	15.2
35	4989.1	to	89.8	4989.45	0.6	2.7	3	7	14.4
36	4990.5	to	91	4990.75	0.5	2.7	3	7	13
37	4991.2	to	92	4991.6	0.8	2.69	3	7	12.3
38	4992.2	to	93	4992.6	0.8	2.71	3	7	11.3
39	4993.3	to	94	4993.65	1.3	2.7	3	7	10.2
40	4994.3	to	95	4994.65	1.2	2.71	3	6	9.2
41	4995.2	to	95.6	4995.4	0.7	2.7	3	6	8.3
42	4996.2	to	97	4996.6	0.7	2.71	3	6	7.3
43	4997.2	to	98	4997.6	1.1	2.71	3	6	6.3
44	4998.2	to	98.5	4998.35	0.8	2.7	3	6	5.3
45	4999	to	99.7	4999.35	0.8	2.71	3	6	4.5
46	5000.2	to	0.8	5000.5	0.9	2.72	3	6	3.3
Plug 1		5001.2		5001.2	2.6	2.7	2	6	2.3
Plug 2		5001.8		5001.8	6.01	2.68	2	6	1.7
47	5002	to	2.6	5002.3	5.3	2.71	2	6	1.5
48	5003.4	to	3.4	5003.4	0.6	2.71	2	6	0.1
49	5003.5	to	5006				7	1	0
50	5006		5016					13	-2.5

Strat Position is footage above or below (-) the Hunton/Sylvan contact at 5003.5 ft., core depth.

Table 7-33: McBride South 1-10 Porosity and Facies Codes

Marjo McBride South 1-10 Porosity and Facies codes										
Core #	From	To	Mid-Depth	Phi	Grain Density	Pore Code	Facies Code	strat position	Thin Section	
			Core Depth	CORE PHI						
1	4962.6	to	63	4962.8	6.5	2.74	9	7	33.7	
2	4963.3	to	64	4963.65	6.5	2.76	9	7	33	
3	4964	to	64.7	4964.35	4.7	2.78	9	7	32.3	
4	4965.3	to	66	4965.65	1.5	2.72	2	7	31	
5	4966.4	to	67	4966.7	4.4	2.73	9	7	29.9	
6	4967	to	67.7	4967.35	4.4	2.8	7	7	29.3	
7	4968	to	68.7	4968.35	1.6	2.72	3	7	28.3	
8	4969	to	69.7	4969.35	2.6	2.72	3	7	27.3	
9	4970.2	to	71	4970.6	7.8	2.83	5	7	26.1	
10	4971.3	to	71.9	4971.6	2.3	2.75	11	7	25	
11	4972.7	to	73	4972.85	1.5	2.71	3	7	23.6	
12	4973	to	73.8	4973.4	1.6	2.72	3	7	23.3	
13	4974	to	74.7	4974.35	1.5	2.72	3	7	22.3	
14	4975.3	to	76	4975.65	2.9	2.71	1	7	21	
15	4976	to	76.7	4976.35	1	2.72	3	7	20.3	
16	4977	to	77.6	4977.3	2	2.71	1	7	19.3	
17	4978	to	78.6	4978.3	2.6	2.71	3	7	18.3	
18	4979.3	to	79.9	4979.6	1.8	2.72	3	7	17	
19	4980	to	80.6	4980.3	1.5	2.71	4	7	16.3	
20	4981.3	to	82	4981.65	1.2	2.72	3	7	15	
21	4982.6	to	83	4982.8	1.9	2.72	1	7	13.7	
22	4983.6	to	84	4983.8	0.6	2.71	3	6	12.7	
23	4984	to	84.7	4984.35	2.4	2.72	1	6	12.3	
24	4985	to	85.4	4985.2	2.8	2.72	1	6	11.3	
25	4986	to	86.6	4986.3	0.9	2.72	3	6	10.3	
26	4987	to	87.7	4987.35	1.6	2.71	3	6	9.3	
27	4988	to	88.7	4988.35	3.4	2.72	1	6	8.3	
28	4989.4	to	90	4989.7	2.4	2.72	3	6	6.9	
29	4990.3	to	91	4990.65	1.4	2.73	12	3	6	
30	4991	to	91.5	4991.25	1.6	2.71	4	3	5.3	
31	4992	to	92.7	4992.35	4.2	2.72	3	3	4.3	
32	4993.6	to	94	4993.8	4.1	2.72	3	6	2.7	
33	4994.3	to	95	4994.65	4.3	2.72	3	6	2	
34	4995	to	95.6	4995.3	4.8	2.72	3	6	1.3	
35	4996.3	to	96.7	4996.5	6.2	2.91	7	1	0	
36	4997.4	to	98	4997.7	5.4	2.86	7	1	-1.1	

Strat Position is footage above or below (-) the Hunton/Sylvan contact at 4996.3 ft., core depth.

Table 7-34: Marjo Toles 1-10 Porosity and Facies Codes

Marjo Toles 1-10 Porosity and Facies codes										
Core #	From	To	Mid-Depth	Phi	Grain Density	Pore Code	Facies Code	strat position	Thin Section	
			Core Depth	CORE PHI						
1	4964.4	to	65	4964.7	3.1	2.71	1	7	39.3	* 4964.2 c bracc pkstn, vugs are matrix dissolved -SV
2	4965	to	65.6	4965.3	2.1	2.71	1	6	38.7	
3	4966	to	66.6	4966.3	1.8	2.71	1	7	37.7	* 4967.8 c bracc pkstn, TV with frac
4	4967	to	67.8	4967.4	2.3	2.71	1	7	36.7	
5	4968	to	68.8	4968.4	4.4	2.71	1	6	35.7	
6	4969.2	to	69.8	4969.5	1.8	2.71	3	6	34.5	
7	4970.3	to	71	4970.65	2.4	2.72	1	7	33.4	
8	4971.5	to	72	4971.75	2.6	2.71	1	7	32.2	* 4971.4 c collapsed grnstr
9	4972.3	to	73	4972.65	3.5	2.71	4	6	31.4	
10	4973.3	to	74	4973.65	2.5	2.71	4	6	30.4	
11	4974.3	to	75	4974.65	3.3	2.7	4	6	29.4	
12**	4975.5	to	76	4975.75	4.5	2.71	4	5	28.2	
13**	4976.3	to	76.9	4976.6	3.5	2.71	4	5	27.4	
14	4977.3	to	78	4977.65	3.1	2.7	3	4	26.4	
15	4978.1	to	78.8	4978.45	3.7	2.7	4	5	25.6	
16	4979.2	to	80	4979.6	2.7	2.7	3	4	24.5	
17	4980	to	80.7	4980.35	1.6	2.7	3	4	23.7	
18	4981	to	81.5	4981.25	2.2	2.7	3	4	22.7	
19	4982	to	82.8	4982.4	2.1	2.7	3	4	21.7	
20	4983	to	83.4	4983.2	5	2.71	2	7	20.7	
21**	4984	to	84.8	4984.4	4.2	2.7	2	5	19.7	
22**	4985.5	to	86	4985.75	5.2	2.7	3	4	18.2	
23**	4986	to	86.5	4986.25	3.4	2.7	3	4	17.7	
24**	4987	to	87.7	4987.35	6.1	2.71	2	7	16.7	
25**	4988	to	88.8	4988.4	4.9	2.71	2	7	15.7	
26**	4989.2	to	90	4989.6	7	2.7	2	7	14.5	
27	4990.3	to	91	4990.65	6.7	2.71	4	9	13.4	
28	4991.3	to	91.9	4991.6	2	2.7	4	9	12.4	* 4991.1 bracc-co-cri grnstr
29	4992	to	92.4	4992.2	2	2.72	4	5	11.7	frac with karst infill
30	4993	to	93.3	4993.15	1.8	2.71	4	5	10.7	
31	4994.6	to	95	4994.8	2.9	2.71	4	5	9.1	
32	4995.3	to	95.8	4995.55	2.5	2.71	1	5	8.4	* 4995.9 cri bracc co strom grnstr, vugs
33+	4996.1	to	*	4996.1	2.3	2.7	2	5	7.6	4996.6
34	4997	to	97.5	4997.25	1	2.71	4	4	6.7	* 4996.9 - 97 cri (bracc) grnstr, tight
35	4998.5	to	99	4998.75	1.6	2.7	4	5	5.2	
36	4999.3	to	100	4999.65	2.2	2.71	1	5	4.4	
37	5000	to	0.5	5000.25	2.6	2.71	4	5	3.7	
38	5001	to	1.8	5001.4	2.1	2.71	2	5	2.7	Ls c cri
39	5002.2	to	2.8	5002.5	5.9	2.86	5	4	1.5	Dol, f cri grnstr with sparse big bracc
40	5003	to	3.4	5003.2	3.8	2.87	5	1	0.7	* 5003.7 Dol, calcite IX
41	5004.1	to	4.3	5004.2	3	2.79	11	1	-0.4	"Sh", Dol, argill mdstr

Strat Position is footage above or below (-) the Hunton/Sylvan contact at 5003.7 ft., core depth.

Table 7-35: Marjo Wilkerson 1-3 Porosity and Facies Codes

Marjo Wilkerson 1-3 Porosity and Facies codes									
Core #	From	To	Mid-Depth	Phi	Grain Density	Pore Code	Facies Code	strat position	Thin Section
			Core Depth	CORE PHI					
1	4950							13	49.8
2	4952.4							14	47.4
3	4952.7	to	53.3	4953	2.1	2.64		13	47.1
4	4953.4			4953.4				7	46.4
5	4953.6	to	54	4953.8	5.8	2.71	2	7	46.2
6	4954.5	to	55	4954.75	5.9	2.71	1	7	45.3
7	4955	to	55.7	4955.35	5.9	2.71	1	7	44.8
8	4956.5	to	57	4956.75	6.7	2.71	1	7	43.3
9	4957.3	to	57.3	4957.3	5.5	2.71	1	7	42.5
10	4958.6	to	59	4958.8	3.2	2.71	1	7	41.2
11	4959	to	59.4	4959.2	3.1	2.71	1	7	40.8
12	4960	to	60.5	4960.25	4.4	2.71	1	7	39.8
13	4961.1	to	61.7	4961.4	5.4	2.7	1	7	38.7
14	4962	to	62.4	4962.2	3.8	2.71	1	7	37.8
15	4963.1	to	63.8	4963.45	2.6	2.69	2	7	36.7
16	4964.2	to	64.6	4964.4	3.9	2.69	2	7	35.6
17	4965.4	to	66	4965.7	4.3	2.71	1	7	34.4
18	4966.5	to	66.9	4966.7	3.5	2.7	2	7	33.3
19	4967.1	to	67.9	4967.5	1.8	2.71	2	7	32.7
20	4968	to	68.5	4968.25	1	2.72	2	7	31.8
21	4969.1	to	69.7	4969.4	2.2	2.71	2	7	30.7
22	4970.1	to	70.7	4970.4	1.3	2.72	1	7	29.7
23	4971.1	to	71.7	4971.4	0.9	2.72	2	7	28.7
24	4972.1	to	72.8	4972.45	1.1	2.72	2	7	27.7
25	4973.4	to	74	4973.7	5	2.71	2	7	26.4
26	4974	to	74.5	4974.25	9.7	2.7	1	7	25.8
27	4975	to	75.2	4975.1	10.4	2.7	1	7	24.8
28	4976.1	to	76.8	4976.45	1.3	2.71	2	7	23.7
29	4977.1	to	77.8	4977.45	1.7	2.72	2	7	22.7
30	4978	to	78.6	4978.3	1.4	2.71	2	6	21.8
31	4979	to	79.5	4979.25	1.1	2.72	3	6	20.8
32	4980.1	to	80.7	4980.4	1.2	2.71	3	6	19.7
33	4981.1	to	81.6	4981.35	1.4	2.71	3	6	18.7
34	4982.3	to	82.9	4982.6	3.1	2.71	3	6	17.5
35	4983.3	to	83.9	4983.6	3.4	2.71	2	4	16.5
36	4984.1	to	84.8	4984.45	2.5	2.71	2	4	15.7
37	4985.3	to	86	4985.65	2.2	2.72	2	7	14.5
38	4986.3	to	86.9	4986.6	1.5	2.71	2	5	13.5
39	4987.1	to	87.8	4987.45	1.2	2.71	2	5	12.7
40	4988	to	88.5	4988.25	1	2.71	2	4	11.8
41	4989.1	to	89.8	4989.45	2.3	2.71	2	4	10.7
42	4990.3	to	90.9	4990.6	1.8	2.71	2	5	9.5
43	4991.1	to	91.8	4991.45	4	2.71	2	5	8.7
44	4992.1	to	92.7	4992.4	3.2	2.71	2	5	7.7
45	4993.5	to	94	4993.75	1.9	2.71	2	5	6.3
46	4994.4	to	95	4994.7	1.6	2.71	2	5	5.4
47	4995.4	to	96	4995.7	6.6	2.7	2	6	4.4
48	4996	to	96.4	4996.2	8.4	2.69	2	6	3.8
49	4997.1	to	97.7	4997.4	6.1	2.71	2	6	2.7
50	4998.1	to	98.7	4998.4	7.9	2.78	11	3	1.7
51	4998.7	to	99.4	4999.05	11.2	2.81	6	3	1.1
52	4999.6	to	4999.8				7	12	0.2
53	4999.8	to	5004.2					1	0
Strat Position is footage above or below (-) the Hunton/Sylvan contact at 4999.8 ft., core depth.									

Table 7-36: Williams 1-3 Porosity and Facies Codes

Marjo Williams 1-3 Porosity and Facies codes									
Core #	From	To	Mid-Depth	Phi	Grain Density	Pore Code	Facies Code	Strat position	Thin Section
	4942.0	to	43.0	4942.5				41.7	
1	4943.5	to	44.0	4943.75	1.0	2.74	12	7	40.2
2	4944.3	to	44.8	4944.55	2.1	2.71	4	7	39.4
3	4945.3	to	45.7	4945.5	0.8	2.71	4	7	38.4
4	4946.3	to	47.0	4946.65	0.8	2.72	4	7	37.4
5	4947.2	to	48.0	4947.6	1.5	2.72	1	7	36.5
6	4948.3	to	49.0	4948.65	1.2	2.72	4	7	35.4
7	4949.2	to	50.0	4949.6	3.0	2.72	1	7	34.5
8	4950.0	to	50.4	4950.2	3.5	2.71	1	7	33.7
9	4951.0	to	51.8	4951.4	4.9	2.71	1	7	32.7
10	4952.0	to	52.6	4952.3	2.8	2.71	1	7	31.7
11	4953.3	to	54.0	4953.65	3.2	2.72	1	7	30.4
12	4954.0	to	54.8	4954.4	1.3	2.72	1	7	29.7
13	4955.2	to	56.0	4955.6	1.5	2.71	4	7	28.5
14	4956.2	to	57.0	4956.6	1.8	2.71	4	7	27.5
15	4957.1	to	57.8	4957.45	0.9	2.71	4	7	26.6
16	4958.2	to	59.0	4958.6	0.9	2.72	4	7	25.5
17	4959.3	to	60.0	4959.65	1.2	2.71	4	7	24.4
18	4960.0	to	60.8	4960.4	1.7	2.71	4	7	23.7
19	4961.2	to	62.0	4961.6	1.4	2.71	4	7	22.5
20	4962.3	to	63.0	4962.65	1.6	2.72	4	7	21.4
21	4963.0	to	63.7	4963.35	1.2	2.71	1	7	20.7
22	4964.2	to	65.0	4964.6	2.3	2.72	4	7	19.5
23	4965.2	to	66.0	4965.6	2.1	2.72	1	7	18.5
24	4966.0	to	66.5	4966.25	0.8	2.71	4	7	17.7
25	4967.2	to	68.0	4967.6	1.6	2.71	4	7	16.5
26	4968.3	to	69.0	4968.65	2.0	2.71	4	7	15.4
27	4969.2	to	70.0	4969.6	2.9	2.71	4	7	14.5
28	4970.1	to	70.8	4970.45	2.6	2.71	4	7	13.6
29	4971.2	to	71.9	4971.55	1.7	2.72	4	7	12.5
30	4972.0	to	72.6	4972.3	1.1	2.72	4	7	11.7
31	4973.2	to	73.8	4973.5	1.4	2.72	4	7	10.5
32	4974.0	to	74.5	4974.25	1.7	2.71	4	7	9.7
33	4975.0	to	76.7	4975.35	2.7	2.71	4	10	8.7
34	4976.0	to	76.4	4976.2	3.6	2.71	1	7	7.7
35	4977.0	to	77.7	4977.35	1.5	2.72	4	12	6.7
36	4978.2	to	79.0	4978.6	5.2	2.76	9	7	5.5
37	4979.6	to	80.0	4979.8	6.6	2.79	6	7	4.1
38	4980.5	to	81.0	4980.75	8.7	2.81	6	7	3.2
39	4981.3	to	82.0	4981.65	9.2	2.80	6	7	2.4
40	4982.0	to	82.5	4982.25	6.8	2.78	6	7	1.7
41	4983.0	to	83.4	4983.2	7.7	2.77	11	12	0.7
42	4984.3	to	84.7	4984.5	5.2	2.87	7	1	-0.6
42	4984.7	to	87.5	4986.1			7	1	-1.0
43	4987.5	to	91.0	4989.25				13	-3.8

Strat Position is footage above or below (-) the Hurton/Sylvan contact at 4983.7, core depth

7.1.11. Graphic Core Data and Well Log Plots of Individual Wells, with graphic plots of Porosity Types and Lithofacies Types on described cores

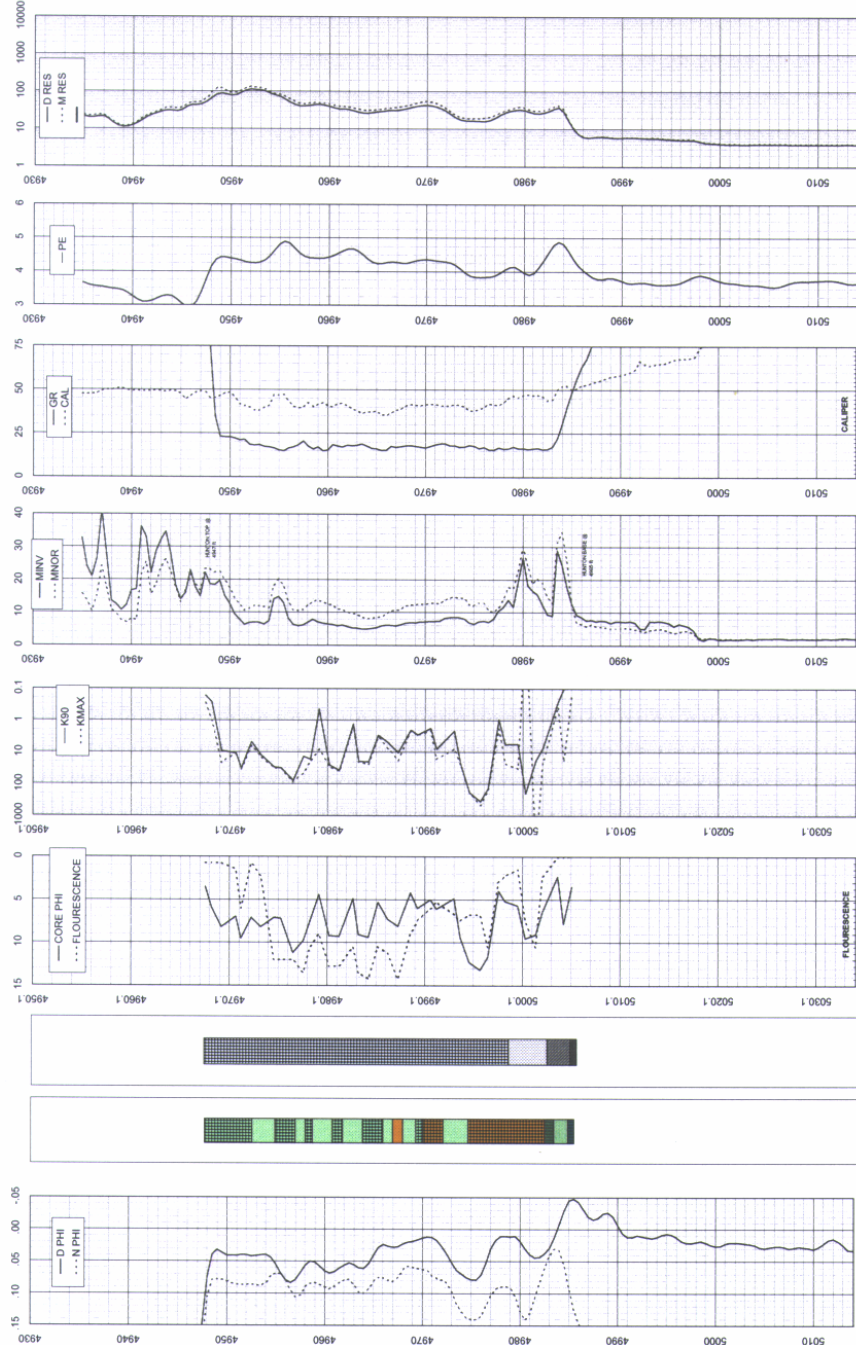


Figure 7-7: Marjo Anna well log plot

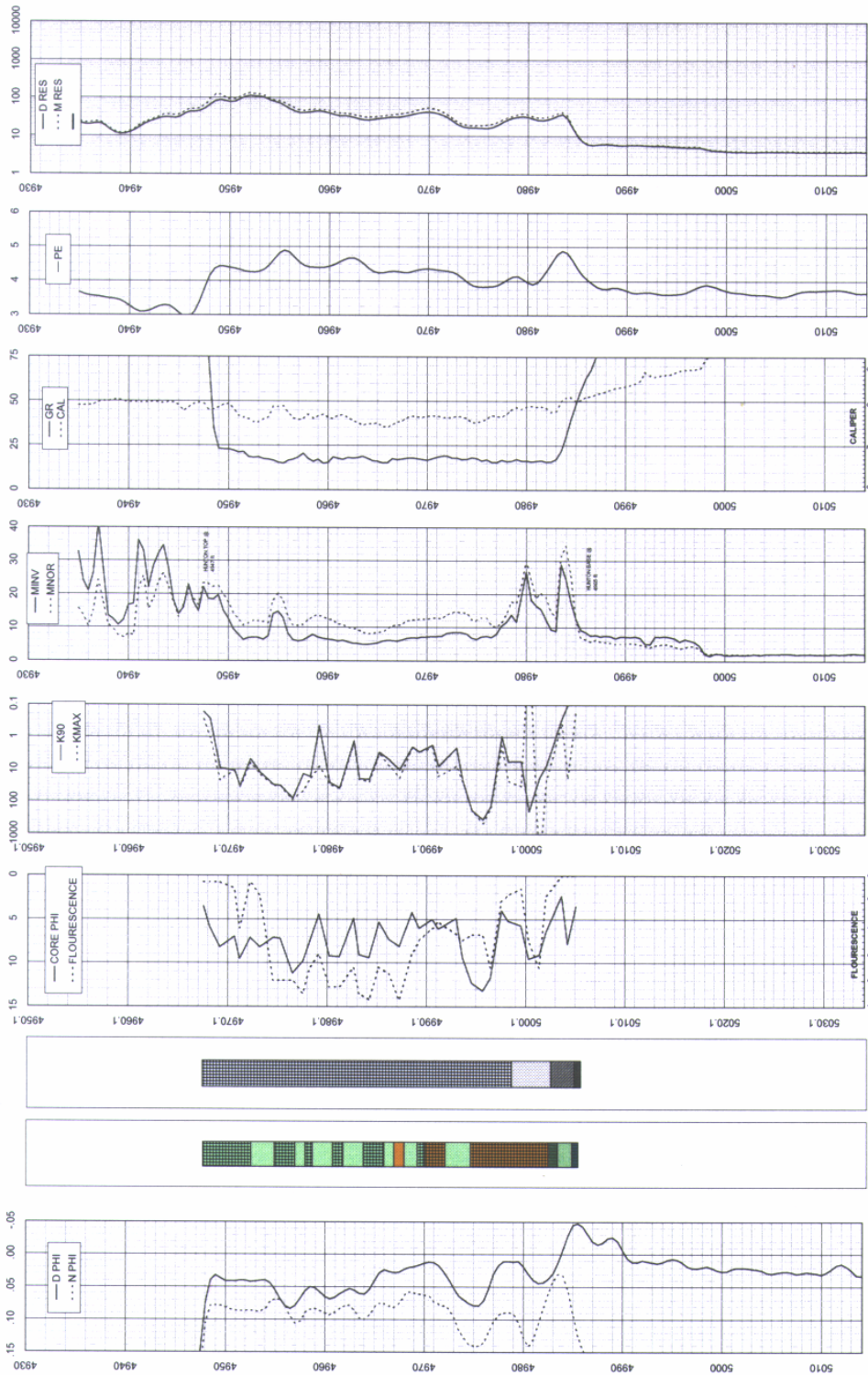


Figure 7-8: Bailey 2-6 well log plot

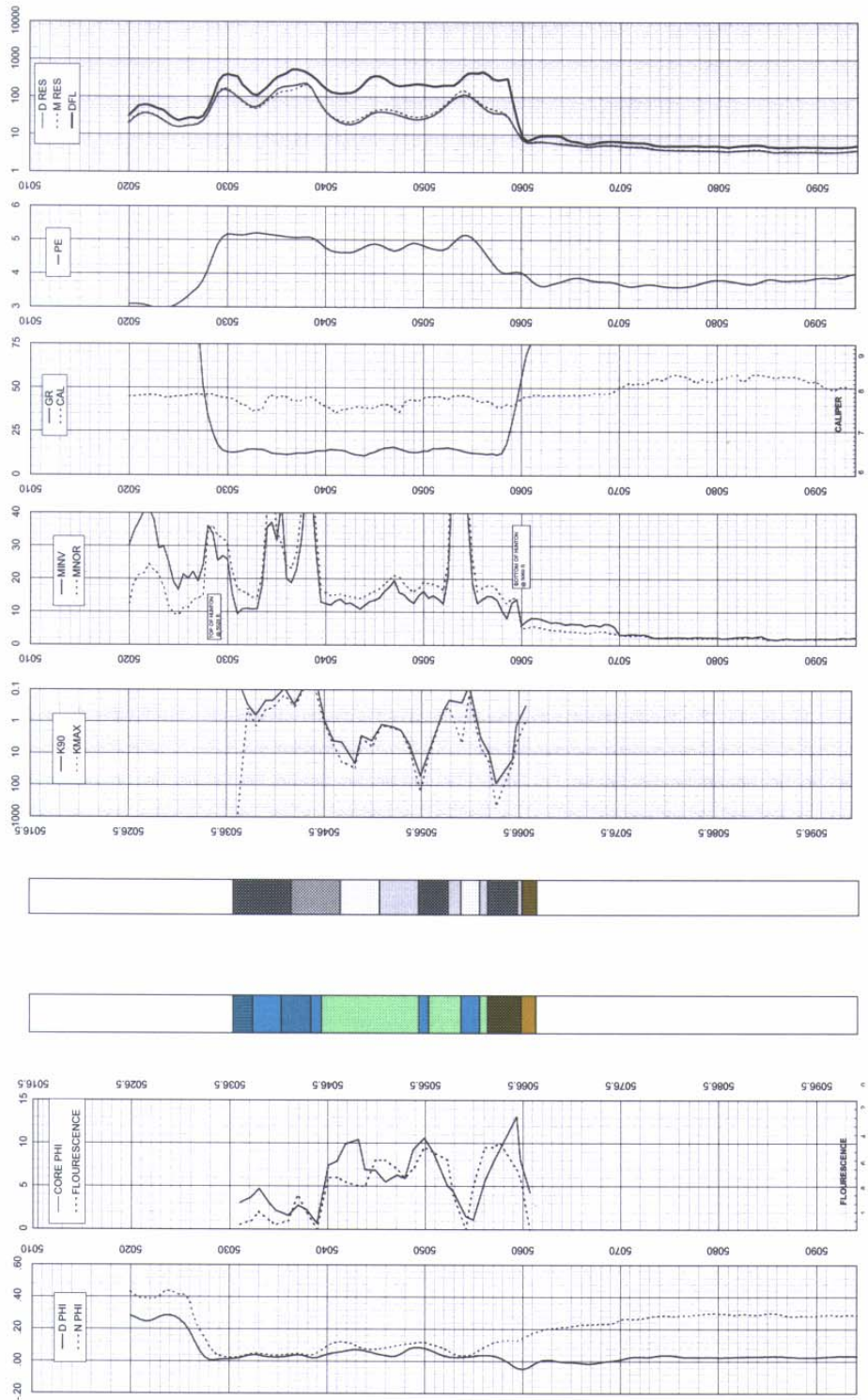


Figure 7-9: Marjo Boone 1-4 well log plot

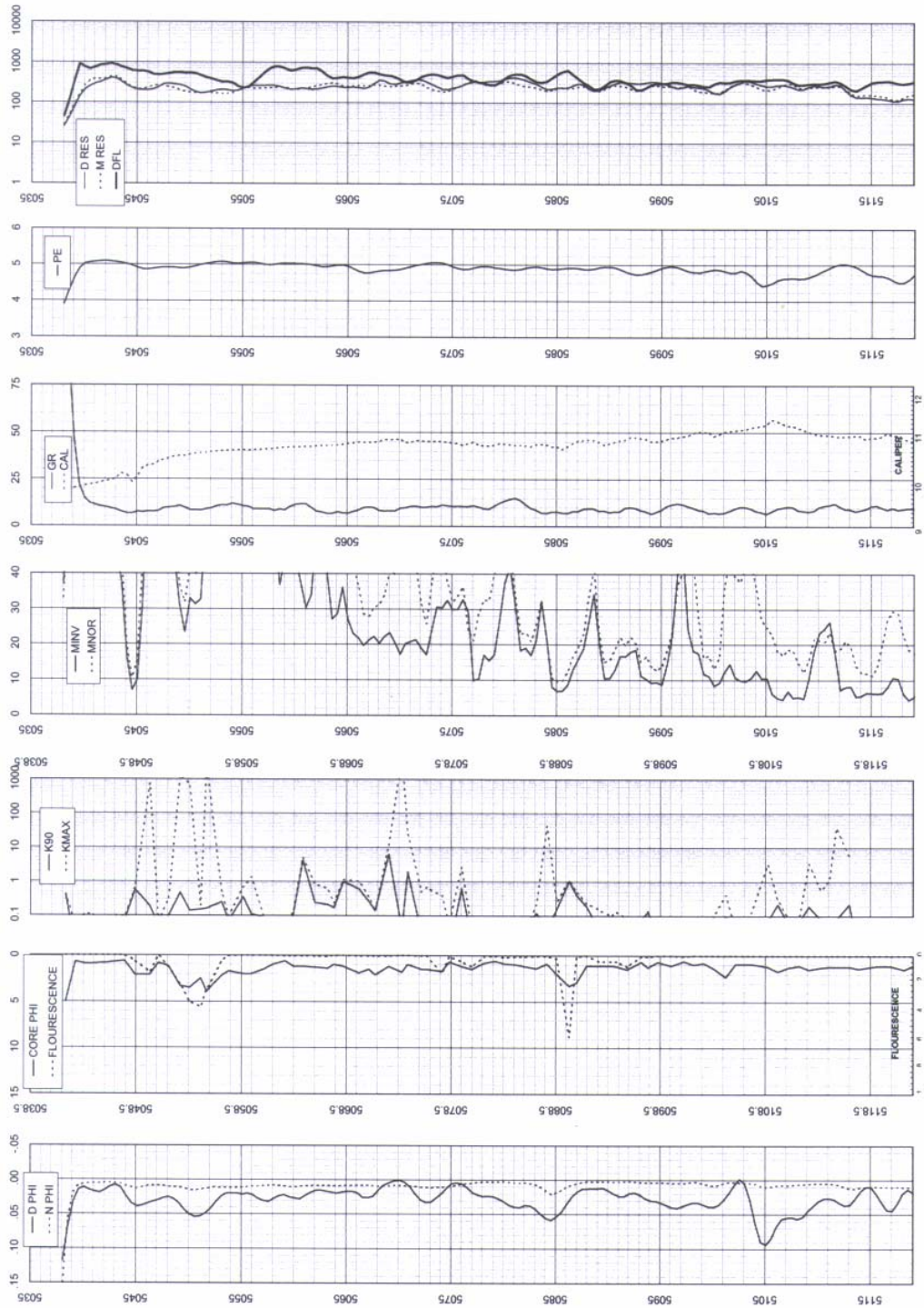


Figure 7-10: Marjo Carney Extension SWDW well log plot #1

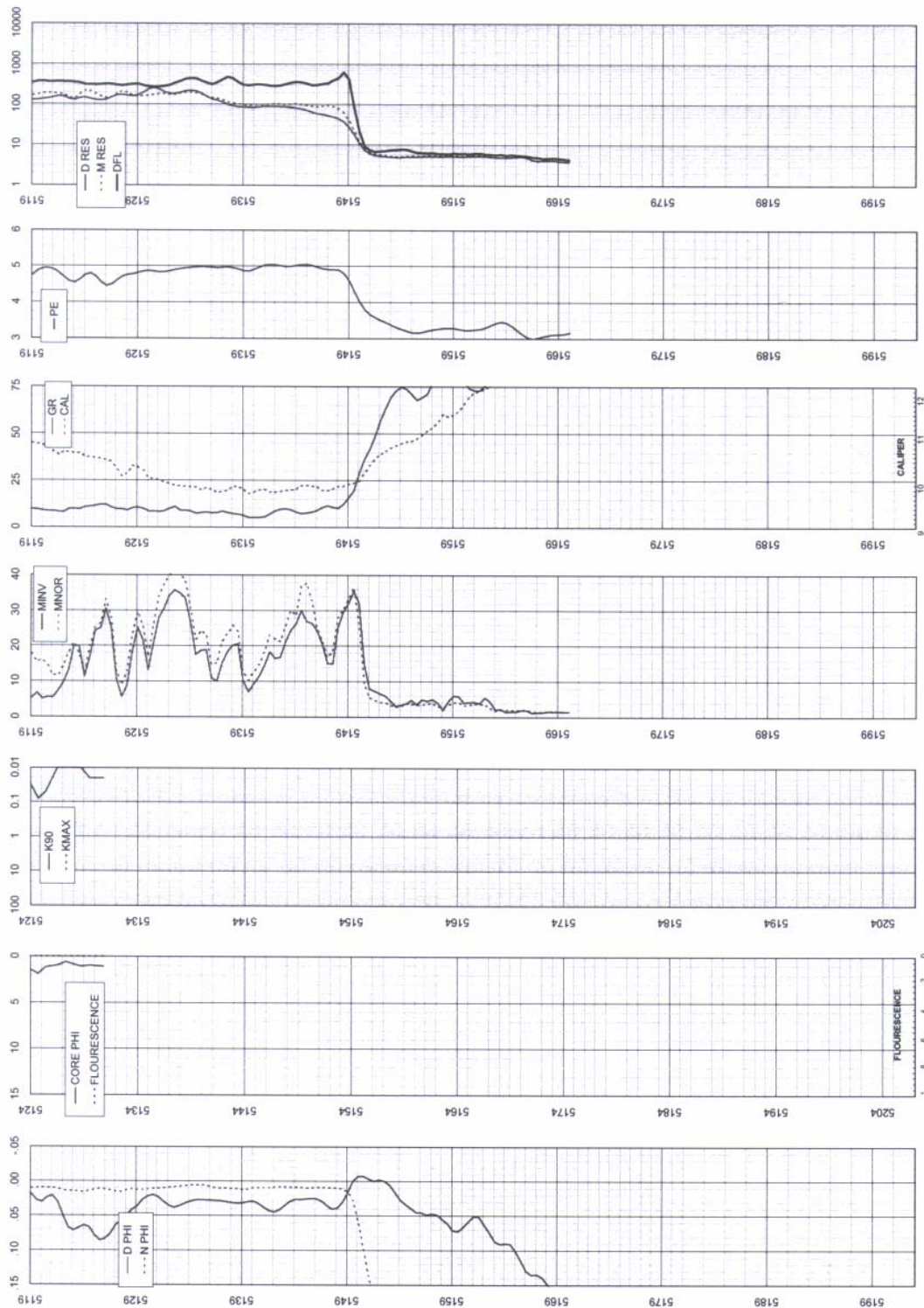


Figure 7-11: Marjo Carney Extension SWDW well log plot #2

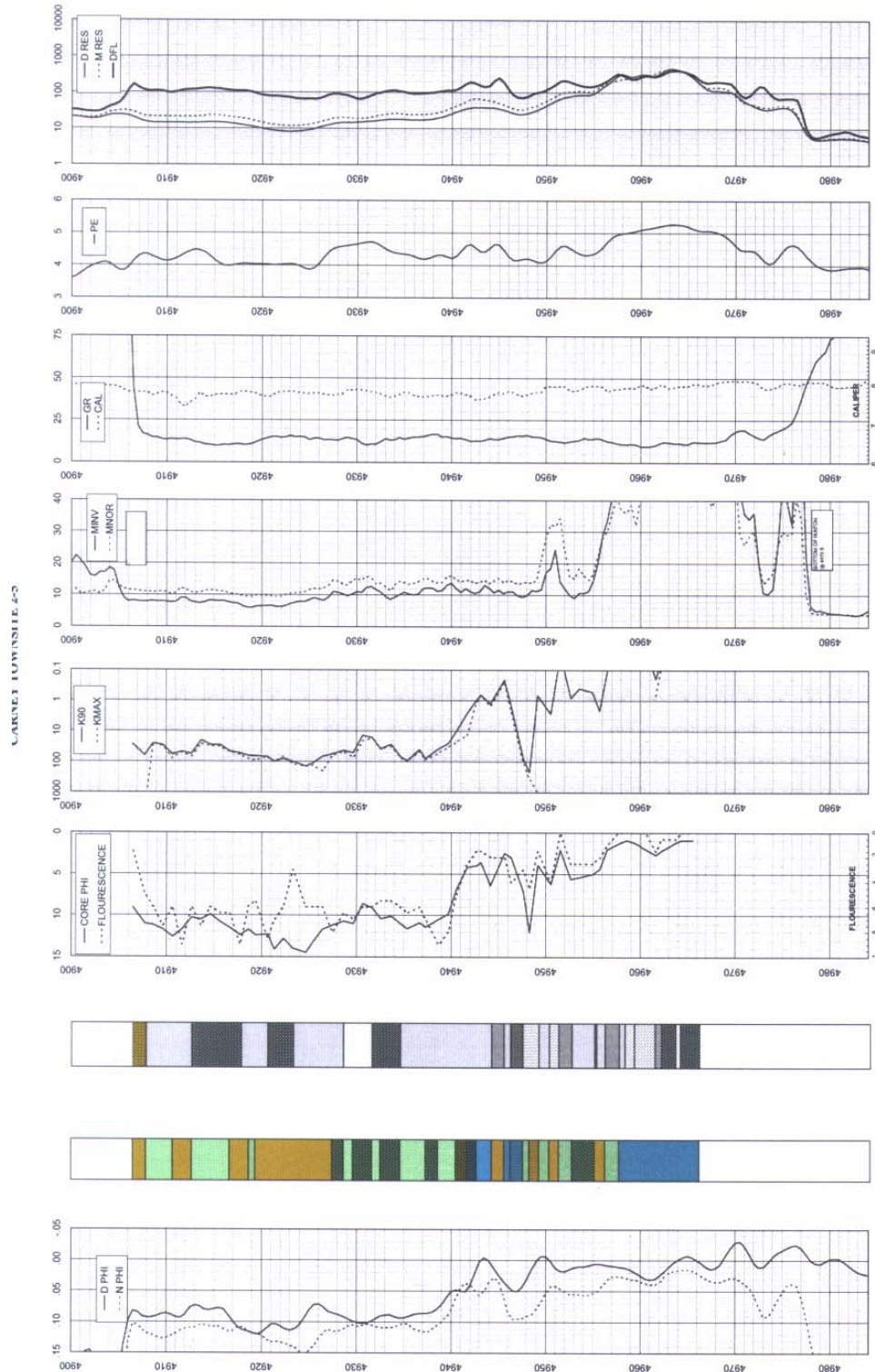


Figure 7-12: Marjo Carney Townsite 2-5 well log plot

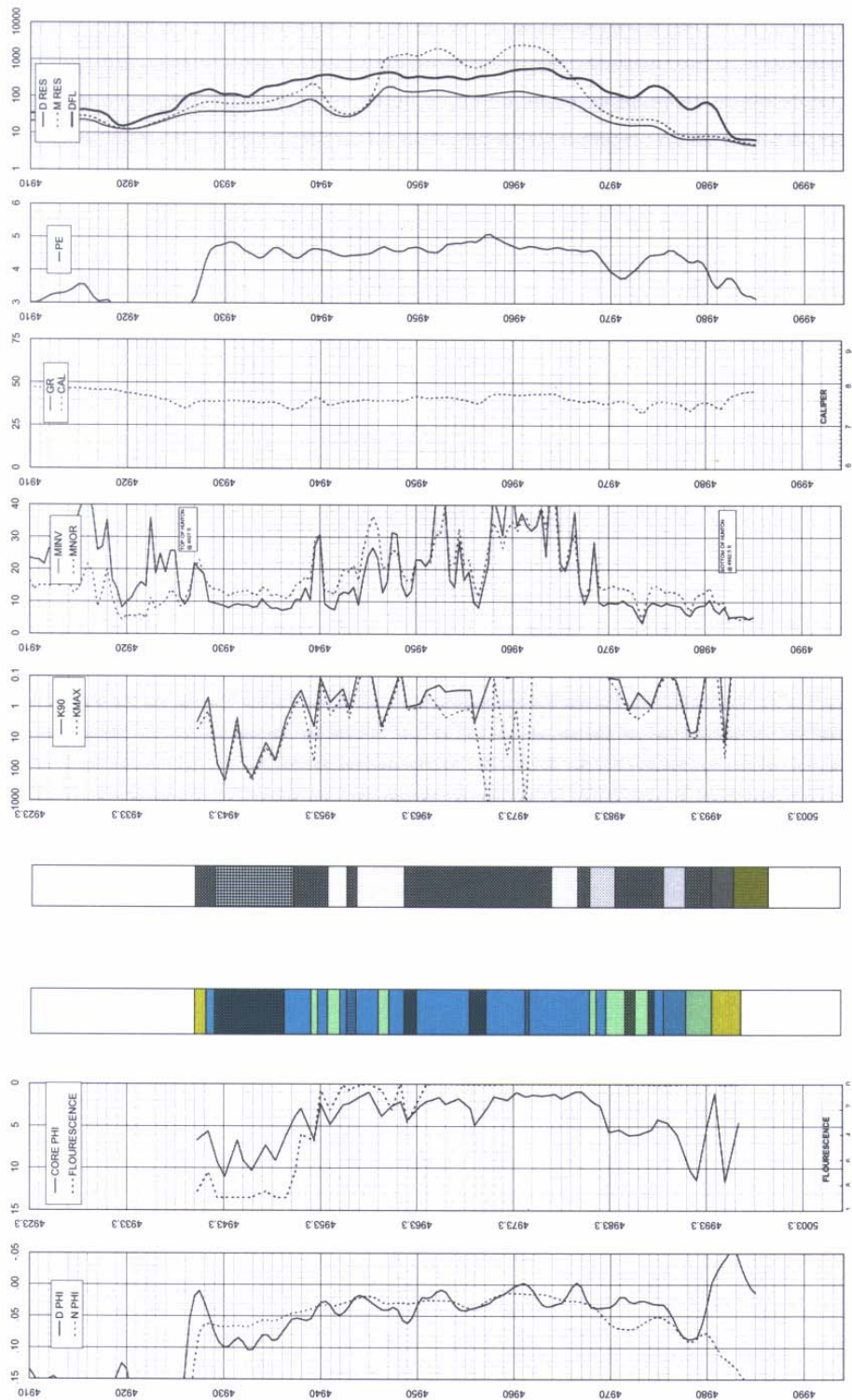


Figure 7-13: Marjo Carter well log plot

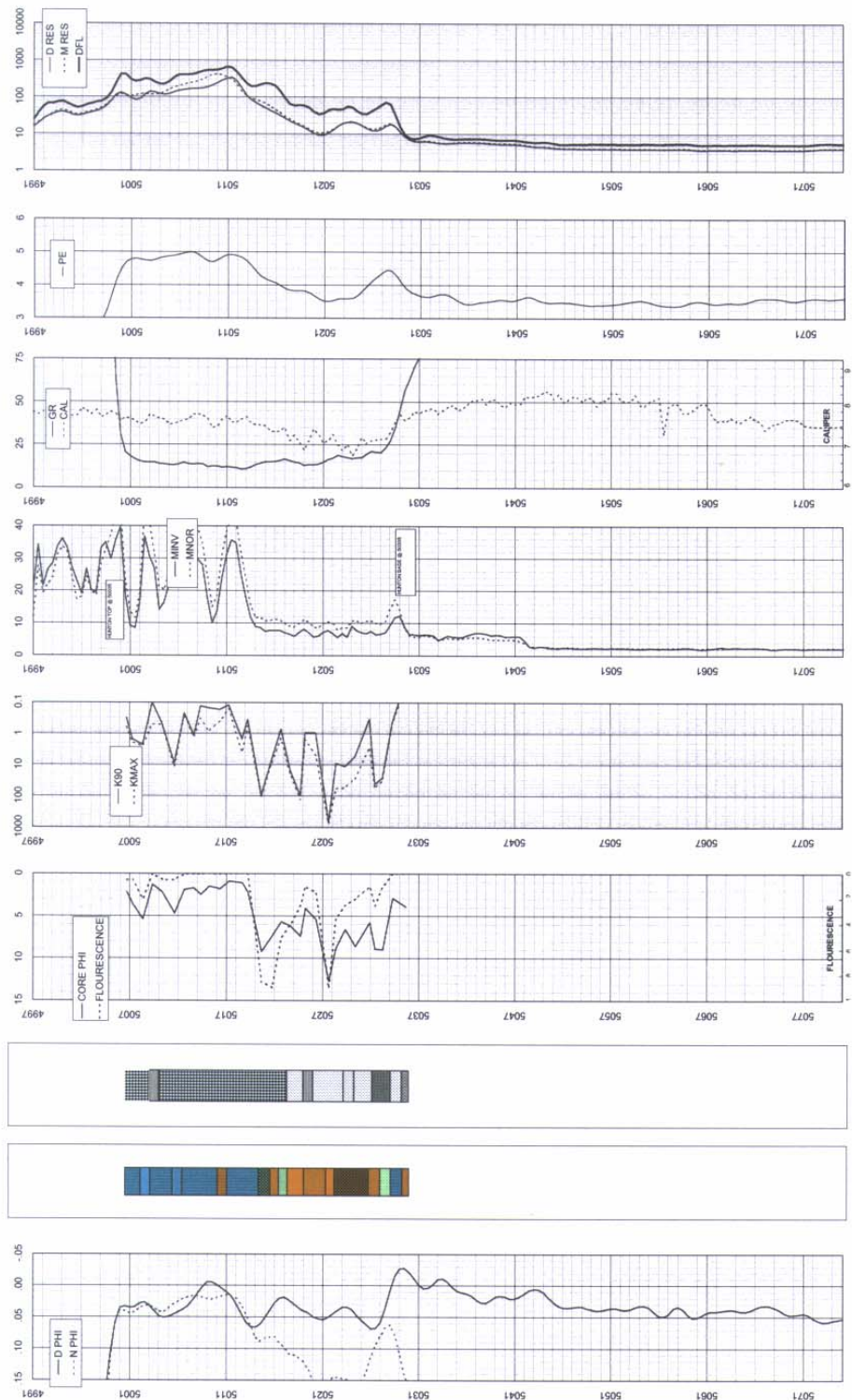


Figure 7-14: Marjo Carter Ranch well log plot

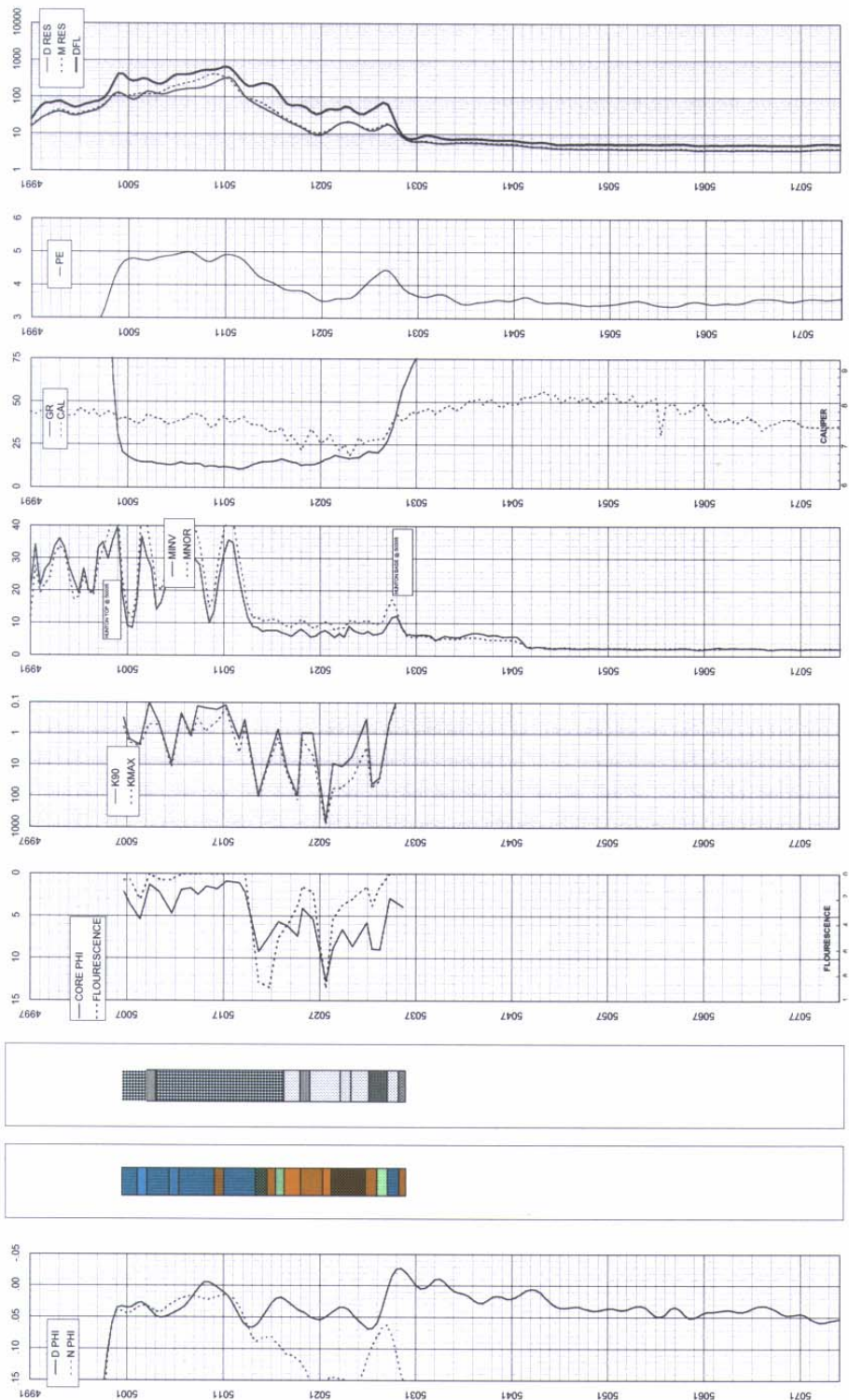


Figure 7-15: Marjo Danny 2-34 well log plot

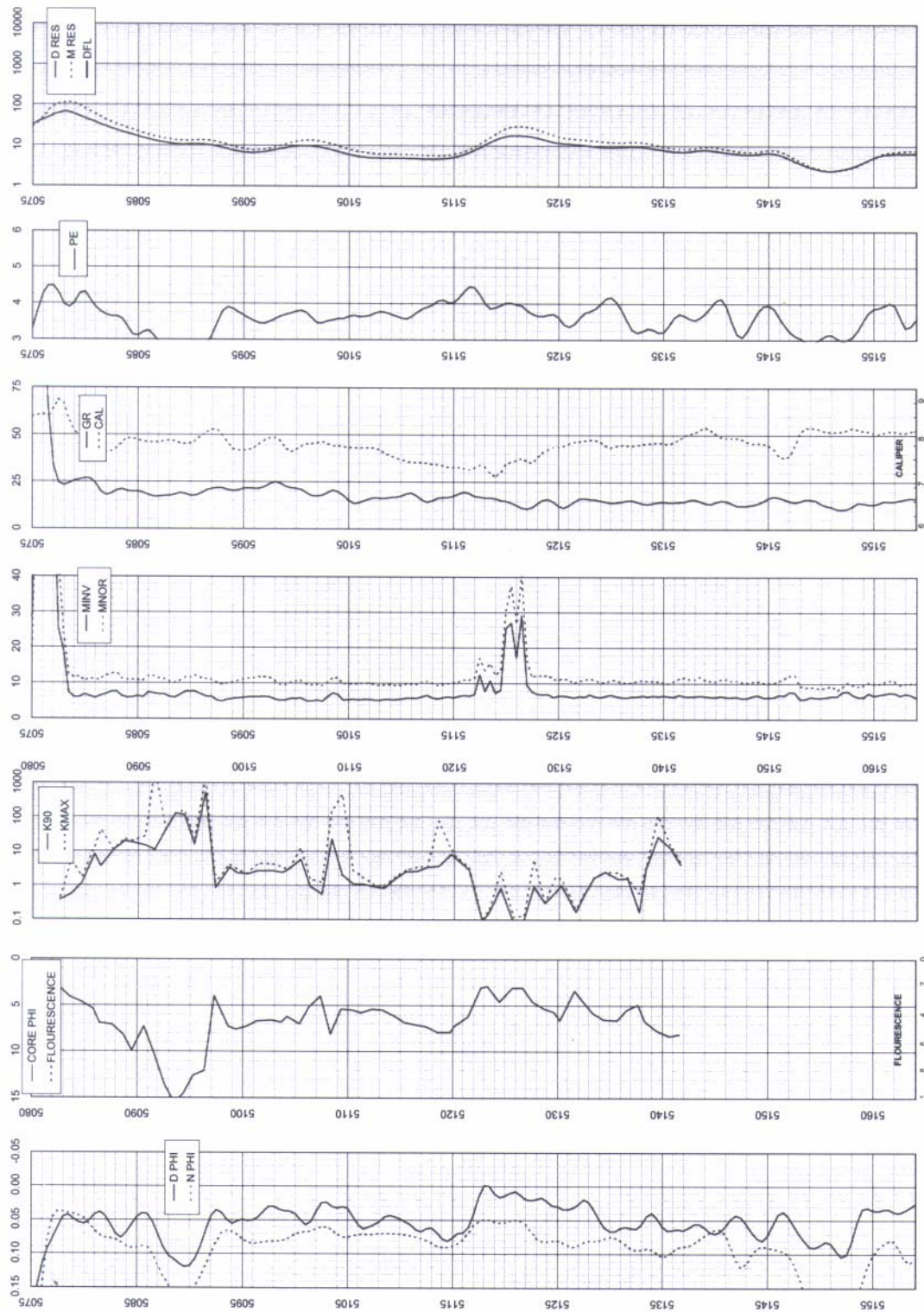


Figure 7-16: Marjo Griffin well log plot #1

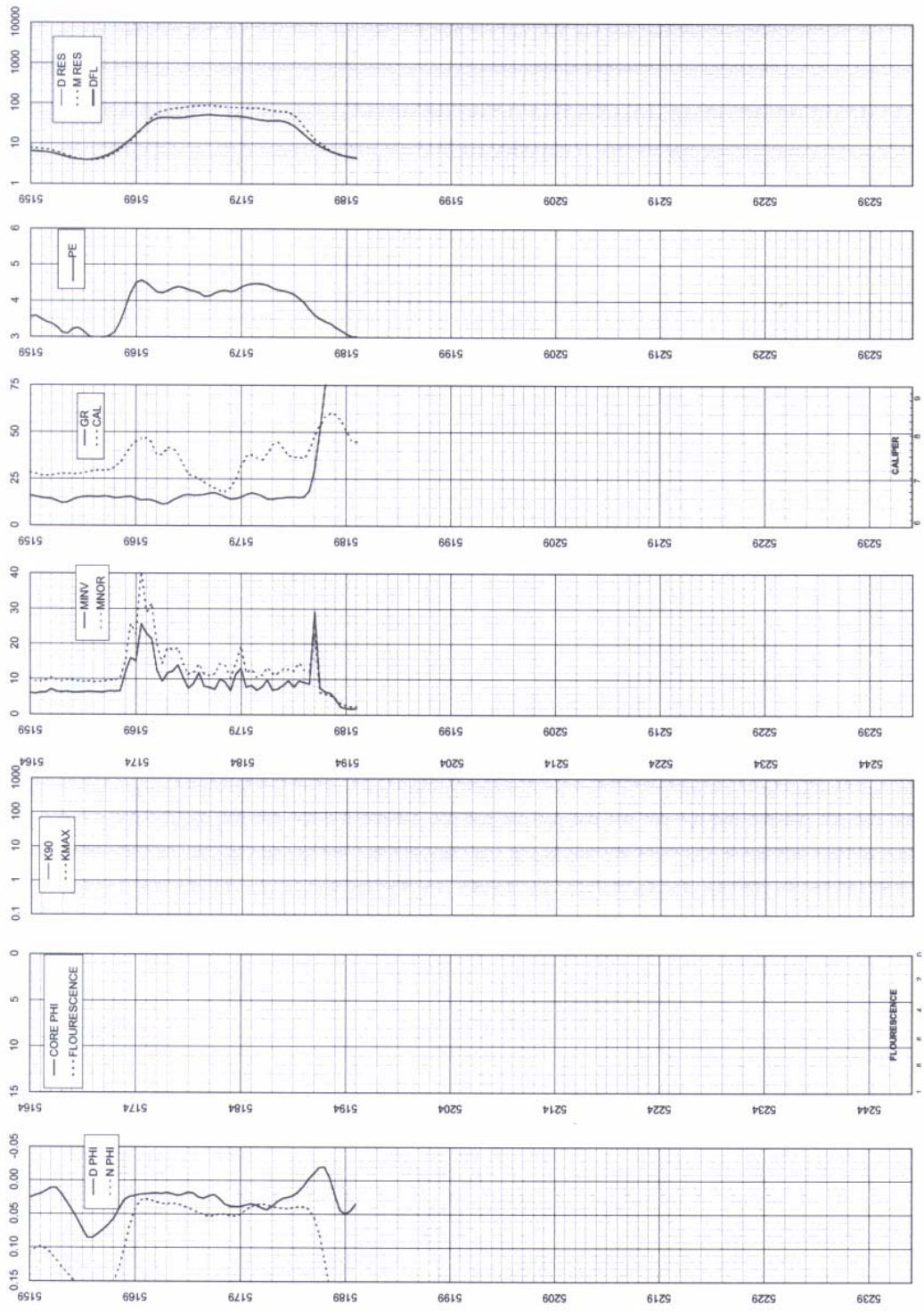


Figure 7-17: Marjo Griffin well log plot #2

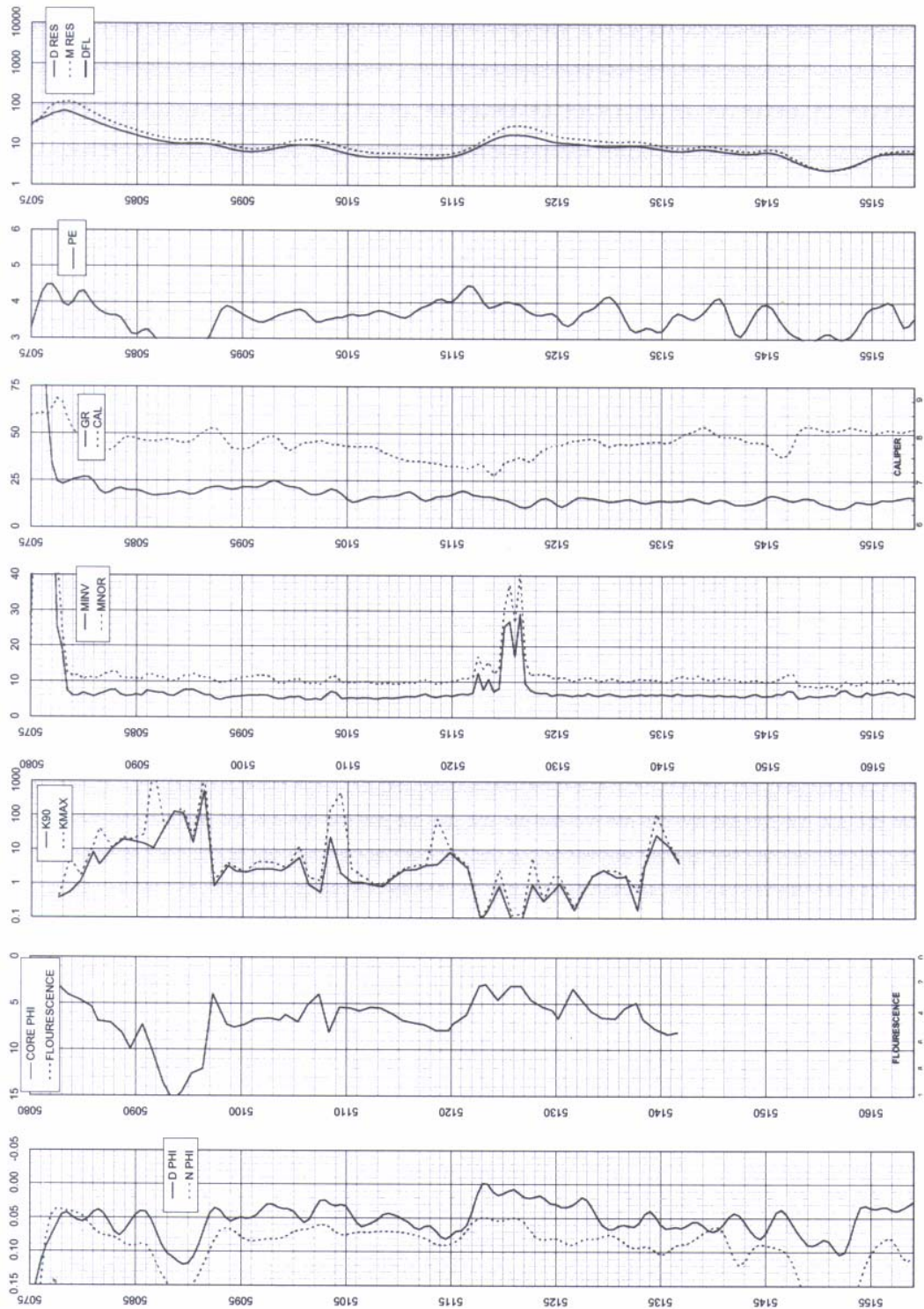


Figure 7-18: Marjo Henry 1-3 well log plot

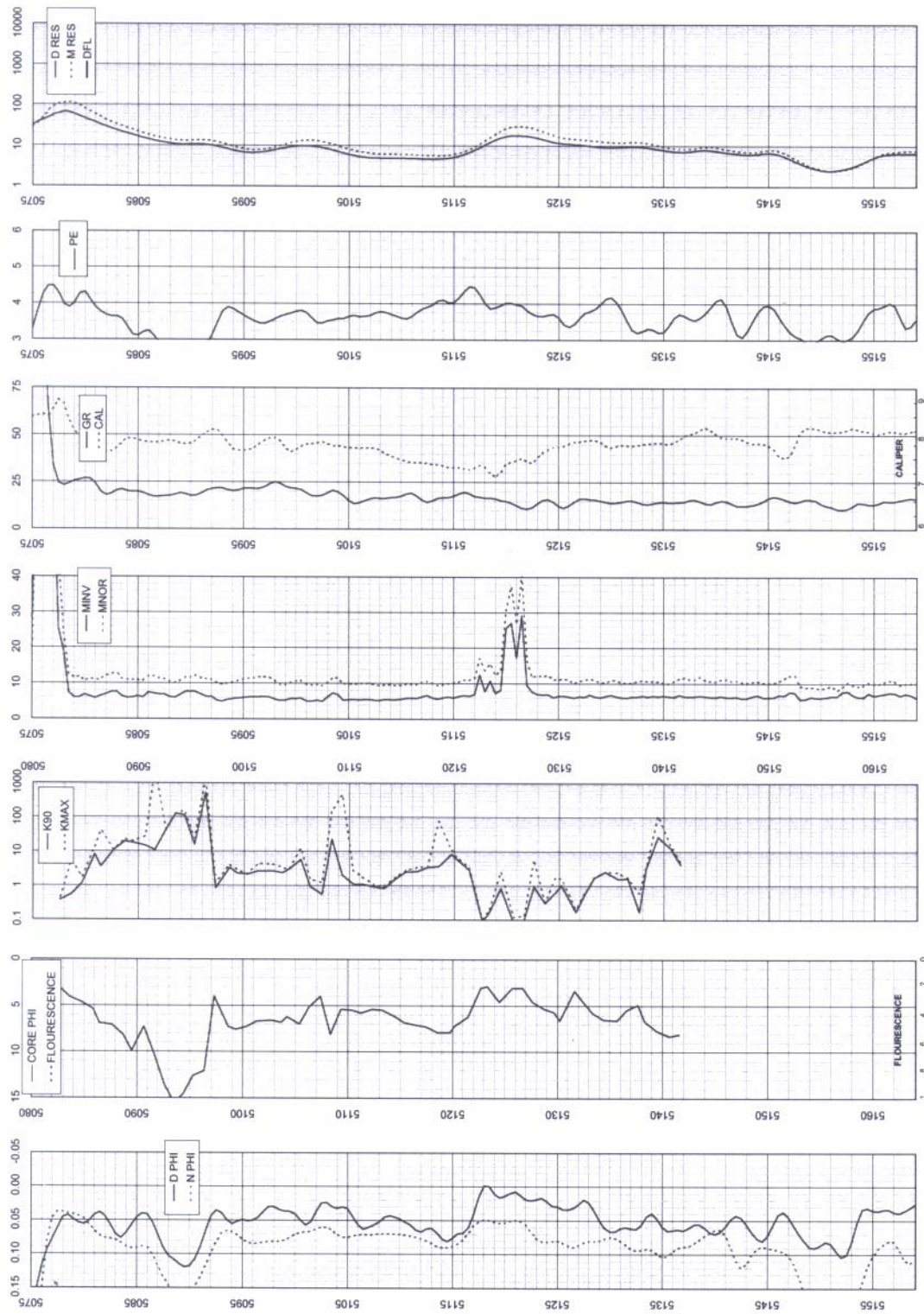


Figure 7-19: Marjo Joe Givens 1-14 well log plot

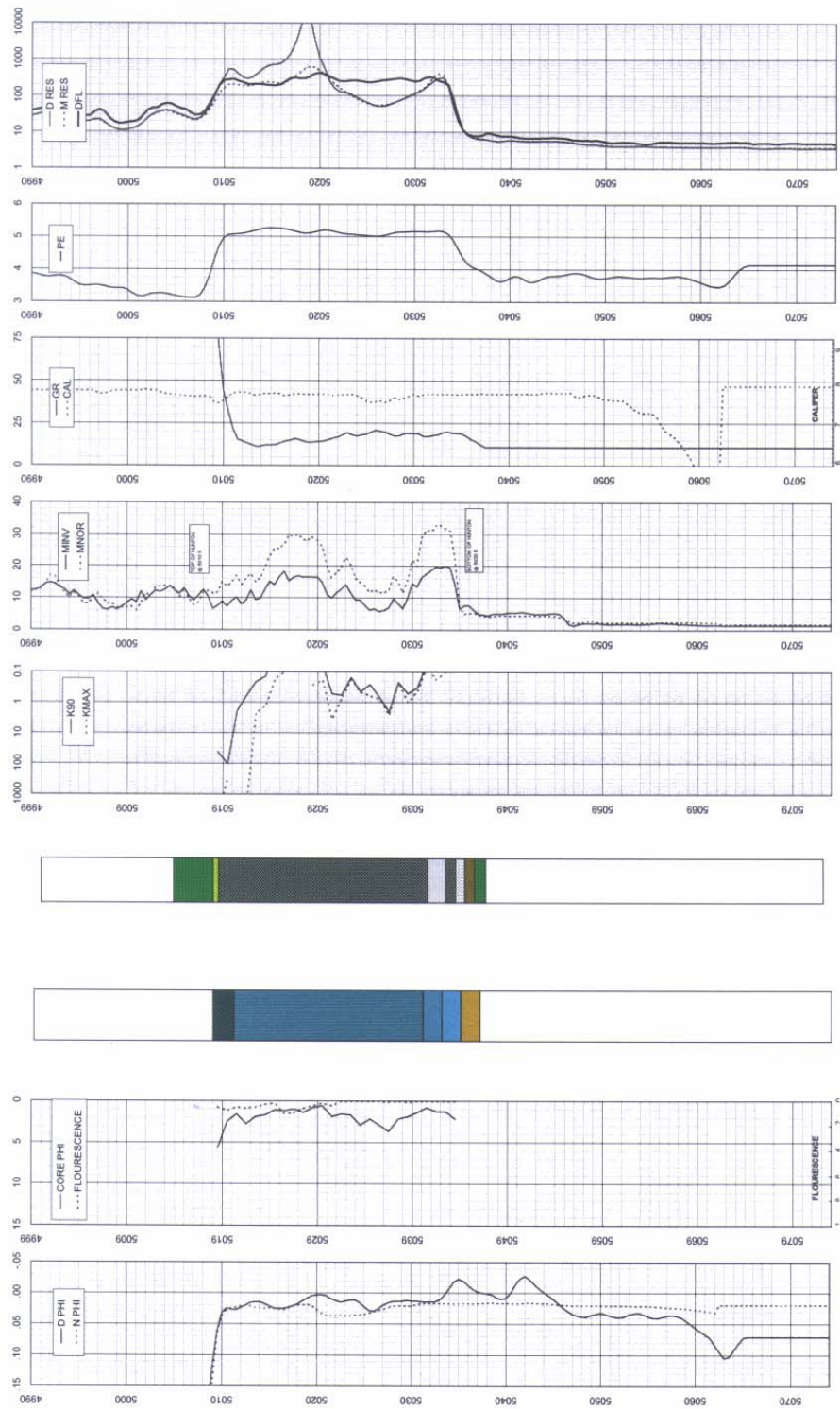


Figure 7-20: Marjo Mary Marie 1-11 well log plot

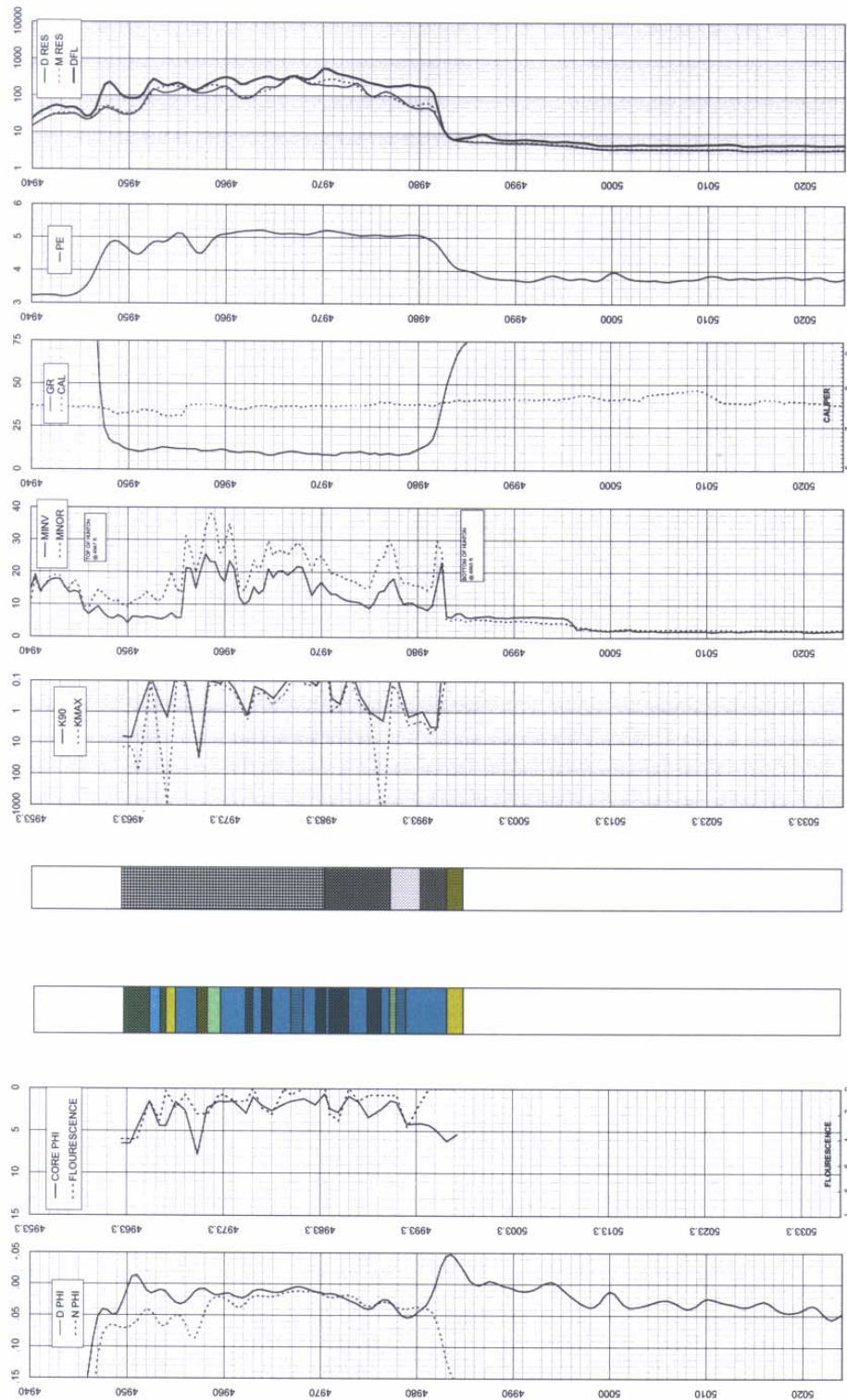


Figure 7-21: Marjo McBride South1-10 well log plot

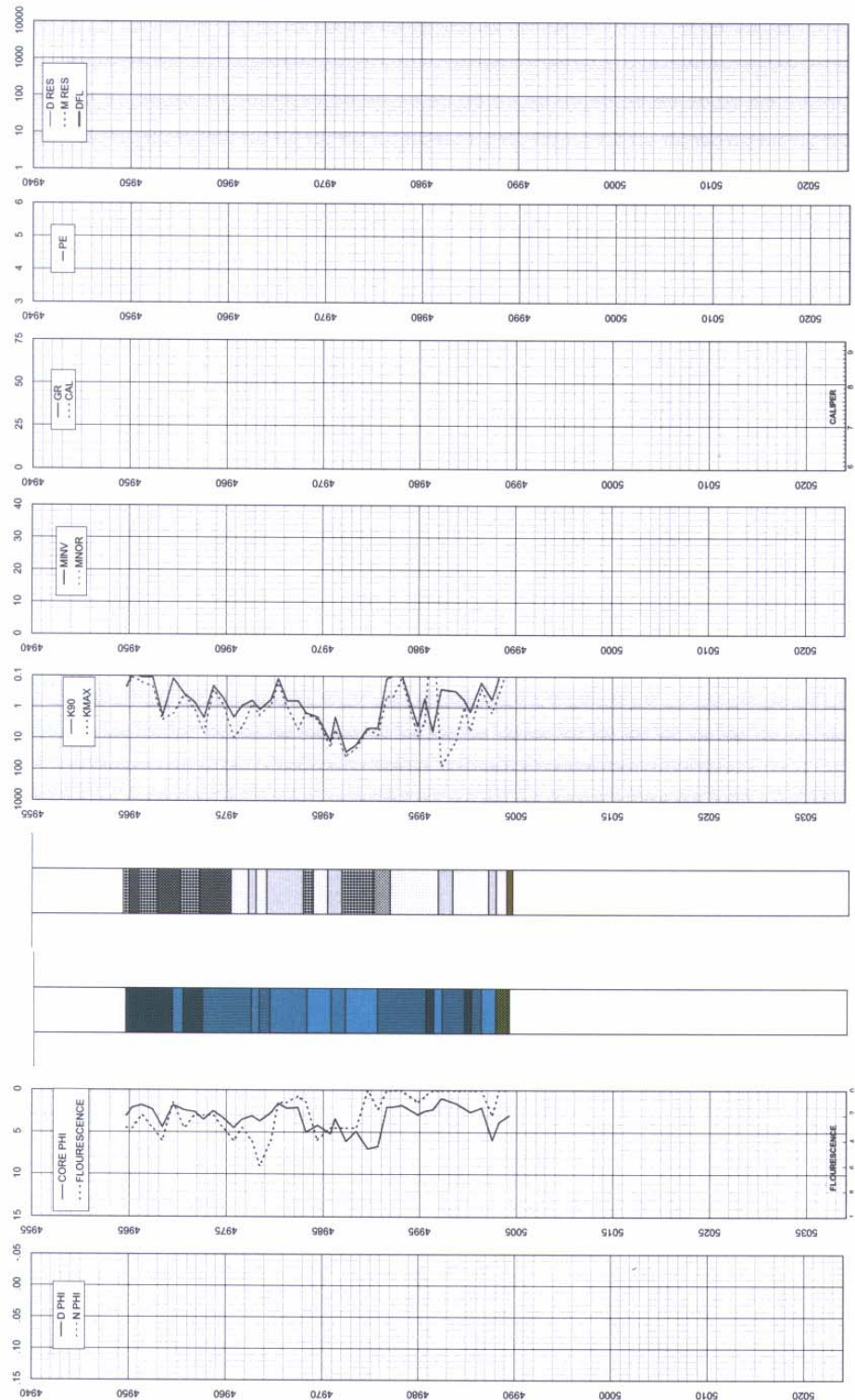


Figure 7-22: Marjo Toles 1-10 well log plot

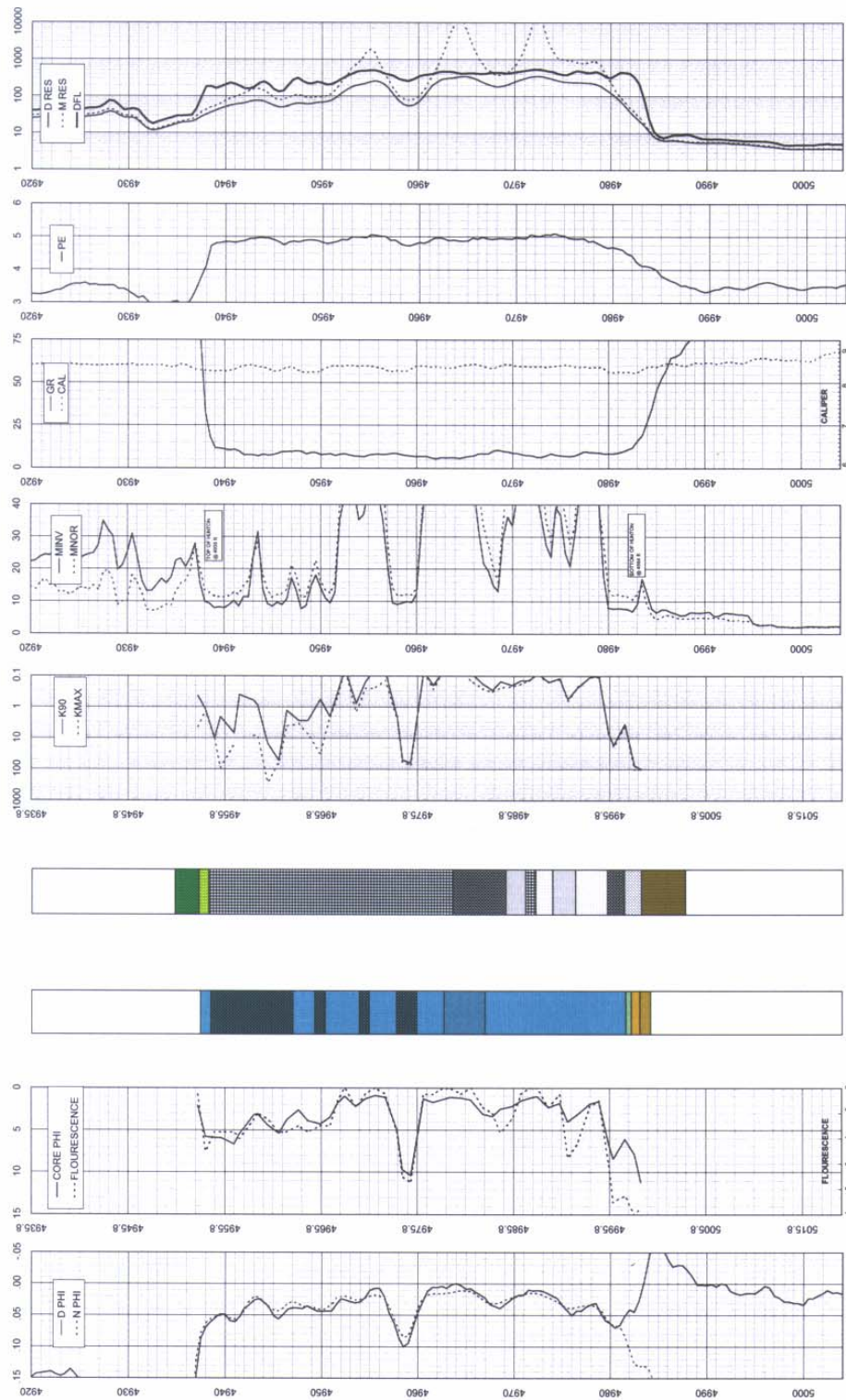


Figure 7-23: Marjo Wilkerson 1-3 well log plot

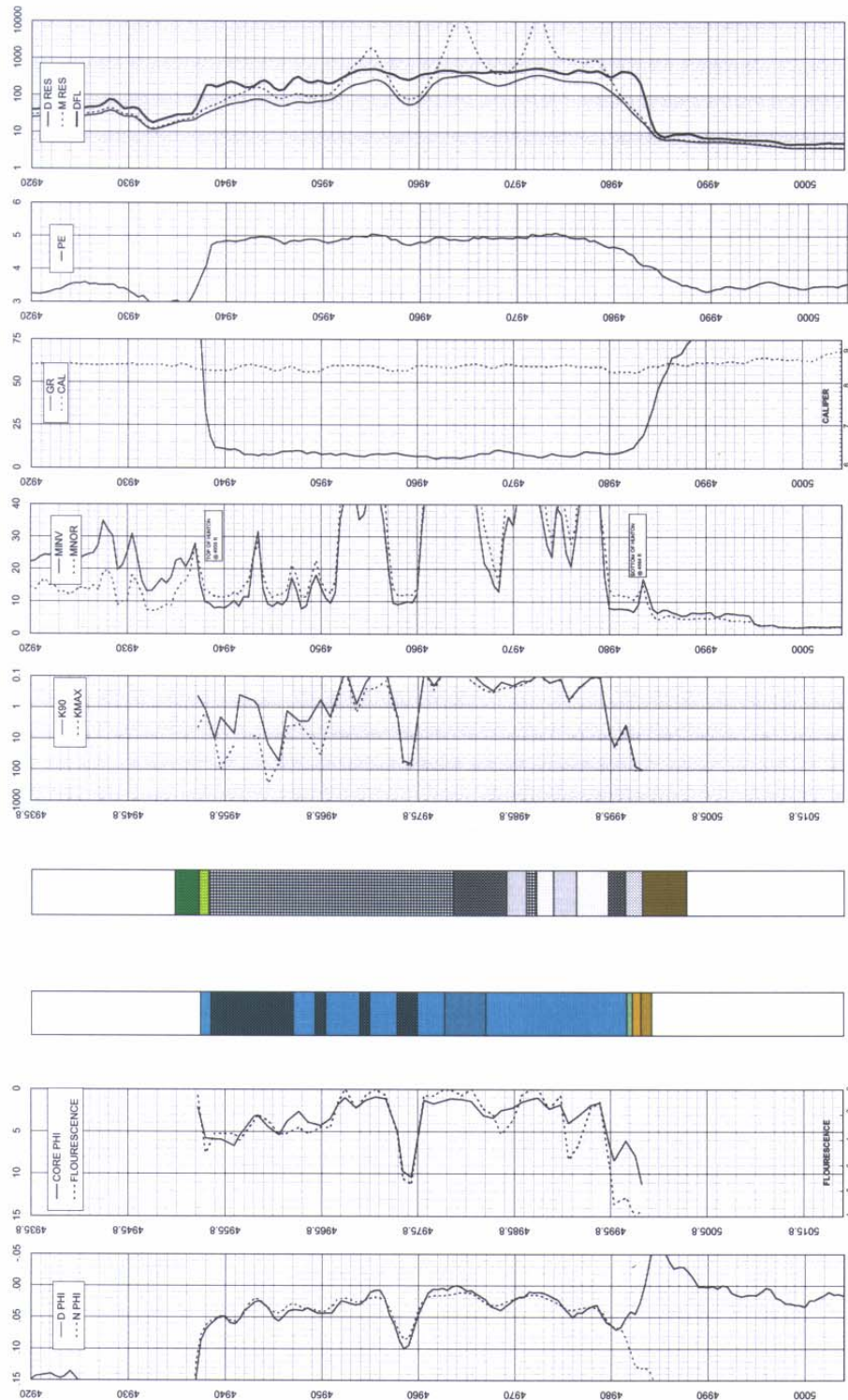


Figure 7-24: Marjo Williams 1-3 well log plot

**7.1.12. Preliminary Report on Conodont Faunas of the Hunton Group
(PaleoAppendix1)**

Dr. James E. Barrick, Texas Tech University, Lubbock Texas, is the leading student of Silurian conodonts in North America. He has extracted and studied the conodonts from 85 samples selected from 8 wells (**Appendix Table 7-37**), and provided the zonal classification of Silurian strata. For the purpose of this report, we simplified the conodont zones into a scheme of 7 “zones” numbered from 0 to 6 (**Figure 4-13**). Dr. Barrick provided the following summary of the faunas.

Conodont zonation, Lincoln and Logan County wells, James E. Barrick , March 6, 2002

Zone 0 – Late Ordovician. Sylvan Shale.

Faunas assigned to Zone 0 include a number of genera and species that occur in Late Ordovician strata, but not Silurian strata. These faunas were obtained only from samples that had previously been placed in the Sylvan Shale on lithological grounds.

Zone 1 – Latest Ordovician (Hirnantian) Keel Formation.

No conodont species diagnostic of the Hirnantian fauna of the Keel were recovered.

Zone 2 – Early Silurian (early Llandovery: Rhuddanian to early Aeronian).

No conodont species indicative of this interval of time were recovered. The presence of carbonates of this age in the Oklahoma region has not been demonstrated.

Zone 3 – Early Silurian (mid-Llandovery: middle Aeronian to early Telychian) – "Lower Cochrane"

A large number of samples contain a distinctive conodont fauna that is characterized by a robust species of *Oulodus* and a heavily costate species of *Walliserodus*. The exact ranges of these forms are unknown, and the age of the fauna is based on a few rarely occurring species. *Distomodus staurognathoides* appears in the middle to late Aeronian (middle Llandovery) and ranges through the late Aeronian and Telychian (late Llandovery). This species places the lower age limit on the fauna. The upper age limit of the fauna is poorly constrained, and only placed in the early Telychian because of the absence of any species restricted to the more diverse middle and late Telychian conodont faunas. The Cochrane Formation in southern Oklahoma appears to fall in the same age range as Zone 3.

Paleoecological information. The Zone 3 fauna from Lincoln County is more diverse than that of the Cochrane in outcrop. During the Early Silurian, it appears that the *Oulodus*-dominated faunas of moderate diversity were more characteristic of shallow marine settings with an abundant shelly fauna. The lower diversity *Panderodus* and *Walliserodus* faunas of the outcrop Cochrane are shelf faunas that workers place offshore of carbonates with diverse coral-brachiopod associations.

Zone 4 – Early Silurian (late Llandovery: middle to late Telychian) – "Upper Cochrane".

This fauna is characterized by common *Ozarkodina polinclinata* and *Panderodus unicostatus*, and smaller numbers of *P. recurvatus* and *Oulodus petila?* The less common elements of species of *Pterospathodus* indicate a late Telychian age for the fauna. In the Bailey well, zonal species for at least four of the *Pterospathodus* zones and subzones occur in succession. No strata bearing this fauna has been previously recovered from carbonate units in the Oklahoma region, with the

possible exception of one or two relatively poor samples at the top of the Cochrane Formation in the Anadarko Basin. In the southern Oklahoma outcrop area, this interval of time occupies the hiatus that separates the Cochrane from the overlying Wenlock Clarita Formation.

Zone 5 – Late Silurian (Wenlock: Sheinwoodian) – "Lower Clarita"

The faunas of this zone contain an abundant, but low diversity coniform fauna strongly dominated by *Dapsilodus obliquicostatus*. The abundance of this species, in association with *Pseudooneotodus bicornis*, comprises the typical conodont fauna of the lower Clarita in outcrop and the subsurface of the Anadarko Basin. Although not occurring in the samples analyzed here, species of *Ozarkodina* and *Kockelella* found in the lower Clarita place it in the Sheinwoodian, or early Wenlock. Zone **5a** represents a basal Clarita fauna that contains the youngest species of *Pterospodus*, *P. amorphognathoides amorphognathoides*, an earliest Wenlock species. Zone **5a** occurs sporadically at the base of the Clarita in outcrop.

Paleoecologic information: The *Dapsilodus*-dominated faunas of the lower Clarita occur with a widespread early Wenlock flooding event across southern North America. Except in the most offshore sections, lower Wenlock carbonates show a shallowing upward trend that is accompanied by a loss of the *Dapsilodus*-dominated fauna.

Table 7-37: Local Biostratigraphic relationship of selected wells in the West Carney Hunton Field

Age	Series	Formation	Zone	Selected Wells with Completed Conodont Study							
SILURIAN	Wenlock	Upper Clarita	6	Marie Marie No. 1	Mcbride South No. 1	Boone No. 1	Carter No. 1	Carney Townsite No. 2	Bailey No. 2	W. Carney SWDW No. 1	Griffin No. 1
		Lower Clarita	5	Marie Marie No. 1	Mcbride South No. 1	Boone No. 1	Carter No. 1	Carney Townsite No. 2	Bailey No. 2	W. Carney SWDW No. 1	Griffin No. 1
	Llandovery	Upper Cochrane	4	Marie Marie No. 1	Mcbride South No. 1	Boone No. 1	Carter No. 1	Carney Townsite No. 2	Bailey No. 2	W. Carney SWDW No. 1	Griffin No. 1
		Lower Cochrane	3	Marie Marie No. 1	Mcbride South No. 1	Boone No. 1	Carter No. 1	Carney Townsite No. 2	Bailey No. 2	W. Carney SWDW No. 1	Griffin No. 1
		Missing	2	Marie Marie No. 1	Mcbride South No. 1	Boone No. 1	Carter No. 1	Carney Townsite No. 2	Bailey No. 2	W. Carney SWDW No. 1	Griffin No. 1
	ORDOVICIAN	Ashgill	Keel	1	Marie Marie No. 1	Mcbride South No. 1	Boone No. 1	Carter No. 1	Carney Townsite No. 2	Bailey No. 2	W. Carney SWDW No. 1
Sylvan			0	Marie Marie No. 1	Mcbride South No. 1	Boone No. 1	Carter No. 1	Carney Townsite No. 2	Bailey No. 2	W. Carney SWDW No. 1	Griffin No. 1
Local Biostratigraphic relationship of Selected Wells in the West carney Hunton Field, Logan County, Oklahoma.				Marie Marie No. 1	Mcbride South No. 1	Boone No. 1	Carter No. 1	Carney Townsite No. 2	Bailey No. 2	W. Carney SWDW No. 1	Griffin No. 1

	SERIES	STAGES	CONODONTS	"Zone"	Formation	
SILURIAN	PRIDOLI		<i>O. costinbomanale</i> - <i>O. s. detoria</i>			
			<i>O. remscheldensis</i> Interval zone			
		LUDLOW		<i>O. crassa</i>		
				<i>O. snajdri</i> Interval zone		
				<i>P. siluricus</i>		
				<i>A. ploeckensis</i>		
			<i>K. "variabilis"</i>			
	WENLOCK	HOMERIAN		<i>O. bohemia</i>	5	Clarita
				<i>O. sagitta sagitta</i>		
		SHEINWOODIAN		<i>K. ortus ortus</i>		
				<i>K. walliseri</i>		
				<i>O. rhenana</i>		
			<i>K. ranulliformis</i> Superzone			
			<i>P. p. procerus</i> Superzone			
			<i>Ps. bicornis</i> Superzone			
			<i>P. a. amorphognathoides</i>			
		LLANDOVERY	TELYCHIAN			
				<i>P. seopennatus</i>		
	AERONIAN			<i>D. staurogathoides</i>	3	Lower Cochrane
				<i>D. kentuckyensis</i>		
	RHUDDANIAN		<i>O. ? nathani</i>	1	Keel	
		<i>A. Ordovicicus</i>	0			Sylvan Shale

Figure 7-25: Local zonation of Conodont stratigraphy divided into 7 zones

7.1.13. Tables of Conodonts Recovered from 8 Wells (PaleoAppendix2)

Table 7-38: Conodont Samples, Marjo Bailey 2-6

CONODONT SAMPLES-Marjo 2-6 Bailey												
E/2-SW-6-16N-3E, Lincoln Co., OK-												
Depth		Spl #	Fm	LITHOLOGY	Grams	# Cono	Age	Series	ZONE	Strat Position	TS	Sent Barrick
FROM	TO											
4876.0	4876.3	1	Basal Clarita	Dol, moldic, foss	500.0	>100	Silurian	Wenlock	5a	85.2	x	8/31/2001
4878.3		2	Up Cochrane	Dol, dk, oil stn						82.9	x	
4881.2	4881.9	3	Up Cochrane	Dolc ls, crin. pkstn	650.0	32.0	Silurian	Llandov	4	80.0	x	8/31/2001
4887.0	4887.4	4	Up Cochrane	Ls, cri grstn	500.0	53.0	Silurian	Llandov	4	74.2	x	9/19/2001
4890.7		5	Up Cochrane				Silurian	Llandov	4	70.5	x	8/31??
4891.4	4892.0	6	Up Cochrane	Dolc br-cri pkstn	750.0	41.0	Silurian	Llandov	4	69.8	x	
4899.4	4900.0	7	Up Cochrane	Br-cri, small brachs	1180.0	23.0	Silurian	Llandov	4	61.8	x	9/19/2001
4905.0	4905.2	8	Up Cochrane	Big brach coquina			Silurian	Llandov	4	56.2	x	
4910.8	4911.0	9	Up Cochrane				Silurian	Llandov	4	50.4	x	
4913.0	4913.1	10	Up Cochrane				Silurian	Llandov	4	48.2	x	
4915.0	4915.6	11	Up Cochrane	Big Br, micrite infill	660.0	28.0	Silurian	Llandov	4	46.2	x	9/19/2001
4916.0	4916.7	12	Up Cochrane	brachs	1000.0	78.0	Silurian	Llandov	4	45.2	x	8/31/2001
4919.4		13	Up Cochrane	Poss seq bndry, paleosol?	500.0	42.0	Silurian	Llandov	4	41.8	x	9/19/2001
4920.3	4921.0	14	Up Cochrane		600.0	37.0	Silurian	Llandov	4	40.9	x	9/19/2001
4923.0	4923.4	15	Up Cochrane	Karst mud infill, lam	500.0	1.0	Silurian	Llandov	?	38.2	x	9/19/2001
4925.0	4925.2	16	Up Cochrane				Silurian	Llandov		36.2	x	
4927.4	4928.0	17	Up Cochrane	Brachs; vuggy & tite	600.0	4.0	Silurian	Llandov	4?	33.8	2.0	9/19/2001
4930.0	4930.5	18	Up Cochrane	Foss wk/pkstn, small brachs	650.0	4.0	Silurian	Llandov	4?	31.2	x	9/19/2001
4932.0	4932.6	19.0	Lw Cochrane	F. br/cri ls; soln fract & fill						29.2	x	
Strat Position is footage above or below (-) the Hunton/Sylvan contact at 4961.2 ft., equivalent to core footage. Contact is at 4964 log depth												
All footages are core depth.												
Note : Lithology is limestone, unless mentioned otherwise												

Table 7-39: Conodont Samples, Marjo Boone 1-4

CONODONT SAMPLES- MARJO BOONE # 1-4, SEC. 4, T15N-R2E												
Lincoln County, Oklahoma												
[On log-plots, enter the top or "from" depth]												
Depth		Spl #	FM	LITHOLOGY	Grams	# Cono	Age	Stage	Zone	Strat Position	TS	
FROM	TO											
5038.3	5039	B-1	Lw Cochrane	f foss pkstn	700	31	Early Sil	Llandov	3	28.2	x	
5046.1	5047	B-2	Lw Cochrane	coral-cri grstn	650	80	Early Sil	Llandov	3	20.4	xx	
5051	5051.8	B-3	Lw Cochrane	c cri grstn	700	5	Early Sil	Llandov	3	15.5	x	
5061	5061.9	B-4	Lw Cochrane	c cri grstn	700	213	Early Sil	Llandov	3	5.5	x	
5065.7	5066	B-5	Lw Cochrane	dol c foss pkstn	350/80u	33	Early Sil	Llandov	3	0.8		
5066.5	5067	B-6	Sylvan	argil dol mdstn	350/120u	15	Early Sil?	?		0	x	
Position is footage of top of sample. above or below (-) the Hunton/Sylvan contact, at 5066.5												
Note : Lithology is Limestone, unless mentioned otherwise												

Table 7-40: Conodont Samples, Carney Townsite 2-5

CONODONT SAMPLES- CARNEY TOWNSITE 2-5, SEC. 15, T15N-R3E												
LINCOLN CO, OKLAHOMA											Strat	
[On log-plots, enter the top or "from" depth]												
Depth	Spl #	FM	LITHOLOGY	Detailed Lithology	Grams	# Cono	Age	Series	"Zone"	Position	TS	
From	To											
4906.2	4906.9	CT-1	Lw Clarita	Dol, lt gy f xln	open vert fract, with xln lining 4906-4908.4	900	7	Silurian	Wenl.	5	73.1	x
4916.3	4917	CT-2	Lw Clarita	Dol, limy f xln	micro vug + 1 lining 1"x11/2" vug	680	26	Silurian	Wenl.	5	63	x
4924.3	4925	CT-3	Lw Clarita	Dol, limy, v lt gy	many microvugs	620	30	Silurian	Wenl.	5	55	x
4931.3	4932	CT-4	Lw Clarita	Ls, sli dol v lt gy	chalky, pp, foss, f foss wkstn-pkstn with spares lg cri	550	22	Silurian	Wenl.	5	48	x
4946	4946.7	CT-5	Lw Clarita	Ls, lt gy, dense hard	mdstn/wkstn, sli pp, with tan silt cavity fill	600	71	Silurian	Wenl.	5	33.3	x
4947.3	4948	CT-6	Lw Clarita	Dol, f xln, lt gy	intersecting vertical fractures, sli xtls in fractures						32	
4956.8	4959	CT-7	Lw Clarita	Ls, lt tan gy	open vert fract in tight Ls, healed frac below 4959, Ls very dense, foss, wkstn/pkstn						22.5	
4959.3	4959.8	CT-8	Up Cochrane	Ls, f foss, wkstn/pkstr	v dense and tight 1% porosity	650	>100	Silurian	Llandov	4	20	x
4962	4963	CT-9	Up Cochrane	Ls, c brac pkstn	huge soln enhanced frac 0.5" long x 0.2" wide, a pipeline !						17.3	
4964.7	4965	CT-10	Up Cochrane	Ls, m-c. brach grnsth	cri-brach-ost grnst						14.6	x
Strat Position is footage above base of Hunton, corrected to core depth; = 4979.3												

Table 7-41: Conodont Samples, Marjo Carter 1-14

CONODONT SAMPLES- MARJO CARTER 1-14, SEC. 14, T15N-R2E												
LINCOLN CO, OKLAHOMA											Strat	
[On log-plots, enter the top or "from" depth]												
Depth	Spl #	FM	LITHOLOGY	Detailed Lithology	Grams	# Cono	Age	Series	"Zone"	Position		
FROM	TO											
4940	4940.9	CR 1-14 #1	Lw Cochrane	dol grstn		1100	24	Early Sil	Llandov	3	55.8	
4941.4	4942	CR 1-14 #2	Lw Cochrane	c foss grstn	smooth tril, ost, frags lg brac	600	15	Early Sil	Llandov	3	54.4	
4945	4945.1	CR 1-14 #3	Lw Cochrane	vuggy br grstn					Llandov		50.8	
4950.4	4951	CR 1-14 #4	Lw Cochrane	c br-cri grstn	c.br, tril, cri	350	4	Early Sil	Llandov	3	45.4	
4951	4951.7	CR 1-14 #5	Lw Cochrane	c br-cri grstn	big brac-pent	500	9	Early Sil	Llandov	3	44.8	
4955	4956	CR 1-14 #6	Lw Cochrane	f foss pkstn	few lg cri - cri sparite, no other foss	1400	17	Early Sil	Llandov	3	40.8	
4961.5	4962	CR 1-14 #7	Lw Cochrane	c foss grstn	sparte, lg brac-pent	700	40	Early Sil	Llandov	3	34.3	
4962	4962.6	CR 1-14 #8	Lw Cochrane	c br grstn	leached vuggy, v big pent brac, tril, lg cri	500	3	Early Sil	Llandov	3	33.8	
4975	4975.7	CR 1-14 #9	Lw Cochrane	br-cri pkstn	sm v big pent brac, v lg cri, lg ost or tril	500	8	Early Sil	Llandov	3	20.8	
4976.8	4977.5	CR 1-14 #10	Lw Cochrane	c cri grstn	lg cri, med pent brac	500	3	Early Sil	Llandov	3	19	
4984	4984.6	CR 1-14 #11	Lw Cochrane	m-c brac grstn		950	2	Early Sil	Llandov	3	11.8	
4990.9	4991.4	CR 1-14 #12	Lw Cochrane	f foss wkstn	pp porosity chalky	500	4	Early Sil	Llandov	3	4.9	
4994.5	4994.9	CR 1-14 #13	Lw Cochrane	dol grstn	f xln, vuggy&tight, loc washouts	550	>200	Early Sil	Llandov	3	1.3	
4995	4995.5	CR 1-14 #14	Lw Cochrane	coralline lst	altered to c dol, moldic			Early Sil	Llandov	3	0.8	
4995.6	4996	CR 1-14 #15		contact ?	f xln gy dol & gm gy argill dol	250	7	Late Ord	Ashgill	0	0.2	
4996.3	4997	CR 1-14 #16	Sylvan	grn gy argill dol		700	Many	Late Ord	Ashgill	0	-0.5	
4997.6	4998.5	CR 1-14 #17	Sylvan	grn gy argill dol		400	Many	Late Ord	Ashgill	0	-1.8	
4999.6	5000	CR 1-14 #18	Sylvan	grn gy shaly argill dol		400	Many	Late Ord	Ashgill	0	-3.8	
Strat Position is above or below Hunton/Sylvan contact												
Hunton/Sylvan contact is at 4995.8, core depth; = 4982.5 log depth.												
Note : Lithology is limestone, unless mentioned otherwise												

Table 7-42: Conodont Samples, Marjo Griffin 1-14

CONODONT SAMPLES- Marjo 1-14 Griffen, 14-15N-1E, Logan co, OK												
On log-plots, enter the top or "from" depth											Strat	Sent to
Depth	Spl #	Gp/Fm	LITHOLOGY	Grams		Age	Series	"Zone"	Position	TS	Barrick	
FROM	TO											
5082.3	5083	1	Hunton/ Clarita	Doltc Ls, karst fill	600	Many	Silurian	Wenlock	5	109.2		2/1/2002
5085	5085.7	2	Clarita	Ls mdstn	900	Many	Silurian	Wenlock	5	106.5	X	2/2/2002
5087.3	5088	3	Clarita	Doltc Ls, vuggy	1220	Many	Silurian	Wenlock	5	104.2		2/3/2002
5090.4	5090.9	4	Clarita	Doltc Ls, vuggy	1000	Many	Silurian	Wenlock	5	101.1	X	2/4/2002
5095	5096	5	Clarita	"	1000	Many	Silurian	Wenlock	5	96.5		2/5/2002
5100	5100.7	6	Clarita	Doltc Ls, sabkha mdstn	1500	Many	Silurian	Wenlock	5	91.5		2/6/2002
5105	5105.7	7	Clarita	"	1400	Many	Silurian	Wenlock	5	86.5	X	2/7/2002
5110	5110.7	8	Clarita	Mdstn, sabkha	1750	Many	Silurian	Wenlock	5	81.5		2/8/2002
5115	5115.7	9	Clarita	"	1100	Many	Silurian	Wenlock	5	76.5	X	2/9/2002
5119.5	5120	10	Clarita	Mdstn, sabkha	850	Many	Silurian	Wenlock	5	72		2/10/2002
5127.3	5128	11	Clarita	"	1450	Many	Silurian	Wenlock	5	64.2	X	2/11/2002
5135.3	5138	12	Clarita	doltc Ls, vuggy, fract w/ karst fill	1400	Many	Silurian	Wenlock	5	56.2		2/12/2002
5137.3	5138	13	Clarita	doltc ls, mottled	1400	Many	Silurian	Wenlock	5	54.2	X	2/13/2002
5140.3	5141	14	Clarita	doltc ls, vuggy	1200	Many	Silurian	Wenlock	5	51.2	X	2/14/2002
Strat Position is footage above or below (-) the Hunton/Sylvan contact at 5191.5 ft. (log base at 5186.5, adjusted to core depth).												
Note: Many samples contain late Middle Devonian conodonts that are typical of Misener leak.												

Table 7-43: Conodont Samples, Mary Marie 1-11

CONODONT SAMPLES- MARY MARIE 1-11, SEC. 11, T15N-R2E											
LINCOLN CO, OKLAHOMA											Strat
[On log-plots, enter the top or "from" depth]											
Depth	Spl #	FM	LITHOLOGY	Grams	# Cono	Age	Series	"Zone"	Position	TS	
From	To										
4961.5	4962	MM-1	Lw Cochrane	brach pkstn, grnstn	400	1, 6 indet					42
4967	4967.5	MM-2	Lw Cochrane	c brach pkstn	500	2, indet					36.5
4973	4973.5	MM-3	Lw Cochrane	c brach pkstn	500	2, 1 indet					30.5
4980	4980.5	MM-4	Lw Cochrane	c brach pkstn	600	6					23.5
4987	4987.5	MM-5	Lw Cochrane	f-c brach pkstn	500	0					16.5
4990.5	4991	MM-6	Lw Cochrane	c brach grnstn	650	27	Early Sil	Llandov	3		13
4997.2	4998	MM-7	Lw Cochrane	cri, brach grnstn	750	48	Early Sil	Llandov	3		6.3
5000.2	5000.8	MM-8	Lw Cochrane	cri, brach pkstn grnstn	550	64	Early Sil	Llandov	3		3.3
5003	5003.3	MM-9	Lw Cochrane	shale pyritic	150	18	Early Sil	Llandov	3		0.5
5003.5	5004	MM-10	H/S	CONTACT	650		Lt. Ord	Ashgill	0		0
				lt gy dol / grn gy argill dol							x
5004.6	5005.2	MM-11	Sylvan	grn gy argill dol	750		Lt. Ord	Ashgill	0		-1.1
5006	5006.6	MM-12	Sylvan	grn gy argill dol	850		Lt. Ord	Ashgill	0		-2.5
5007.3	5008	MM-13	Sylvan	shale pyritic	800	many	Lt. Ord	Ashgill	0		-3.8
5014	5016	MM-14	Sylvan	shale pyritic	650	many	Lt. Ord	Ashgill	0		-10.5
Strat Position is footage above or below (-) the Hunton/Sylvan contact at 5003.5											
Note: Lithology is limestone unless otherwise noted.											

Table 7-44: Conodont Samples, Marjo W. Carney Extension SWDW No. 1

CONODONT SAMPLES- Marjo W. Carney Extension SWDW* No. 1											Sent to
SW-NE-14-T15N-R1E, Logan Co. Ok. *SWDW = Salt Water Disposal Well											Strat
Depth	Spl #	Formation	LITHOLOGY	Grams	# Cono	Age	Series	"Zone"	Position	TS	Barrick
FROM	TO										
		Hunton									
5042.7			Top of Hunton						113.3		
5044.1	5044.7	1	Lw Cochrane	Ls, small brachs, Misener karst sed	500	7	Silurian	Llandov	3	111.9	x 8/31/2001
5045.4	5046	2	Lw Cochrane	Br pkstn, Ca-fill	520	35	Silurian	Llandov	3	110.6	x 8/31/2001
5054.3	5055	3	Lw Cochrane	dns pkstn, open SF	200	2	Silurian	??		101.7	x 9/19/2001
5055.4	5056.3	4	Lw Cochrane	Big brachs, vuggy, vert fract, karst fill	650	5	Silurian	??		100.6	x 8/31/2001
5059	5059.1	5	Lw Cochrane	Karst brecc, Wfd fill						97	x
5061.2	5061.8	6	Lw Cochrane	Dns br/cri pkstn	530	20	Silurian	Llandov	3	94.8	x 8/31/2001
5069.4	5070	7	Lw Cochrane	karst filled coral						86.6	x
5077.3	5078	8	Lw Cochrane	dns cri/br pkstn	650	7	Silurian	??		78.7	x 8/31/2001
5082	5083	9	Lw Cochrane	Coral/brach pkstn, streptelasmid & favositid	500	22	Silurian	Llandov	3	74	x
5091.7	5092.3	10	Lw Cochrane	Cavity fill?	700	48	Silurian	Llandov	3	64.3	x 9/19/2001
5097	5097.7	11	Lw Cochrane	Pent brachs, favositid coral						59	x
5107	5108	12	Lw Cochrane	Pkstn, ?karst infill or burrow						49	x
5117.9	5119	13	Lw Cochrane	favositid coral	1000	57	Silurian	Llandov	3	38.1	x 9/19/2001
5126	5130	14	Lw Cochrane	Rubble, fractured tite ls: Br/cri facies w/streptelasmid & favositid corals	2300	>100	Silurian	Llandov	3	30	x 9/19/2001
Strat Position is footage above or below (-) the Hunton/Sylvan contact at 5156 ft, core depth equivalent of log base of Hunton.											
Note : Lithology is limestone, unless mentioned otherwise											

7.1.14. Thin Section Samples of Individual Wells

Table 7-45: Thin Sections, Marjo Anna 1-15

THIN SECTION SAMPLES- MARJO ANNA 1-15, SEC. 15, T15N-R2E LINCOLN CO, OKLAHOMA						
Depth		Std	2x2	SEM	LITHOLOGY:	Details
From	To				hand lens	
4969.5	69.7		x		Dolc pkstn, vuggy	big Pent. Brach facies; karst silt infill
4977.3	77.5		x		same	same
4983.4			x			
4989	89.2		x		same	
4994.3	94.5		x		Dol, wkstn & pkstn	vugs under big brach shells
4999.2	99.4		x		Dol, mdstn, wkstn	small brach facies?
5001	5001.2		x		Dol, mdstn, wkstn	facture porosity
5001.8	1.9		x		Dol, mdstn	fractures
5004.6	4.8		x		Dolc, f. grnstn/ argill dol.	Hunton/Sylvan contact @ 5004.7

Table 7-46: Thin Sections, Marjo Bailey 2-6

THIN SECTION SAMPLES- MARJO BAILEY 2-6, SEC. 6, T15N-R3E LINCOLN CO, OKLAHOMA						
Depth		Std	2x2	SEM	LITHOLOGY: hand	Details
From	To				lens	
4876.3			x		Dol, moldic	poss rxllzd corals
4879.3			x		C dol, w/ cavity fill	karst cave fill
4881.2			x		Doltc Ls, cri pkstn	poss corals or stroms
4887.2			x		Dol, dns cri pkstn	also corals, bry, brachs
4890.7			x			
4891.7			x		Doltc brach pkstn	Large brachs, mud infill in shelter pores
4899.9			x		Ls, brach-cri pkstn	small brachs
4905			x			
4910.8			x			
4913			x			
4915.3			x		Ls, br pkstn, mud matrix	karst cavity, silt fill;
4916.3			x		Ls, c. br-cri pkstn	
4920.3			x		Ls, c. br-cri pkstn	big pent brachs
4923			x		Ls, c br pkst, vuggy	laminated karst infill
4925			x			
4927.4			x		Ls, br pkstn, vuggy	
4927.9			x		Ls, br pkstn, tite	
4930			x		Ls, wkstn/pkstn	foss, br, etc
4932.3			x		Ls, f gr, br, big cri	fracture w/ fill

Table 7-47: Thin Sections, Marjo Boone 1-14

THIN SECTION SAMPLES- MARJO BOONE 1-14 LINCOLN CO, OKLAHOMA						
Depth		Std	2x2	SEM	LITHOLOGY:	Details
From	To				hand lens	
4940	4940.1					
4941.1	4941.2				f foss pkstn	
4941.9	4942				co-cri grstn	
4950.9	4951				c cri grstn c cri grstn	
4955	4955.1				dol c foss pkstn	
4961.5	4961.6				argil dol mdstn	
4962	4962.1					
4975	4975.1					
4976.8	4976.9					

Table 7-48: Thin sections, Marjo Carney Townsite 1-14

THIN SECTION SAMPLES- MARJO CARNEY TOWNSITE 1-14, SEC. 14, T15N-R2E LINCOLN CO, OKLAHOMA						
Depth		Std	2x2	SEM	LITHOLOGY	DETAILS
From	To					
4906.2	4906.9	x			Dol, lt gy f xln	open vert fract, with xln lining 4906-4908.4
4916.3	4916.4	x			Dol, limy f xln	micro vug + 1 lining 1"x1 1/2" vug
4924.3	4924.4	x			Dol, limy, v lt gy	many microvugs chalky, pp, foss, f foss wkstn-pkstn
4931.3	4931.4	x			Ls, sli dol v lt gy	with spares lg cri
4946.4	4946.6	x			Ls, lt gy, dense hard	silt tan cavity fill
4946.8	4946.9		x		Ls, lt gy, dense hard	mdstn/wkstn, sli pp
4960.1	4960.2	x			Ls, lt tan gy	v dense and tight 1% porosity
4964.9	4965	x			Ls, f foss, wkstn/pkstn	

Table 7-49: Thin section, Marjo Carter 1-14

THIN SECTION SAMPLES- MARJO CARTER 1-14, SEC. 14, T15N-R2E LINCOLN CO, OKLAHOMA						
Depth From	To	Std	2x2	SEM	LITHOLOGY	DETAILS
4940	4940.1	x			dol grstn	
4941.1	4941.2	x				
4941.9	4942	x			c foss grstn	smooth tril, ost, frags lg brac
4945	4945.1	x			vuggy br grstn	
4950.9	4951	x			c br-cri grstn	c.br, tril,cri
4955	4955.1	x			c br-cri grstn	big brac-pent few lg cri - cri sparite, no
4961.5	4961.6	x			f foss pkstn	other foss
4962	4962.1	x			c foss grstn	sparite, lg brac-pent leached vuggy, v big pent
4975	4975.1	x			br-cri grstn	brac, tril, lg cri sm v big pent brac, v lg cri,lg
4976.8	4976.9	x			br-cri grstn	ost or tril
4984.6	4985		x		m-c brac grstn	
4991.3	4991.4	x			f foss wkstn	pp porosity chalky f xln, vuggy&tight, loc
4994	4994.2	x			dol grstn	washouts
4995.4	4995.5	x			coralline lst	altered to c dol, moldic
4995.7	4995.9	x			contact ?	f xln gy dol & grn gy argill dol
4998.2	4998.3	x			grn gy argill dol	

Table 7-50 Thin section, Mary Marie 1-11

THIN SECTION SAMPLES- MARY MARIE 1-11, SEC. 11, T15N-R2E LINCOLN CO, OKLAHOMA						
DEPTH		Std	2x2	SEM	LITHOLOGY	DETAILS
From	To					
4963.9				x		
4965.7				x		
4966.5				x	x	
4968.5				x		
4968.8				x		
4970.6				x		
4972.2				x		
4973.6				x		
4974.3	4974.4			x	x	
4976.3				x		
4977.8				x		oil stained vugs
4979.8				x	x	
4981.8				x		
4983.8				x	x	
4984.2				x		
4985.2				x		
4986.9				x		
4987.9				x		
4989.9				x		
4990.5				x		
4993.2				x		
4994.3				x		fractures
4996.2	4996.3			x		fractures/stylolites
4997.2				x		vertical fracture -water
4998.2				x		vertical fracture -oil stain
4999.6	4999.7			x		from end of full diameter sample
5001.2		x	x			vertical fractures
5001.6				x		across contact
5001.8		x	x			fractures
5002.2				x		fractures
5003.3	5003.4			x		across stylolite
5003.5	5003.6	x				Contact; lt gy dol/grn gy argill dol
5004.1	5004.2	x				grn gy argill dol
5006.2	5006.3	x				grn gy argill dol CS = Cover Slip

Table 7-51: Thin section, McBride South 1-10

THIN SECTION SAMPLES- MC BRIDE SOUTH 1-10, SEC. 10, T15N-R2E LINCOLN CO, OKLAHOMA						
Depth		Std	2x2	SEM	LITHOLOGY	DETAILS
From	To					
4979.6	4979.8	x			Dol Ls with sed filled frac	dense foss pkstn/wkstn strongly recrystallised c xln brac pkstn, big brac facies, ? Misener infill

Table 7-52: Thin section, Marjo Toles #1

THIN SECTION SAMPLES- MARJO TOLES #1, SEC. 10, T15N-R2E LINCOLN CO, OKLAHOMA						
Depth		Std	2x2	SEM	LITHOLOGY:	Details
From	To				hand lens	
4964.2					Ls, Pkstn	
4967.8					Ls, Pkstn	
4971.4					Ls, Grnstn	
4979.2					Ls, Grnstn	
4991.1					Ls, Grnstn	
4995.9					Ls, Grnstn	
4996.6					Ls, Grnstn	
4997					Ls, Grnstn	
5003.7					Dol, Crystalline	

Table 7-53: Thin Section, Marjo W. Carney Extension SWDW 1-14

THIN SECTION SAMPLES- MARJO W. Carney Extension SWDW 1-14 SEC. 14, T15N-R1E LINCOLN CO, OKLAHOMA						
Depth		Std	2x2	SEM	LITHOLOGY: hand	Details
From	To				lens	
5041.4					TOP OF CORE	Woodord Fm.
5042.7					Top of Hunton	Sharp, irregular contact
					Ls, small brach	
5044.1			X		pkstn	Misener infill in Karst solution cavities
5045.4			X		Ls pkstn, calcitic fill	
5054.3	54.5		X		Pkstn, dense	Open solution fractures
5055.7	55.8		X		brach pkstn, vuggy	
					Karst mosaic	
5059	59.1		X		breccia	Woodford infill
5061.2	61.3		X		Br-cri pkstn	karst infill
					Corals, karst sed fill	
5069.5	69.6		X		Cri-brach pkstn,	
					dense	
5077.3	77.4		X		Corals & brachs,	
					pkstn	Streptelasmids, Favositids
5082.2	82.3		X			Or deep-water mdstn at sequence boundary?
5092			X		Cavity fill mud?	
					Pent brachs over	
5097.3	97.5		X		Corals	
					Pkstn,	
5105	5.2		X		stromatoporoid	
5107	7.2		X		Pkstn, karst infill?	or Burrow?
5118	18.2		X		Favositid coral	
5129	29.1		X		Corals	Streptelasmids, Favositids

Table 7-54: Thin section, Marjo Wilkerson 1-3

THIN SECTION SAMPLES- MARJO WILKERSON 1-3, SEC. 3, T15N-R2E LINCOLN CO, OKLAHOMA						
Depth		Std	2x2	SEM	LITHOLOGY	DETAILS
From	To					
4953.3			X			
4953.3			X			
4954.3			X			
4958.5			X			
4960.7			X			
4964	4964.1		X			
4966.4			X			
4968.7			X			
4970.9	4971		X			
4974.9			X			
4975.5			X	X		
4979.8			X			
4983.1			X			
4986			X			
4986			X			
4988.6			X			
4990.9	4992		X			
4996.7			X			
4999.6			X			

*** Note : Sample is polished

7.1.15. Introduction to Core Photographs

Every core cut by Marjo for this project is taken directly to Stim-Lab of Duncan, Oklahoma, where the following is performed:

- Whole core plain light photography
- Whole core ultraviolet light photography, showing fluorescent oil-saturated intervals
- Plain light photography of the slabbed core.

The core is photographed in 10-foot segments, arranged in 5 columns each 2 feet long. The highest part of the core is to the left, and footages are marked.

Core photographs in digital form are presented in the following appendix files.

7.1.16. Core Photographs of Individual Wells

Ctrl+Click to view [Core Photographs](#).

7.2. *Geologic Appendix*

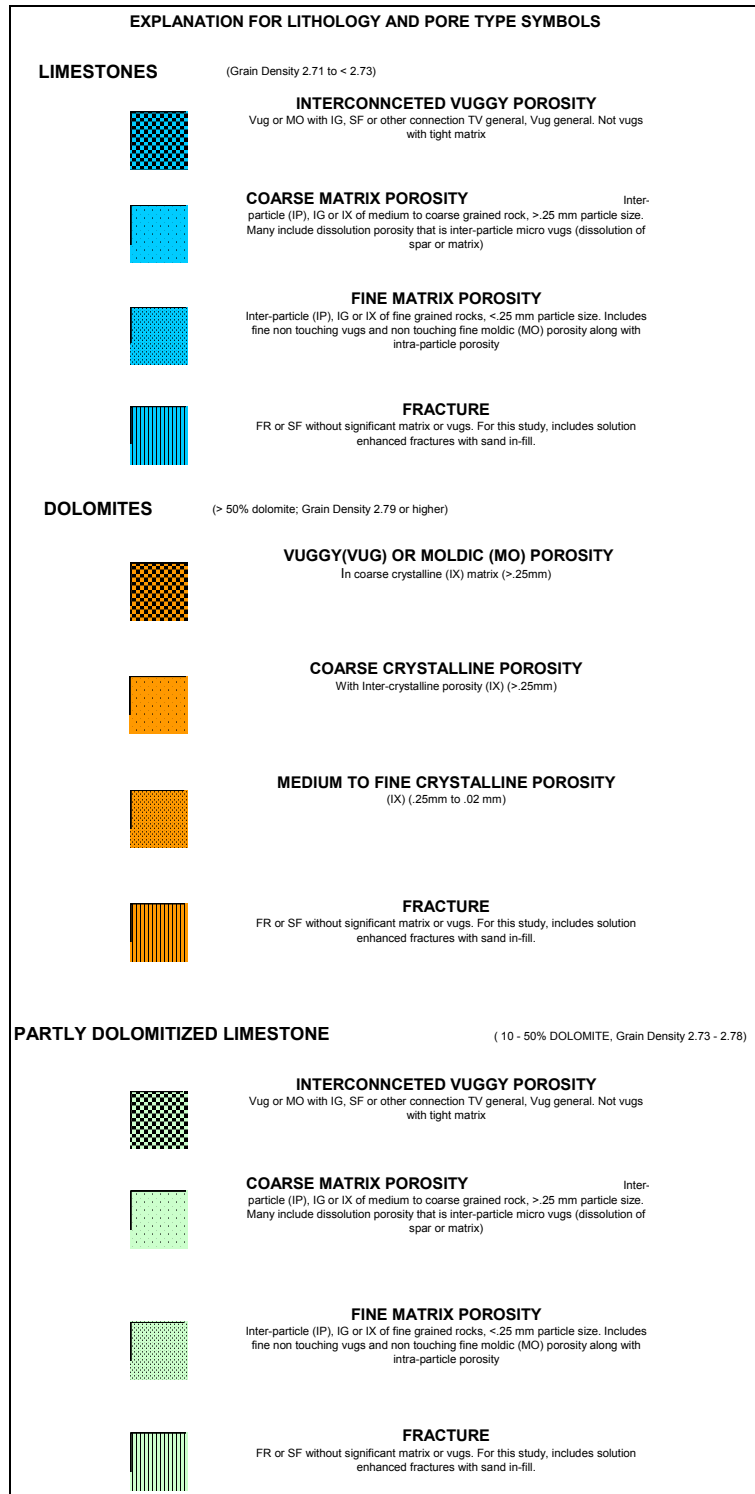


Figure 7-26: Explanation for Lithology and Pore Type Symbols







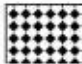
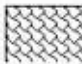
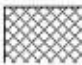

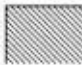
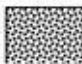


EXPLANATION FOR FACIES TYPE SYMBOLS	
	ARGILLACEOUS DOLOMITE
	CRYSTALLINE DOLOMITE
	SMALL BRACHIOPOD GRAINSTONE/PACKSTONE/WACKESTONE
	FINE CRINOID GRAINSTONE/PACKSTONE/WACKESTONE
	COARSE CRINOID GRAINSTONE/PACKSTONE
	MIXED CRINOID -BRACHIOPOD GRAINSTONE/PACKSTONE/WACKESTONE
	BIG PENTAMERID BRACHIOPOD COQUINA
	CORAL AND DIVERSE FAUNA
	CORAL AND CRINOID GRAINSTONE / WACKESTONE
	SPARSE FOSSIL WACKESTONE
	MUDSTONE
	FINE - MEDIUM GRAINSTONE
	SHALE
	FINE SANDSTONE

Figure 7-27: Explanation for Facies Type Symbols

7.3. Production Appendix

Jeff Frederick and Mohan Kelkar (The University of Tulsa), Brian Keefer (Marjo Operating Company)

Equivalent times and the relationship between constant rate and constant pressure production.

$$t_{eL}(t) = Q(t) / q(t), \dots\dots\dots (A-1)$$

$$t_{eG}(t) = \frac{\mu_{gi} c_{gi} z_i G_i}{q(t) 2 p_i} [m(p_i) - m(\bar{p})], \dots\dots\dots (A-2)$$

$$q_{D,CP}(t_D) = \frac{1}{p_{D,CR}(t_{eD})}, \dots\dots\dots (A-3)$$

Variable used to calculate r_e and ultimate recovery.

$$q_{DdL} = \frac{141.2q(t)B_l\mu_l}{kh(p_i - p_{wf})} \left[\ln\left(\frac{r_e}{r_{wa}}\right) - 0.75 \right], \dots\dots\dots (A-4)$$

$$Q_{DdL} = \frac{5.615N_p B_l}{Ah\phi c_t (p_i - p_{wf})}, \dots\dots\dots (A-5)$$

$$1 - Q_{DdL} = q_{DdL}, \dots\dots\dots (A-6)$$

$$N_{p \max} = \frac{Ah\phi c_t (p_i - p_{wf})}{5.615B_l}, \dots\dots\dots (A-7)$$

$$RF_{oil} = \frac{N_{p \max}}{IOIP}, \dots\dots\dots (A-8)$$

$$RF_{water} = \frac{N_{p \max}}{IWIP}, \dots\dots\dots (A-9)$$

$$q_{DdG} = \frac{1422(T + 460)q(t)}{kh[m(p_i) - m(p_{wf})]}, \dots\dots\dots (A-10)$$

$$Q_{DdG} = \frac{28.27(T + 460)z_i G_i}{\phi h A p_i} \left[\frac{m(p_i) - m(\bar{p})}{m(p_i) - m(p_{wf})} \right], \dots\dots\dots (A-11)$$

$$1 - Q_{DdG} = q_{DdG}, \dots\dots\dots (A-12)$$

$$m(\bar{p}) = m(p_i) - \frac{Ah\phi p_i [m(p_i) - m(p_{wf})]}{28.27(T + 460)z_i G_i}, \dots\dots\dots (A-13)$$

$$G_{p \max} = G_i \left(1 - \frac{\bar{p} z_i}{z p_i} \right), \dots\dots\dots (A-14)$$

$$RF_{gas} = \frac{G_{p \max}}{G_i}, \dots\dots\dots (A-15)$$

Laplace solutions.

$$\hat{p}_{D,CR,infinite}(r_D; s) = \frac{K_0(\sqrt{s}r_D)}{s\sqrt{s}K_1(\sqrt{s})}, \dots\dots\dots (A-16)$$

$$\hat{p}_{D,CR,bound}(r_D; s) = \frac{K_0(\sqrt{s}r_D)I_1(\sqrt{s}R_{eD}) + I_0(\sqrt{s}r_D)K_1(\sqrt{s}R_{eD})}{s\sqrt{s}[K_1(\sqrt{s})I_1(\sqrt{s}R_{eD}) - I_1(\sqrt{s})K_1(\sqrt{s}R_{eD})]}, \dots\dots\dots (A-17)$$

$$\hat{q}_{D,CP,infinite}(r_D; s) = \frac{1}{s^2 \hat{p}_{D,CR,infinite}(r_D; s)}, \dots\dots\dots (A-18)$$

$$\hat{q}_{D,CP,bound}(r_D; s) = \frac{1}{s^2 \hat{p}_{D,CR,bound}(r_D; s)}, \dots\dots\dots (A-19)$$

$$p_{D,CR,infinite}(r_D, t_D) = \mathfrak{S}^{-1}[\hat{p}_{D,CR,infinite}(r_D; s)], \dots\dots\dots (A-20)$$

$$p_{D,CR,bound}(r_D, t_D) = \mathfrak{S}^{-1}[\hat{p}_{D,CR,bound}(r_D; s)], \dots\dots\dots (A-21)$$

Variables used to evaluate the Laplace solutions.

$$r_D = \frac{r}{r_{wa}}, \dots\dots\dots (A-22)$$

$$R_{eD} = \frac{r_e}{r_{wa}}, \dots\dots\dots (A-23)$$

$$t_{eDL} = \frac{0.006328kt_{eL}}{\phi\mu_l c_l r_{wa}^2}, \dots\dots\dots (A-24)$$

$$t_{eDG} = \frac{0.006328kt_{eG}}{\phi\mu_{gi} c_{gi} r_{wa}^2}, \dots\dots\dots (A-25)$$

$$t_{DL} = \frac{0.006328kt}{\phi\mu_l c_l r_{wa}^2}, \dots\dots\dots (A-26)$$

$$t_{DG} = \frac{0.006328kt}{\phi\mu_l c_l r_{wa}^2}, \dots\dots\dots (A-27)$$

$$q_{DL} = \frac{141.2\mu_l B_l q(t)}{kh(p_i - p_{wf})}, \dots\dots\dots (A-28)$$

$$q_{DG} = \frac{1422(T + 460)q(t)}{kh[m(p_i) - m(p_{wf})]}, \dots\dots\dots (A-29)$$

Miscellaneous variables.

$$G_i = \frac{520\pi}{(1000)(14.7)} \frac{r_e^2 \phi h p_i}{z_i (T + 460)}, \dots\dots\dots (A-30)$$

$$IOIP = \frac{Ah\phi(1-S_w)}{5.615B_{oi}}, \dots\dots\dots (A-31)$$

$$IWIP = \frac{Ah\phi S_w}{B_{wi}}, \dots\dots\dots (A-32)$$

$$\frac{\bar{p}}{\bar{z}} = \frac{p_i}{z_i} \left(1 - \frac{G_p}{G_i} \right), \dots\dots\dots (A-33)$$

$$r_{wa} = r_w e^{-S_f}, \dots\dots\dots (A-34)$$

7.4. Laboratory Testing Appendix

Kishore Mohanty (The University of Houston)

Table 7-55: Hydrodynamic Properties of the fluids used in the experiment

Fluids	Viscosity (cp)	Density (g/cc)
Reservoir dead oil	4.4	0.84
Reservoir brine	1.5	1.13

Table 7-56: Imbibition Relative Permeability of core#3 by JBN method

	Krw	Kro
0.0825	0	1
0.465866	0.130109	0.095619
0.471877	0.133678	0.090531
0.489825	0.144121	0.076374
0.513614	0.157524	0.059875
0.536574	0.170069	0.046233
0.554813	0.179822	0.036877
0.570874	0.188296	0.029652
0.582584	0.194427	0.024949
0.59336	0.200048	0.021022
0.601982	0.20454	0.018144
0.60987	0.208651	0.015711
0.616651	0.21219	0.013766
0.623853	0.21596	0.011845
0.63726	0.223025	0.00865
0.642768	0.225952	0.007477
0.647201	0.228323	0.006589
0.677659	0.245163	0.001788
0.684833	0.249368	0.000972
0.693792	0.259418	0

Table 7-57: Drainage Relative Permeability of core#3 by JBN method

Sw	Krw	Kro
0.7082	0.241255	0
0.690629	0.23527	0.109749
0.674323	0.229715	0.185419
0.663211	0.225929	0.22383
0.63672	0.216905	0.292866
0.626842	0.21354	0.316456
0.620245	0.211293	0.333508
0.615707	0.209747	0.346532
0.612398	0.20862	0.357065
0.609071	0.207486	0.368899
0.60655	0.206627	0.378993
0.605586	0.206299	0.383178
0.600255	0.204483	0.411159
0.599925	0.20437	0.413262
0.595954	0.203018	0.46494

Table 7-58: Imbibition Relative Permeability of core#5 by JBN method

Sw	Krw	Kro
0.0256	0	1
0.311548	0.16003	0.142777
0.352749	0.194577	0.09525
0.366208	0.205301	0.082298
0.377668	0.214241	0.072195
0.385535	0.220285	0.065733
0.393373	0.226235	0.059664
0.40032	0.231451	0.054585
0.405259	0.23513	0.051141
0.422585	0.247847	0.040116
0.435254	0.256979	0.033046
0.446102	0.264697	0.027619
0.455175	0.271086	0.023504
0.463154	0.276659	0.020191
0.469922	0.281353	0.017596
0.476101	0.285614	0.015396
0.484073	0.291077	0.012785
0.489898	0.295043	0.011034
0.495183	0.298624	0.009558
0.499657	0.301641	0.008389
0.503857	0.304461	0.007357
0.50765	0.306996	0.006479
0.511144	0.309323	0.005715
0.5367	0.326755	0

Table 7-59: Drainage Relative Permeability of core#5 by JBN method

Sw	Kro	Krw
0.4969	0	0.067536
0.358221	0.181526	0.003152
0.358221	0.181526	0.003152
0.350518	0.185714	0.000782
0.347618	0.187066	0.000382
0.345888	0.188182	0.000223
0.344745	0.189175	0.000144
0.343943	0.190062	9.91E-05
0.343312	0.190917	6.96E-05
0.342826	0.191703	4.99E-05
0.34244	0.192431	3.61E-05
0.342126	0.193108	2.6E-05
0.341816	0.193875	1.7E-05
0.341531	0.194688	9.45E-06
0.34124	0.19566	2.63E-06
0.341123	0.206828	0

Table 7-60: Imbibition Relative Permeability of core#6 by JBN method

Sw	Krw	Kro
0.3795	0	1
0.378725	0.014436	0.688668
0.4235	0.29573	0.358508
0.447216	0.429807	0.249174
0.462024	0.50803	0.197563
0.472279	0.559577	0.167898
0.486301	0.626369	0.134094
0.497651	0.677144	0.111578
0.506395	0.714147	0.096745
0.513667	0.743466	0.085868
0.520311	0.769065	0.076966
0.526495	0.791851	0.069483
0.53168	0.810169	0.063753
0.535842	0.824339	0.059488
0.540006	0.838042	0.055497
0.544231	0.851454	0.051713
0.548074	0.863217	0.048489
0.551492	0.873327	0.045787
0.554838	0.882906	0.043282
0.557889	0.891358	0.041116
0.560862	0.899339	0.039106
0.563485	0.906171	0.037412
0.566161	0.912933	0.035758
0.616431	0.99359	0

Table 7-61: Drainage Relative Permeability of core#6 by JBN method

Sw	Krw	Kro
0.5184	0.296063	0
0.518494	0.155971	0.069893
0.505342	0.017467	0.409063
0.492781	0.003262	0.3996
0.48818	0.001875	0.387094
0.484949	0.00129	0.377737
0.482361	0.000964	0.370137
0.480604	0.000793	0.364976
0.478322	0.000619	0.358307
0.476362	0.000502	0.352634
0.475157	0.000442	0.349175
0.474096	0.000396	0.346152
0.473293	0.000364	0.343879
0.472314	0.000329	0.341126
0.471849	0.000314	0.339823
0.4612	0	0.341693